# Microwaves and Radar Institute

## A Retrospective 1908 – 2008

From Early Radio Experiments to TerraSAR-X and TanDEM-X

DLR

**German Aerospace Center**
A member of the Helmholtz Association

**Microwaves and Radar Institute**

**Director of the Institute** Prof. Dr.-Ing. habil. Alberto Moreira

**Address** Oberpfaffenhofen
D-82234 Weßling
www.dlr.de/HR

**Editorial Team** Gerhard Krieger
Alberto Moreira
Markus Peichl
Andreas Reigber
Manfred Zink

**Proofreading** David Hounam

**Layout** Björn Döring
Jens Fischer
Renate Weist

**Printed by** Richard Thierbach Buch- und Offset-Druckerei GmbH,
Mülheim an der Ruhr

November 2008

**Cover** The Radio Telegraphic and Air Electricity Test Station Gräfelfing (DVG), founded 1908

# Microwaves and Radar Institute

## A Retrospective 1908 – 2008

From Early Radio Experiments to TerraSAR-X and TanDEM-X

# Preface

On November 27, 2008 we commemorated the centennial anniversary of the Microwaves and Radar Institute! The fact that the history of our Institute can be traced back to the beginning of radio frequency and microwave research is a source of great pride to us. On October 14,1908, Prof. Dr. Max Dieckmann founded his private research laboratory for "wireless telegraphy and air electricity" in a suburb of Munich. Later in 1937 he moved his laboratory to Oberpfaffenhofen, originating the present research campus of DLR.

Many fantastic achievements were made in course of the last 10 decades. The Institute's history can be divided into several phases: DVG (Radio Telegraphic and Air Electricity Test Station, Gräfelfing, 1908 – 1936), FFO (Flugfunk Forschungsinstitut – Aircraft Radio Research Institute, Oberpfaffenhofen, 1937 – 1945; München Riem, 1954 – 1955), Institut für Flugfunk - Aircraft Radio Institute, 1956 – 1962, Institut für Flugfunk und Mikrowellen - Aircraft Radio and Microwaves Institute, 1962 - 1978, Institut für Hochfrequenztechnik (Radio Frequency Technology Institute, 1978 – 2000) and Institut für Hochfrequenztechnik und Radarsysteme (Microwaves and Radar Institute, 2000 – today). The first 40 years were undoubtedly dominated by the two world wars. It is undeniable that the research was strongly influenced by these events, which also led to strong growth in the research activities. Following the restart of the research activities in Oberpfaffenhofen in 1956 after the American occupation, the research concentrated on microwave technology, aircraft radio, landing systems and position finding. In the 1960s the use of microwaves for space applications (satellite control, communication and tracking) became a new research area at the Institute. Later in the 1970s research on navigation as well as microwave remote sensing started, the later representing the current focus of the Institute's research.

With its know-how and expertise in passive and active microwave remote sensing, the Microwaves and Radar Institute contributes today to the development and advancement of ground-based, airborne and spaceborne sensors. The focus of its research work is on the conception and development of new synthetic aperture radar (SAR) techniques and systems, as well as sensor-specific applications.
The Institute's strength is the execution of long-term research programs with applications in remote sensing, aeronautics and traffic monitoring, as well as reconnaissance and security. In line with the German space program, the Institute works in close collaboration with other DLR institutes, the German Space Administration, the European Space Agency, German industry, and responsible ministries. The education of young scientists in the form of hosting and supervising internships, as well as diploma and doctoral theses is also an important part of the Institute's mission.

I would like to thank many colleagues that contributed to this report, in particular Prof. Wolfgang Keydel (former Institute's Director, 1978 – 2001), Karl-Heinz Bethke, David Hounam, Rudolf Schmid and Bernd Röde for their support in compiling the historical account of the research activities. I hope it will be of interest to members and friends of the Institute as we proceed on our journey through the second hundred years.

Oberpfaffenhofen, December 2008

*Alberto Moreira*
*Institute's Director, 2001 – today*

# Contents

## Institute's History (1908-2000)



## The Institute Today (2000-2008)

Spaceborne SAR



Airborne SAR

# Institute's History



# Institute's History

**Figure 1-1: Max Dieckmann, picture, oil on wood. Painter: O. Pippel, 1935, Location: Institute's foyer.**

## Introduction

The present "Microwaves and Radar Institute" of the DLR was founded in 1937 as the "Flugfunk-Forschungsinstitut Oberpfaffenhofen – FFO" (Aircraft Radio Research Institute Oberpfaffenhofen) under the leadership of Prof. Max Dieckmann. This is the origin of the DLR research site in Oberpfaffenhofen near Munich.

However, the Institute's history can be traced back to 1908 when Dr. Max Dieckmann founded his private "Drahtlostelegraphische und Luftelektrische Versuchsanstalt Gräfelfing – DVG" (Wireless Telegraphic and Air Electricity Test Station Gräfelfing) located in Gräfelfing near Munich, 13 km from Oberpfaffenhofen. The goals of the DVG were the application of electromagnetic waves for communication, navigation, and radio location as well as the research of electric processes in the atmosphere. Using modern terminology, the work encompassed microwave technology, radio measurement techniques (radar), jamming, and determination of aircraft signatures by model measurements. Particularly in the early years, antenna development was predominant.

Remembering that Heinrich Hertz had discovered electromagnetic waves twenty years beforehand, the DVG Institute seems to be the first microwave laboratory world wide dedicated to the research of microwave techniques and applications.

## The Radio Telegraphic and Air Electricity Test Station Gräfelfing (DVG)

100 years ago, on October 14, 1908, Max Dieckmann, Assistant Professor at the Technical University Munich, hired a meadow with a small cabin in Gräfelfing near Munich and founded the DVG. The purpose was to develop the then very new and exciting area of wireless techniques, to investigate the effects of natural electrostatic phenomena and to use that facility as an experimental station for his students.

One of the very early developments was the "safe" spark gap transmitter for operation on board Zeppelin airships, which were then filled with highly inflammable hydrogen gas. Together with the former Telefunken Company (now EADS Defence), Dieckmann succeeded in constructing a hermetically sealed cabinet containing the spark gap

transmitter and an antenna which was adequately isolated from the gondola environment. A very successful field trial was conducted to demonstrate the usefulness of airborne wireless radio stations in 1911/12, when the airships "Victoria Luise" and "Hansa" exchanged telegrams over distances of 250 km (see Figures 1-2 and 1-3). The antenna was the first developed in Gräfelfing. As a result of this success, almost all Zeppelin airships were equipped with such radio stations that communicated with the first ground station near Frankfurt.

This was indeed the birth of airborne radio communication. Further developments included the development of simple methods for locating the position of an airship by comparing signal strengths received from different ground stations. Also, the DVG developed a special gas-tight skin which had a certain degree of electrical conductivity. This feature guaranteed that static electricity would not accumulate and give rise to sparks.

In 1914 the DVG also developed a first frame direction finder and used it for ship navigation on the nearby lake Ammersee. During the First World War, such instruments were installed on airships for navigation via ground based transmitters (see Figure 1-4).

During the First World War, the research in Gräfelfing decreased. Prof. Dieckmann served in the Imperial German Army as a director of the Air Force Wireless Research Laboratory at Döberitz near Berlin. During this time, he invented and developed an apparatus for the detection of phone cables (1914) and a system whereby an observer in a basket lifted by a balloon was connected to a ground station by a 1000 m long wire (see Figure 1-5). Later this was performed with an airship flying above the clouds and, therefore, invisible from the ground. He also developed a first instrument for radio transmission of images (facsimile). The necessity of such techniques came from the airborne reconnaissance units for supporting the artillery. Detected enemy positions were conveyed more swiftly and accurately by the transmission of hand sketches and annotated map sections.

These inventions proved to be of great importance for the Institute when the image transmission technique was further developed in the years 1922 to 1929. During 1926, first attempts were

Figure 1-2: Dr. Max Dieckmann and the wireless radio station on-board the airship "Victoria Luise", 1912.

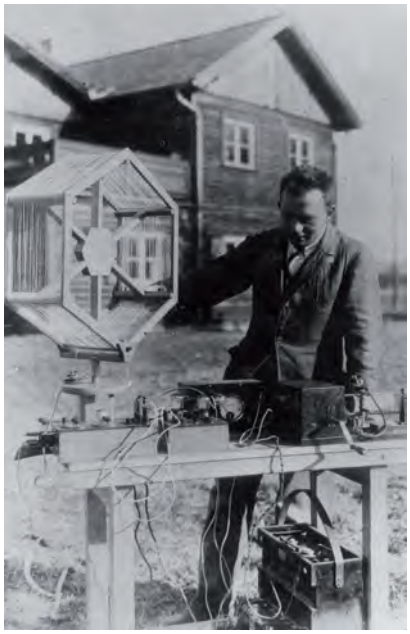

Figure 1-4: Experiment equipment with a DVG frame direction finder.

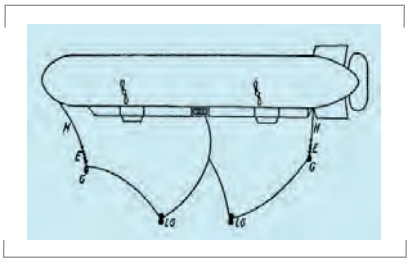

Figure 1-3: Zeppelin airship with an early wire antenna.

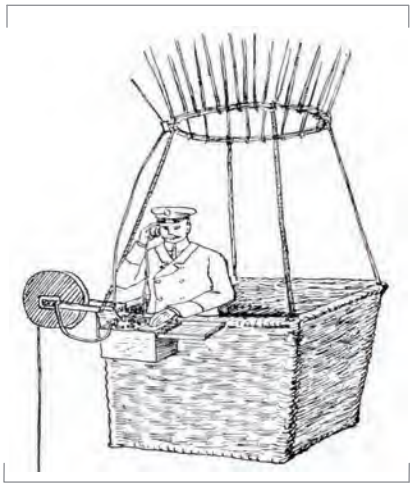

Figure 1-5: Observer in a balloon basket with a communication link to the ground.


**Figure 1-6: Radio weather map sent in 1926 from Radio Norddeich to the "Westphalia" over 4600 km via the DVG radio technique with a thank-you and congratulations message from the ship's captain.**

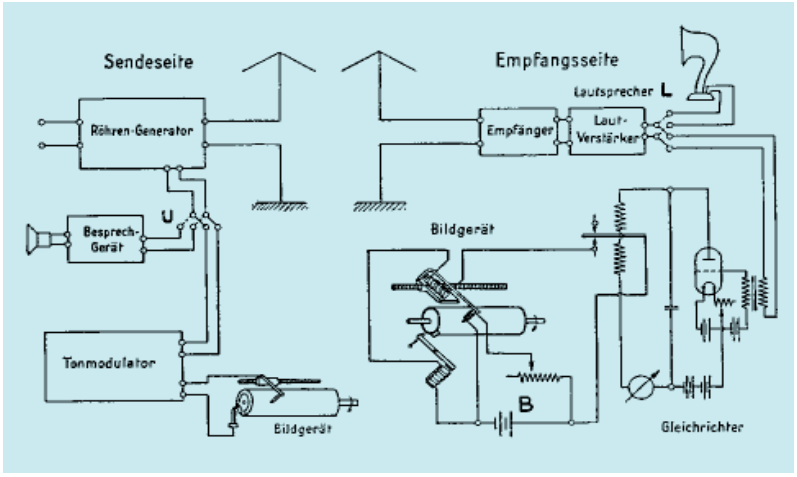


**Figure 1-7: Circuit diagram of the DVG image transmission system used for weather map transmission in 1926 to "Westphalia".**


**Figure 1-8: Image of the DVG building at Gräfelfing, painted by Max Dieckmann and transmitted with the DVG image radio transmission technique.**

made to operationally transmit weather maps to the public at large via the medium wave broadcast transmitter in Munich, and via the German coastal radio station in Norddeich to ships on intercontinental routes. Figure 1-6 shows an example of such a weather map of the North Atlantic sent to the liner "Westphalia" over a distance of approx. 4600 km. A block circuit diagram in Figure 1-7 shows the principle of the system. The originals were scanned on a cylinder with a two-bit resolution. Several different printing techniques had been investigated for the receiver, e.g. an ink-jet process, also in colour (see Figure 1-8), or a hot stylus process to melt and transfer the colour from a colour carrier sheet.

The other problem intensively investigated was the localization of aircraft, either from the ground or from the aircraft itself. The growth of civil air transportation services imposed an urgent need for a reliable system for localizing aircraft and thereby maintaining air traffic security.

Several patents were awarded to the Gräfelfing team for the development of specialized airborne receivers to measure the angular bearings of ground transmitters, either to get a reference for its own position, or to estimate the correct air traffic route. Figure 1-9 shows such an instrument from around 1935, which used a fixed loop antenna in conjunction with the main communication wire antenna to derive the angular deviation from a ground transmitter relative to the aircraft axis. At the left in the figure, the cockpit instrumentation can be seen which indicated this deviation. Later on, receivers of this type were installed in fighter aircraft of the newly established German Air Force.

In the year 1928, an additional test site on the western shore of Lake Ammersee near the village of Riederau was established. Experiments on precise

direction finding devices require well defined natural surroundings for proper estimation of system performance and propagation parameters. The water surface of the lake was therefore an ideal choice for such a test site. At Riederau, first experiments for remote radio controlled vehicles were carried out. These experiments generated widespread public interest, as can be seen in a newspaper clip from the "Gelsenkirchener Allgemeine Zeitung" dated September 24,1928 (Figure 1-10).

# The Airborne Radio Research Institute Oberpfaffenhofen (FFO)

After 1935, the German Air Ministry identified that the German research facilities in the field of RF techniques were insufficient for the applications to communications, navigation and radio detecting systems required by the German Air Force. Therefore, Prof. Dieckmann was asked by the Air Force to intensify his experimental work to establish a new institute for airborne radio research. Prof. Dieckmann accepted this task and looked for a location somewhere between Gräfelfing and Riederau. He found a place large enough in the immediate neighbourhood of the Dornier airfield near the village Oberpfaffenhofen. This newly established facility bore the name "Flugfunk-Forschungsinstitut Oberpfaffenhofen (FFO)" and activities formally commenced in the year 1937.

The key personnel came from the Institute in Gräfelfing. The FFO started with a staff of 115 members:
17 executive engineers and autonomous scientists, 35 engineers, technicians and scientific assistants, 15 other employees, 34 mechanics and craftsmen, as well as 17 labourers and assistants. They were divided into the following branches:

- General sciences (8): General scientific and theoretical work, reports, patents, library, scientific secretariat
- Research branch A (14): Direction finder in all wavelengths, wave propagation and multipath effects, short time measurement techniques, ultra short waves (today VHF and UHF), tubes (valves) and tube systems
- Research branch B (14): Self-excitation, energy lines, on board equipment
- Mechanical workshop and operations (38): Construction, precision and coarse mechanics, assembling, house keeping
- Flight department (13): Air traffic for research, travelling, training, aircraft maintenance and repair


**Figure 1-9: Specialised airborne receiver for direction and route finding.**

**Figure 1-10: Experiments for remote radio controlled vehicles.**


2. Blatt. Nr. 265. 26. Jahrgang. Gelsenkirchener

Die Strohpuppe am Steuer

75

**Figure 1-11: Building of the Flugfunk-Forschungsinstitut Oberpfaffenhofen at the beginning in 1937.**

**Figure 1-12: An engineer during experiments with wave guide and Fresnel lens antennas.**

**Figure 1-13: Junkers W-34 aircraft carrying the DVG experimental short-wave height measuring radar at the Schleißheim airfield near Munich, autumn 1935.**

At first, the FFO consisted of a laboratory building and a hangar. The building is still being used (see Figure 1-11).

The enthusiastic beginning was, however, marred by a tragic accident when a Ju52 aircraft with six engineers and pilots on board crashed near Kassel during the night of November 4, 1937 while on its way back to Oberpfaffenhofen.

In the following years, research was mainly concentrated on developing the emerging microwave technology; and antenna research and development was a central topic. Figure 1-12 shows an engineer during experiments with wave guide and Fresnel lens antennas.

Especially radar problems required an ever-growing part of human and technical resources. Direction finding techniques for different purposes had been developed during the war and in the twenties and early thirties, due to the worldwide progress in the development of innovative electronic devices, like high-power magnetrons, detector devices and the forgotten invention of Hülsmeyer for detecting objects via the reflection of electromagnetic waves gained increasing importance. Both the DVG and the FFO took up that topic, which is now called radar, as a central research activity. Because radar research has been a key topic since the thirties, the next three chapters will be dedicated to the radar research and development in FFO and DVG.

**The Development of Pulsed Airborne Radar for Height Determination**

A very early development of a radar system was undertaken at the beginning of 1935 and continued in the following years at the DVG. The aim was to determine the real height of an aircraft above ground by means of an electrical echo sounder (altimeter). At this time, the ionospheric echo sounding method by transmitting short RF pulses in the zenith direction was already known. This method had been developed by Breit and Tuve in the US in the late twenties and was used later at different sites in Europe to analyse ionospheric phenomena, which were important in order to predict commercial intercontinental short-wave links.

To our knowledge, it was at the DVG that this sounding principle was applied for the first time by measuring the delay of RF echoes reflected from the ground from flying aircraft, in order to measure the precise height over ground. This apparatus used a wavelength of $\lambda = 7$ m (equivalent to a carrier frequency f = 42 MHz) and a transmitter pulse length of less than 0.5 μs. Some rare pictures on glass-plates of the apparatuses survived the war and were found in the cellar of the Institute some years ago. A selection is shown in the next figures. These very early experiments with an airborne radar had been undertaken in the second half of the year 1935 using a Junkers W-34 aircraft of the DVL organisation (Figure 1-13) which was stationed on the Schleißheim airfield, some 20 kilometres north of Munich. A sketch of the aerials fitted to this aircraft is shown in Figure 1-14.

For displaying the results at high resolution and distances of at least 10 km, the developers initially used a Cathode Ray Tube (CRT) of an early Telefunken TV set, exhibiting a screen

diameter of about 20 cm (huge at the time) with magnetic electron beam deflection (see Figure 1-15).

The circuit diagram of the first developmental stage is shown in Figure 1-18.

The engineers tried to expand the distance co-ordinate (to obtain a more precise reading) into a zigzag line. Experiments showed this not to be sufficient, so that in a later stage (during 1936) a circular electron beam trace was written onto the CRT screen with a dark-point triggered by the ground echo. This gave better readings with a much clearer picture.

A photograph of such a CRT display is depicted in Figure 1-16, which shows the case of an aircraft flying at a height of 2500 m. Later on, an advanced CRT construction using electrostatic deflection made the deflection amplifier more sensitive, requiring a much lower RF output power. The installation of the radar transmitter and the CRT deflection amplifier during a measurement campaign in 1935/36 inside the Junkers W-34 aircraft can be seen in Figure 1-17. The transmitter delivered a peak power of about 200 W at a pulse repetition rate (PRF) of 15 kHz.

The observations described in the test report showed that the influence of the reflecting surface had a strong impact on the precision of the reading. Especially during the very early experiments, the strong absorption of RF waves of forested areas caused difficulties because of insufficient echo strength and strong signal fluctuations. Optimal results were observed over water. Furthermore, there were interesting observations regarding the detection of coasts or lake shores, because of the wide antenna beams. The observer could detect the approaching coastal reflections from the off-nadir angles on the screen and could relatively accurately determine the moment of a coastal approach.

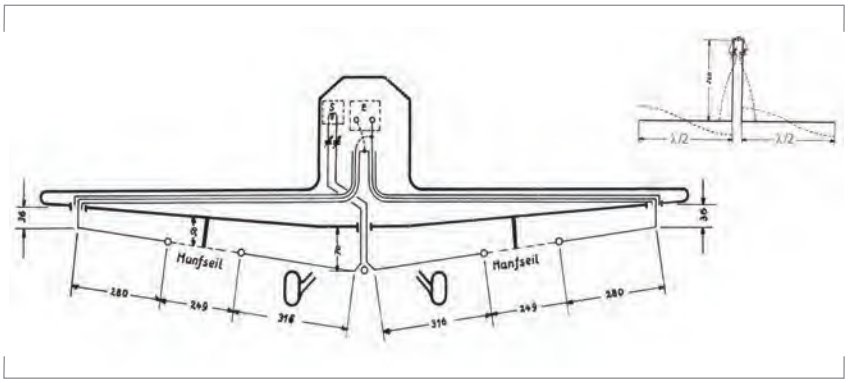


**Figure 1-14: Sketch of short-wave antennas developed for the first experiments with the electrical echo sounder of the DVG mounted on a Junkers W 34 aircraft.**

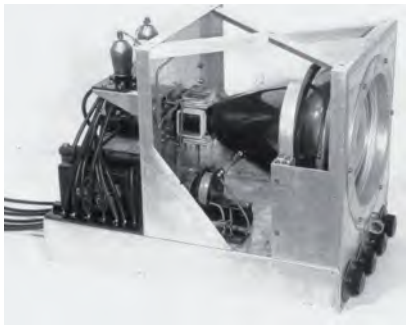

**Figure 1-15: Monitor module, the first development stage of the DVG echo sounder; CRT diameter 20 cm with magnetic beam deflection from an early television set.**

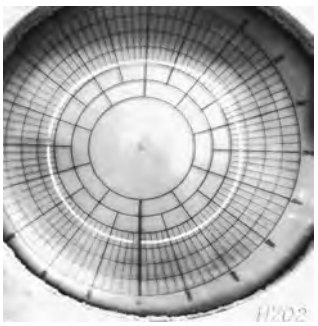

**Figure 1-16: Echo sounder CRT display during a flight test at a height of 2500 m above ground. The deviation from a circle shows the problems of non-ideal magnetic deflection coils and other stray fields.**

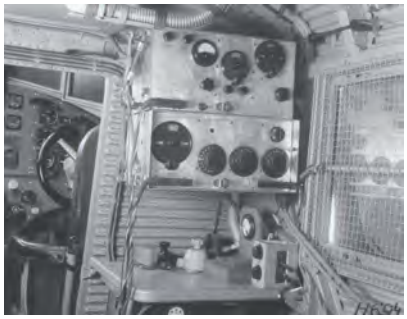

**Figure 1-17: Installation of two echo sounder modules. Above the pulse transmitter, λ = 7 m (42.9 MHz) and the CRT deflection amplifier and PRF generator, fixed by elastic ropes.**

The date of completion of the modified prototype is not known exactly. However, there is a copy of the preliminary description of the apparatus in the archives dated August 1941. After this date, the device, now under the official designation FuG 102, was used by the German Air Force. The transmitter frequency was then f = 182 MHz ($\lambda$ = 1.65 m) at a peak pulse power level of about 80 W and a pulse length of 0.3 µs. This wavelength resulted in compact dipole aerials installed below the wings using this surface as a reflector. This installation caused very low additional air resistance. One original CRT of the FFO production with a flat, screen and internal scale remained intact in the archives of our Institute in Oberpfaffenhofen. The scale of this CRT extends only up to 5000 m. The FuG 102 device could be used, however, up to a maximum height of 10000 m. The precision of the whole device (including reading errors) was given as less than ±100 m over flat terrain.

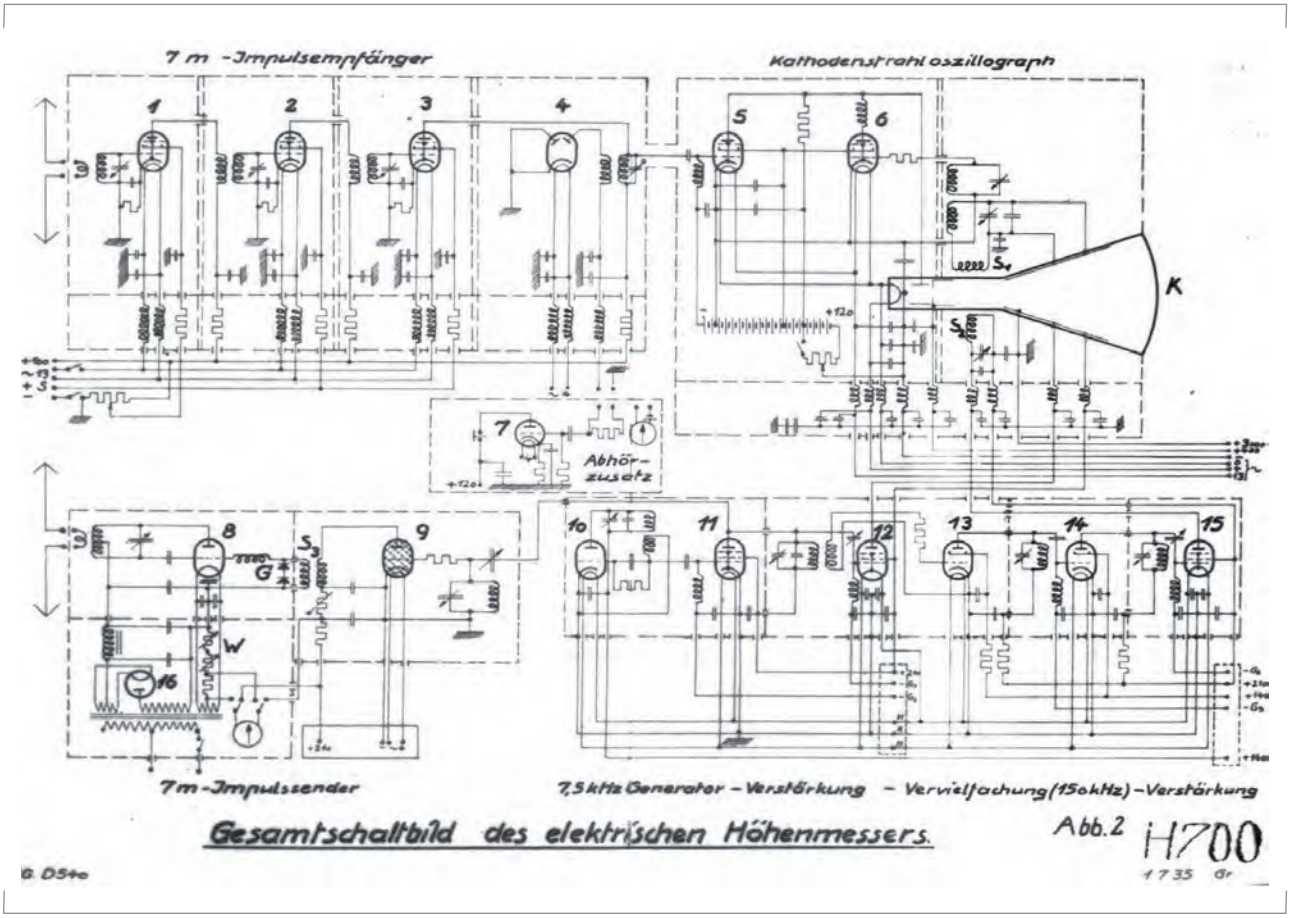


**Figure 1-18: Circuit of the first version of the DVG electrical echo sounder for aircraft (1935).**

**Early Experiments with Microwave CW Radar**

There is some evidence in the Institute's archives which indicates that as early as 1936 radar experiments had been undertaken on the shore of Lake Ammersee near Riederau to detect ships and determine their line-of-sight velocity components by measuring the frequency shift of the microwave echoes due to the Doppler effect.

A field trial using such an apparatus during August 1937 is depicted in Figure 1-19. The lower reflector antenna with a 1 m diameter is the transmitter antenna with a magnetron installed behind it. A view into this open transmitter construction can be seen in Figure 1-20. The wavelength chosen in these early experiments was $\lambda = 6$ cm. The exact type of the magnetron could not be determined, but it was probably a two-slit construction with a CW output power of less than 0.1 W. This can be deduced from a published account two years later, where a microwave link for telephony over 160 km was described and where the same transmitters had been used. In those days, the front-end of the receiver used either crystal diodes for rectification and mixing or Barkhausen-Kurz valves. These devices were crude predecessors of microwave devices like klystrons.

The CW power coupled out of the magnetron was led via a Lecher line to small dipole feeder in the reflector focus. In Figure 1-20 this Lecher line is shown from the side, therefore only one wire can be seen. It seems that the feeder line together with the feeder dipole was mechanically fixed at only two positions by ¾ $\lambda$ double wire stubs to the left and right sides. It should be emphasised that these magnetron valves were constructions of the DVG valve laboratory. One of the experimental magnetron types is shown in the right Figure 1-22; it is likely to be of the type

**Figure 1-19: The first CW radar of the DVG during experiments in 1937 at Lake Ammersee.**

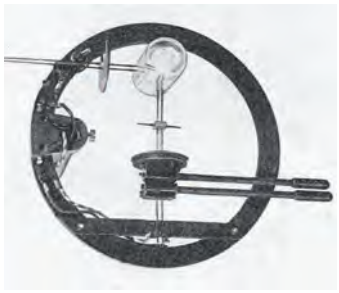

**Figure 1-21: A receiver detector using a special triode valve in a retarding field condition. The receiving dipole is in the centre with variable matching disks on one side.**

**Figure 1-22: A (probably) two-slit magnetron valve for cm-wavelengths from DVG valve laboratory.**

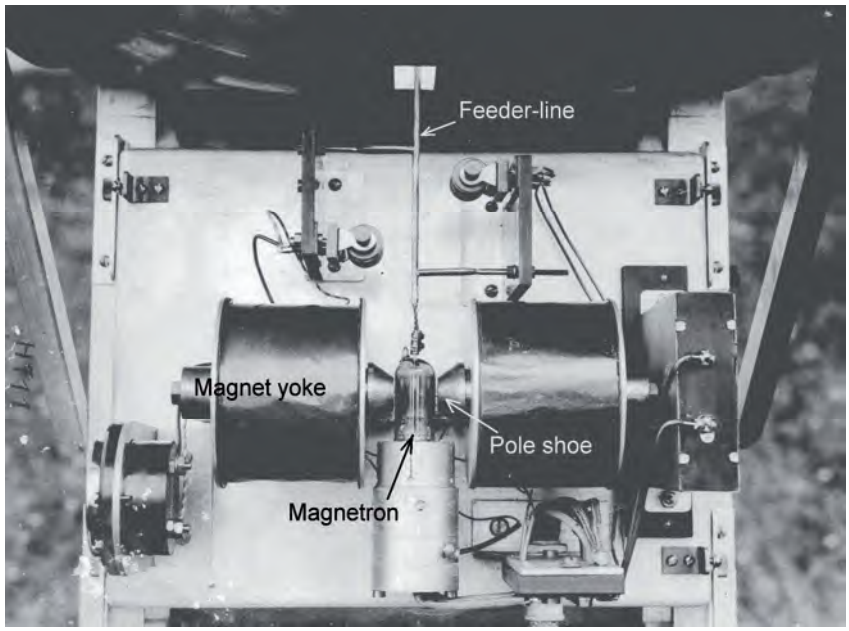


**Figure 1-20: View into the transmitter box of the experimental microwave radar apparatus of 1937.**

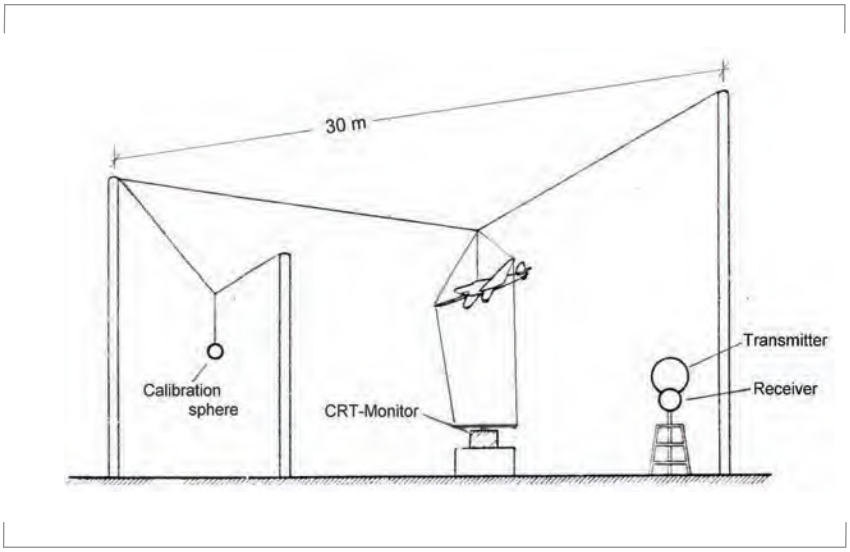


**Figure 1-23: Arrangement of radar and targets during the RCS measurements in Oberpfaffenhofen, 1940.**

**Figure 1-24: Magnetron transmitter of the DVG for RCS measurements of 1:10 scaled aircraft models. This microwave source delivered 10 W CW power at λ = 5.2 cm.**

used in the transmitter shown in the Lake Ammersee photograph taken in 1937. The receiver detector inside the upper 0.7 m reflector was probably a special triode valve operated in a retarding field condition in a configuration as shown in Figure 1-21.

**First Experiments to Evaluate Quantitative Radar Cross Sections (RCS) of Aircraft**

Because of a growing demand for basic research in the field of radar development during the early years of the Second World War, a quantitative description of the maximal range of ground-based radar to detect aircraft in different heights was missing.

After some very preliminary field experiments by the DVL on a proving ground of the Telefunken works near Templin (north of Berlin) in 1939 which gave some first hints of the reflectivity of a Ju-52 transport aircraft in flight, a programme was initiated in the years 1940/41 at the FFO to measure the reflectivity of different aircraft types flown by the German Air Force. Because initial experiments showed that field trials required enormous effort, it was decided to use scaled models of the targets.

Calibration of the model measurement setup was a prerequisite to obtain quantitative results. In the FFO, a calibration device consisting of a short dipole resonant to the transmitted radar wave was the ultimate reference, the theory of the scattering of such a dipole being known at that time. However, the dipole could not be directly used during the model measurements because of its relatively low reflectivity and the necessary high precision in aligning the dipole. Therefore, the dipole equivalent number, *z*, for a more convenient calibration reflector, a metallic sphere with a 5λ diameter, was determined with high precision. During the following two years, this sphere served as a reference for all the experiments with the 1:10 downscaled aircraft models. A confirmation of this indirect model method was able to be obtained in a campaign 1943/44, when small clouds of a known number of free flying dipoles (chaff cloud) were dropped from an aircraft over the Baltic see.

Later on during the war, the backscatter cross-section replaced the dipole equivalent number as the measure of reflectivity. A sketch of the measurement arrangement is shown in Figure 1-23. The radar system was located 30 m away from the targets, i.e. the calibration sphere and the aircraft model.

First experiments used a wavelength of λ = 5.2 cm. Later on, measurements at λ = 6 cm were conducted. Figure 1-24 shows the transmitter antenna with the magnetron oscillator of about 10 W CW output power installed immediately behind the reflector. The received echo signal of the CW transmission was rectified, amplified and used to deflect the electron beam of a CRT in a radial direction. The bright spot of the beam was caused to continuously write a reference circle onto the CRT screen, and was synchronised to a motor which

rotated the aircraft model by very thin increments (Figure 1-25). The radial deviations of the bright spot from the basic circle served as a quantitative measure of the target reflectivity when compared to the echo of the calibration sphere at the same distance.

Two examples of such measurements can be seen in the Figures 1-25 and 1-26. The first shows the reflectivity of a Dornier Do 17 model in the azimuth plane. The other example displays the reflectivity of the Messerschmitt Me 109 fighter aircraft model in the vertical plane aligned to the aircraft main axis. The inserts in both pictures represent the received echo intensities of the calibration sphere with a diameter of 30 cm. The strong echoes on both sides of the aircraft in the left Figure are caused mainly by specular reflections from the fuselage, while the main reflections from the upper and lower sides of the Me-109 model are more asymmetric because of the much smaller radius of curvature of the upper part of the fuselage. The choice of the wavelength $\lambda = 5.2$ cm in connection with the 1:10 scaled model measurements was selected in order to simulate a wavelength of $\lambda = 52$ cm (corresponding to a frequency of 576 MHz) which had been used since 1939 by the ground-based targeting radar system of Telefunken, widely known by its code name "Würzburg".

After evaluation of the measurements it was possible to calculate the range of detection of the radar equipment for the different aircraft types. The results were validated later during field trials ordered by the Air Force.

Note that the calculation procedure to determine the radar range (radar equation) was already known in 1940. The theoretical minimal detection ranges for three types of aircraft for the "Würzburg" radar system with an assumed effectively radiated TX pulse power of 1 kW were determined. The results in the table were obtained, which proved to be quite realistic later.

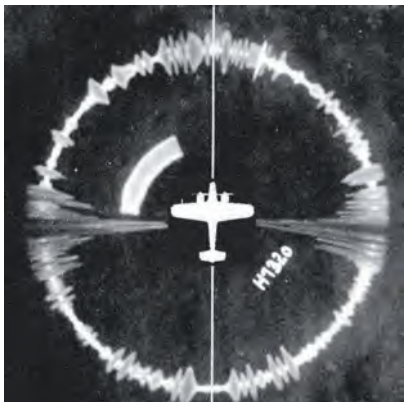

**Figure 1-25: Backscatter of a 1:10 down-scaled Dornier Do 17 aircraft model at $\lambda = 5.2$ cm, azimuth plane.**

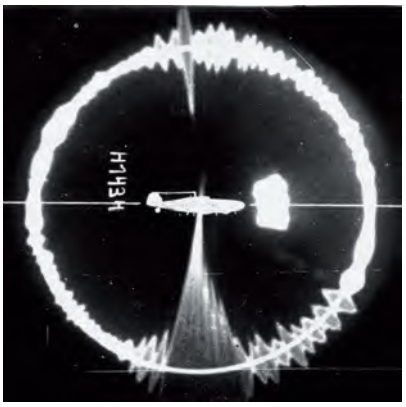

**Figure 1-26: Backscatter of a 1:10 down-scaled Messerschmitt Me 109 aircraft model at $\lambda = 5.2$ cm, elevation plane.**

| | Me 109 | Ju 87 | Do 17 | Comment |
|---|---|---|---|---|
| **R max** [km] | 26 | 26 | 35 | Side aspect |
| **R min** [km] | 12 | 14 | 14 | Mean of other aspects |

**Figure 1-27: Results of radar range computations based on measured radar cross sections.**

A less well known activity during the war was the discovery of the jet streams in the stratosphere. Together with Prof. Georgii from the "Institut für Segelflug", the FFO developed mobile direction finders in the short wave spectrum and at a wavelength of 20 cm in order to track balloon-mounted transmitters. With five direction finders, deployed in different regions of Germany, weather balloon ascents were regularly conducted. An example of one of these balloon tracks and the derived wind velocity measurements is shown in Figure 1-28.

During the war, because of the increasing danger due to air raids,

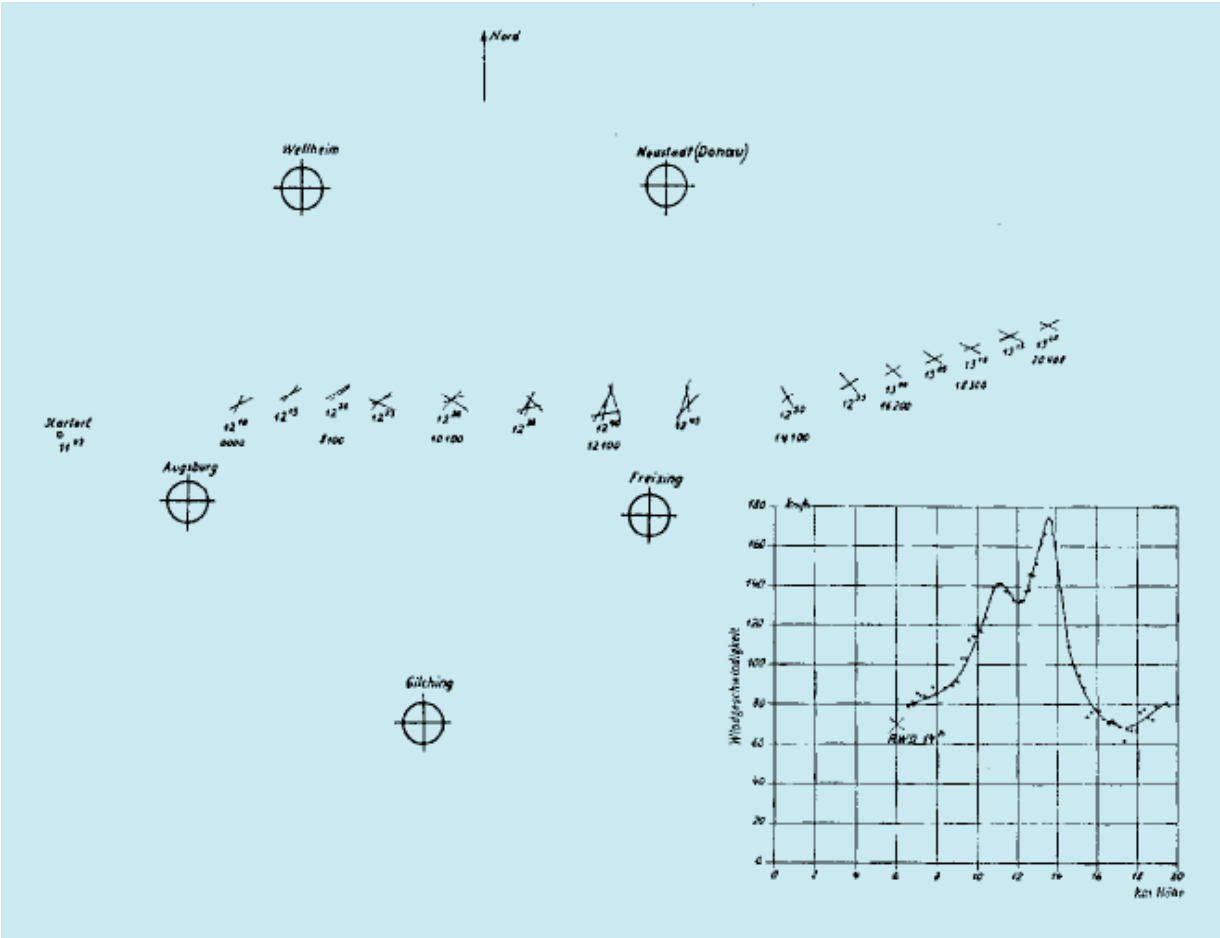


**Figure 1-28: Example of a balloon track measurement and the derived wind velocity gained with direction finders installed at Kehlheim, Neustadt/Danube, Augsburg, Freising, Gilching. The lower diagram shows the measured wind velocity as a function of the balloon position.**

it became necessary for parts of the Institute to be relocated to other places in the nearby surroundings. One of these sites was the observatory building on top of the Hohenpeißenberg hill, now belonging to the German Weather Service and then used for wave propagation research. Other places were Seeshaupt at Lake Starnberg, Gauting and castle Wartaweil on the edge of Lake Ammersee. The FFO grew constantly during the war. In May 1945, together with all of the remote locations it had more than 2000 employees on its payroll. During the war, no air raids were directed at the Institute, the only exception being when two fighter aircraft made a low-level approach and shot with their cannons into the hangar. At the second approach one of the aircraft was hit by the Institute's own flak and crashed near St. Gilgen.

On 8 May 1945, American troops occupied the still intact Institute and after a short time of evaluation of the developments, almost all machines and instrumentation were destroyed. The valuable library was moved to the Wright-Patterson Laboratories near Dayton/Ohio, however, most of the

books returned in the sixties. This is the reason that even today one occasionally finds older volumes of our publications marked "US Property"!

In the following years, radio research in this modern field ceased because all the buildings of the Institute were confiscated and used by the US Forces. Evidence of this time came to light, when paintings were discovered under wallpaper, when a laboratory room was given away for an extension of the canteen. They depict some humorous and satirical scenes of US military personnel sporting Greek attire (see Figure 1-29). They were painted by a local artist, Maria von Rebay, in 1946 and can still be seen in the canteen.

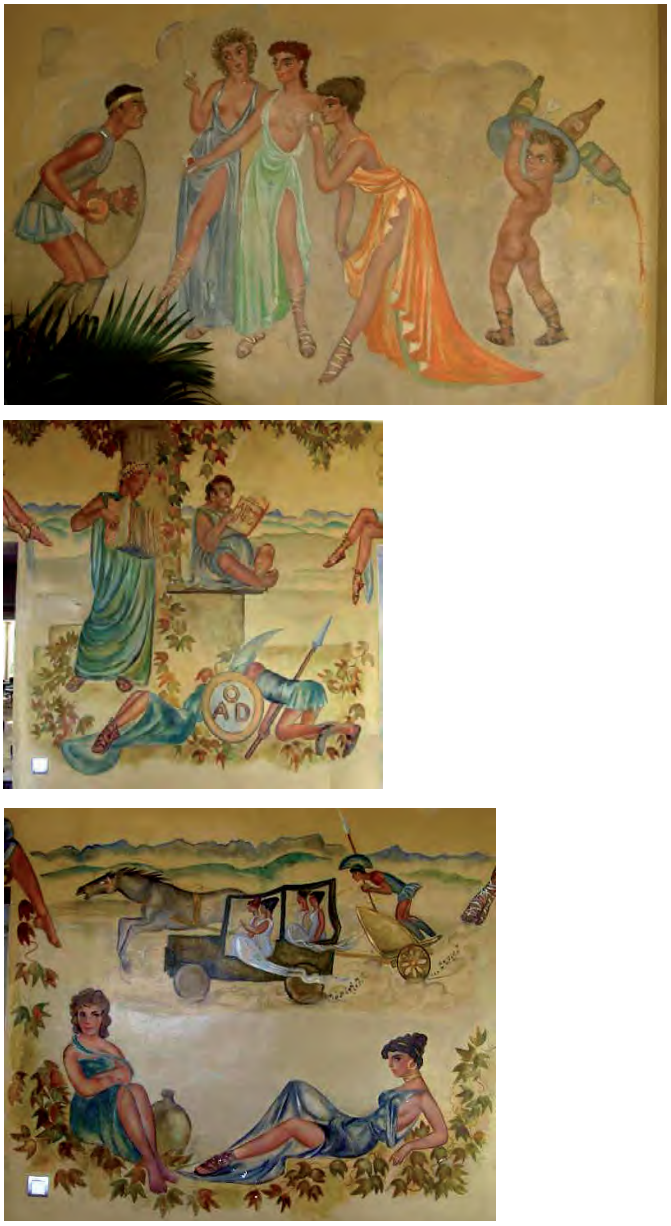

**Figure 1-29: Paintings discovered under wallpaper, US military sporting Greek attire. The paintings can still be seen in the canteen of DLR Oberpfaffenhofen.**

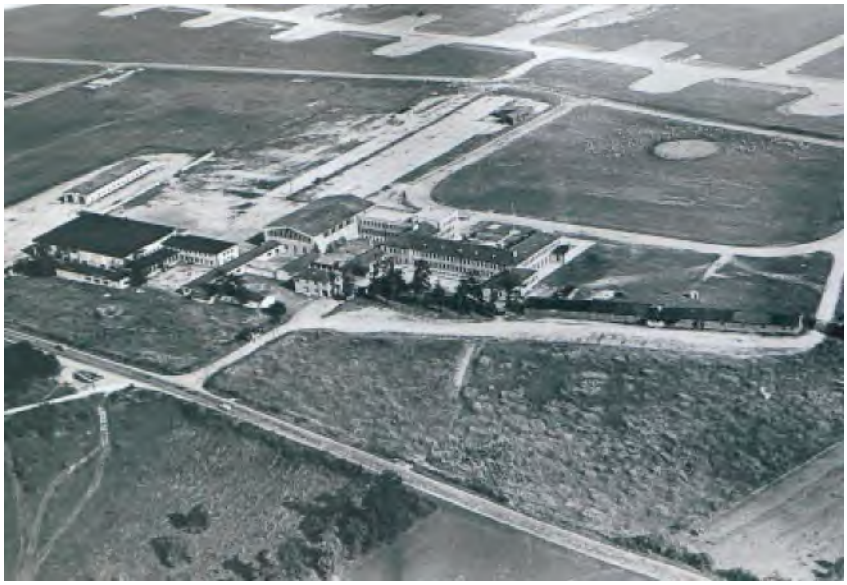

**Figure 1-30: Beginning after the Second World War, Oberpaffenhofen site in 1954/1955.**

# The Time after the Second World War

**Organisational History**

In 1953, first attempts were made to revitalise radio science in the old buildings at Oberpfaffenhofen which had been left empty after the American occupation. The property was now in the possession of the German government. At that time, the main impetus came from the German Air Navigation Service and the Ministry of Transport which realised the urgent need for radio research in the field of instrument landing systems and direction finding devices. Furthermore, there was also the need to investigate basic microwave physics because knowledge in this important field was widely lost after the war as a consequence of the restriction imposed on this research, and also because many of the leading FFO engineers had left Germany to work abroad. On July 31, 1954 the members of the FFO resolved to reanimate the FFO under the umbrella of the German Aeronautics Research Centre, the Deutsche Versuchsanstalt für Luftfahrt (DVL). On September 29, 1955 the board of directors of the DVL finally agreed the new development.

This led to the formation of an interim establishment, the "Flugfunk-Forschungsinstitut München-Riem", which was located in what had been the old main building of the Munich airport in Riem.

The Institute started immediately to work with a staff of 30 persons under the leadership of Dr. Hans J. Zetzmann from the Siemens & Halske Company. First tasks were:

- Research on and development of a three-dimensional air traffic control system
- Research on and development of instrument landing systems
- Development of millimetre-wave measurement techniques and components

Figure 1-31 shows an experimental assembly of an analogue computer for an automatic landing system built at the airport Munich-Riem. While work was in progress at Riem, a complete renovation of the empty buildings in Oberpfaffenhofen took place.
Figure 1-30 depicts the state of development around 1954/55. After the renovations were complete, the Institute moved to its past location in Oberpfaffenhofen in November 1956, this time under the name "DVL-Institut für Flugfunk" (DVL Aircraft Radio Institute).

Since 1953 there had been two other DVL Microwave Institutes in Mülheim/Ruhr: the Institute for Radio Frequency Technology under the directorship of Dr. A. Esau and the Institute for Microwaves, the acting head being Dr. W. Fogy. Subsequently, Dr. G. Ulbricht, who came from the Telefunken Company, became the director. Because the already designated

director, Dr. H. Zetzmann, had a bad accident and was unable to take over the task, Ulbricht also took the leadership of the Aircraft Radio Institute in Oberpfaffenhofen. In 1960, the three Institutes (two of them from Mülheim in North West Germany) were unified in Oberpfaffenhofen under the name "Institut für Flugfunk und Mikrowellen" (Institute for Aircraft Radio and Microwaves), still under the directorship of Dr. G. Ulbricht.

The goals of the new Institute were the applications of radio frequency techniques and technology in the field of aviation for communication, navigation and position finding, the research topics being antennas and wave propagation, radar, direction finding, landing support, and altimetry.

In 1968 Prof. Ulbricht retired and Dr. Werner Fogy became the acting head. On December 1, 1978, Dr. Wolfgang Keydel who came from the AEG-Telefunken Company in Ulm, became the new director and the Institute's name changed to Institute for Radio Frequency Technology. This name remained until 2000 where a reorganisation of the DLR research areas in Earth observation, navigation and communication took place. Since then, the Institute has its current name "Institut für Hochfrequenztechnik und Radarsysteme" (Microwaves and Radar Institute, DLR-HR). After the retirement of Dr. Keydel, on August 1, 2001, Prof. Dr. Alberto Moreira took over the leadership as the new director in conjunction with a chair at the Karlsruhe Institute of Technology (KIT). Figure 1-32 shows the whole Institute's development from the beginning in 1908 until 2008.

**Figure 1-31: Experimental assembly of an analogue computer for an automatic landing process at Riem, about 1955.**

During the first 20 years after the Second World War, the complete aircraft research landscape in Germany changed mainly due to the upcoming and rapidly growing space activities. From 1961, the

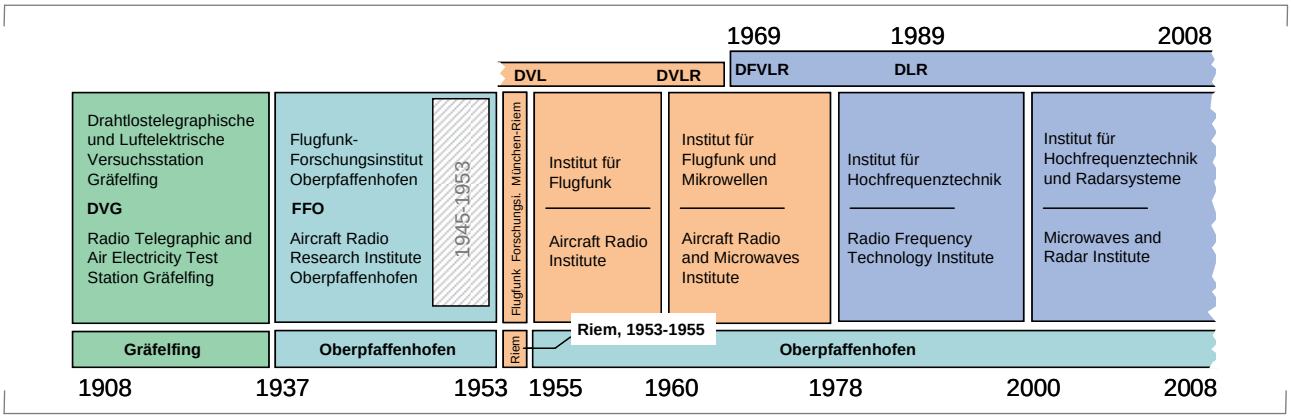


**Figure 1-32: Complete Institute's development from the beginning in 1908 until 2008.**

**Figure 1-33: Experimental installation of an electronically switched Doppler direction finder.**

**Figure 1-34: The test monopulse tracking antenna in Oberpfaffenhofen (diameter 11 m).**

DVL was called Deutsche Versuchsanstalt für Luft- und Raumfahrt, DVLR (German Aerospace Testing Establishment). In 1969, the DVLR was merged with three other aviation and aerodynamics laboratories forming the Deutsche Forschungs- und Versuchsanstalt für Luft- und Raumfahrt, DFVLR (German Aerospace Research and Testing Establishment). Since 1989 its name is DLR and in 1997, after the merger with the German Space Agency (Deutsche Agentur für Raumfahrtangelegenheiten, DARA) the name was changed again to its current name of DLR, Deutsches Zentrum für Luft- und Raumfahrt, German Aerospace Centre.

Further research on the problem of direction finding, which had been a traditional research topic, was ceased in 1962. The last but, nevertheless, important construction of an electronically switched Doppler direction finder came to a successful conclusion as a very early circular phased array; it was developed further in industry in the following years and became a familiar sight on airports all over the world (see Figure 1-33). The other areas of research, however, continued over the next 15 years.

**The Implementation of Large Scale Research Activities**

Increasingly, the work in the Institute was reoriented towards space activities encompassing projects in communications, navigation and remote sensing. The first major activity was the development of the Central German Ground Station. The Institute was prime contractor for the major antenna systems and provided systems engineering. It also selected and procured the site in Lichtenau, Weilheim, approximately 40 km south of Oberpfaffenhofen. This was the beginning of space activities in both the Institute and DLR.

A first monopulse tracking antenna with a diameter of 11 m for the reception of satellite signals in the VHF band was constructed in cooperation with an industrial partner (Rohde & Schwarz) and set up some hundred meters behind the Institute for testing purposes (see Figure 1-34). An identical tracking antenna and a similar slaved telecommand antenna were set up in Lichtenau used for first communication links.

On November 20, 1967, at an inaugural ceremony Franz Josef Strauß (Bavaria's Prime Minister, 1978 – 1988) officially launched the development of the satellite ground station at Lichtenau (Figure 1-35).

**Figure 1-35: Franz Josef Strauß (Bavaria's Prime Minister, 1978 – 1988) laying the foundation stone for the German central ground station at Lichtenau, November 20th,**

One of the first two major ground station projects was the design and construction of a high-precision tracking interferometer. At that time all satellites emitted beacon signals in the 136-138 MHz band. Interferometers with fixed, wide beam antennas were used for tracking the satellites. Many such stations were needed to provide sufficient data to determine the orbit. The DLR VHF interferometer used three steerable, high-gain antennas spaced 57 wavelengths (126 m) apart in an L configuration. The system was able to track satellites from horizon to horizon and provide sufficient data for complete orbit determination. The antennas were steered in unison by slaving them to the monopulse tracking antenna. The system was completed in time to position the joint German/French communications satellite SYMPHONIE A, which was launched on the December 12, 1974. Figure 1-36 gives an impression of the size of the interferometer antenna with the dipole array monopulse tracking antenna in the background.

**Figure 1-36: One of the interferometer antennas at the DLR ground station in Lichtenau.**

**Figure 1-37: A 34-m Cassegrain dish antenna of DLR.**

The other major project was the construction of the 30-m-parabolic dish antenna for S-Band communication with the joint US/German solar probe Helios, supporting the Deep Space Network (Figure 1-37). This antenna is a shaped Cassegrain system with an elevation over azimuth mount. The antenna provided telecommand transmission in the 2110 – 2120 MHz band with a transmit power of 10 kW. It could also receive telemetry in the 2290 – 2300 MHz range with a hydrogen maser amplifier. The close proximity of the transmit and receive frequencies required a high-quality waveguide diplexer, which was


Figure 1-38: The experimental ship terminal (ringed) on its way to the Faroe islands. The antennas were mounted on a container housing the electronic equipment (hidden in the cargo bay).

Figure 1-39: The AMA antenna test range measuring a scaled down Space Shuttle.

built in the Institute. The antenna beam width was 0.2°, so calibration was a challenge. Fortunately, the ALSEP (Apollo Lunar Surface Experimental Package) transmitters were still working on the moon and could be used as measurement sources. The Helios A and B probes were launched in 1974 and 1976, respectively. Later the antenna was extended to cover C and X-band and used to support the scientific space missions Giotto, AMPTE and Equator-S.

Today, the satellite ground station has grown tremendously and hosts more than 10 large-diameter antennas. It is operating by the German Space Operations Centre (DLR-GSOC), which is responsible for the operations of numerous spaceflight missions, recent ones being TerraSAR-X, TanDEM-X, GRACE, Galileo and Columbus.

Figure 1-40: The AMA control room.

The development of the ground station at Lichtenau represented the beginning of a series of large-scale research activities, as well as the beginning of numerous national and international cooperations.

With the great interest in maritime communication satellites in the nineteen seventies, the Institute built an experimental L-Band ship terminal to investigate the influence of multipath effects at low elevation angles. The terminal had a high-gain dish antenna and an array antenna with switchable gain mounted on an elevation over azimuth pedestal. The station was commissioned to operate with the Marisat communication satellites. As the wider beam array antenna was more susceptible to multipath reflections from the sea's surface than the high-gain antenna, comparing the signals gave a measure of the influence. The ship terminal was mounted on two ships and went on journeys to the Faroe Islands and the Azores (see Figure 1-38). The latter campaign was in conjunction with the Italian Laboratorio per l'Automazione Navale in Genoa. Finally, it was shipped to the Antarctic to investigate the possibility of communications close to the horizon.

In the nineteen seventies, a new antenna measuring system (AMA) was constructed (see Figures 1-39 and 1-40). The facility was designed for radar cross section measurements of airborne and spaceborne vehicles as well as for the characterisation of antenna systems. For this purposes three different free field test ranges were established. Distances up to 220 meters were possible, measuring between the two towers where the device under test was

mounted on a heavy duty, two-axis positioner in a height of 15 meters over ground.

Several projects were performed in the past, like RCS measurements of fighter aircrafts (1:1 model), characterisation of conformal phased array antennas and measuring the radiation pattern of antennas mounted on airborne and spaceborne vehicles with the help of down-scaled models.

Standard measurements for internal and external customers were carried out over more than 30 years, up to 2008. With the construction of the new HF-TechLab building, the AMA will be replaced by a more suitable indoor Compact Test Range (CTR). Basic principle of the CTR is a two reflector system which gives a measurement area, called quiet zone, of 3.8 meters in diameter. Inside the quiet zone far field conditions are achieved. The new CTR facility will deliver high quality products for the tasks done by the AMA before as well as introducing new measurement tasks and methods under fully controlled environmental conditions.

Microwave radiometry became a research topic in the sixties. One of the world's first imaging linescanner systems using cooled receivers was developed in the late nineteen seventies (Figure 1-41), operating at Ka and W-band for many experiments in the nineteen eighties. Here, a highly oscillating parabolic mirror was used to scan the antenna beam rapidly across the flight direction. An upgrade for new non-cooled receiver technology and more efficient PC based data acquisition was implemented in the late nineties. A similar multi-frequency system MERES (W, Ka and Ku-band) was developed in the late eighties and put into and kept in service during the nineties. In parallel, the imaging principle of aperture synthesis was investigated since 1990. This method coming from radio astronomy uses highly thinned arrays in order to synthesise large antennas for very high spatial resolution. A two-element interferometer (Figure 1-42) as the key unit of an aperture synthesis radiometer was developed and built in Ka-band, and some of the world's first two-dimensional millimetre-wave high-resolution images were recorded. These results demonstrated basically the applicability of the imaging principle for Earth observation, demanding much larger and more complex scenes than in radio astronomy, even for high frequencies and resolution. Since the mid nineties up to now, security applications of microwave radiometry have attracted notice. Consequently many quite different imaging principles, and the whole range of microwaves from 1 to 300 GHz and beyond are investigated in order to satisfy challenging requirements concerning penetration depth, resolution, sensitivity, image size, and image acquisition time. These newer fields of interest are outlined in more detail in section

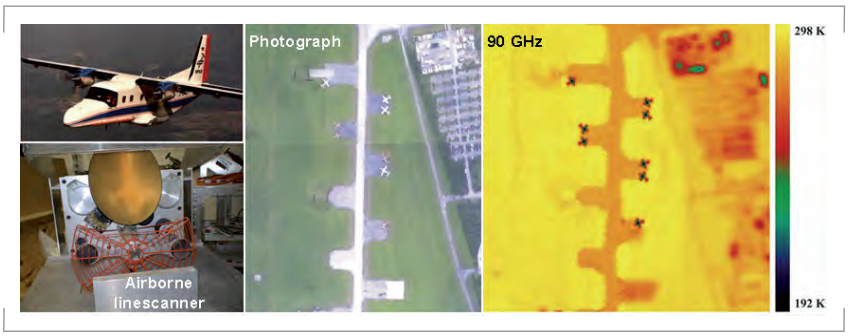


**Figure 1-41: Photographs of the airborne linescanner, an imaged airport area and the corresponding 90 GHz imaging example of the airport area.**

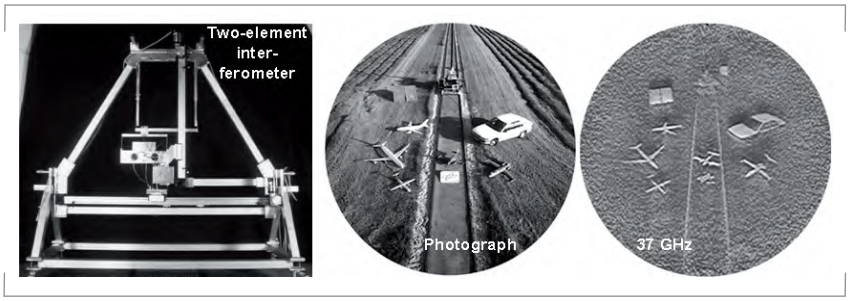


**Figure 1-42: Photograph of the aperture synthesis two-element interferometer and corresponding 37 GHz imaging example of a test scene.**

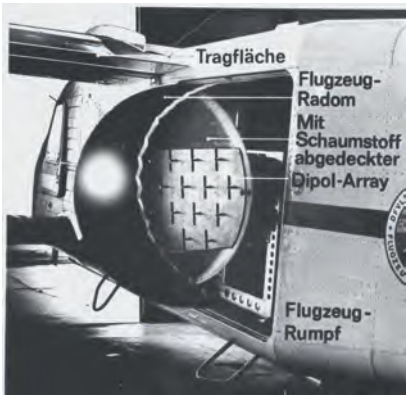


**Figure 1-43: Two-frequency scatterometer (SARSCAT), L-band.**

**Figure 1-44: The E-SAR of DLR, operated by the Institute, P-band antenna underneath the cockpit.**

**Figure 1-45: View inside the cabin of the DO228 aircraft. The racks are approximately 1.2 m high.**

*Microwave Systems: Research and Technology*.

A coherent two-frequency scatterometer was developed and flown by the Institute on a Dornier Do28 aircraft. This scatterometer, denoted as SARSCAT (see Figure 1-43), was a predecessor to the experimental SAR, E-SAR (Figures 1-44 and 1-45). First successful flight experiments with the two-frequency scatterometer in a SAR mode were carried out in the early eighties by the Institute.

Airborne SAR technology and its operation has been a major subject at the Institute for nearly three decades. It began with the development of E-SAR in 1983, which was intended as a technology test-bed to establish expertise in SAR system design, signal processing and image analysis. In April 1988, after five years in development, E-SAR, having been installed on board a Dornier Do28 Skyservant, generated the first imagery in L-band during an experiment on oil slick detection in the North Sea. Only a year later, the instrument had been installed in a new Dornier Do228 aircraft and the first C-band imagery was obtained.

In the 12 years that followed, the E-SAR instrument was continuously upgraded, with RF segments in X-band and later in P-band. The system's performance was gradually improved by integrating a more modern data recording system by replacing the old 6-bit A/D-converters, implementing a new high power TWT and the introduction of solid-state transmitter amplifiers. The integration of a DGPS/IMU-based precision navigation and positioning system in 1998, an IGI CCNS4/Aerocontrol system, resulted in a quantum leap in system performance and data quality.

In the final configuration, E-SAR operated in four frequency bands (X, C, L and P-band) covering a range of wavelengths from 3 to 85 cm and was fully calibrated. An arbitrary waveform generator provided radar chirps with a programmable bandwidth between 1 MHz and 100 MHz. The polarisation of the radar signal was selectable between horizontal or vertical. Data rate restrictions limited system operation in X-band to single polarisation (either HH or VV) per pass. C-band offered a dual polarisation mode (either HH-HV or VV-VH). In polarimetric mode (L and P-band only), the polarisation was switched from pulse to pulse in a HH-HV-VV-VH sequence.

The Do228, which by the end of the 1980s had replaced the Do28, is a twin-engined short take-off and landing turbo-prop aircraft: a 900 m long landing strip is sufficient and the type of runway may be concrete, gravel or even grass. The cabin is not pressurised and the aircraft can carry a payload of up to 1000 kg. Special modifications (28 VDC and 220 VAC instrumentation power supply, hardpoints, bubble windows, circular mounts in the roof, and a hatch with a roller door) make it ideal for scientific payloads. With E-SAR installed on board, the maximum operating altitude was about 6000 m above sea level. For SAR operation, the average ground speed was 175 kt. Depending on E-SAR's configuration, the endurance varied between 2.5 and 4 hours.

The demand for high quality SAR data products by external partners and customers in research and industry, such as CNES, ESA and Infoterra, stimulated the progress of both the E-SAR instrument and processor. For many years, E-SAR was heavily used in SAR experiments and measurement campaigns. It evolved to be an important tool for SAR research and applications in Europe: more than 30 important scientifical and technical SAR missions and projects were carried to completion with great success. However, there is an end to every success story. The aging of key components in the instrument, the maintenance and repair of up to 25-year

old sub-systems and components were no longer feasible or economical. The future belongs to F-SAR, the new advanced DLR airborne SAR system (see Section *Airborne SAR*).

Antenna research and development as well as research on both microwave propagation and sounding of the atmosphere are classical tasks in Oberpfaffenhofen since the early beginnings in the DVG. Beside others, the modelling of the atmosphere based on measurements from the ground is an essential feature for microwave propagation research. In the eighties, the Institute designed and developed one of the most advanced polarimetric cloud radars with full polarimetric operation in C-band. Only very few weather radars provide the capability of polarisation diversity. POLDIRAD is located on the roof of the DLR's Institute for Atmospheric Physics and operated since 1986 (see Figure 1-46). By using different polarisations it is possible to identify and quantify the different types of precipitation particles (rain, snow, graupel, hail) as well as to observe differential propagation effects of electromagnetic signals in the atmosphere under varying weather conditions. Polarimetric weather radar data particularly help to measure, understand and predict the influence of multi-path propagation effects on both SAR systems and navigation systems.

Radar cross section measurements started in both the DVG and the FFO in the middle nineteen thirties. Until today, this activity represents an indispensable research task for understanding the scattering mechanisms, the development of scattering models, and deriving inversion algorithms for feature extraction. Such investigations are not only prerequisites for reliable data utilisation but also necessary steps to optimise the sensor. Several groups have worked from the beginning until today on scattering measurements, simulation and modelling as well as image data interpretation (see Figure 1-47). The Institute's expertise in man-made target radar signatures has been used to solve stealth problems for airborne, spaceborne and ground-based equipment. Additionally, an intensive research on the polarimetric behaviour of electromagnetic waves, including propagation and scattering phenomena has been performed.

Within the time frame from 1980 up to now the Institute conducted five Space Shuttle missions in cooperation with the German Industry and with international and national research organisations and universities.


**Figure 1-46: The full polarimetric weather radar, POLDIRAD.**

**Figure 1-47: Radar signatures of an Airbus A340 measured on a turntable using a 1:20 scale model with inverse SAR, X-band. White arrows indicate the illumination direction, for easier interpretation the aircraft contours have been overlaid in green. Spatial resolution is 24 cm.**

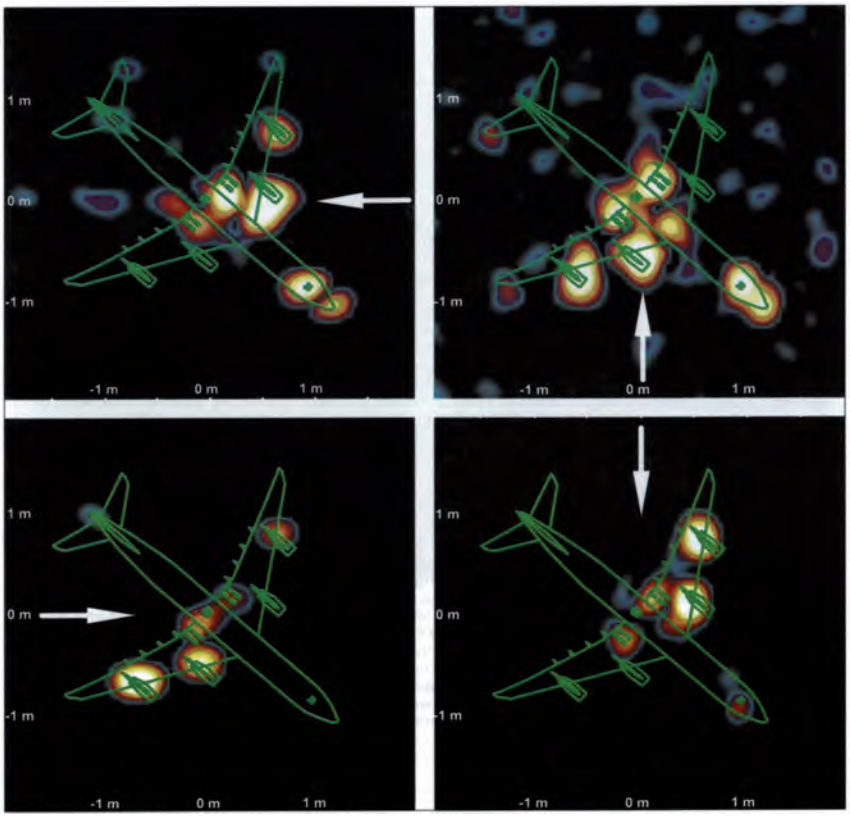

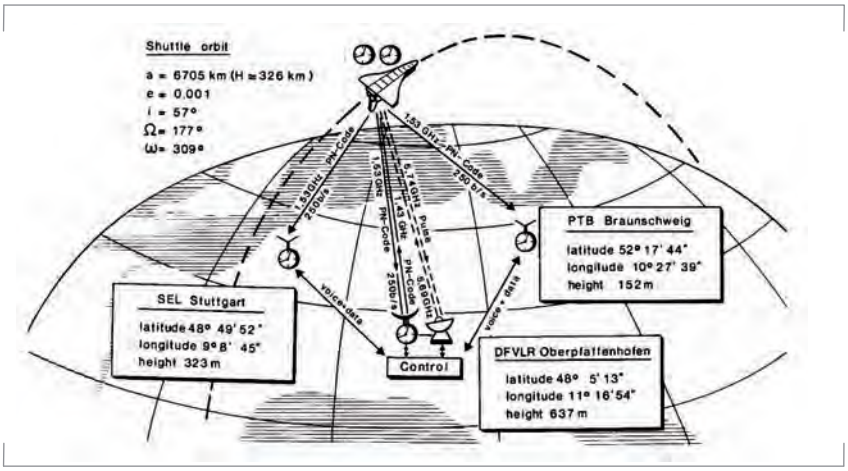


**Figure 1-48: Sketch of the NAVEX experiment configuration.**

NAVEX was an experimental system successfully flown 1985 on the first German Spacelab Mission D1 to investigate basic technical problems significant for operation and control of a future generation of navigation satellites. A sketch of the NAVEX experiment configuration is depicted in Figure 1-48. A remarkable result amongst others was the accuracy with which the relativistic effect could be measured. During the whole measurement period the relativistic frequency shifts could be measured with an accuracy of 0.1%.

**Figure 1-49: MRSE result brightness temperature/Kelvin at 9.6 GHz along a swath over the north west coast of France (Penmarch), and Belgium (Brussels).**

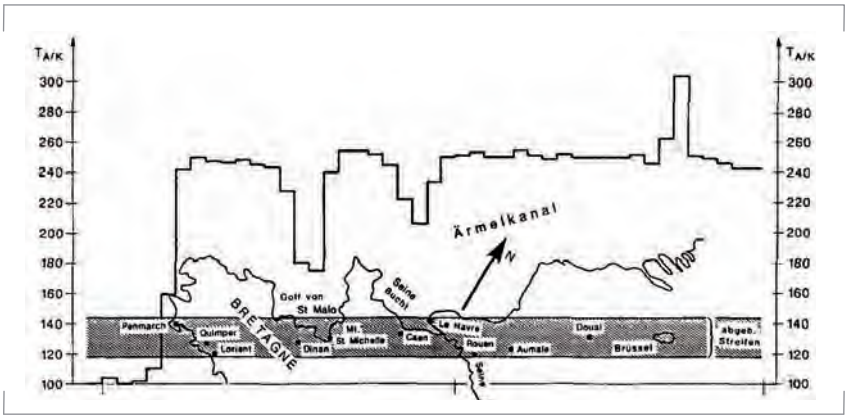


With MRSE, the Microwave Remote Sensing Experiment, an X-band SAR, a two frequency scatterometer and a microwave radiometer all at 9.6 GHz, were flown on the Space Shuttle in 1983 (Figure 1-49). The microwave radiometry mission was successful. The SAR and scatterometer mission failed due to a manufacturing problem that caused a high voltage brake down of the TWT under the Shuttle pressure conditions. This mission, our first space instrument, was however a most important experience that enabled our participation in the follow-on Shuttle missions.

X-SAR was an X-band radar developed as a joint German/Italian project to supply the X-band system of the Shuttle Imaging Radar (SIR) mission. Together with NASA's SIR-C operating in L-band and C-band, this mission provided multi-spectral polarimetric images from space for the very first time during its two flights over hundreds of test areas around the world in April and October 1994.

SRTM, the Shuttle Radar Topography Mission (Figure 1-50), was the third mission from February 12-21, 2000. The goal was to generate a digital elevation model of the Earth's landmass between ± 60 degrees latitude by means of measurements with SAR interferometry in both C-band (NASA) and X-band (DLR) with height accuracy down to 6 m. For that purpose the X-SAR sensor was extended by adding a complete second RF receiver with an additional antenna in order to construct an X-band interferometer with a 60-m baseline.

Preparation, realisation, mission operation and evaluation of all three X-SAR Shuttle missions influenced the goals of the research, development and operational radar activities in Oberpfaffenhofen tremendously with respect to ground based, airborne, and space activities. Research in the field of interferometry and polarimetry, for

example, got a new push as well as all the processing and data evaluation activities, and the development of operational systems. The Institute gave both functional and scientific support to all the European SAR satellites.

Radar calibration is an important and central task of the Institute. Calibration activities for SAR started with an airborne German/Canadian measurement campaign with the Canadian CV-580 SAR which was organised by the Institute in 1979. The consequence was that the Institute developed special experience in the field of SAR calibration. The determination of an antenna diagram of SIR-B in 1985 using ground receivers represented the first time that the antenna diagram of a spaceborne SAR has been measured during flight for calibration purposes (Figure 1-51). For different SAR missions the Institute meanwhile has established calibration fields in Bavaria with an extension of several hundred kilometres in both north/south and east/west directions.

Mainly for logistic reasons these calibration fields are selected in South Germany which can be operated and maintained from Oberpfaffenhofen, the location of the Institute. The existing infra-structure of the Institute is well prepared for executing calibration campaigns over large test sites. One example is shown in Figure 1-52, bottom. This calibration field has been deployed and maintained for both the TerraSAR-X and the TanDEM-X mission. Enclosing an area of 120 km x 40 km and consisting of 30 target positions this field enables a high number of passes across deployed reference targets and consequently a large number of measurements in-flight can be performed. Only then, an accurate calibration of a SAR system can be ensured within a time restricted by the commissioning phase.

More details on the different calibration procedures and activities performed by

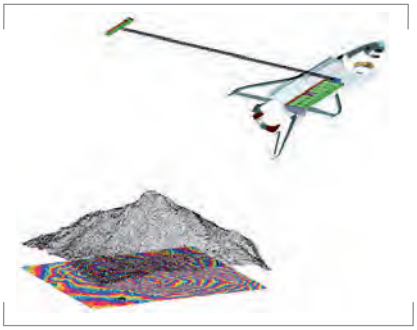

Figure 1-50: Sketch of the SRTM configuration with its 60 m long boom over the digital elevation model together with the respective interferometry fringes.

Figure 1-51: Ground measurement of the SIR-B antenna diagram, during flight October 9, 1984.

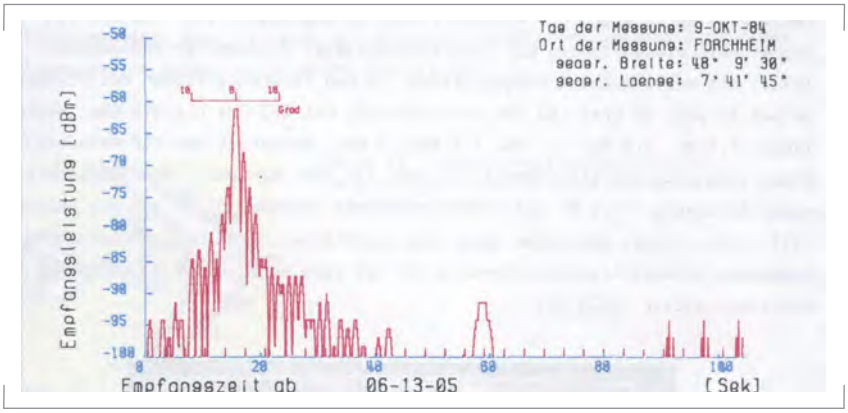


Figure 1-52: Example of a DLR calibration field in South Germany consisting of 30 target positions and enclosing an area of 120 km x 40 km.

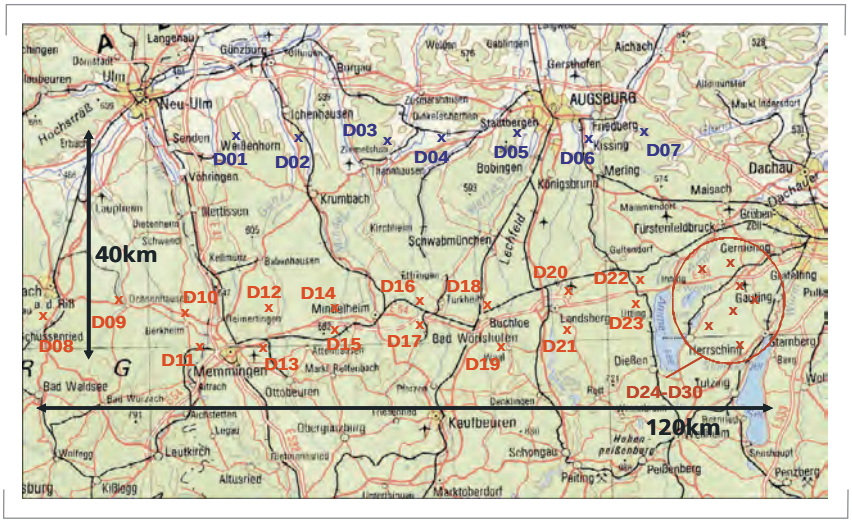

the Institute can be found in section *Spaceborne SAR*.

The cooperation with NASA on SIR-C/X-SAR and SRTM accounts for the first successful milestones in the German Radar Remote Sensing Program. It prepared both DLR and industry for the first national SAR mission TerraSAR-X, which was implemented in public private partnership between DLR and EADS Astrium GmbH. After the launch in June 2007 the TerraSAR-X system became operational in January 2008 and is since then providing high-quality X-Band radar images to a growing commercial market and scientific user community.

TerraSAR-X opened a new era in our SAR program and initiated widespread R&D activities on future concepts, which resulted in the Institute's proposal for TanDEM-X (Figure 1-53) in collaboration with EADS Astrium GmbH. This bi-static SAR mission is formed by adding a second, almost identical spacecraft, to TerraSAR-X and flying the two satellites in a closely controlled formation with typical distances between 250 and 500 m. The primary mission objective is the generation of a consistent global digital elevation model with an unprecedented accuracy according to the HRTI-3 specifications. Beyond that, TanDEM-X provides a highly reconfigurable platform

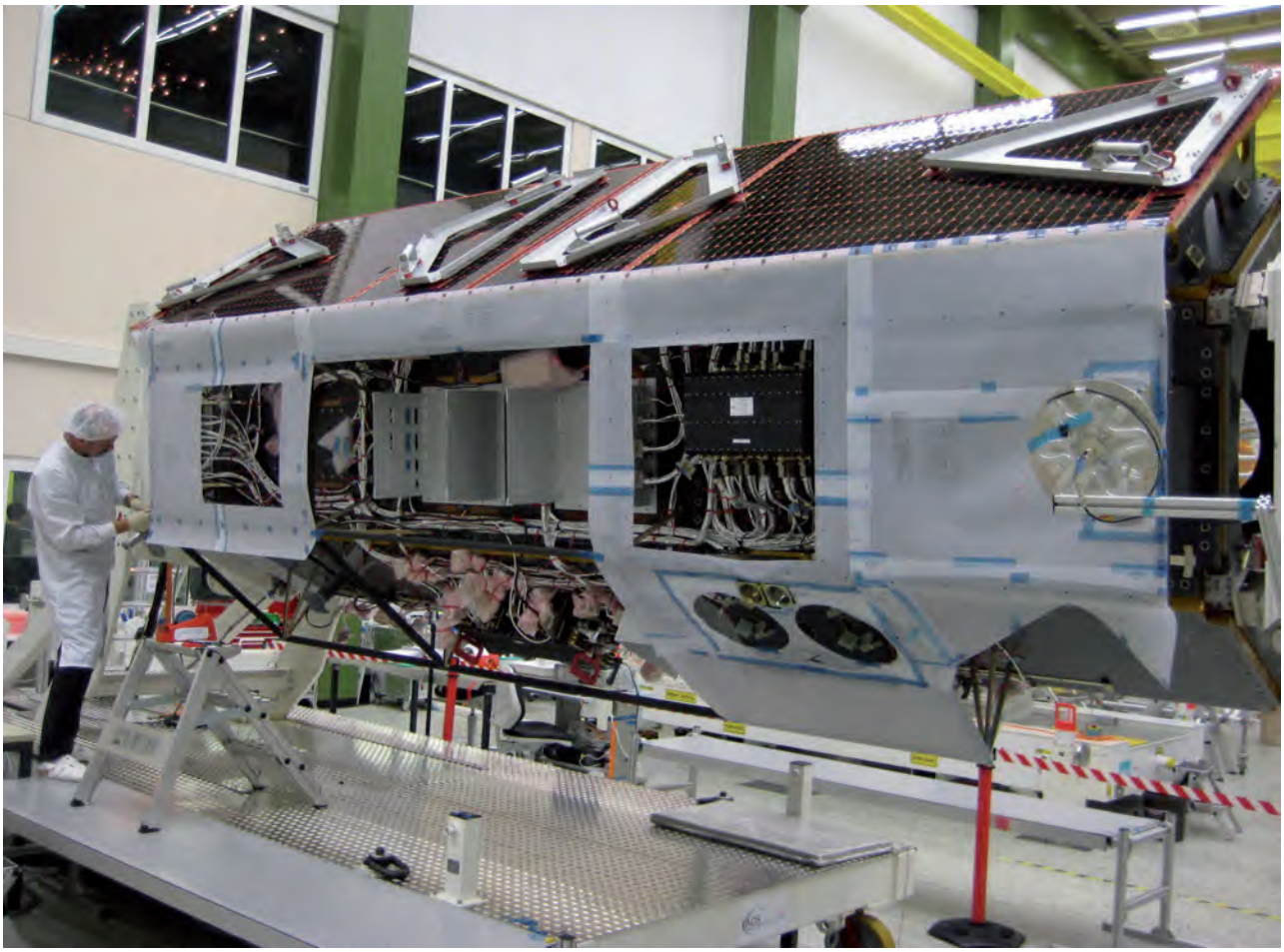

**Figure 1-53: Integration of the TanDEM-X satellite (courtesy of EADS Astrium GmbH).**

for the demonstration of new SAR techniques and applications. For detailed descriptions on TerraSAR-X and TanDEM-X, see section *Spaceborne SAR*.

**Outlook**

Looking ahead to the next 5 years, the Institute will continue to initiate and contribute to several projects that will be decisive for its long-term strategy. By means of the Institute's contributions to the TerraSAR-X, TanDEM-X and SAR-Lupe projects, a highly qualified project team has been established. Due to the high degree of innovation in science and technology, the mission proposal Tandem-L represents the most important project for the Institute in the years to come and can be seen as a next milestone in the national radar roadmap after TanDEM-X.

In a changing and dynamic world, high-resolution and timely geospatial information with global access and coverage becomes increasingly important. Constellations of SAR satellites will play a major role in this task, since SAR is the only spaceborne sensor that has all-weather, day-and-night, high-resolution imaging capability. Examples of applications for such a constellation are environmental remote sensing, road traffic, hazard and disaster monitoring, as well as reconnaissance and security related applications.

In some respect, the vision of a SAR sensor network for an Earth observation system with a global and quasi-continuous coverage is not too far away. The Institute is committed to increase its role in the development of future microwave satellites for remote sensing, reconnaissance and traffic monitoring. It aims to expand its expertise and leadership in strategically important projects and research areas. Together with its cooperation partners in DLR, industry and science, the Institute will play a key role in the realisation of this vision.

# Summary of the Institute's History (1908 – 2000)

**1908** On October 14, Dr. Max Dieckmann founded the private "Drahtlostelegraphische und luftelektrische Versuchsanstalt Gräfelfing" (DVG -Research Laboratory for Wireless Telegraphy and Air Electricity). Goals were application of electromagnetic waves for communication, navigation, radiolocation, and research of electric processes in the atmosphere.

Research laboratory and DVG staff in Gräfelfing, 1908.

**1910** Radio telegraphic exchange of messages between air ships.

**1912** Birth of airborne radio communication. Use of a "safe" spark gap transmitter for operation on board of Zeppelin airships which were filled with hydrogen gas. That made the use of spark gap transmitters onboard very hazardous particularly when the ventilation of the airship gondola was not effective enough in evacuating residual hydrogen gas.

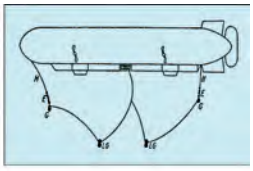

Zeppelin airship with an early wire antenna.

Dr. Max Dieckmann beside the wireless station onboard the airship "Victoria Luise".

**1914** First frame direction finder for ship navigation.

**1917/18** Radio image transmission of annotated map sections by the aircraft crew for airborne reconnaissance.

**1925** Colour image transmission.

**1925** Frame direction finder for aircraft navigation.

First Oberpfaffenhofen building and hangar, 1937.

**1935** First airborne radar altimeter (echo sounder).

**1937** Dr. Dieckmann founded the "Flugfunkforschungsinstitut Oberpfaffenhofen" (FFO) (Airborne Radio Research Institute) with a staff of 115 coming from the DVG. It was located besides the former Dornier airfield near the village Oberpfaffenhofen. The laboratory building and the hangar were the first buildings of the present campus and they exist till today.

Focal points of research were investigation of techniques and technology for radio location, navigation and communication with electromagnetic waves. Radar experiments were already performed with respect to moving target indication long before the word "radar" had been coined.

Detection and velocity estimation of a damper on Lake Ammersee at 1 km distance, 1937.

**1938** Experiments with waveguide and Fresnel lens antennas.

**1939** Tube developments for cm wavelengths (Triodes, Magnetrons etc.).

Communication experiments at cm wavelengths.

**Communication experiment: 5 cm transmitter on the Zugspitze (left photo), receiver on the 250 km distant Mount Arber, 1939.**

**1940/41** The research on backscatter phenomena was intensified. Measurement of backscattering cross section of a model aircraft at a scale of 1:10. The aim was to determine the frequency dependence of the cross section.

**Backscatter diagram of a 1:10 down-scaled Ju52 aircraft model, wavelength 6 cm, 1940.**

**1944/45** Invention of the field effect transistor (Patent 1945).

**1945** American troops occupied on May 8 the still intact Institute which was spared from bomb attacks. After evaluation of FFO developments, almost all machines and instrumentation were destroyed. The valuable library was moved to the Wright-Patterson-Laboratories near Dayton/Ohio.

**1954** Reactivation of an interim establishment of the "Flugfunk-Forschungsinstitut in Riem nearby Munich" using rooms and laboratories in the old main building of the Munich airport. First tasks were research and development of three dimensional air traffic control system, instrument landing systems and millimetre wave measurement techniques and respective devices.

**Institute campus at the beginning after the war, 1956.**

**1955** Integration into the „Deutsche Versuchsanstalt für Luftfahrt" (DVL-German Laboratory for Aviation).

**1956** November 1956 - The Institute moved back to Oberpfaffenhofen under the name "DVL-Institute für Flugfunk" (Institute for Aircraft Radio and Microwaves).

**1960** In 1960 the two other DVL Institutes in Mühlheim/Ruhr, the Institute for Microwaves and the Institute for Radio Frequency Technology have been transferred to Oberpfaffenhofen and became unified with the Institute für Flugfunk under the name "Institut für Flugfunk und Mikrowellen" (Institute for Aircraft Radio and Microwaves).

Goals of the Institute were application of radio frequency technique and technology in the field of aviation for communication, navigation and position finding with the research areas antennas and wave propagation, radar, direction finding, landing support and altimetry.

Research on the problem of direction finding was one of the important research topics. An important construction of an electronically switched Doppler direction finder came to a successful conclusion. This system was further developed from industry in the following years.

**Experimental set-up of an electronic switched direction finder (left), VHF monopulse tracking antenna for satellite signal reception, diameter 11 m (right).**

**1967** Laying of the foundation stone for the satellite control station in Lichtenau.

At this outer location (RF distortion free) near Weilheim/Oberbayern, the Institute developed the central scientific satellite control station in Germany and later in 1972 an interferometer system for precise satellite position finding.

**1969** The Institute became a member of the newly founded "German Aerospace Research Establishment" (DFVLR, today DLR).

**1978** The Institute's name changed to "Institut für Hochfrequenztechnik" (Institute for Radio Frequency Technology). Focus of research activities: remote sensing of the Earth and its atmosphere for environment, reconnaissance and security.

**1978/79** Development of a 90 GHz radiometer.

Development of a far field antenna measurement facility (AMA).

**1980** First extended SAR calibration activities for the German/Canadian CV 580 SAR campaign.

Development of possibly Europe's first GPS Receiver for measuring GPS time.

**1981** Radar cross section and microwave radiometry measurement and analysis.

**1982** Experiments with the German experimental ship station. Joint Italian-German measurement campaign with respect to maritime radio communication.

Experiments with 140 GHz radiometry.

Research for the application of polarimetric radiometry. Detection of oil pollution becomes central application for microwave radiometry.

**1983** Development of airborne SAR (Synthetic Aperture Radar), E-SAR. E-SAR was operated in 4 frequency bands (X, C, L and P-band), hence it covered a range of wavelengths from 3 to 85 cm. The polarisation of the radar signal was selectable, horizontal as well as vertical.

34 m Cassegrain antenna.

Space interferometer antenna, 1972.

AMA – antenna measurement facility.

POLIRAD – weather radar, 1986.

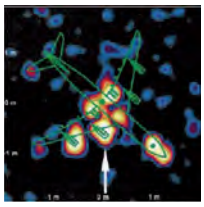

ISAR image of an A340 1:20 model.

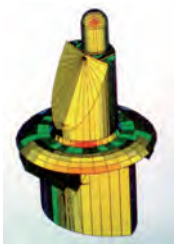

Periscope model for backscatter analysis.

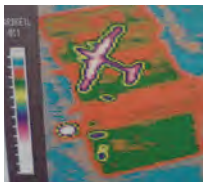

Radiometric image of an aircraft and vehicles at 140 GHz.

E-SAR on a Do228 and a fully polarimetric C-band image of Oberpfaffenhofen acquired with E-SAR.

**1983** MRSE (Microwave Remote Sensing Experiment) on SPACELAB-1 with an X-band SAR instrument.

L-Band satellite communication and wave propagation experiment in the Arctic from the Argentinean Arctic Research Station "General Belgrano II".

Crew of Spacelab-1 and the MRSE instrument in the Shuttle cargo bay (red circle).

**1984** First field strength measurements on the ground for the determination of the SIR-B antenna diagram during flight.

**1985** Navigation experiment NAVEX on the first German Spacelab mission D1 (clock-synchronization experiments and one-way ranging measurements).

NAVEX on Spacelab, D1 mission: Antennas T/R (left) and receiver, atomic clocks (Cs/Rb) and receiver (right).

**1986** Participation in the ESA/ERS-1 radar system development with a scientific and technical support. Development of the polarimetric weather radar (POLIRAD).

**1992** Proposal for a geostationary satellite overlay to GPS, key patent for EGNOS.

**1992** Real-time SAR processing on-board E-SAR. At this time, E-SAR was a four-frequency radar acquiring data in several European campaigns.

Development of a three-dimensional SAR simulator.

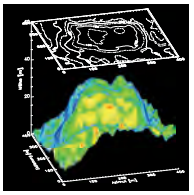

DEM using E-SAR single-pass interferometry in X-band.

**1993** Demonstration of airborne SAR interferometry with E-SAR.

**1990ies** MERES (MEhrfrequenz Radiometer zur Erkundung der Seeoberfläche, Multi Frequency Radiometer for Remote Sensing of the Sea Surface) becomes operational. It has been used since then for operational monitoring of oil spills in the North Sea.

Multi-frequency radiometer MERES, oil spill imaged in 89, 36 and 18 GHz (right, top down).

**1994** SIR-C/X-SAR – The Shuttle Imaging Radar Missions consisted of two flights in April and September 1994 aiming to demonstrate the potential of fully polarimetric radar systems in three different carrier frequencies for a variety of applications. Germany developed the X-SAR radar system in cooperation with Italy, the United States developed the radar systems in C and L-band. Both SIR-C/X-SAR missions opened a new era in scientific remote sensing with multi-frequency, multi-polarimetric SAR systems. The combination of L, C and X-band, as well as the different polarisations of the acquired data takes are unique – until today.

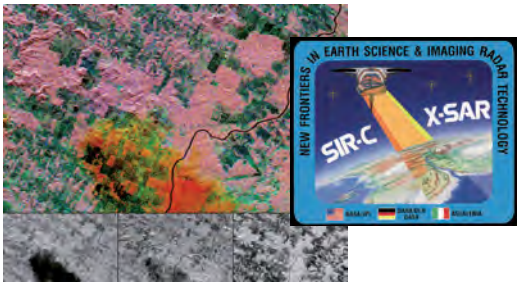


Multi-frequency image of the X-SAR/SIR-C mission.

**1997** First demonstration of Polarimetric SAR Interferometry (Pol-InSAR).

**1999** First demonstration of SAR Tomography with airborne data.

**2000** SRTM, the Shuttle Radar Topography Mission, was a highlight in Germany's radar activities in cooperation with NASA/JPL. Space Shuttle Endeavour started on February 11, 2000 with the goal to map the topography of the Earth surface using two radar systems. In total 3600 gigabyte have been recorded in the course of only eleven days. Secondary antennas mounted at the end of a 60 m long boom allowed a topographic mapping of 80 percent of the Earth's land surface with a height accuracy of approximately 10 metres. Germany participated in the mission with an interferometric X-band radar system (X-SAR) that acquired approximately 40 percent of land surface with the increased accuracy of approximately 6 metres.

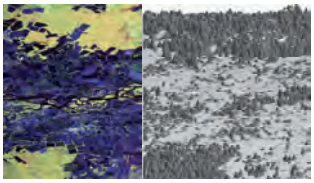

**First forest height estimation with Pol-InSAR (SIR-C acquisition, Kudara, Russia).**


**Shuttle Radar Topography Mission (SRTM) and the first DEM obtained with X-SAR (White Sands, USA).**

The next sections of this report describe the research activities and project highlights of the Institute in the timeframe from 2000 to 2008.

# The Institute Today

## Spaceborne SAR

- Shuttle Radar Topography Mission – SRTM
- TerraSAR-X
- TanDEM-X
- Sentinel-1
- TanDEM-L
- Advanced Land Observing Satellite – ALOS
- Multi-Application Purpose SAR – MAPSAR
- BIOMASS
- Reconnaissance Systems

## Airborne SAR

## Microwave Systems: Research and Technology

## Institute's Personnel

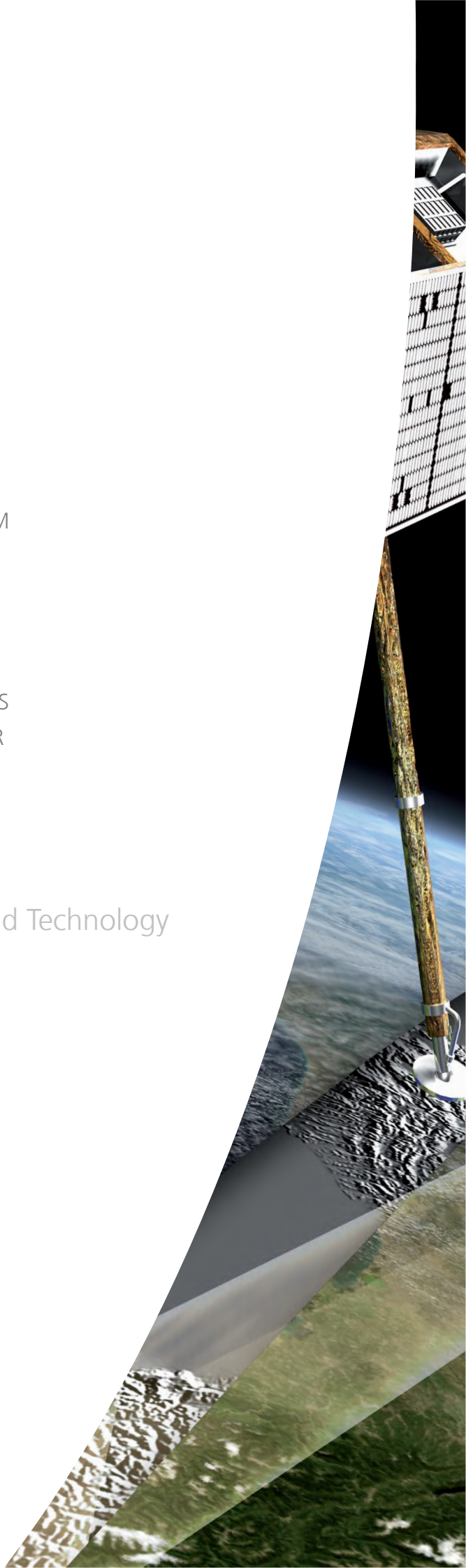

# Spaceborne SAR


## Shuttle Radar Topography Mission – SRTM

On February 22, 2000 one of the most complex space shuttle missions was successfully completed, the Shuttle Radar Topography Mission (SRTM). The main objective of this mission was to collect interferometric radar data for the generation of a near global Digital Elevation Model (DEM), covering the Earth's surface between -56° and +60° latitude.

The SRTM mission was a follow-on to the Shuttle Imaging Radar-C/X-band Synthetic Aperture Radar (SIR-C/X-SAR) missions that were successfully conducted twice in April and October 1994. For SRTM, the SIR-C (5.6 cm wavelength) and X-SAR (3 cm wavelength) radar instruments had each to be supplemented by a second receive channel, as well as a second receive only antenna at the end of a 60 m long deployable mast forming the first spaceborne single-pass interferometer.

SRTM was a cooperative project between NASA, NGA (National Geospacial-Intelligence Agency) and DLR. NASA's Jet Propulsion Laboratory (JPL) was responsible for the C-band radar system, the mast and the Attitude and Orbit Determination Avionics (AODA). DLR was responsible for the X-band radar system (X-SAR). The Institute had the project lead and was responsible for the specification, system engineering, mission operations (with support from DLR-GSOC), calibration and the scientific exploitation. Data processing, archiving and data distribution was the task of DLR-CAF. EADS Astrium GmbH was the main contractor for the X-SAR flight hardware development, integration and test.

**Figure 2-1: View into Endeavours cargo bay with the deployed 60 m SRTM mast (By courtesy of NASA).**

**Single-Pass SAR Interferometry**

Building a single-pass SAR interferometer requires at least one transmitter and two receivers with antennas separated by a so-called interferometric baseline. For SRTM, the baseline was formed by the 60 m long deployable mast structure reaching out of the orbiter cargo bay and carrying the secondary antennas at its end. The same reflected radar signal from points on the ground is received by both antennas, inboard and outboard, but at slightly different times, or as we call it with a phase difference, due to the tiny difference in distance. This phase difference can be accurately estimated, because single-pass interferometers do not suffer from problems with atmospheric disturbance and temporal decorrelation of the target backscatter encountered with repeat-pass interferometry.

With the precise knowledge of the shuttle's position and the baseline vector in space relative to the spot on the ground at any time, the height of the

target can be processed. Orbit and baseline were measured with the AODA system: a set of GPS receivers, gyros, electronic distance meters, and star trackers. The position of the interferometer was measured by GPS with an accuracy of 1 m. The baseline angle was measured with an accuracy of about 2 arcseconds (short-time) and 7 arcseconds (mission). The baseline length was determined to millimetre accuracy.

**The Mission**

Seven hours after launch the mast had been successfully extracted and soon the first test data take was acquired over New Mexico / USA and processed by DLR. Figure 2-3 shows the first interferogram with the oscillations of the mast still uncompensated and without calibration.

The mapping of the continents was performed by operating the radar only over land with 5 to 15 seconds coverage over the ocean before and after the land. These acquisitions served as an absolute height reference using the well known ocean heights. More than 700 data takes were performed to map the earth in 11 days. Additionally, several long data takes only over ocean have been acquired to support the calibration and verification of the system.

The only problem during the mission was the malfunctioning of a cold gas valve. In consequence, the baseline orientation had to be maintained by corrective firings of the attitude control thrusters about every 90 seconds. These firings lead to increased oscillations of the mast and in consequence, to increased processing complexity and DEM errors. Nevertheless, after 159 orbital revolutions the C-band system with its 225 km wide swath had managed to cover the required surface. The X-band coverage, limited due to a swath width of 50 km, still comprises more than 60 million square kilometres.

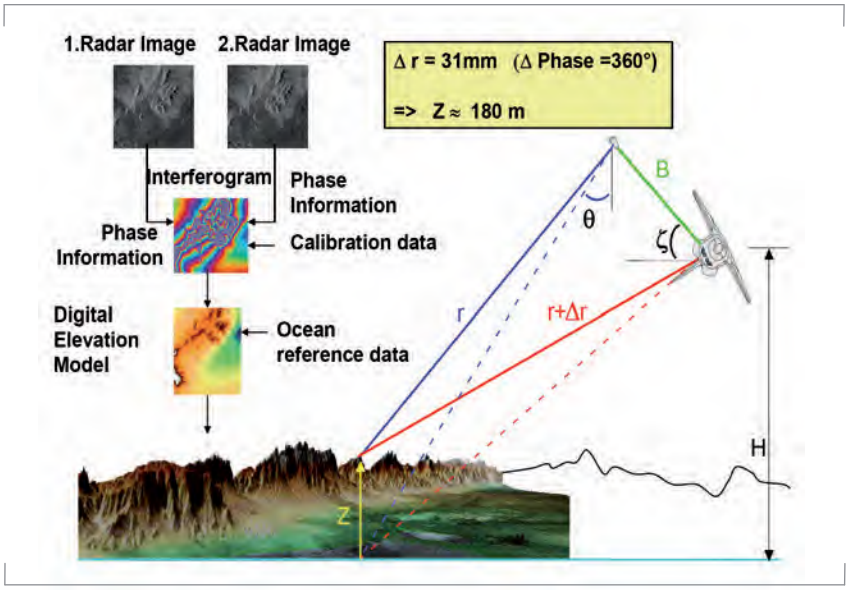


Figure 2-2: Single-pass SAR interferometry principle and baseline definition.

**Data Analysis and Results**

The mission analysis revealed an excellent stability of the radar systems and a homogenous data quality with respect to the basic radar parameters, like received echo level, antenna azimuth beam alignment, interferometric coherence and Doppler centroid frequency. During

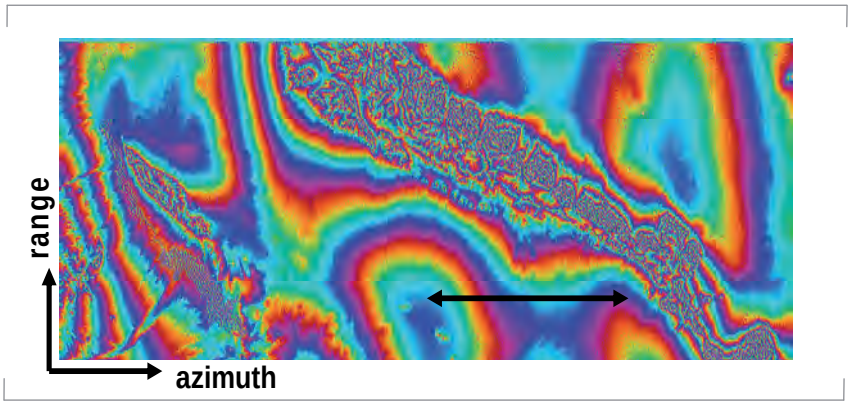


Figure 2-3: First X-SAR interferogram of the Shuttle Radar Topography Mission. The arrow shows the effects of uncompensated mast oscillations.

| Flat terrain | | | |
|---|---|---|---|
| | number | μ [m] | σ [m] |
| Forested areas | 2329 | -6.20 | 6.74 |
| Urban areas | 1683 | -2.63 | 4.10 |
| Open landscape | 20786 | -0.94 | 4.31 |
| Σ | 24798 | -1.55 | 4.84 |

| Moderate relief | | | |
|---|---|---|---|
| | number | μ [m] | σ [m] |
| Forested areas | 1970 | -1.98 | 7.60 |
| Urban areas | 725 | -1.14 | 4.86 |
| Open landscape | 8000 | +0.15 | 4.54 |
| Σ | 10695 | -0.33 | 5.33 |

| Highlands | | | |
|---|---|---|---|
| | number | μ [m] | σ [m] |
| Forested areas | 2272 | -4.43 | 8.62 |
| Urban areas | 766 | -1.04 | 5.29 |
| Open landscape | 7693 | -0.74 | 5.36 |
| Σ | 10731 | -1.54 | 6.37 |

**Table 2-1: SRTM DEM validation with navigation points in the western part of Germany.**

**Figure 2-4: SRTM X-band digital elevation model shows topography plus vegetation heights, rivers and clear cuts in the Kongo rain forest.**

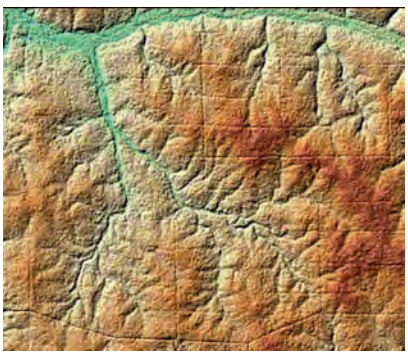

a collaborative calibration phase after the mission that lasted more than one year, the processing teams calibrated all the timings, offsets and dynamic behaviour of the instruments.

The relative height error was specified to be 6 meters (90 %). This accuracy was generally confirmed by DLR investigations, e.g. by comparison with navigation points as shown in Table 2-1. Several other investigators confirmed this accuracy, e.g. an independent quality assessment at a 70 km by 70 km test site south of Hanover, Germany, using trigonometric points and the Digital Terrain Model ATKIS DGM5 concludes with a mean value of the height differences μ of 2.6 m and a standard deviation σ of 3.4 m.

The small height errors of ±2.5 m correspond to a line-of-sight mast motion compensation accuracy of 0.44 mm, which was an incredible achievement. Nevertheless, residual, uncompensated first order oscillations of the mast translate to this measurable error on an 8 km scale in flight direction.

The long term variations in the 10 to 20 minute scale are of little relevance for the user, as they represent only a small height offset within a DEM product. These slow drift errors are within specification and entirely handled by the ocean calibration and bundle adjustment approach.

With SAR interferometry, the location or height of a representative phase centre of the backscattering resolution cell is measured. In principle C-band radar waves should have a higher penetration into the vegetation than X-band waves leading to differences in the interferometric height measured in the two systems over forested areas. In order to compare the penetration between C- and X-band, for instance in rain forest, several areas in Brazil and Kongo (see Figure 2-4) have been investigated. A relatively flat terrain and visible clear-cuts along roads have been selected to remove any offset between C- and X-band not due to penetration effects.

The resulting height differences of about 1 m are not very significant and well within the height error boundaries of both systems.

In response to the announcement of opportunity (AO) 102 proposals have been accepted and more than 1200 DEM and radar products for scientific evaluation with regard to validation, calibration and geoscience applications have been ordered. Hundreds of papers have been written using SRTM data for their investigations.

Though the X-band data from SRTM have a better performance than the C-band data, the gaps in the coverage and the cost for the data access have reduced the worldwide use considerably.

For many applications, the 1 arcsec posting and the accuracy of the SRTM dataset is still not sufficient and the area north and south of 60 degrees latitude is still only available with 30 arcsec resolution. A satellite mission like TanDEM-X will provide DEM performance of the next higher quality level and fill the gaps.

# TerraSAR-X

TerraSAR-X is Germany's first national remote sensing mission being implemented in a public-private partnership between the German Aerospace Centre (DLR) and EADS Astrium GmbH. TerraSAR-X was launched on June 15th, 2007 and is supplying high-quality radar data for purposes of scientific observation of the Earth for a period of at least five years. At the same time it is designed to satisfy the steadily growing demand of the private sector for remote sensing data in the commercial market.

TerraSAR-X is the successor of the scientifically and technologically successful radar missions X-SAR (1994) and SRTM (2000). EADS Astrium GmbH has developed the TerraSAR-X satellite, whereas DLR is responsible for the overall mission and provides the necessary ground segment infrastructure and its operation.

**Mission and System**

The TerraSAR-X satellite was launched on a Russian DNEPR-1 with a 1.5 m long fairing extension. All launch vehicle elements except for the fairing inter-stage are unmodified components of the original SS-18 intercontinental ballistic missile. The lift capability into the selected orbit is 1350 kg.

For the orbit selection, an altitude range between 475 km and 525 km has been investigated. The sun-synchronous dawn-dusk orbit with an 11-day repeat period showed the best performance with respect to order-to-acquisition and revisit times.

The satellite is being operated by the German Space Operation Centre (GSOC) in Oberpfaffenhofen using two primary ground stations in Germany. Weilheim serves as the telemetry and telecommand station, and Neustrelitz is used as the central receiving station for the X-band downlink of the SAR data. Beyond that, additional Direct Access Stations, commercial partners of Infoterra GmbH, are extending the baseline receiving station concept.

TerraSAR-X carries an advanced high resolution X-band Synthetic Aperture Radar (SAR) based on active phased array technology which allows the operation in Spotlight-, Stripmap- and ScanSAR Mode in various polarisations. It provides the ability to acquire high resolution images for detailed analysis, as well as wide swath images for overview applications.

The X-band SAR instrument operates at a centre frequency of 9.65 GHz and

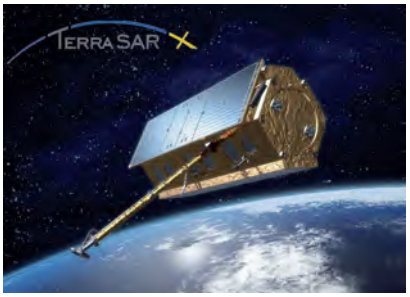


**Figure 2-5: Artist's view of the TerraSAR-X spacecraft.**

**Figure 2-6: TerraSAR-X modes of operation.**

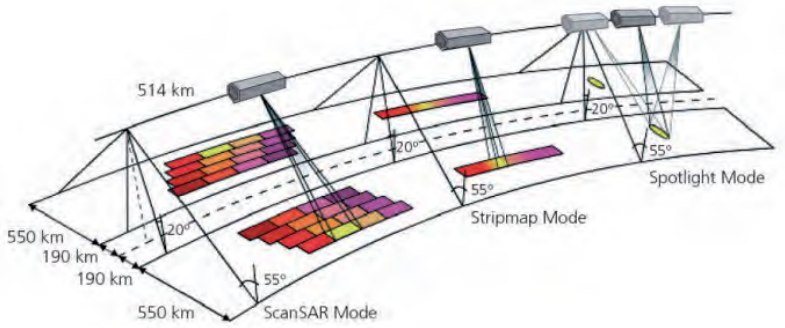


**Table 2-2: TerraSAR-X orbit parameters.**

| *Parameter* | *Mission Orbit* |
|---|---|
| Orbit Type | Sun-synchronous repeat orbit |
| Repeat Period | 11 days |
| Repeat Cycle | 167 orbits in the repeat cycle |
| Orbits per Day | 15 2/11 |
| Equatorial Crossing Time | 18.00 h ±0.25 h ascending pass |
| Eccentricity | 0.0011 – 0.0012 |
| Inclination | 97.443823° |
| Argument of Perigee | 90° |
| Altitude at Equator | 514.8 km |
| Ground Track Repeatability | within ±250 m per repeat cycle |

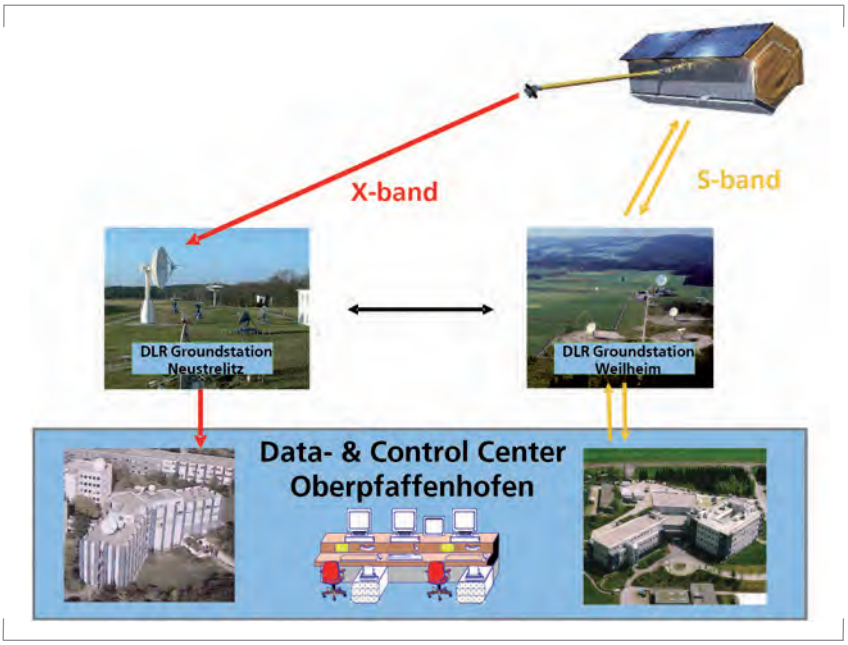


Figure 2-7: TerraSAR-X data flow concept.

with a maximum bandwidth of 300 MHz. The antenna is capable to operate in two polarisations: H and V on transmit as well as on receive and consists of 12 panels with 32 dual polarised slotted waveguide subarrays stacked in elevation. Each sub-array is fed by a dedicated Transmit/Receive Module (TRM). The SAR antenna's approximate dimensions are 4800 mm in length, 800 mm in width and 150 mm in depth. It features electronic beam steering in azimuth (±0.75°) and elevation (±20°). The acquired SAR data are stored in a Solid State Mass Memory Unit (SSMM) of 256 Gbit end-of-life capacity before they are transmitted to ground via a 300 Mbit/s X-band system.

All payload sub-systems are fully redundant, i.e. main and redundant functional chains exist. This allows the utilisation of a new concept that involves activation of both functional chains at the same time, one being the master for timing purposes. As a result operation in an experimental Dual Receive Antenna (DRA) Mode, where the echoes from the azimuth antenna halves can be received separately, becomes possible. This new experimental mode enables interesting new features like Along-Track Interferometry (ATI), fully polarimetric data acquisition and the enhancement of azimuth resolution.

**Ground Segment**

The TerraSAR-X Ground Segment is the central facility for controlling and operating the TerraSAR-X satellite, for calibrating the SAR instrument, archiving the SAR-data and generating and distributing the basic data products. The overall TerraSAR-X Ground Segment and Service Segment consist of three major parts:

- Ground Segment which is provided by DLR,
- TerraSAR-X Exploitation Infrastructure (TSXX) under the responsibility of Infoterra and
- Science Service Segment coordinated by DLR.

**SAR System Engineering**

SAR System Engineering is the key responsibility of the Microwaves and Radar Institute. It provides the SAR know-how to operate the instrument within the required specifications and to monitor the payload hardware. It also provides support to the ground segment integration and the overall project management.

Examples for major tasks of SAR System Engineering are:

- Specification of TerraSAR-X modes and imaging beams
- Overall SAR system performance control
- Instrument shadow engineering
- Support in instrument acceptance tests
- Technical support for project management decisions

- Algorithm development for Spotlight SAR processing
- Attitude steering definition law for Doppler centroid minimisation

In the following, typical examples of SAR System Engineering tasks are presented in more detail.

*Spotlight Processing Algorithms*

The Extended Chirp Scaling Algorithm for Steering Spotlight has been enhanced for the processing of TerraSAR-X sliding Spotlight raw data. The enhancement consists more of
a detailed analysis of the sliding Spotlight geometry and raw data signal.

*Zero-Doppler Attitude Steering*

The Total Zero Doppler Steering developed for TerraSAR-X enables SAR data acquisition with Doppler centroids close to zero independent
of incidence angle and terrain height variation. This is achieved by introducing a slight pitch steering on top of the standard yaw steering to align the satellite attitude to its velocity vector.

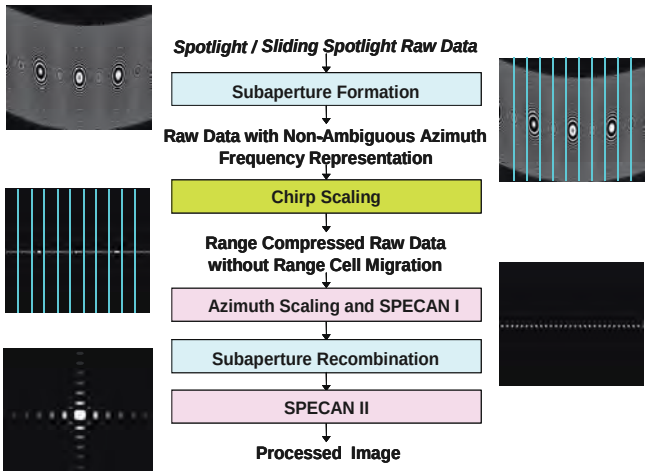


**Figure 2-8: Algorithmic steps of Extended Chirp Scaling processor for Sliding Spotlight Mode products.**

**Figure 2-9: Measured Doppler centroids in Hz at the swath center for all data takes acquired since begin of the operational phase. All TerraSAR-X data pass a systematic screening process which includes Doppler centroid estimation. The results of the screening are provided via a so-called Data Quality Check Product to the Long-Term Data Base of the IOCS system.**

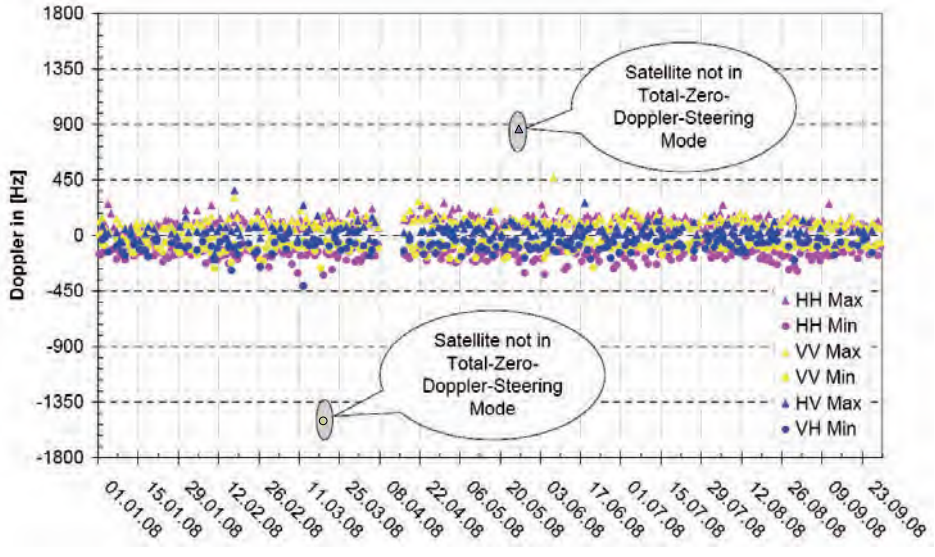

**Figure 2-10: This 150 MHz TerraSAR-X Spotlight image of Amsterdam and its many canals was taken on December 9, 2008.**

The implementation in TerraSAR-X is based on a look-up table with a step width of two degrees in argument of latitude and linear interpolation in-between. The look-up table implementation and satellite pointing errors result in a residual Doppler centroid below 250 Hz for left and right looking geometries.

*Operationalisation of 300 MHz Spotlight Products*

Use of the full 300 MHz bandwidth was originally limited for experimental modes only. A strong demand from the commercial customers triggered the inclusion of 300 MHz spotlight products into the standard product portfolio. It required an optimisation of the acquisition parameters and a corresponding upgrade of the commanding chain as well as adaptations of the SAR processor. The 300 MHz option became operational already\ during the Commissioning Phase and is since then being heavily used for high-resolution imaging.

*Special Instrument Commanding*

Our *System Command Generator* enables the exploitation of the full flexibility of the TerraSAR-X SAR instrument by providing tools for commanding data

**Figure 2-11: 300 MHz Spotlight image of Venice/Italy taken by TerraSAR-X on October 3, 2008.**

takes with special instrument settings. This feature of the Instrument Operations and Calibration System is being regularly used to command special data takes, for example:

- Aperture switching mode for along-track interferometry applications (e.g. traffic monitoring): for this mode either the forward or backward half of the antenna is activated on receive for sub-sequent pulses.
- Special beams using for example notch patterns for antenna pointing calibration.
- Special nadir data takes for investigations on the nadir interference.
- Split-bandwidth operation for delta-k interferometry.
- TOPSAR data takes for large area acquisitions with improved quality w. r. t. ScanSAR.

*TOPSAR Demonstration*

TOPSAR is a new and promising mode of operation for future SAR satellite missions. It overcomes the inherent SNR variations in standard ScanSAR (scalloping) by an additional azimuth scanning during the burst acquisition. Future sensors like Sentinel-1 will primarily rely on this mode. The active phased array antenna on TerraSAR-X does allow for electronic scanning in both range and azimuth direction. This feature is already being used for ScanSAR and Spotlight acquisitions. Using the *System Command Generator*, the required combined range and azimuth scanning can be achieved. The first spaceborne demonstration of TOPSAR operation was successfully achieved early in the Commissioning Phase.

**The Instrument Operations and Calibration Segment**

TerraSAR-X is the first mission to implement the novel concept of a dedicated ground segment facility

**Figure 2-12: Image over the Amazon rain forest acquired with a notch beam pattern. The gamma profiles derived from such images show a well established drop around the position of the pattern null. Using fitting techniques this position and hence the antenna beam pointing can be determined with milli-degree accuracy.**

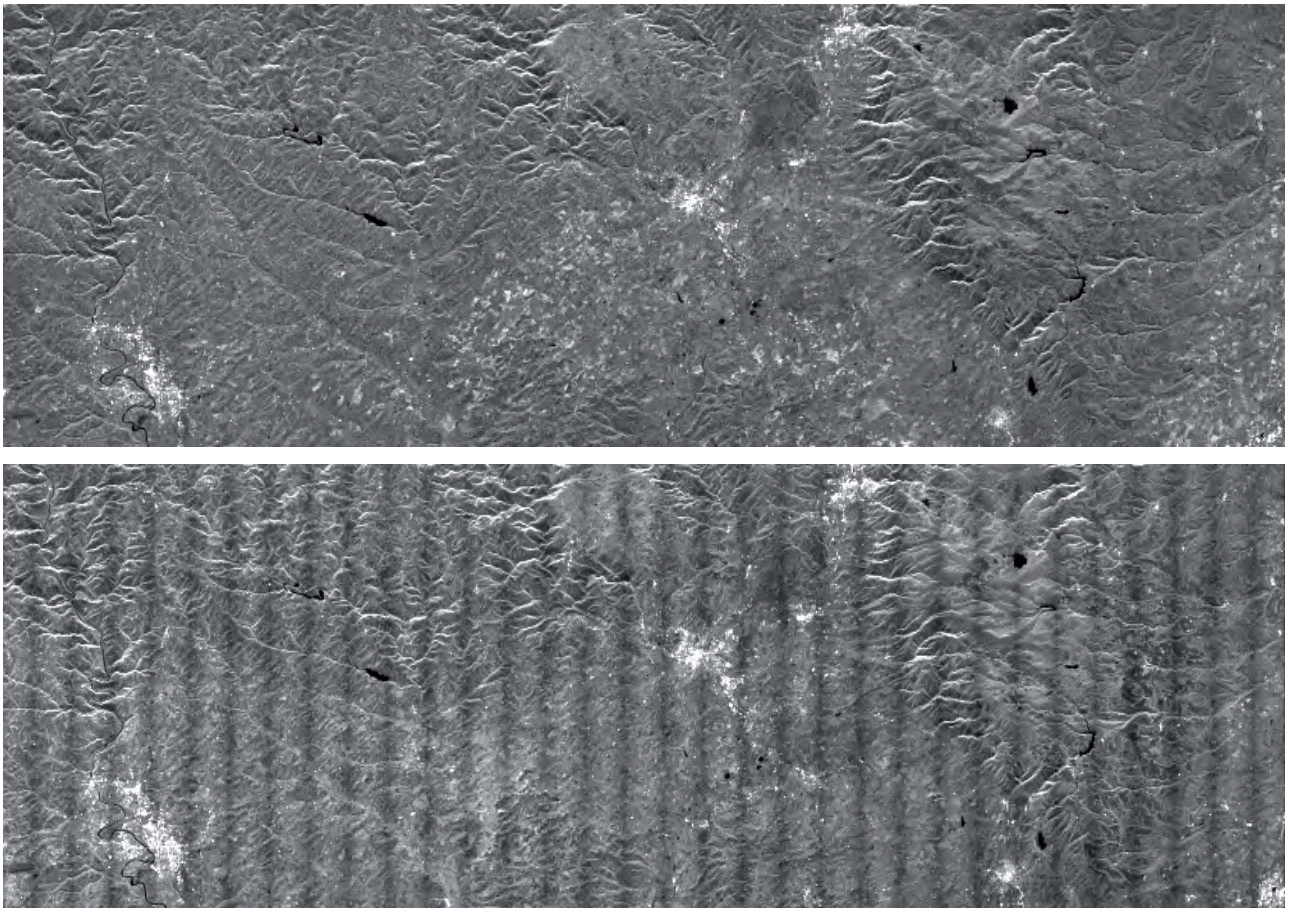

**Figure 2-13: TOPSAR (top) and ScanSAR (bottom) comparison. The first subswath of data takes acquired over Toulouse has been processed. No scalloping correction has been performed. The measured scalloping in the ScanSAR image is around 1.2 dB, compared to 0.3 dB in the TOPSAR image. Thirty-three ScanSAR bursts were necessary in contrast to only nine required by the two TOPSAR modes. The advantage in using the TOPSAR technique in terms of scalloping and therefore signal-to-noise ratio is clearly visible.**

comprising all the tools for instrument operations, performance monitoring as well as system and product calibration and verification.

*The Instrument Operations Section* has the function to operate the SAR instrument in its different operational SAR modes Stripmap, ScanSAR, Spotlight and in the experimental modes. The main tasks are to:

- generate, maintain, archive and distribute all required instrument tables for use on-board and on-ground, generate radar parameters and command information for each SAR data acquisition,
- generate flight procedures with respect to the SAR instrument for nominal and contingency operations,
- provide and maintain a Long Term Data Base (LTDB) for archiving all relevant instrument information throughout the whole mission,
- provide auxiliary products with all calibration and instrument information required in the SAR data processing.

A key element of the IOCS is the LTDB. The central role of this archive is to provide all required data for system performance prediction and execution of corrective measures throughout the whole mission lifetime. In previous SAR missions, this information was often

distributed over different locations. With the LTDB architecture, all mission data relevant for SAR system performance assessment are brought together and can be accessed by calibration, characterisation, monitoring, and verification tools. These tools are able to quickly provide a more complete picture of the whole TerraSAR-X system and its performance in shorter time. The effort for contingency analysis and the identification of counter-measures can be reduced. Under long-term system monitoring aspects, it is possible to detect performance degradations with more anticipation and to provide more room for degradation mitigation.

**Figure 2-14:** ***Above*****: Imbalance statistic of the complex raw data recorded by TSX-1. The data of all nominal images is checked automatically against its limits (red lines): The raw data imbalance is well below its limit. The gap in April 2008 is the result of a maintenance phase where no images were acquired.** ***Below*****: Typical examples of long-term system monitoring showing the performance of the on-board start time correction since begin of the operational phase.**

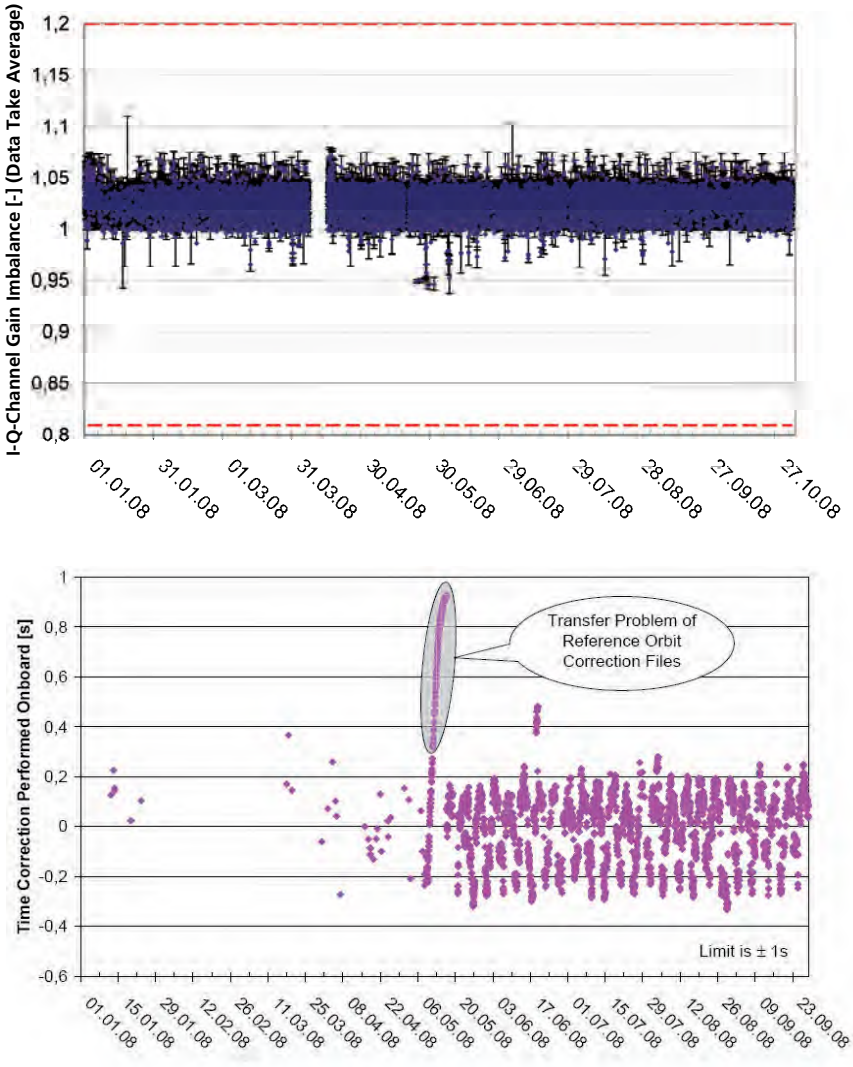

**Figure 2-15: First TerraSAR-X image, Tsimlyanskoye reservoir, taken on 19 June 2007, 15:03:24 UTC. During this acquisition, a thick cloud cover prevailed. Nevertheless, radar satellites such as TerraSAR-X offer imaging capability even in case of cloudy skies and at night. However, exceptional strong precipitation events like heavy thunderstorms may influence even radar imaging. Such an event can be seen at the upper left part of the radar image as a bright veil.**

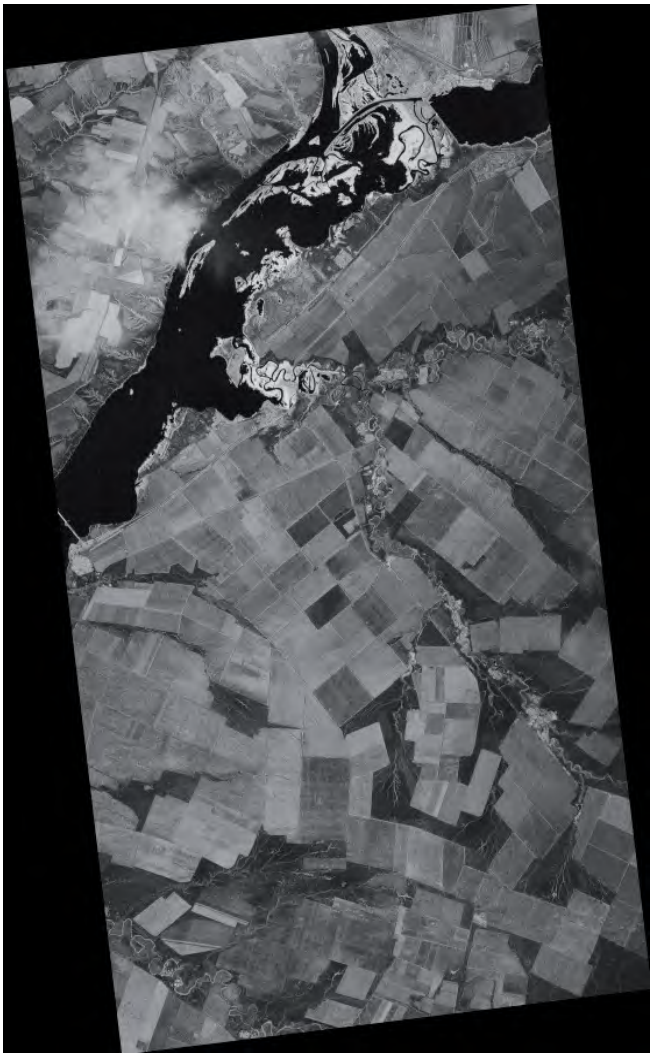

*The Verification Section* ensures the correct in-orbit operation of the entire SAR system from data take instrument command generation to ground processing and has to technically release the SAR products. The complete SAR system verification is performed during the commissioning phase and at regular intervals during the mission. Specific verification activities can be triggered by faults and failures for trouble shooting. Typical tasks performed by this section are: data take verification, long-term SAR system monitoring, and instrument health monitoring.

*The Calibration Section* comprises all the analysis tools necessary for the internal and external calibration, antenna pattern determination including optimisation of beam coefficients, control of ground equipment, and noise characterisation. Further details on the TerraSAR-X calibration concept and its implementation are described in *Chapter Microwave Systems*.

**Mission Status**

Only four days after launch the first SAR image was processed successfully. An 30 km x 60 km area in Russia, west of Wolgograd has been imaged in the stripmap mode, HH polarisation at a resolution of 15 m. The successful processing of the first image demonstrated the functional capability of the satellite on one hand and the operability of the ground segment on the other hand. The entire processing chain including order input, scheduling, commanding, data acquisition, on ground data reception, SAR processing, and archiving of the images has been verified. This result was also the consequence of a comprehensive pre-launch testing program including numerous space-to-ground segment tests.

The commissioning phase was finished right on schedule after 5.5 month and the goal was attained to ensure

optimum SAR product quality and to accomplish the full operational readiness of the space and ground segment in December 2007. The TerraSAR-X team executed a very comprehensive program involving tasks such as calibration, characterisation and verification of the SAR instrument and overall SAR system performance, and verification of the final image products. During the commissioning phase 12000 data takes were executed and all imaging modes were tested and verified. In most cases the obtained results even exceeded the initial specifications. Consequently, TerraSAR-X turned out to be a very stable precision instrument for radar imaging.

On January 7th, 2008 the operational phase was kicked off and the image production for scientific and commercial users is running extremely satisfactory since then.

**Figure 2-16: Trainspotting with TerraSAR-X: This image shows a valley located approx. 100 km north of Los Angeles, California. It contains the highway 58 (dark line) and a railway (bright line) connecting Bakersfield to Mojave, crossing the Tehachapi Pass. The Tahachapi Loop was build to reduce the slope and can be recognised as the bright circle in the center of the image. The bright circle is the railway track; the ellipse touching the circle is a very long, running train which appears displaced from the tracks. The displacement between the train and the rails in azimuth direction is a SAR effect for objects moving in range direction. For this imaging geometry, the speed of the train can be estimated from the azimuth displacement of 360m to 25 km/h.**

# TanDEM-X

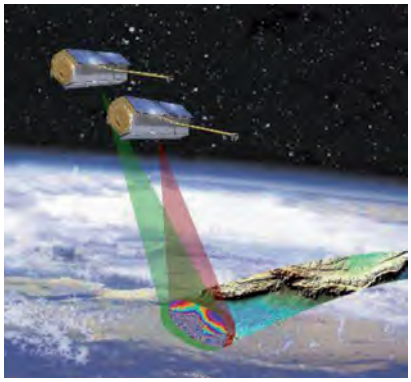

Figure 2-17: TSX-1 and TDX in tandem formation flight.

After the successful participation in the Shuttle missions SIR-C/X-SAR and SRTM, the first national SAR mission TerraSAR-X opened a new era in the German Space Programme and provided a major push for our R&D activities on high-resolution X-band SAR. In this spirit, the proposal to add a second, almost identical spacecraft (TDX), to TerraSAR-X (TSX-1) and to fly the two satellites in a closely controlled tandem formation was born.

The TanDEM-X (TerraSAR-X add-on for Digital Elevation Measurement) Mission has the primary objective of generating a consistent, global DEM with an unprecedented accuracy according to the HRTI-3 specifications. Beyond that, TanDEM-X provides a configurable SAR interferometry platform for demonstrating new SAR techniques and applications. TDX has SAR system parameters which are fully compatible with TSX-1, allowing not only independent operation from TSX-1 in a monostatic mode, but also synchronised operation (e.g. in a bistatic mode). The main differences to the TerraSAR-X satellite are the more sophisticated propulsion system to allow for constellation control, the additional S-band receiver to enable for reception of status and GPS position information broadcast by TerraSAR-X and the X-band inter-satellite link for phase referencing between the TSX and TDX radars (the required modifications on the TSX spacecraft have already been implemented). The TDX satellite is designed for five years of nominal operation. Three years of joint operation with TSX-1 will be sufficient to fulfil the TanDEM-X user requirements.

Figure 2-18: HRTI-level versus coverage indicating the uniqueness of the global TanDEM-X HRTI-3 DEM.

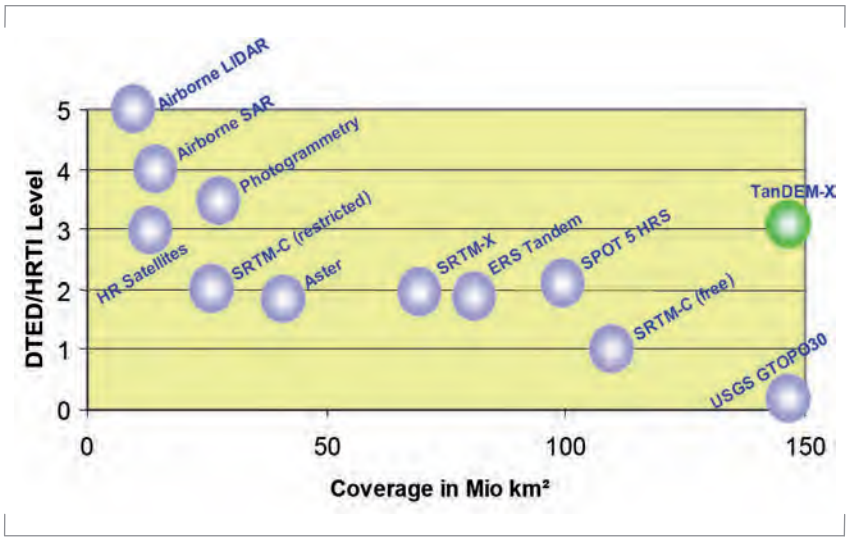


**User Requirements**

The collection of scientific and commercial user requirements for the TanDEM-X mission clearly demonstrates the need of a HRTI-3 DEM data set with global access for both scientific and commercial users. The majority of the geoscience areas like hydrology, glaciology, forestry, geology, oceanography, and land environment require precise and up-to-date information about the Earth's surface and its topography. Digital topographic maps are also a prerequisite for reliable navigation, and the improvements in their precision needs to keep step with advances in the performance of global positioning systems. Hence, TanDEM-X is fortuitously timed to augment the exploitation of the GALILEO programme. From the commercial point of view, DEMs and ortho-rectified images are the most important products for a growing earth observation market.

From a comprehensive user survey, three standard data products have been derived: standard HRTI-3 DEMs, Customised DEMs (CDEM) with even higher height resolution or improved horizontal spacing and Radar Data Products (RDP) acquired by along-track interferometry or new SAR techniques. Both scientific and commercial user

requirements can be satisfied by these products and by the formation and coverage concept.

**The Helix Orbit Concept**

The TanDEM-X mission concept is based on a coordinated operation of two spacecraft flying in close formation. Using two spacecraft provides the highly flexible and reconfigurable imaging geometry required for the different mission objectives. For example, the primary goal of generating a highly precise HRTI-3 DEM requires variable cross-track baselines in the order of 200 to 1000 m.

In this close formation flight collision avoidance becomes a major factor and a minimum safety separation of 150 m perpendicular to the flight direction is to be observed around the orbit at any time. A formation, which fulfils these requirements, is the Helix formation. By an adequate eccentricity / inclination-vector separation, the two satellite orbits can be controlled accurately enough to ensure the minimum safety distance with negligible low risk. Although ground control is the baseline for manoeuvring the satellite, TDX will be able to receive GPS position information of TSX-1 via a dedicated intersatellite S-band link and to react autonomously in a contingency case.

Exposed to the forces of the Earth's geoid, the two satellites start to move around the frozen eccentricity, resulting in a motion of libration. This effect can be advantageously used to achieve the desired height of ambiguity. The phase of libration can be adjusted by orbit manoeuvres, keeping the satellites at any desired phase with low fuel costs.

**TanDEM-X Operational Modes**

Interferometric data acquisition with the TanDEM-X satellite formation can be achieved in three different operational modes: Bistatic, Monostatic, and Alternating Bistatic Mode.

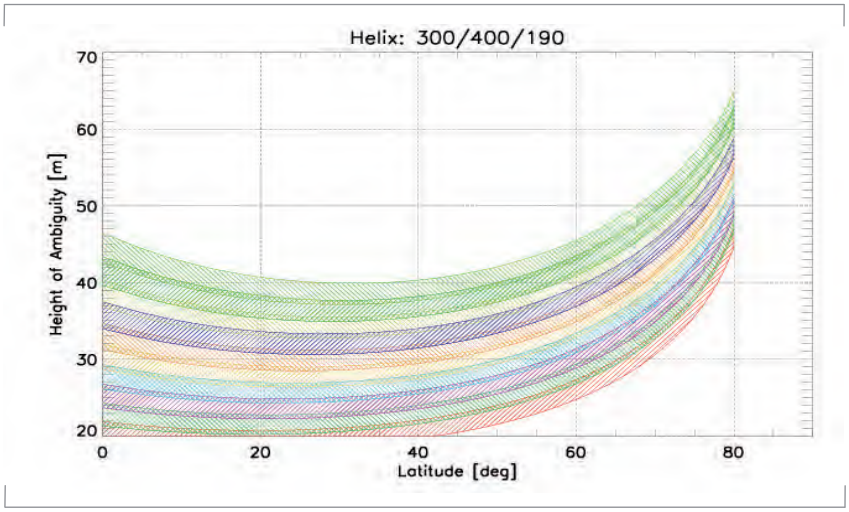


Figure 2-19: Height of ambiguity vs. latitude for the eight TanDEM-X beams from near range (red) to far range (green). Helix vertical separation is 300 m, horizontal separation 400m and the libration phase

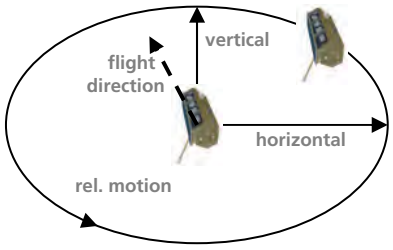


Figure 2-20: HELIX formation and the relative motion of the two satellites. TDX orbits around the centered flight axis of TSX-1 (shown in flight direction).

Operational DEM generation is planned to be performed using bistatic interferometry (Bistatic Mode), which is characterised by the illumination of a scene by one transmitter and the simultaneous measurement of the same scene with two receivers, thereby avoiding temporal decorrelation. To provide sufficient overlap of the Doppler spectra, less than 1 km along-track baselines are required while the effective across-track baselines for high resolution DEMs have to be in the order of 300 m. Robust phase unwrapping can be achieved step-by-step by acquiring two

Figure 2-21: TanDEM-X in bistatic mode: one satellite transmits and both receive the echoes simultaneously.

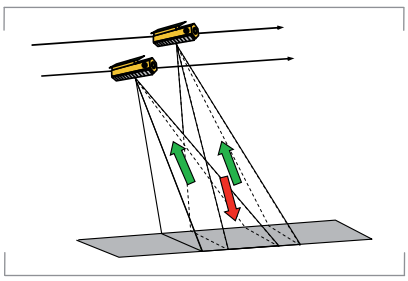

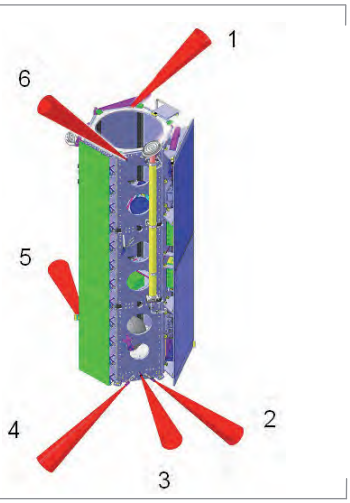


Figure 2-22: Accommodation and ID of synchronisation horn antennas with the beams shown in red.

Figure 2-23: Active synchronisation horn map for transmission. Directions of the baseline vector during one orbit are marked in red.

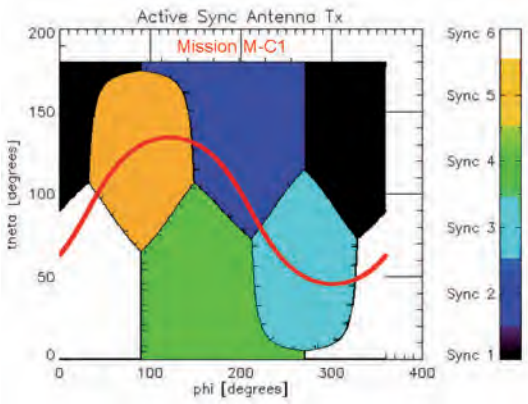


data sets with increasing baseline (decreasing height of ambiguity). For mountainous areas (about 10% of the Earth land surface) additional data acquisitions with different baselines and viewing geometry are required.

Because of the slight differences in the Ultra Stable Oscillator (USO) characteristics of the two instruments PRF synchronisation and relative phase referencing between the satellites (exchange of USO signals via a dedicated X-band inter-satellite link) are mandatory in this mode (see below).

The Radar Data Mode has been introduced as a synonym for the demonstration of innovative SAR modes and applications, offering a large variety of geometric constellations and of radar instrument settings (all SAR modes including 2 + 2 receive phase centres). The instruments are commanded according to the parameters selected by the scientists for Along-Track Interferometry (ATI) applications and for demonstration of new SAR techniques.

**Synchronisation**

In Bistatic Mode the TanDEM-X interferometer is operated with two independent oscillators. Uncompensated frequency drifts and oscillator noise will cause slight deteriorations and significant shifts of the bistatic SAR impulse response, but more importantly substantial interferometric phase errors in case of bistatic interferometric operation. To correct for these phase and frequency errors the TanDEM-X specific SAR instrument features provide a scheme for exchanging synchronisation information through a dedicated link, composed of a set of six horn antennas, optimally distributed to ensure full solid-angle coverage with low phase disturbance. The sync horns are placed identically on TSX-1 and TDX, following the scheme shown in Figure 2-22.

The communication consists of a periodical exchange of synchronisation chirp pulses, which are compressed as normal SAR pulses and provide after proper evaluation the differential phase behaviour of the satellite oscillators. This enables the commanding of leap pulse repetition intervals to correct the frequency drift and the phase correction of the interferometric system in the on ground processing chain.

An accurate phase correction can be achieved by commanding synchronisation pulses with a PRF in the order of 10-20 Hz. For an SNR of 30 dB (a conservative assumption for along-track separations up to 1 km) the remaining interferometric phase error after the synchronisation correction will be kept below 1°.

For assuring maximal SNR in the sync link, the appropriate sync horn pair (on TSX-1 and TDX) has to be selected. Therefore a 3D angle map has been generated showing the ID of the sync antenna that should be active depending on the relative position of the other satellite and the gain pattern of the sync horns. For each time instant, the position on the sync map can be directly calculated from the baseline vector. A similar sync map has to be applied for the opposite satellite.

Figure 2-23 also shows that there will be four sync pair switches per orbit. Assuming that the best sync antennas are chosen for all orbit positions according to the sync maps, the sync link will have the optimal SNR. However, the uncertainty in the a priori knowledge of the along-track component of the baseline is in the order of 200 m. Despite this uncertainty the SNR stays well above 40 dB, which still delivers sufficient performance. Simulations indicate similar results for all mission phases and Helix geometries.

**Predicted DEM Generation Performance**

A detailed DEM calibration concept for the Bistatic Mode has been developed, which comprises a prediction model of the total height errors and the design of DEM correction strategies. The height error simulations show that remaining errors after the monostatic calibration of the satellites need to be corrected in order to fulfil the DEM accuracy requirements.

Therefore, the DEM calibration concept foresees the adjustment of adjacent interferograms by means of a least-square adjustment method and the use of accurate height references to correct absolute offsets.

*TanDEM-X Height Error Simulator*

The simulator covers the main sources of the arising height errors, which can be classified into three groups: inaccuracies in the baseline determination, phase errors in the radar instruments, and interferometric phase errors modelled as uncorrelated, additive random process. Contrarily to the random errors, the baseline inaccuracies and the systematic instrument drifts can be mainly classified as *low frequency errors* in terms of the data take length.

- *Baseline errors:* The interferometric baseline (between the SAR antenna phase centres) is determined through the differential GPS measurement of the TOR/IGOR systems installed in the TanDEM-X satellites, and they have a limited accuracy. This is the main contribution to the baseline error, and Flight Dynamics' simulations predict that the relative error in the baseline product will be a sinusoidal function with amplitude of about 1 mm (one sigma) in any direction and a periodicity usually longer than the typical data take duration. These errors primarily cause a height error offset of ~1m and a systematic phase/height ramp in the cross-track direction of ~3mm/km for typical height of ambiguities of 35 m. Additionally, an unknown but stable offset in the baseline determination may exist (1 to 6 mm). This error contribution is expected to be characterised and cancelled during the TanDEM-X commissioning phase by means of dedicated interferometric acquisitions over test sites with precise height references.
- *SAR instrument drifts*: Automatic temperature compensation measures and adjusts the TR-module amplifiers and phase shifters in the front-end electronics in order to stabilise the operations point of the instrument under temperature variations. However, residual errors still remain.
- *Random errors/coherence loss* result from several contributions like the instrument noise residuals and random errors in the sync link correction, as well as by SAR ambiguities, processing and co-registration errors or volume decorrelation effects. However, the major degradation of the coherence is caused by thermal receiver noise. In order to achieve the required DEM accuracy, overlapping data segments from successive TanDEM-X satellite passes have to be combined to partially compensate the performance decay

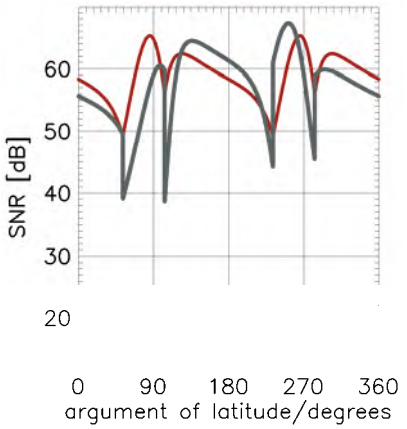


**Figure 2-24: SNR curves by optimal a priori selection of sync horns. Red curve assumes no along-track baseline uncertainty, whereas the gray curve depicts the case of having 200 m offset in the a priori knowledge of the baseline.**

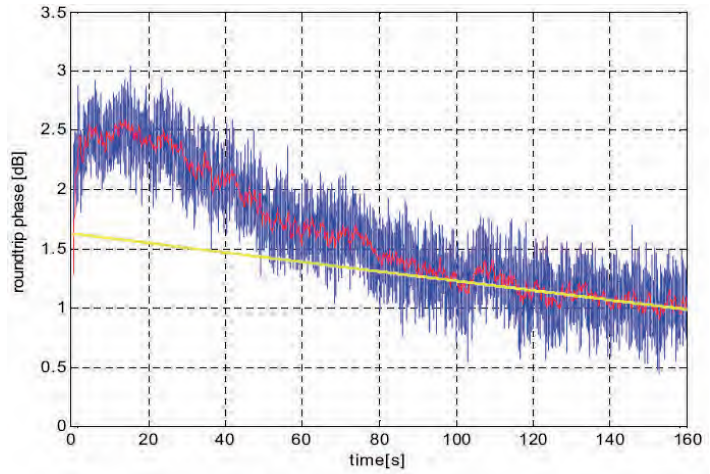


**Figure 2-25: Internal phase calibration: Roundtrip phase in temperature compensation mode measured with the internal calibration loop and linear approximation of the phase derived from the first and last phase sample.**

**Figure 2-26: Point-to-point height accuracy (soil & rock, 90%, VV) for a height of ambiguity of 40 m (dotted) and 30 m (dashed). The solid curve shows the combination of the multiple swaths.**

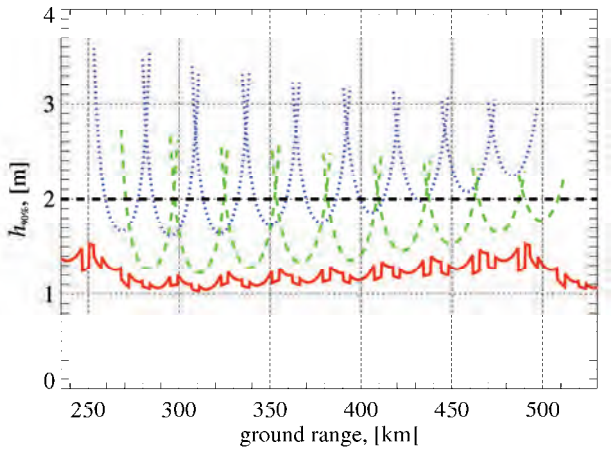


at each swath border. The plot in Figure 2-26 describes the predicted point-to-point height errors for the 90 % confidence interval assuming two sets of DEM data acquisitions with two fixed heights of ambiguity of 30 m (dashed) and 40 m (dotted). The beam coverage on ground is shifted by half a swath width for the two acquisition sets in order to compensate for high errors at the swath edges. The height error from the combination of all acquisitions is shown in solid line yielding an almost constant performance with an accuracy which is well below the 2 m requirement for HRTI-3. However, this only leaves around 0.5 m error margin to the systematic height error budget, which confirms the need of an accurate correction of the systematic height error contributions in the DEM adjustment process.

*DEM Adjustment*

Evaluation of swath overlaps and globally distributed accurate ground control points (GCP) will allow correcting systematic height error trends (typically height ramps in azimuth and range tilts) by means of a simplified polynomial 2-D model and a least-square adjustment method with constraints. The plot in Figure 2-27 shows an example of a typical TanDEM-X parallel adjacent data take scenario with 250 km total range width and around 2000 km azimuth length. The first plot shows the simulated height errors for each interferometric acquisition (phase noise neglected in this simulation). The second plot is the resulting error of the scenario after the application of our adjustment model. Four ground control points (GCPs) provide absolute height references (reference limited accuracy also considered) and data take overlaps also assist in the adjustment. The plots also indicate the remaining 0.48 m relative

error (in equivalent 100 × 100 km regions according to HRTI-3), better than the desired 0.5 m.

The model will be implemented in the Mosaicking and Calibration Processor (MCP), which will simultaneously adjust large scenes, up to continental size, with multiple overlapping data takes, and finally generate the complete and accurate global DEM.

*Absolute Height References (GCPs)*

The HRTI-3 standard has an absolute height requirement of 10 m and a relative of 2 m at a 90% confidence level. To support the least-squares adjustment of the data take scenarios and provide good absolute height accuracy, globally distributed height references are needed. The ICESat Spaceborne Laser Altimeter (GLAS) has been selected as the source for these GCPs.

ICESat's orbit has a 91-day repeat cycle. Its footprint has a diameter of less than 70 m and it sends laser pulses of 40 Hz, which implies spacing between samples of 170 m along-track on the Earth's surface.

The absolute height accuracy of the data is better than 1 m and the data structure provides evaluation and classification information for each sample. The quality parameters comprise information about the orbit determination accuracy, the pointing and geolocation of the laser footprint, about the weighting coefficients for averaging the laser footprint area and about the return echo waveform shape. For example, return echoes from mountainous areas or from forests will have a more scattered waveform than the ones coming from a flat surface reflection.

These parameters allow applying certain selection criteria for ICESat points in order to further improve the GCPs accuracy until 0.5 m. Only narrow echo

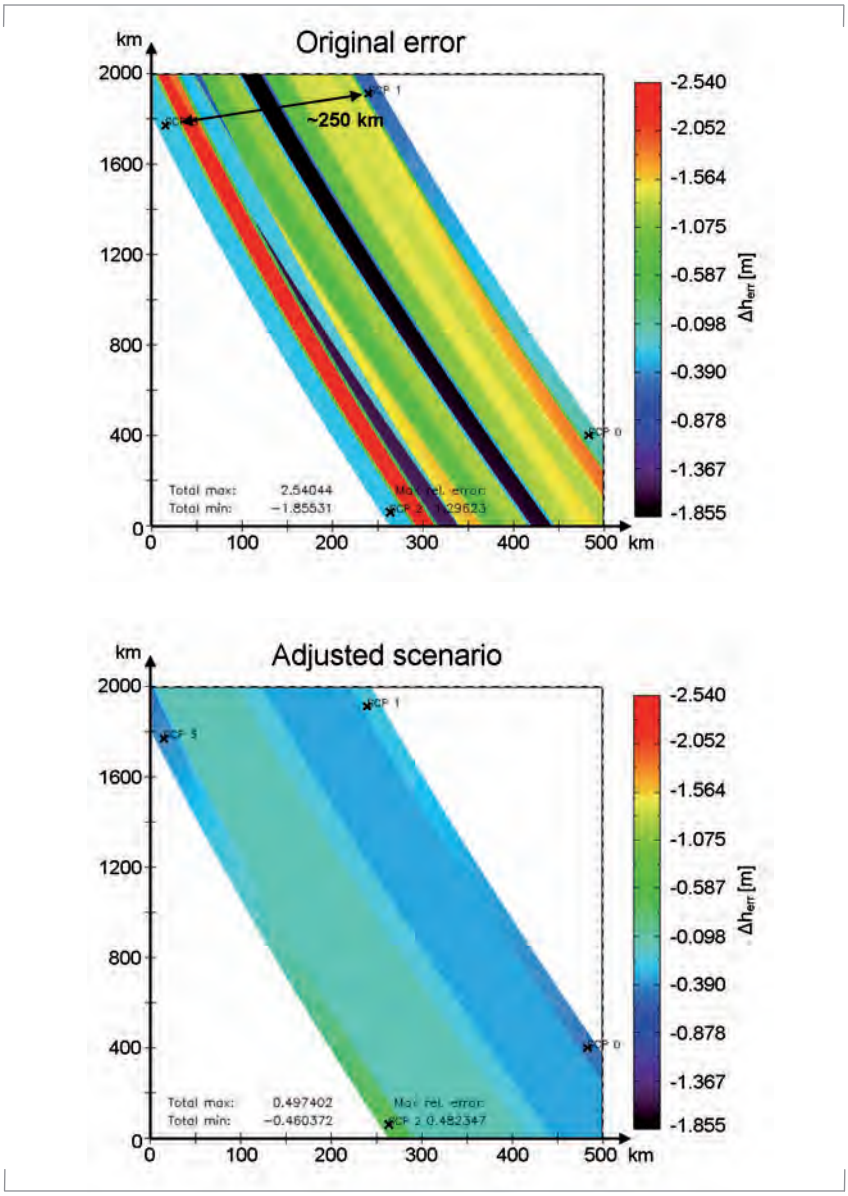


**Figure 2-27: Parallel data take scenario. Upper plot with the simulated systematic height errors. Lower plot with the resulting height error after adjustment.**

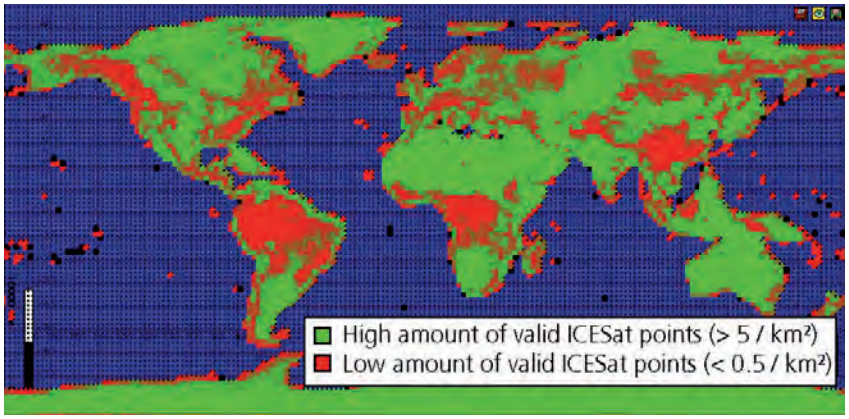


Figure 2-28: ICESat coverage over the Earth (only good quality points).

Figure 2-29: Along-track interferometry modes in TanDEM-X.

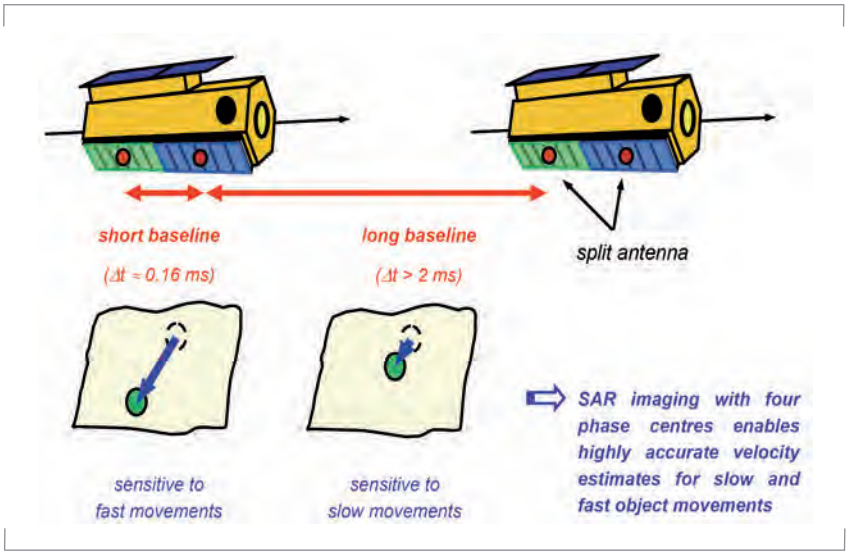


returns from the lidar pulses provide extremely reliable height references, and these will be the ones used for TanDEM-X. In equatorial regions, with less ICESat points density, the acquisition of selected crossing orbits is foreseen to assist the DEM adjustment.

**Radar Data Mode**

The Radar Data Mode stands for any acquisition of TanDEM-X data products which are not covered by the DEM class. Examples are along-track interferometry, polarimetric SAR interferometry, four phase centre moving target indication, bistatic SAR imaging, and digital beamforming.

Along-track SAR interferometry can either be performed by the so-called dual receive antenna mode with a baseline of 2.4 m from each of the satellites or by adjusting the along-track distance of the two satellites to the desired size. The Helix formation allows this distance (called along-track baseline) to be adjusted from zero to several kilometres. This technical feature is essential as this application requires velocity measurements of different fast and slow objects. Mainly four scientific application areas are identified to explore the innovative along-track mode: oceanography, traffic monitoring, glaciology, and hydrology. Scientific interest asks for the identification of moving objects as well as the estimation and the validation of different velocity estimates. In all three application areas the knowledge of the velocity will improve model predictions for environmental, economical, as well as social aspects.

With TanDEM-X, innovative SAR techniques will be demonstrated and exploited, which open up new perspectives for future SAR systems. The focus will be on the research areas:

- Bistatic and multistatic SAR imaging enabling enhanced scene feature

extraction by combination of monostatic and bistatic signatures. This is due to the substantially increased observation space in bistatic SAR.
- Polarimetric SAR interferometry allows for precise measurements of important vegetation parameters like vegetation height and density.
- Digital beamforming and superresolution.

The main interest for these research areas lies in the understanding and the development of new algorithms.

**Mission Scenario**

Contrary to conventional Earth observation missions, the TanDEM-X global mapping strategy has also to account for the formation geometry as well as for given Helix parameters; DEM acquisitions are only possible for a certain range of latitudes. Furthermore, in the parallel operation of the TanDEM-X and TerraSAR-X missions, enough room for the latter has to be reserved and the TanDEM-X acquisitions have to be planned as a quasi complementary mission far in advance.

With these constraints and the assumption of a three-year tandem phase (joint operation of TSX-1 and TDX) and the use of the TerraSAR-X standard stripmap beams covering incidence angles from 20° to 45°, a reference mission scenario has been developed including sufficient time slots for the acquisition of CDEMs and RDPs.

It foresees that all land surfaces will be covered at least twice with different heights of ambiguity to support robust multi-baseline phase unwrapping. During the first year the northern hemisphere will be mapped with ascending orbits, whereas the southern hemisphere with descending orbits, all with the same height of ambiguity. In the second year the process will be repeated with a scaled height of ambiguity. Finally, in the third year the priority will lie on covering difficult areas for a third and even fourth time and to achieve secondary mission goals. The length of the data takes will be maximised within the resource limits in order to simplify the adjustment. Towards the end of the three years the satellites will be separated in along-track e.g. for bistatic monitoring and ATI experiments. In any phase, orbital periods, which are not required for deriving the global DEM, will be used for the generation of CDEMs, RDPs, or TerraSAR-X products.

The TanDEM-X mission encompasses scientific and technological excellence in a number of aspects, including the first demonstration of a bistatic interferometric satellite formation in space, as well as the first demonstration of close formation flying in operational mode. Several new SAR techniques will also be demonstrated for the first time, such as digital beamforming with two satellites, single-pass polarimetric SAR interferometry, as well as single-pass along-track interferometry with varying baseline. TanDEM-X takes advantage of the heritage from the SRTM and SIR-C/X SAR missions, as well as more than 25

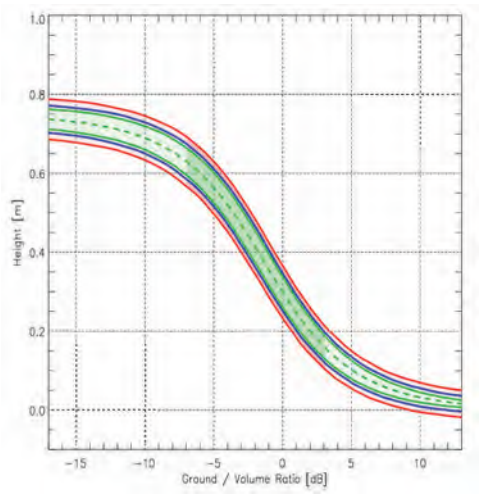


**Figure 2-30: TanDEM-X height estimation performance for sun flower plants based on the Random Volume-over-Ground model. The dashed green line indicates the height variation of the interferometric phase centre with different polarisations (corresponding to a variation of the ground-to-volume ratio on the abscissa). The green tube shows the height errors due to volume decorrelation for different effective baselines and an independent post spacing of 30 m x 30 m. The blue and red tubes show additional errors due to the limited system accuracy for scattering coefficients of -10 dB and -15 dB, respectively. The dark areas of the phase tubes indicate those ground-to-volume ratios which are addressable by the different polarisations.**

# Sentinel-1

As part of European Union's programme, known as Global Monitoring for Environment and Security Programme (GMES), ESA is undertaking the development of Sentinel-1, a polar orbit satellite system for the continuation of SAR operational applications in C-band after the ENVISAT/ASAR is decommissioned. The Sentinel-1 mission requirements have been optimised to enhance the performance and operational capabilities of the GMES Service Element.

As a member of the industrial consortium the Institute develops the system calibration and verification concept as well as the end-to-end performance budgets of the Sentinel-1 SAR system. The concept identifies and describes all facilities and activities necessary to deliver calibrated and verified SAR products within the required performance specification. It defines the associated algorithms and tools and plans the relevant activities. The Sentinel-1 calibration concept is based on the methodology developed for TerraSAR-X (see *Section TerraSAR-X*) which is in turn based on the Institute's heritage from calibration work on ERS-1, SIR-C/X-SAR, SRTM, ENVISAT/ASAR as well as TerraSAR-L. Consequently, Sentinel-1 will profit from new, innovative methods that have been successfully validated on TerraSAR-X and are briefly described in the following.

**Figure 2-31: The Sentinel-1 Satellite (By courtesy of ESA).**


**Efficient System Calibration and Verification Strategy**

Sentinel-1 is an advanced multi-mode synthetic aperture radar system providing stripmap operation with adjustable swath positions or azimuth-sweeped ScanSAR modes (TOPS-SAR), and the Wave mode. This results in a multitude of beams with different antenna patterns for different polarisations. Beam steering and shaping is performed by an active phased array antenna fed by electronic transmit/receive modules controlling the excitation of the individual antenna array elements.

A major challenge for calibration and verification of all operational modes is the short commissioning phase of three months. Calibration must take minimum operation time and cope with system degradation with neither impact on performance nor the need for long re-calibration periods. After the lessons learnt during the ENVISAT ASAR commissioning and with the expertise on the development of TerraSAR-X a more effective calibration philosophy emerges which shifts the effort of system calibration from space to ground. Thus, in-orbit calibration duration is minimised with respect to more detailed pre-launch characterisation and analysis.

The key element of this new concept is a mathematical antenna model based upon accurate on-ground measurements and the antenna beam excitations from the active transmit/receive modules. The

model predicts all antenna patterns and relative beam-to-beam variations. Thus, the number of external measurements during in-orbit commissioning can be reduced for geometric and radiometric calibration. Periodic in-flight internal calibration guarantees both the high radiometric stability of the system as well as the long-term system monitoring over the mission life time of 20 years. The logical flow of these tasks is depicted in the block diagram.

### Antenna Model Approach

Following the great success of TerraSAR-X, the Sentinel-1 calibration concept is also built around an antenna model, which enables the antenna patterns to be accurately derived from pre-flight characterisation and the transmit/receive module excitation coefficients. The antenna model is validated before launch by comparison with on-ground pattern measurements. Once the satellite is in orbit, the modelled patterns are verified against a reduced set of in-flight measurements and will be used from commissioning phase onwards. Input data from ground based characterisation and in-orbit internal characterisation (Pulse Coded Calibration) will be used to provide the actual beam patterns which will be required during data analysis and image processing.

### Pulse Coded Calibration (PCC)

The pulse coded calibration (PCC) is a means of characterising individual rows or modules of an active antenna while rows or modules are operated at the same time. The Sentinel-1 instrument is capable of calibrating each antenna pattern thanks to pulse-coded calibration. The measured excitation coefficients directly feed into the antenna model for dynamic re-calibration. The PCC or PN-Gating method (also see *Section TerraSAR-X*) was developed in the Institute and has been successfully verified for the first time in-orbit on TerraSAR-X.

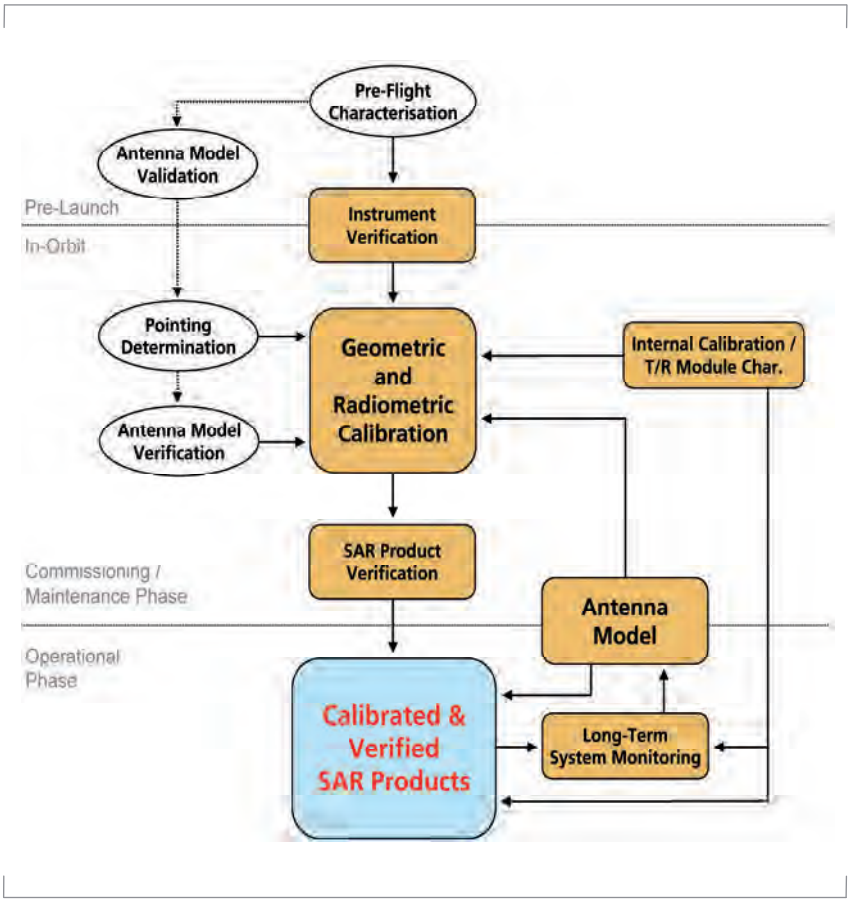


Figure 2-32: Logical flow of Sentinel-1 system calibration and verification.

In the scope of the GMES programme, ESA develops the Sentinel missions and in the case of Sentinel-1 the full implementation of the system has been started. With our current contribution to Phase B up to Preliminary Design Review (PDR) and our long-term experience in SAR calibration we are well prepared to take over responsibility for the detailed Sentinel-1 system calibration and verification plans and budgets, design and development of the required tools and facilities but also for the planning and execution of the campaigns in the commissioning phase. For the latter the Institute is well equipped with calibration targets and operates and maintains a large calibration site in Southern Germany.

# Tandem-L

Tandem-L is a DLR proposal for an innovative interferometric radar mission that enables the systematic and global monitoring of dynamic processes on the Earth's surface with high spatial and temporal resolution. Important application areas are global forest height and biomass inventories, measurement of Earth surface deformations due to tectonic processes, observations of 3-D ice structure and its changes, and the monitoring of ocean surface currents. The innovative mission concept and the high data acquisition capacity of Tandem-L will provide a worldwide unique data set to systematically observe, analyze and quantify a wide range of mutually interacting processes in the bio-, litho-, hydro- and cryosphere. Tandem-L will be an essential step to advance our holistic understanding of the Earth system and its accelerating dynamics in response to a changing climate.

The Tandem-L mission concept relies on a systematic data acquisition strategy using a pair of co-operating L-band SAR satellites flying in close formation. The satellite system operates in two basic data acquisition modes:

- The 3-D structure mode employs fully-polarimetric single-pass SAR interferometry to acquire structural parameters and quasi-tomographic images of semi-transparent volume scatterers such as vegetation, sand, and ice.
- The deformation mode employs repeat-pass interferometry in an ultra-wide swath mode to measure small shifts on the Earth's surface with millimetre accuracy and short repetition interval.

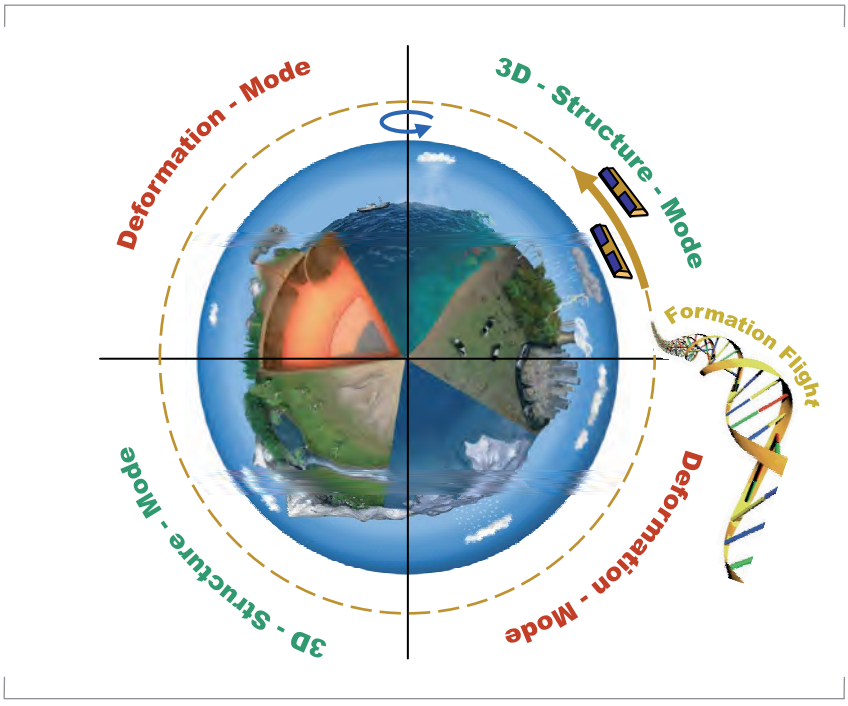


Figure 2-33: Tandem-L mission concept with close formation constellation.

### 3-D Structure Mode

The 3-D structure mode in Tandem-L will provide a worldwide unique data set to assess the status, investigate the dynamics and predict the evolution of the terrestrial bio-, hydro- and cryosphere in response to a changing climate. A key mission objective is the accurate and globally consistent inventory of forest height and biomass with high spatial resolution. Such data are not only urgently required for forest management and environmental monitoring, but they play also a key role for a better understanding of the global carbon cycle. Current estimates assume that on average about one third of all anthropogenic carbon emissions are absorbed by the terrestrial biosphere, but the detailed mechanisms, the spatial distribution and the dynamics of this terrestrial sink are only poorly understood and subject to intense scientific debate. The 3-D structure mode of Tandem-L provides unique observations to significantly improve our understanding of vegetation dynamics and their intricate connection to climate

change. Globally consistent vegetation inventories are moreover an essential basis for present and future international treaties such as the Kyoto protocol and its anticipated successors.

The fully polarimetric data acquired with the 3-D structure mode of Tandem-L are also of immense value for a wealth of further application areas. One example is the simultaneous generation of Digital Terrain (DTM) and Digital Surface (DSM) Models which both represent an ideal complement and update to the DEM acquired by the TanDEM-X mission. Another promising opportunity arises from repeated acquisitions of single-pass interferograms within short time intervals. Their systematic combination can not only be used for tomographic imaging but it has also the potential to reveal otherwise hidden 3-D structural changes within ice sheets, glaciers, wetlands, and permafrost soils. Further applications are large scale measurements of soil moisture and surface roughness, observations of thaw and freeze cycles, measurements of sea ice thickness, agricultural monitoring, detection of dyke damage, and measurement of wave heights and ocean currents.

**Deformation Mode**

Tandem-L is also ideally suited for deformation measurements by repeat pass interferometry. The long wavelength ensures a high temporal coherence over long time intervals and the short repeat cycle allows for unambiguous measurements in the case of fast and nonlinear surface movements. One satellite remains always within a small orbital tube, while the other satellite can be used to simultaneously acquire interferometric datasets with different squint, aspect and/or incident angles without interrupting the time series of the first satellite. The additional acquisitions will improve the retrieval of 3-D motion vectors significantly. Further benefits arise from the opportunity to simultaneously acquire an L-band DEM. The use of both satellites for improved atmospheric corrections is investigated.

**Innovative SAR Technology**

A major challenge for Tandem-L is the development of two cost-effective and at the same time very powerful SAR instruments that fulfil the demanding mission requirements. For this, several options are currently being investigated. A very promising and highly innovative approach is the combination of a large deployable reflector antenna with a digital feed array (see illustration on the bottom). The parallel digitisation of the signals from the individual feed elements enables the generation of highly adaptive antenna beams by software-controlled digital beamforming. The opportunity for digital antenna pattern synthesis increases the flexibility in operating the SAR system and allows for novel and extremely powerful SAR imaging modes that can be optimally adapted to the different requirements of the 3-D structure and deformation modes. The large receiver aperture provided by a deployable reflector enables furthermore a high receiver gain and consequently a reduction of the necessary transmit power without degrading image quality. This allows for frequent large-scale data acquisitions with high orbital duty cycles as required for the systematic observations of large scale dynamic processes in the Earth system.

The combination of highly innovative imaging modes and novel sensor technology for the generation of urgently requested remote sensing products make Tandem-L a unique mission that will set a new observational standard for Earth system research and applications.

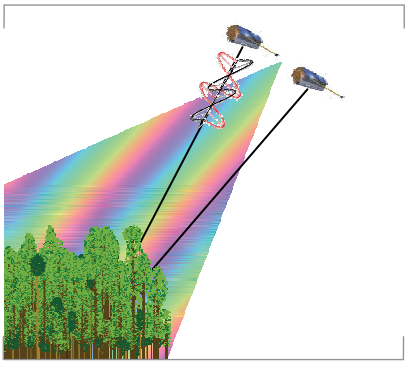

Figure 2-34: 3-D structure mode.

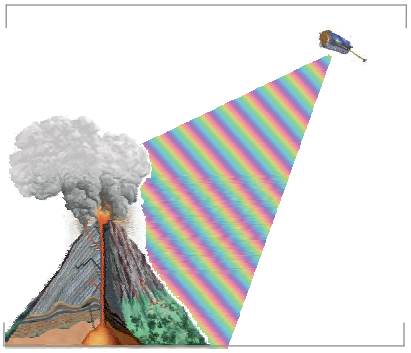

Figure 2-35: Deformation mode.

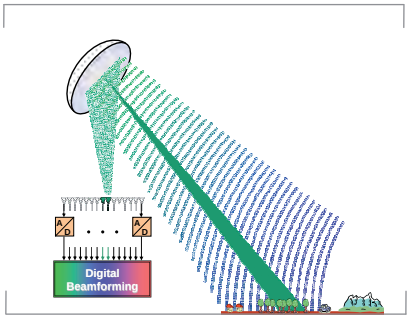


Figure 2-36: Tandem-L will employ innovative SAR instrument technology for high-resolution wide-swath SAR imaging.

# Advanced Land Observing Satellite – ALOS

ALOS, an enhanced successor of the Japanese Earth Resources Satellite 1 (JERS-1), was launched from JAXA's Tanegashima Space Centre in January 2006. ALOS operates from a sun-synchronous orbit at 691 km, with a 46-day recurrence cycle carrying a payload of three remote sensing instruments: the Panchromatic Remote Sensing Instrument for Stereo Mapping (PRISM), the Advanced Visible and Near-Infrared Radiometer type 2 (AVNIR-2) and the polarimetric Phased Array L-band Synthetic Aperture Radar (PALSAR).

The PALSAR sensor has the capacity to operate with a wide range of off-nadir angles and resolutions in a single-, dual-, and quad-pol mode. However, four modes have been prioritised for a simplified observation scenario:

- Single-polarisation (HH), at 34.3° and 10 m resolution
- Dual-polarisation (HH-VH or VV-HV), at 34.3° and 20 m resolution
- Quad-polarisation (HH-HV-VH-VV), at 21.5° and 20 m resolution
- ScanSAR single-polarisation (HH) and 100 m resolution

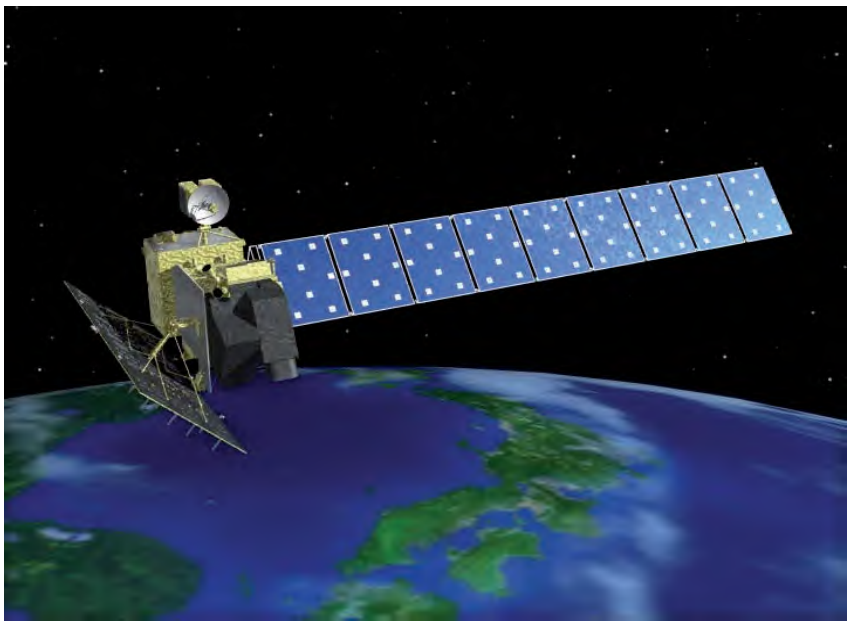

**Figure 2-37: The Advanced Land Observing Satellite – ALOS (By courtesy of JAXA).**

The Institute is involved in science, calibration and validation activities of the ALOS project. It is part of the international science team of JAXA's Kyoto & Carbon (K&C) Initiative.
A MoU signed between JAXA and DLR establishes the framework of the K&C cooperation. Furthermore, the Institute is a member of JAXA's international Calibration and Validation team and supports ESA's calibration and validation activities of ALOS-PALSAR products distributed by the European ADEN node.

**The Kyoto & Carbon Initiative**

The Kyoto & Carbon Initiative is an international collaborative project and forms the continuation of JAXA's JERS-1 SAR Global Rain Forest and Global Boreal Forest Mapping project (GRFM/ GBFM) into the era of ALOS. The initiative is set out to support explicit and implicit data and information needs raised by international environmental Conventions, Carbon Cycle Science and Conservation of the environment (CCCs).
This Initiative is led by JAXA which is responsible for management, data acquisition, processing and distribution. Product development is undertaken jointly by JAXA and an international science team that involves academic and research organisations from 13 countries. The initiative is structured around three main thematic areas: Forests, Wetlands and Desert & Water. The Forest Theme is focused on supporting the UNFCCC Kyoto Protocol and the part of the carbon research community concerned with $CO_2$ fluxes from terrestrial sinks and sources. Key areas considered include the

mapping of land cover (forest), forest change, biomass and structure. Within the Forest Theme the Institute is leading the scientific activities on Polarimetric SAR Interferometry (Pol-InSAR) techniques.

*Polarimetric SAR Interferometry*

ALOS provided, for the first time, the possibility to demonstrate quantitative Pol-InSAR techniques from space. Indeed, based on repeat-pass quad-pol interferometric SAR data acquired by the ALOS/PALSAR sensor during its early calibration/validation phase it was possible to demonstrate model based Pol-InSAR inversion over single isolated stands (see Figure 2-38). However, the high temporal decorrelation levels induced by the 46-day repeat-pass cycle reduce the estimation performance of forest structure parameters significantly and prevent the demonstration of Pol-InSAR inversion on a global scale. However, based on the statistics of the temporal decorrelation patterns, important conclusions and recommendations for upcoming L-band spaceborne interferometric missions have been drawn.

**Pol-InSAR Calibration**

Within the framework of the international JAXA calibration/validation group the Institute is responsible for calibration and validation of Pol-InSAR data and products. The new challenge faced in calibration was to assess and compensate the impact of the ionosphere on Pol-InSAR data. The effect of the ionosphere depends on the Total Electron Content (TEC) in the ionospheric layer below the ALOS orbit and is proportional to the wavelength squared. While being negligible for X-band sensors, ionospheric effects become significant in L-band with a pronounced diurnal variation and a strong dependence on solar activity during the 11-year solar cycle.

In order to address the ionospheric calibration of POL-InSAR data in a more flexible and general framework a new calibration concept based on Coherent Scatterers (CS) has been developed. The fact that CS can be detected on a single-image basis and are characterised by high signal-to-clutter ratios, high interferometric coherence and low polarimetric entropy make them a good candidate for use in radiometric, polarimetric, and interferometric (phase) calibration as well as in the quantification and correction of ionospheric effects.

**Verification of PALSAR products distributed by the European ADEN Node**

Another important contribution to the ALOS mission was the verification and validation of PALSAR products distributed by the European ADEN node. Under a contract with ESA/ESRIN, the Institute assessed ALOS/PALSAR data quality during the commissioning phase

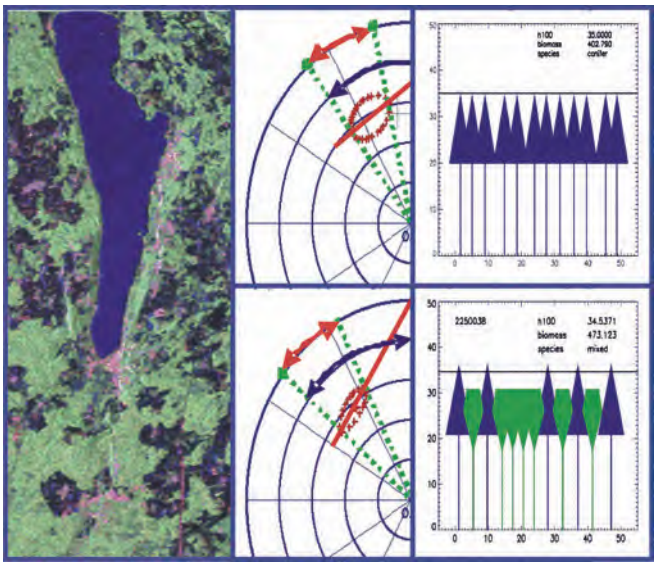

**Figure 2-38: Forest height estimates for two forest stands located within the Oberpfaffenhofen test site obtained from the inversion of dual-baseline quad-pol InSAR ALOS data.**

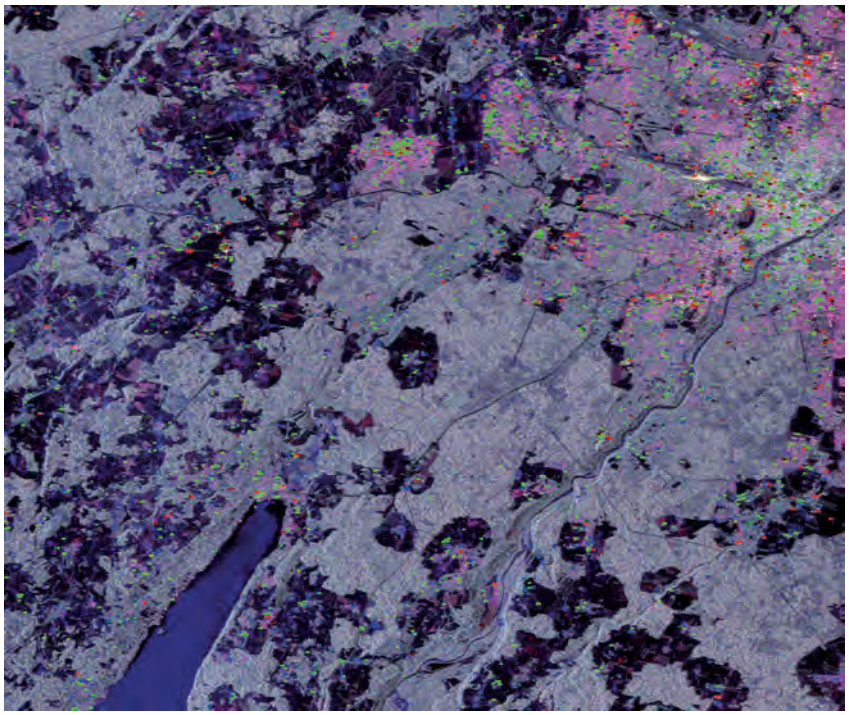

Figure 2-39: Coherent Scaterrers detected in the Oberpfaffenhofen test site using quad-pol InSAR ALOS data. The different colors indicate detection at different polarizations (Red: HH-VV, Blue: HH+VV, Green: HV).

Figure 2-40: Corner reflectors of this type with 1.5 m and 3 m side length have been used for PALSAR product verification.

of the instrument and provided a set of algorithms for quality control throughout the mission lifetime.

Software tools developed and implemented include point target analysis, distributed target analysis, geometric analysis, antenna pattern estimation, polarimetric analysis and the estimation and analysis of propagation effects. The framework for this tool set was the in-house developed CALIX software, which is our standard calibration and verification environment also being used within the IOCS for TerraSAR-X.

During several calibration and verification field campaigns, active and passive calibrators (active transponders and passive dihedral and trihedral reflectors) have been deployed extensively as external reference targets, providing well-defined point target responses for product quality assessment.

# Multi-Application Purpose SAR – MAPSAR

The Brazilian/German MAPSAR is a proposal for an Earth observation mission with a small satellite (500 kg class). As a payload the spacecraft contains an innovative L-band SAR sensor, as satellite bus INPE´s Multi-Mission Platform (MMP) will be used. The main mission objectives are assessment, management and monitoring of natural resources, cartography, disaster monitoring and reconnaissance. Therefore L-Band has been chosen as best frequency band to fulfil the mentioned tasks. MAPSAR is currently being investigated by INPE and DLR in a phase B study (detailed design) as a follow up on a preceding successful phase A study (feasibility analysis). The initiative of the joint study of a small spaceborne SAR is a consequence of a long-term Brazilian/German scientific and technical cooperation that was initiated between INPE and DLR in the seventies.

**User Requirements**

The MAPSAR mission is tailored to optimally support the potential user groups in both countries, taking into account distinct aspects of specific applications. Workshops with potential end-users of MAPSAR were conducted in both countries to develop requirements and recommendations aiming at a joint DLR - INPE spaceborne SAR programme. The consensus was that a spaceborne SAR mission would provide a powerful new tool to acquire data and to derive important and unique information for different applications. Due to the enormous scarcity of up-to-date information, which is fundamental for planning and strategic decision-making about environmental assessment, management and monitoring, the

proposed lightweight spaceborne SAR initiative should be strongly oriented to a quasi-operational ("application-oriented") system. This is dedicated to thematic mapping purposes for topography, vegetation and deforestation, geology, hydrology, biomass estimation, disaster monitoring and security.

Due to INPE´s Multi-Mission Platform performance (mass, power generation, geometric envelope and data rate), main limitations were imposed upon the satellite configuration: use of a single frequency and a lightweight antenna. The resulting reflector antenna concept limits the maximum instantaneous swath width to approximately 55 km. The main mission parameters are shown in Table 2-3, an overview about the different operational modes can be seen in Figure 2-41.

| Parameter | Value |
|---|---|
| Frequency | L-band |
| Polarization | Single, dual and quad. pol. |
| Incidence Interval | 20° - 45° |
| Spatial Resolution | 3 – 20 m |
| Swath | 20 – 55 km |
| Coverage | Global |
| Look Direction | Ascending/descending |
| Revisit | Weekly |
| Data Access | Near real time |
| Additional Requirement | Stereoscopy & Interferometry |

**Table 2-3: MAPSAR mission parameters taking into account user requirements and Multi-Mission Platform constraints.**

### Mission Design

The wide spread applications require different radar polarisations and different spatial resolutions. Furthermore, stereoscopy and interferometry require orbit repetition cycles and coverage sequences with highest accuracy. Nevertheless, the disciplines can be optimised in order to get appropriate coverages. Investigations about the necessary $\Delta v$ for the mission are ongoing. Considering the requirements of the Brazilian Multi-Mission Platform and the SAR sensor, it was concluded to concentrate the investigations on orbit heights between 500 and 700 km.

### MAPSAR Satellite

The L-band SAR sensor is based on a reflector antenna concept. The main advantage is the possibility to realise full polarisation and high bandwidth with low technological risk at low cost. The MAPSAR satellite utilises a modular concept, consisting of a payload module on top of a Multi-Mission Platform.

**Figure 2-41: MAPSAR operational modes. HR: 3 m resolution, single pol.; MR: 10 m resolution dual pol.; LR: 20 m resolution, full pol.**

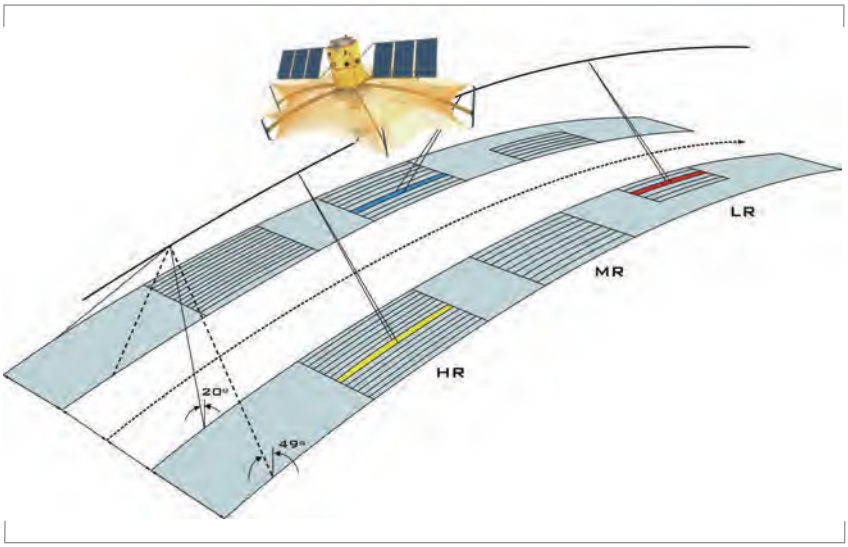

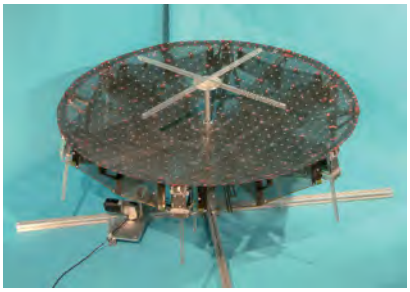

Figure 2-42: Bread-board of the MAPSAR antenna main reflector.

A key problem for an L-band SAR is the large antenna size compared to higher radar frequencies. With respect to launcher constraints a Cassegrain configuration with an elliptical foldable parabolic main reflector with 7.5 m length in azimuth and 5 m width in elevation was considered. Neither the subreflector mounting nor the horn type prime radiator need to be folded. The resulting antenna gain in combination with a low orbit allows very good sensitivity with reasonable power.

The mechanical concept for the antenna main reflector was identified as one of the major challenging technologies. It was developed in cooperation with the Institute of Lightweight Structures of the Technical University of Munich. The reflecting surface is a triaxially woven fabric of carbon fibre reinforced silicone (CFRS). The material is extremely light and fully space qualified. The support structure consists of CFRS rib membranes, which are deployed and stiffened with a pantograph mechanism.

The high power amplifier for generation of the radar pulses was identified to be the second challenging technology for the overall concept. A space qualified amplifier in the class of 1 kW is not yet available on the market. A new design was developed based on combining the power of four space qualified travelling wave tube (TWT) amplifiers with 250 W output power each (see diagram). The power combining is done in wave guide technology where the second stage is directly performed in the orthomode transducer of the L-band horn. The power combining is controlled by low power phase shifters driving the TWTs. This concept also avoids high power switching mechanisms by using polarisation synthesis. The phase of one channel is switched between 0° and 180° for alternating radar pulses. This results in two independent polarisations which are tilted 45° against the horizontal plane. In the receive path of the instrument the phase switching is compensated and the final rotation of the polarisation matrix will be done in the SAR processor.

The total payload mass of 282 kg is just compatible with the specified value of the Multi-Mission Platform. The total mass of the satellite is estimated to be 532 kg. In terms of dimensions, the payload layout is compatible with the majority of MMP considered standard launcher family.

MAPSAR has a high degree of innovation in the design of the small SAR payload, the reflector antenna, and with remarkable sensor performance. The applications will take advantage of high spatial resolution L-band SAR with enhanced capabilities (polarimetry, stereoscopy, interferometry), particularly suitable for German interests, like disaster monitoring and urban mapping. The MAPSAR initiative aims at providing services for public, commercial and military aspects. The Phase B study is planned to be finished by end 2009 and options for a continuation into follow-on phases are being investigated.

Figure 2-43: Block diagram: Power combining and polarization synthesis in the MAPSAR radar payload.

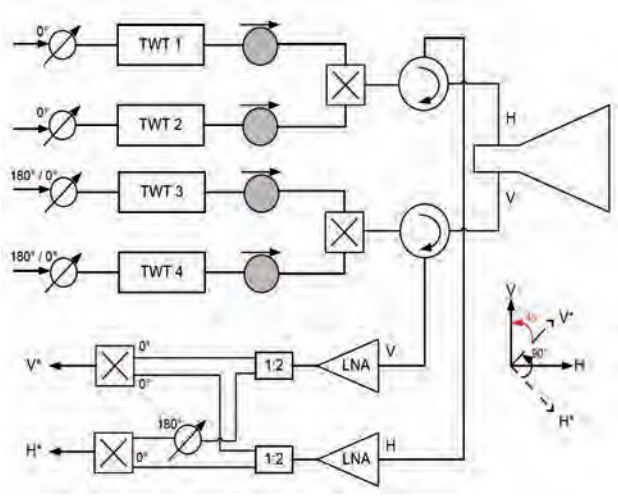

# BIOMASS

BIOMASS is one of the six Candidate Earth Explorer Core missions selected for Assessment Study (Phase 0) following a peer review of 24 proposed mission ideas submitted in response to ESA's Call for Ideas in the frame of the third cycle of Earth Explorer Core missions.

The scientific objective of BIOMASS is to determine for the first time, in a consistent manner, the global distribution of forest biomass to reduce uncertainties in the calculations of carbon stocks and fluxes associated with the terrestrial biosphere. BIOMASS will be used to improve quantification of:

- the terrestrial carbon stocks and fluxes in forests;
- terrestrial carbon sources and sinks, by monitoring and quantifying disturbances and recovery in forests.

The main outcome of the mission will be greatly improved knowledge of the size and distribution of the terrestrial carbon pool, and much improved estimates of terrestrial carbon fluxes.

The Institute is actively involved in the performance and science aspects related to the Pol-InSAR component of BIOMASS mission. This includes performance analysis and mission design tasks, development of innovative inversion methodology as well as performance and evaluation of experimental airborne campaigns dedicated to scientific and technological issues of the BIOMASS mission. The Institute is member of the ESA's BIOMASS Mission Advisory Group (MAG).

**BIOMASS Science**

The release of carbon dioxide into the atmosphere by human activities has been recognised as a major driver of climate change. Terrestrial ecosystems play an important role, both in the release of carbon through land use and deforestation, and in the sequestration of carbon through vegetation growth processes. Over the last 25 years, there is strong evidence that the terrestrial biosphere has acted as a net carbon sink, removing from the atmosphere approximately one third of the $CO_2$ emitted from fossil fuel combustion. However, terrestrial ecosystems have the largest single source of uncertainty in the global carbon budget (IPCC, 2007). The uncertainties lie in the spatial distribution of carbon stocks and carbon exchange, and in the estimates of carbon emissions due to human-induced or natural disturbances.

A central parameter to the terrestrial carbon budget is forest biomass which represents a proxy for carbon. Despite its crucial role in the terrestrial carbon budget, forest biomass is poorly quantified across most parts of the planet due to the great difficulties in measuring biomass on the ground and consistently aggregating measurements across scales.

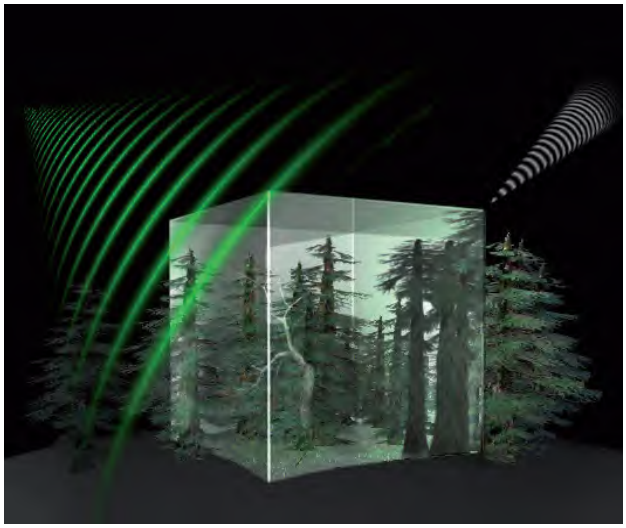

**Figure 2-44: BIOMASS – A mission proposal for mapping forest biomass on a global scale (By courtesy of ESA).**

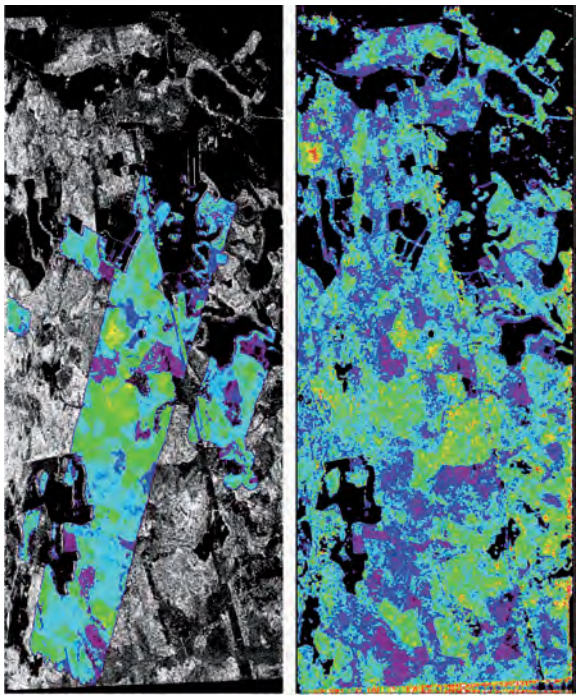

Figure 2-45: Left: P-band (100 MHz) HH amplitude image and lidar forest height map. Right: Pol-InSAR derived forest height map. Test Site: Remningstorp, Sweden (BIOSAR 2008 campaign).

**BIOMASS Mission**

BIOMASS will be implemented in terms of a P-Band Synthetic Aperture Radar (SAR) mission, which will provide first observations of the global distribution of forest biomass at a resolution and accuracy compatible with the needs of international reporting on carbon stocks and terrestrial carbon models. The mission will exploit the unique sensitivity of P-Band SAR to forest biomass and exploit advanced retrieval methods to map forest biomass globally across the entire biomass range encountered in tropical, temperate and boreal forests. BIOMASS will also provide the first opportunity to explore the Earth's surface at the P-Band wavelength.

**Pol-InSAR for BIOMASS**

To cover the full range of the world's biomass, and to estimate the carbon emission from deforestation in the tropics, BIOMASS relies on forest height estimation from space by means of Pol-InSAR. The estimated height should be used to improve forest biomass estimates derived by intensity measurements. The major advantage of using forest height instead of intensity is the unsaturated sensitivity of Pol-InSAR to height and hence biomass levels. Methods to be assessed and explored for deriving biomass information from Pol-InSAR consist of: a) using known relationships between biomass and height (or allometry), and b) combining intensity with Pol-InSAR height in biomass retrieval based on regression.

The inversion of forest height is based on Pol-InSAR data which require interferometric acquisitions of the fully-polarimetric complex scattering matrix. While there are several sources of error affecting height retrieval, the largest impact on the retrieved height accuracy is expected from temporal decorrelation. Temporal decorrelation biases Pol-InSAR forest height estimates and increases their dispersion. While the dispersion can be compensated at a cost of spatial resolution, the bias (i.e. overestimation of forest heights) cannot yet be compensated. The biases due to temporal decorrelation have been studied both theoretically and experimentally using airborne SAR data (see Figures on the left). Already moderate temporal decorrelation of about 10% is sufficient to introduce errors larger that the specification of the level 2 height product (> 30%).

Temporal decorrelation is related primarily to the temporal stability of the location and dielectric properties of the scatterers within a SAR resolution cell. Pol-InSAR height inversion is affected because temporal decorrelation is superimposed on the volume decorrelation contribution which carries the information about the general vertical forest structure, and forest height in particular. With respect to temporal decorrelation the use of the longer

P-Band wavelength has two main advantages:

- Waves with long wavelengths penetrate deeper into the vegetation layer and interact more with the ground beneath the canopy as well as with larger tree structures than for shorter wavelength. Both the ground and large tree structures constitute more stable scatterers over time than smaller tree elements such as branches. This results in higher temporal coherence at P-band.
- The decorrelation caused by a given movement of the scatterers within the resolution cell scales is a function of wavelength and is therefore lower for longer wavelengths. The temporal decorrelation due to different magnitudes of movement as a function of wavelength (shown in Figure 2-46) clearly demonstrates the advantage of P-Band.

As a consequence, the interferometric coherence at P-Band as a function of time is expected to decrease more slowly for than for any other frequency band allocated to EO. For a single-satellite repeat-pass SAR mission, only the higher coherence of P-Band is expected to permit forest height retrieval at a global scale and fulfil the BIOMASS scientific objectives.

**Figure 2-46: Temporal decorrelation caused by movement as a function of wavelength for three movement amplitudes of the scatterers.**

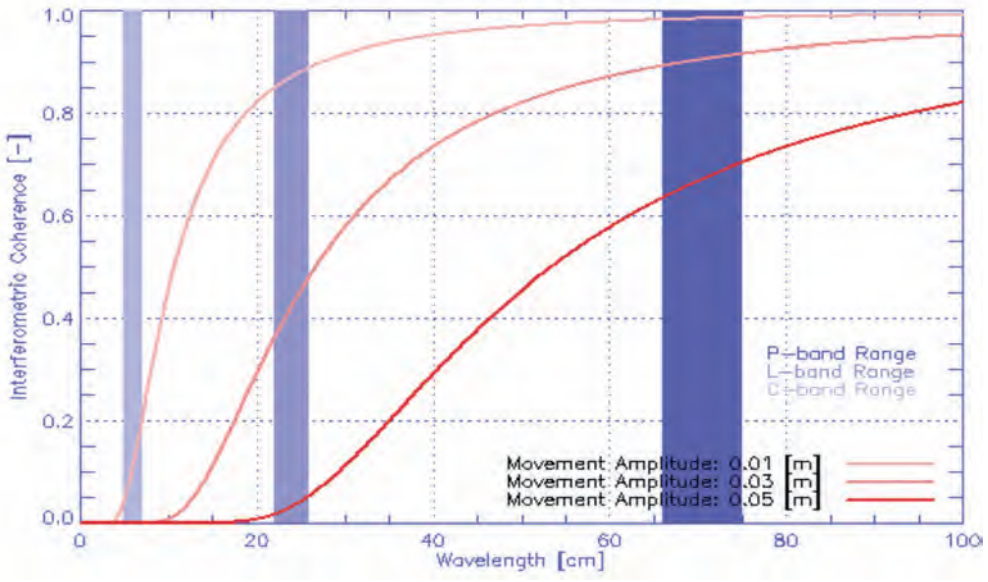

# Reconnaissance Systems

The information demand for future spaceborne reconnaissance systems can only be covered by multi-sensor systems on different satellite platforms. Current spaceborne reconnaissance systems are optimised only to a limited number of selected parameters, e.g. type of the sensor, revisit time, incidence angle, etc. Future reconnaissance missions have to be provided with imaging capabilities independent of weather and time (SAR), capabilities for heat detection (IR) and material determination (hyper-spectral). Multi-sensor systems with very high spatial and radiometric resolution cannot efficiently be integrated on a single platform, because of different image acquisition geometries, platform size and resources. The illustration shows a possible generic scenario for such a multi-platform system consisting of image (IMINT), signal (SIGINT) and human (HUMINT) intelligence sensors on different ground, air and space based platforms.

For analysing and increasing the efficiency of existing and future reconnaissance systems (also valid for civil Earth observation), the design and development of tools to simulate the interactions between the single elements of the complete system is necessary. An end-to-end simulation concept was realised with the main focus on the principal user. The modular simulation concept guarantees the necessary continuous flexibility. It can presently handle nearly all possible platforms e.g. cars, trucks, airplanes, UAVs, ships, and spacecraft in a wide variety of scenarios.

The three major parts of this tool are the mission simulator, the SAR end-to-end simulator and the ground segment simulator.

With respect to given user requests the tasks of the mission simulator are to plan and analyse the geographical or time dependent coverage of the regions of interest and to optimise the mission with regard to major aspects, like platform resources, and sensor characteristics. The mission simulation is described in more detail in the next section.

The SAR end-to-end simulator has the task of generating a simulated SAR image from an optical image, another radar image or a map. The simulator consists of modules for target and scenario generation, modelling the platform and sensor behaviour, processing of the simulated raw data, and analysing the simulated image quality. Further tools for assistance of the simulator are the parameter generator, which is suited for a very first design of a spaceborne SAR system, and the performance estimator, which can predict the image quality parameters to be expected very exactly without processing the raw data.

The ground segment simulator includes a variety of planning, processing and assessment tools, which can be used to simulate a whole ground segment.

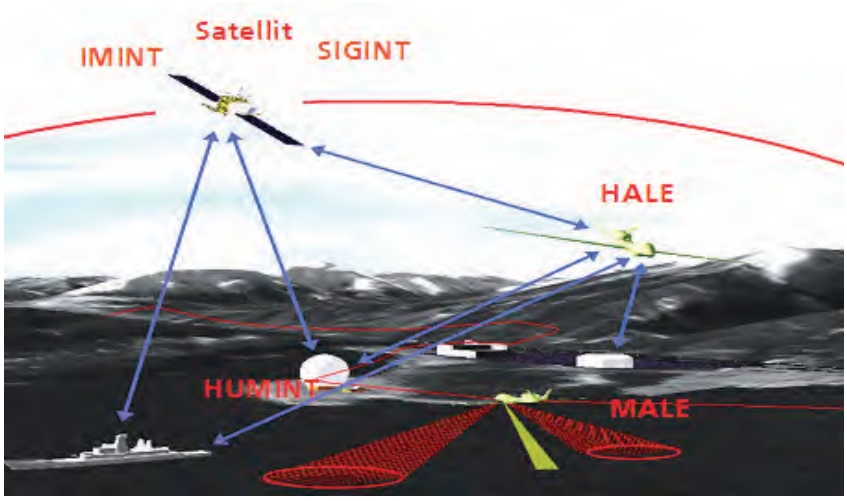


**Figure 2-47: Multi-platform reconnaissance system consisting of different information sources (IMINT, SIGINT and HUMINT) and data links to dislocated ground stations.**

### Mission Simulator

The mission simulator is a tool to simulate a complete multi-platform reconnaissance system considering multi-user aspects. The user can define different multi-mission scenarios and system constraints. The tool allows geographical coverage analyses, field of view analyses, global coverage and contact calculations, as well as time dependent coverage analyses, like the calculation of response time, revisit times and image information age. These results can be used for subsequent mission optimisations. Finally, the mission planning capability can be used to optimise multi-user driven imaging requests for different parameters, like number of images or short time intervals between image acquisition and image delivery to the user's ground segment. The analyses are supported by external data bases, which can communicate with the mission simulation via existent interfaces. It is also possible to carry out collision analyses with space debris using the NORAD data base or predicting shadowing effects, if a digital elevation model of the area of interest with sufficient resolution and quality is available. The functions are shown in Figure 2-49.

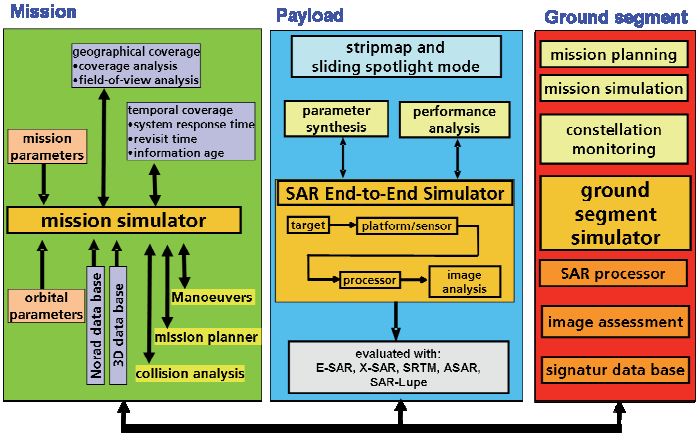


Figure 2-48: Generic reconnaissance system simulation concept; the mission simulator generates the principal geometry for the SAR end-to-end simulator according to the user requirements.

The mission simulator consists of four core modules: the mission analyser, the mission planner, the satellite simulator, and the coverage analysis tool, which is supported by commercial orbit propagators.
To analyse external scenarios, the mission simulator provides an interface to two commercial software tools, the Satellite Tool Kit (STK) and the FreeFlyer.

*Mission Analysis Tool*

Using the mission analysis tool all parameters of a simulated mission can be calculated and analysed. For example it is possible to make

Figure 2-49: Scheme of mission simulator displaying the data flow from user inputs to different simulation results supported by external data bases.

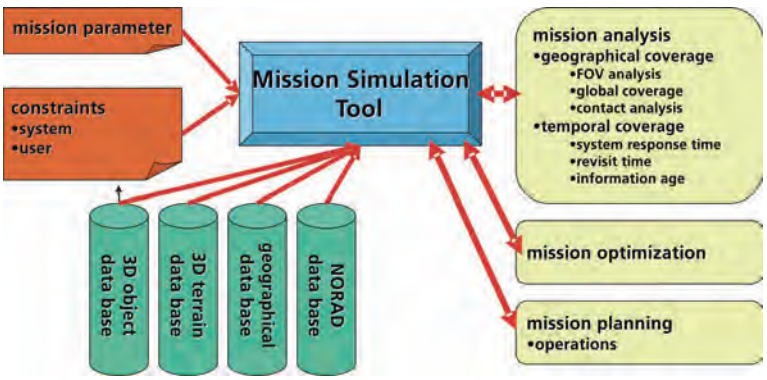

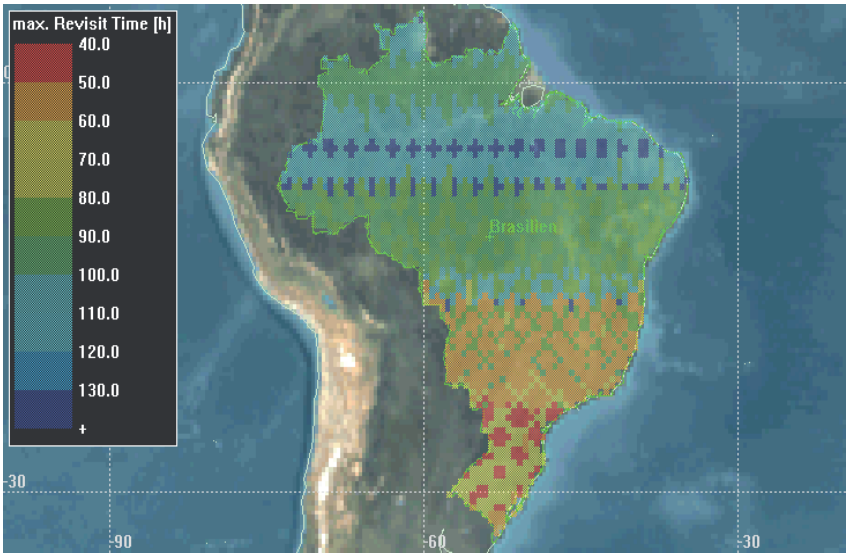


**Figure 2-50: Coverage analysis for the MAPSAR mission. The colour scale indicates the different region-dependent revisit times for Brazil.**

**Figure 2-51: Ground station contact analysis with a limited field of view caused by high trees in the ground station area.**

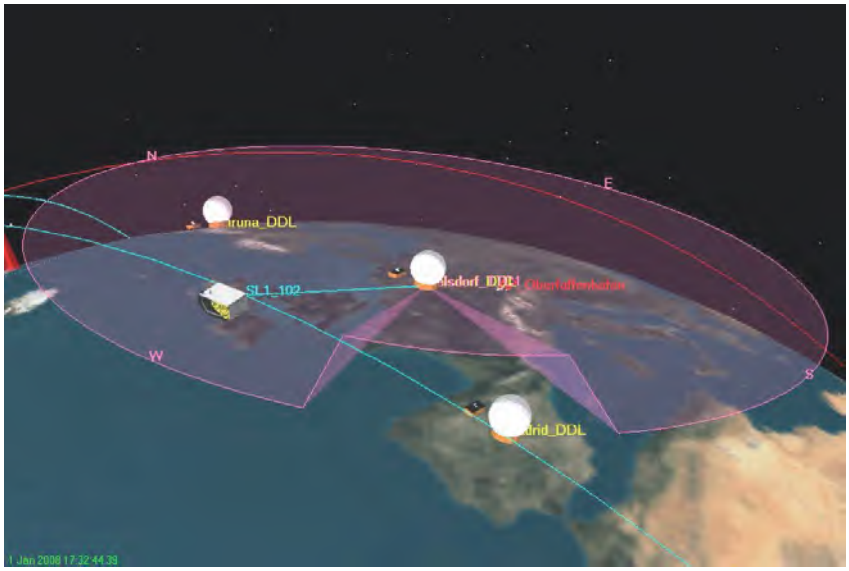


a coverage analysis of an area of interest to determine the revisit time of the system. Figure 2-50 shows the coverage analysis for Brazil produced for the MAPSAR project.

Further analysis examples are the determination of the system response time, the image information age, and the field of view analysis of moving or stationary sensors. Figure 2-51 shows the result of the contact analysis of a satellite ground segment considering local terrain aspects.

In addition, the mission analysis tool is able to calculate the necessary input parameters for the mission planning tool, like ground station contacts, inter-satellite data link contacts and contacts to other platforms mentioned above. If a DEM is available, the calculation of the contact times also considers the three dimensional geographical coordinates. For better visualisation, the overlay or registration of the scene with a satellite image is possible.

*Mission Planning Tool*

The mission planning tool can be used for the definition, design and analysis of multi-user driven multi-mission and multi-platform scenarios. Starting with a list of orders generated by the user, the coordinates of all targets on the order list will be converted by a target generator to a special format readable by the mission planning tool. In a second step, all possible contacts of the satellites to one or more ground stations and to all targets are calculated. Considering the constraints given on the resources of the system (e.g. power, data storage, priority of orders, etc.), the mission scheduler creates an optimised scheduling and shows it within a result list. The results are displayed graphically. A further feature is the option to prioritise particular orders. The mission plan can be optimised by iterations.

*Satellite Simulator*

The satellite simulator models the most important satellite sub-systems and can be used to calculate the satellite system driven constrains of the reconnaissance system required for the mission analysis, optimisation and planning activities. Presently, five of the satellite subsystems are modelled: the SAR sensor imaging geometry and field of view aspects, the orbit control system, the power system, the attitude control system, and the data storage system. These five systems significantly influence the capability of the reconnaissance system regarding the feasibility and number of orders, geographical location of the targets, and system response time. As an example, Figure 2-52 depicts an image acquisition manoeuvre of a SAR reconnaissance system, showing the important coordinate systems. The satellite has to be manoeuvred from its nominal mode to the image acquisition location by pre-defined quaternion files considering the speed and acceleration constraints. The simulation of the manoeuvre allows the analysis, if the image coordinates have been hit by the SAR beam within the required constraints. These aspects are very important for platforms with reflector antennas and mechanical beam steering.

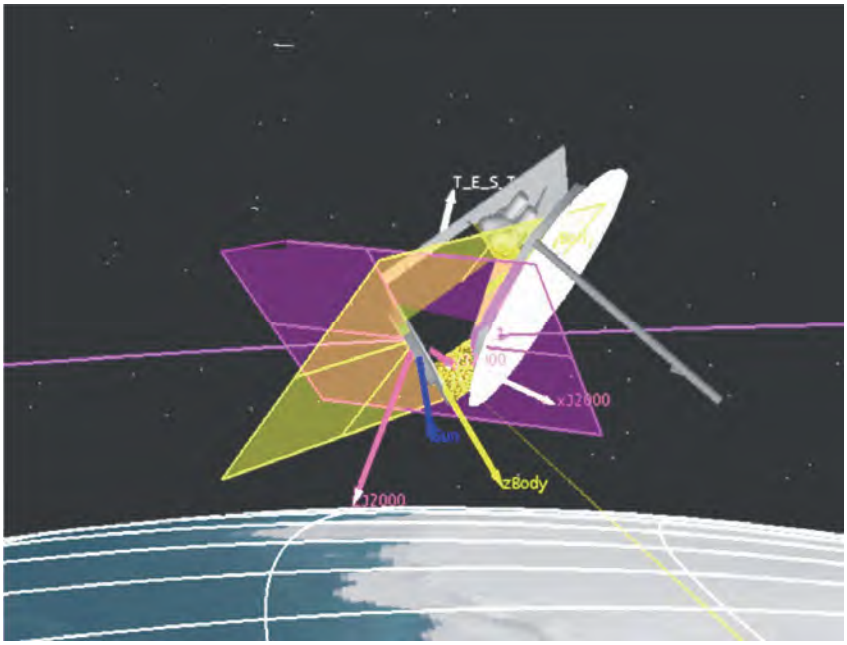


**Figure 2-52: Image acquisition manoeuvre of a SAR reconnaissance satellite with a reflector antenna simulated and analysed with the satellite simulator using a pre-calculated quaternion file.**

*Coverage Analysis Tool*

The coverage analysis tool contains several modules for the valuation of alternative mission concepts concerning complete sensor coverage aspects. The Coverage Analysis Tool was developed by the Institute and is based on the Microsoft Excel environment for the graphic user interface (GUI) in combination with interfaces to the mission simulator. The current version includes capabilities for analysis of orbit nodal drift aspects, latitude dependent coverage and especially, investigation of information age and the system response time which can be achieved for the image products from reconnaissance

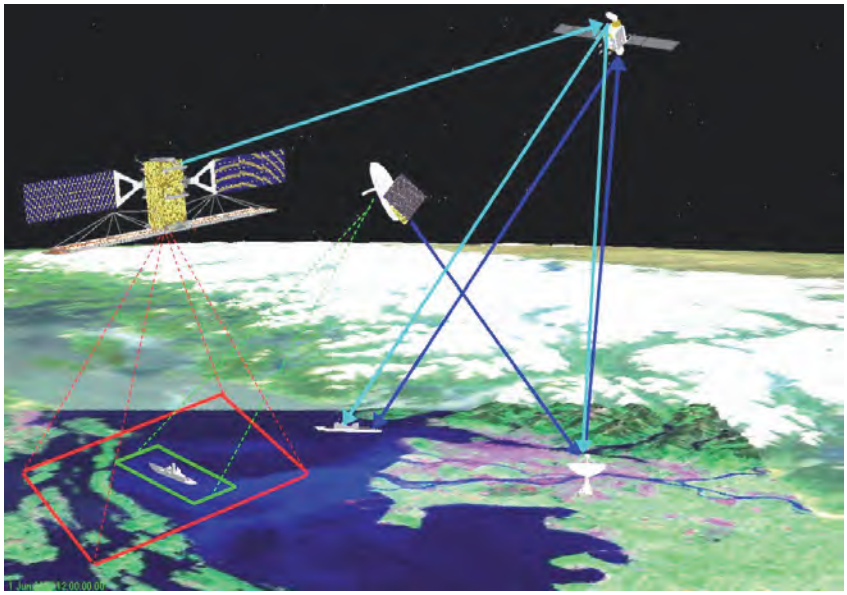

Figure 2-53: Ship detection: Multi-mission reconnaissance system consisting of Radarsat-2 and an additional high-resolution imaging system.

satellites. It is important for the validity of the calculated results that as much as possible operational constraints are considered, such as available satellite data storage, minimum time between two satellite target accesses and other user or satellite defined access restrictions.

**Simulation Example of a Multi-Platform Reconnaissance System**

The following example demonstrates the simulation of a multi-platform reconnaissance mission consisting of two satellite platforms with a SAR payload on each. In Figure 2-53 for example, the Canadian Radarsat-2 with a moderate spatial resolution detects an unknown ship near the coastline. The acquired image is transferred via a geostationary communication satellite to the ground station, where a SAR image is generated. The position and the velocity vector of the ship can be determined. A short time later after the analysis of the data, a high-resolution reconnaissance system is commanded to acquire an image with sufficient resolution for the identification of the ship, the determination of the technical characteristics and activities.

One of the main objectives of the ongoing developments of the mission simulator is to provide an automated, optimised mission planning and design tool for future multi-sensor reconnaissance missions and satellite constellations.

The developments will focus on a corresponding simulation tool and an operations plan optimiser. The corresponding boxes are marked blue in Figure 2-54).

This simulation module will contain new features, like an integrated sensor performance analysis tool with different constellation configurations, different target and mission scenarios and with the possibility to consider inter-satellite links for commanding, as well as for data transmission.

The operations plan optimiser will be a completely new developed module that extends the presently used first-in first-out (FIFO) planning method. It will allow the optimisation of multiple mission objectives and calculates optimal solutions driven by specific performance figures of merit e.g. the minimisation of system time response, the minimisation of the information age, the maximisation of the number of data takes in a given time span, etc.

These goals will be realised by modification and development of existing constraint satisfaction techniques to fit them to space operations planning and scheduling problems. Different optimisation techniques for constraint satisfaction optimisation problems will be compared, such as combinatorial optimisation approaches, deterministic and heuristic approaches, and genetic algorithms. These techniques will be realised in the operations plan optimiser module.

The final version of the mission simulator will be realised as an end-to-end simulation environment for reconnaissance systems. It will be used during system studies and development phases, system analyses and system realisation, and finally to support the system operations.

Figure 2-54: Work flow of the next generation mission planning tool.

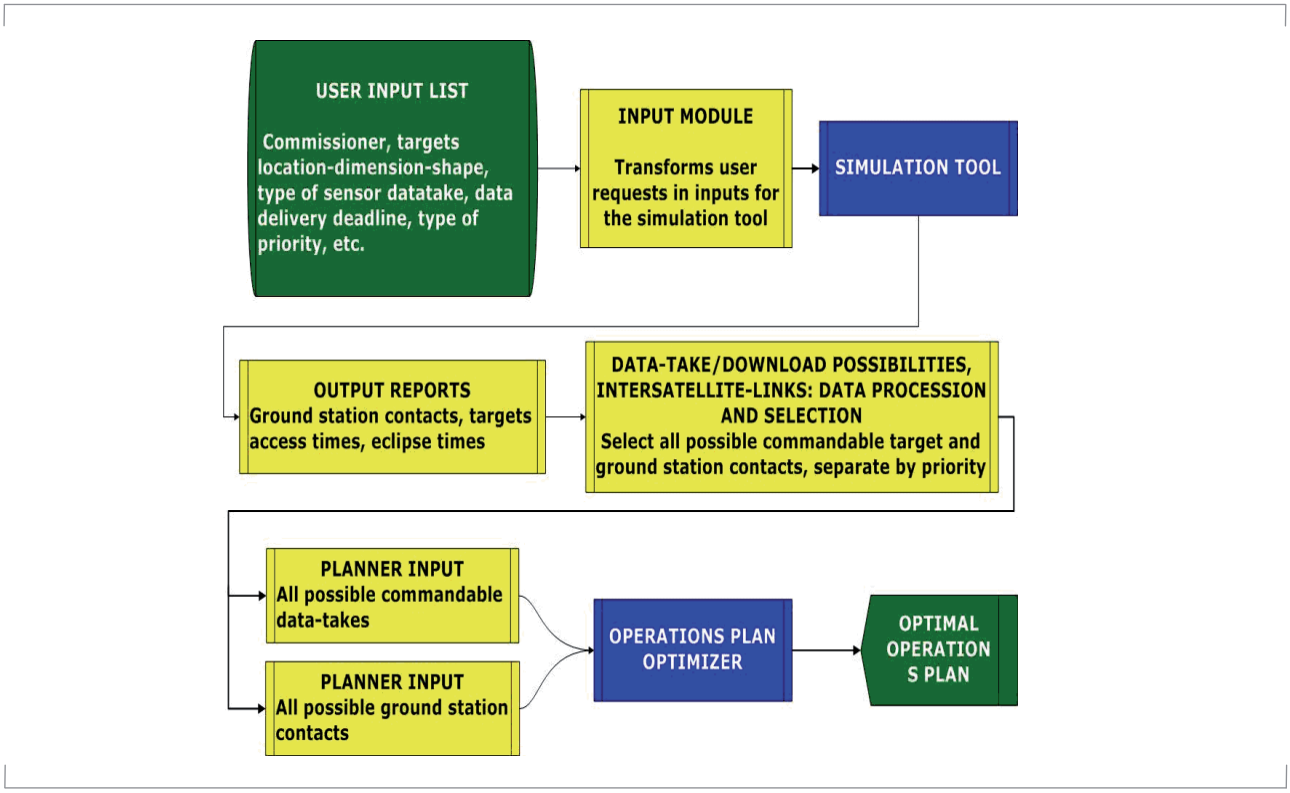

# The Institute Today

## Spaceborne SAR

## Airborne SAR

- Experimental SAR – E-SAR
- Polarimetric SAR Interferometry
- Tomography
- The New Airborne SAR – F-SAR

## Microwave Systems: Research and Technology

## Institute's Personnel

# Airborne SAR


**Figure 3-1: E-SAR onboard DLR's Dornier DO228-212 aircraft touching down after a successful measurement flight (Photo: Courtesy of Renato Burkhart).**

**Figure 3-2: View inside the cabin of the DO228 aircraft. The racks are approximately 1.2 m high.**

**Table 3-1: E-SAR Technical Parameters**

| | X | C | L | P |
|---|---|---|---|---|
| **RF** [MHz] | 9600 | 5300 | 1300 | 350 |
| **Bw** [MHz] | 100 or 50 (selectable) | | | |
| **Sampling** | 6 or 8 bits, complex (I and Q) | | | |
| **Data rates** | 8 or 16 MByte/s (selectable) | | | |
| **Rg res.** [m] | 2 or 4 (selectable) | | | |
| **Az res.** [m] | 0.25 | 0.3 | 0.4 | 1.5 |
| **Rg cov.** [km] | 3 or 5 (selectable) | | | |

## Experimental SAR E-SAR

E-SAR identifies the DLR airborne Experimental Synthetic Aperture Radar system, which is operated by the Microwaves and Radar Institute in cooperation with the DLR flight facilities on-board a Dornier DO228-212 aircraft. Being developed in the Institute, E-SAR delivered first images in 1988 in its basic system configuration. Since then the system has been continuously upgraded to become what it is today: a versatile and reliable workhorse in airborne Earth observation with deployments worldwide.

The DO228 is a twin-engined short take-off and landing aircraft. The landing strip must have a minimum length of about 900 m. The cabin is not pressurised. It can carry up to 1000 kg of payload. Special modifications (28 VDC and 220 VAC instrumentation power supply, hardpoints, bubble windows, circular mounts in the roof, and a hatch with a roller door) make it ideal for scientific instrumentation. The operational costs are comparatively low.

The maximum operating altitude with E-SAR onboard is about 6000 m above sea level. For SAR operation, the ground speed ranges from 140 kt to 200 kt. Depending on the SAR configuration, the endurance varies between 2.5 and 4 hours.

E-SAR operates in 4 frequency bands (X, C, L and P-band) - hence it covers a range of wavelengths from 3 to 85 cm. The polarisation of the radar signal is selectable, horizontal as well as vertical. In polarimetric mode the polarisation is switched from pulse to pulse in a HH-HV-VV-VH sequence.

E-SAR offers high operational flexibility. The measurement modes include single channel operation, i.e. one wavelength and polarisation at a time, and the modes of SAR interferometry and SAR polarimetry. The system is polarimetrically calibrated in L and P-band. Single-pass SAR interferometry is operational in X-band (XTI and ATI). Repeat-pass SAR interferometry in combination with polarimetry is operational in L- and P-band.

A real-time D-GPS/INS System (IGI CCNS4/ Aerocontrol IId) combined with a FUGRO OmniStar 3000L D-GPS receiver allows most precise navigation and positioning. E-SAR is hence able to generate geocoded image products of very high geographical precision.

Repeat-pass SAR interferometry at baselines of less than 10 m is possible, allowing the realisation of advanced and innovative techniques like Pol-InSAR and tomography, as well as coherent change detection.

Part of the system is the operational E-SAR ground segment. After transcription from HDDC (SONY SD-1) to hard disk drive, the E-SAR Extended Chirp Scaling (ECS) processor converts

the SAR raw data to calibrated image data products. To increase the product quality level to CEOS level 1b, radiometric and polarimetric calibration, DEM generation and geocoding are operationally implemented. Finally, the ground segment is completed by DLR's DIMS archiving system and the EOWEB internet portal, which provides an user access point.

For calibration, 12 trihedral radar corner reflectors are set up on the former Kaufbeuren military airfield and six in the neighbourhood of the DLR Oberpfaffenhofen research centre. Their size varies between 0.9 m and 3 m leg length. The geographical positions of their phase centres are precisely known.

Since many years, E-SAR has been heavily used for SAR experiments and measurement campaigns. It has evolved to be an important tool for SAR research and applications in Europe. A number of scientifically and technically important SAR missions and projects which were executed in recent years with great success are summarised later in this chapter.

Many questions could be answered in the past. However, new challenges have come up requiring new solutions. The Institute is developing a new airborne SAR facility identified as F-SAR (described at the end of this chapter). F-SAR will have enhanced measurement capabilities, such as simultaneous full-polarimetric measurements at four wavelengths (X, C, L and P-band). It will also offer simultaneous X- and S-band single-pass polarimetric interferometry.

While F-SAR is in the building phase, E-SAR is still maintained and used for campaigns. Minor upgrades are implemented to cover immediate scientific needs such as those for TerraSAR-X.

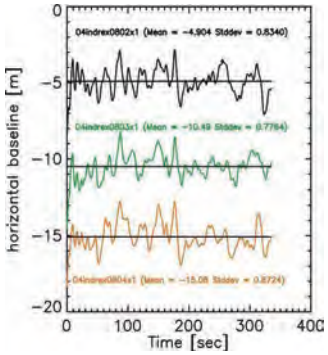


**Figure 3-3: Repeat-pass SAR interferometry baselines achieved during the INDREX-II campaign in Indonesia. Example for the precision of in-flight track maintenance. Three consecutive passes of about 6 minutes duration each flown with a nominal baseline of 5 m. Deviations of less than 1 m (rms) for each of the 3 passes were achieved.**

**Figure 3-4: The new DLR airborne SAR calibration site at Kaufbeuren, Germany: A former military airfield. Corner reflectors (purple) aligned with the runway. Radar Geometry Image Product (RGI) example: E-SAR L-band, fully polarimetric, high resolution. HH (red), HV (green), VV (blue). Image size: 3 km ground range, 7.5 km azimuth.**

**Processing Algorithms**

Synthetic Aperture Radar systems, in particular airborne SAR, require sophisticated signal processing in order to obtain the desired information from the data. Spatial resolution as well as radiometric and interferometric calibration accuracy have direct influence on the potential to measure or infer physical parameters.

As the E-SAR and F-SAR systems are often employed to experiment with innovative operating modes to establish new applications, the development of new algorithms to provide the new information and to improve the quality of the associated data products is an ongoing process.

In addition, the increasing amount of acquired and processed airborne SAR data poses strong requirements on efficient algorithm implementation. About 300-400 data takes per year were acquired during the last 8 years, corresponding in average to approx. 300-400 GB of raw data per year and the same amount of processed data products.

The E-SAR and F-SAR processors are based on an advanced SAR processing algorithm that was developed at the Institute.

The Extended Chirp Scaling (ECS) algorithm is able to accommodate the requirements posed by the high resolution, phase-preserving data processing and at the same time allows accurate motion error correction. All processing steps are performed without interpolation, as in the original version of the Chirp Scaling algorithm. The ECS processor has also been extended for the processing of ScanSAR and Spotlight mode data. This extension has been adopted for the operational processing of the TerraSAR-X satellite. Recently, also a dedicated processor for the innovative TOPS mode has been developed.

Linked to the requirements of high resolution and precise motion compensation together with the high number of flight campaigns abroad, the E-SAR processing software has been

**Figure 3-5: Fully polarimetric E-SAR image of Oberpfaffenhofen, incl. DLR facilities in image centre; composite obtained from two dual-polarized data takes in C-band (HH-green, HV-red, VV-blue), corner reflectors (light blue) aligned with the runway.**

extensively adapted to run on individual LINUX-PCs while accessing common data storage for the raw and processed data. During campaigns outside of Europe (India, Indonesia, and Tunisia) this concept allowed on-site data processing and quality checks.

The E-SAR processor provides the following operational products: Radar Geometry Image products (RGI) including polarimetric multilook and single look complex (SLC) data in slant range and ground range, Geocoded Terrain Corrected Data (GTC product), Digital Elevation Models (DEM product) and Repeat-Pass Interferometric Data (RP-InSAR product).

Dedicated software has been developed to segment long data takes, as acquired during INDREX, SVALEX, and ICESAR campaigns and to allow perfectly overlapping data products for a specific area (e.g. areas acquired at different frequency bands). For archiving purposes, each data product is ingested into the Data Ingestion and Management System (DIMS) of the German Remote Sensing Data Centre (DLR-DFD), allowing a world wide access via EOWEB (eoweb.dlr.de). In the last 8 years the algorithm development activities for the airborne SAR processor focused on the needs imposed by the Pol-InSAR and tomographic imaging modes as well as by differential and along-track airborne SAR interferometry. The processing software for the new F-SAR system keeps the main interfaces for product generation and archiving, but is optimised with respect to throughput and handling of large data volumes. In the following sections some of the most important developments are described.

**DEM Generation**

Digital Elevation Models are one of the standard E-SAR products. However, large scale mapping is a challenge due to the small E-SAR swath width of only 3.5 km.

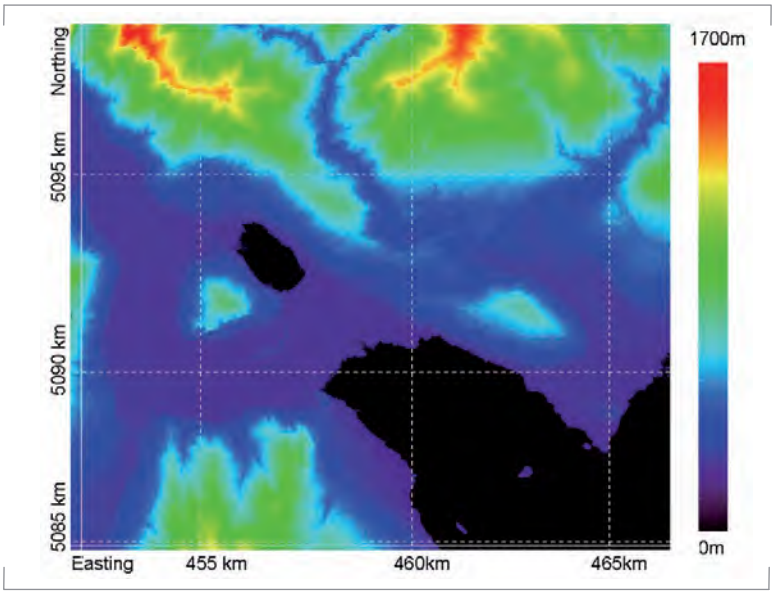


**Figure 3-6: Digital elevation model of the Lago Maggiore area near Verbania, Italy. Obtained from single-pass interferometric E-SAR data in X-band of 15 km x 15 km (WGS-84, UTM zone 32). No-signal areas are indicated in black: Lago di Mergozzo (small lake) and parts of Lago Maggiore (lower left corner) with three islands.**

Therefore, a mosaicking procedure is used to generate large area DEMs. With the opportunity of data acquisition near Lago Maggiore (Italy), the mosaicking procedure was extended to incorporate iterative topography adaptive compensation of residual motion errors.

An elevation model covering an area of 15 km x 15 km was generated from 15 different tracks. Horizontal posting is 2 m and the height accuracy is better 2 m rms (> 5 m rms on steep slopes). Total height variations about 1500 m. Black areas correspond to areas where no signal information is available (e.g. lakes).

**Airborne Repeat-Pass SAR Interferometry**

A dedicated processing chain for repeat-pass SAR interferometry was implemented, demanding high complexity in the algorithm developments.

Accurate processing is a precondition to obtain high quality Pol-InSAR data products as input to the model-based

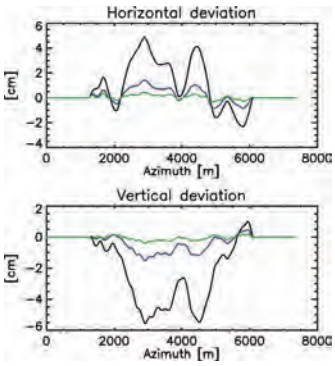


**Figure 3-7: Residual track errors measured and corrected by the repeat-pass processing approach. Almost perfect compensation is reached after 3 iterations, corresponding to a correction of residual motions errors to millimetre accuracy.**

inversion approaches. The performance of standard airborne SAR processing is limited by the accuracy of the navigation data available to perform the motion compensation (state-of-the-art is a combination of inertial and GPS sensors).

Although the relative accuracy is very good, enabling well focused data, the absolute performance is limited by the absolute precision of the differential GPS signal, which is in the order of 5-10 cm (approx. one interferometric phase cycle assuming SAR data at L-band and the two-way propagation delay). It is obvious that this accuracy is insufficient for repeat-pass interferometry.

A robust error estimation approach was developed based on the so-called multi-squint technique. Residual errors (in horizontal and vertical directions) between the two tracks of the interferometric acquisitions are iteratively estimated from the processed interferometric SAR data using special algorithms. The original residual track errors are in the order of 3-5 cm and are in accordance with the accuracy of the navigation system based on differential GPS and INS. Without this compensation approach, phase errors and coherence degradations would occur, which have strong impact on the interferometric data quality.

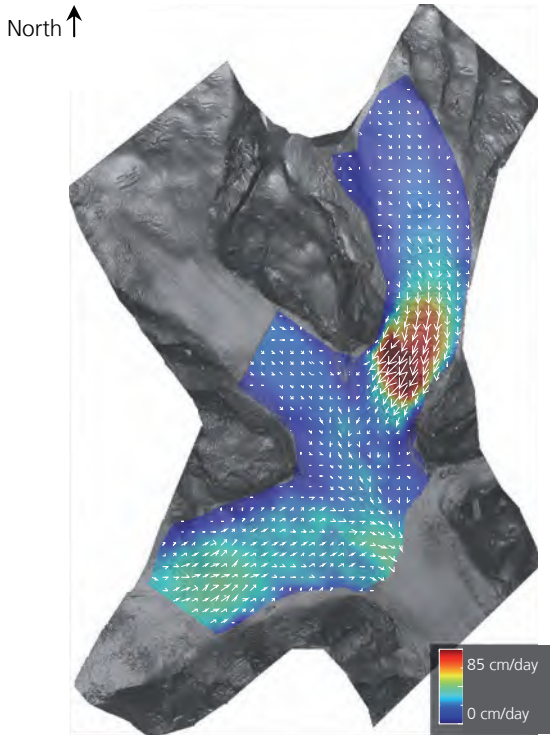


**Figure 3-8: Estimated surface velocity field over the Aletsch glacier after one day interval. Displacements range from 0 to 85 cm per day.**

### Topographic Motion Compensation

During the development and refinement of the airborne repeat-pass processing strategy it was recognised that the usual approximations for motion compensation are not sufficient and that topography needs to be taken into account very precisely. This led to the development of new algorithms for topography and aperture dependent motion compensation. They are based on short time FFT codes and thus make effective use of the quasi-linear azimuth time-frequency correspondence of the SAR signal. Its application is imperative, not only for processing airborne data in differential SAR interferometric mode, but also for repeat-pass SAR applications in hilly and mountainous areas in general.

### Airborne Differential SAR Interferometry

Differential SAR interferometry (D-InSAR) is an extension of SAR interferometry where changes of the Earth's surface in the order of a fraction of the wavelength can be detected. This awesome capability has been exploited to monitor different scenarios, like cities, volcanoes, earthquakes, or glaciers, among others. Typically, it is performed with satellite-borne sensors, as their stable trajectory allows the interferometric processing with high precision. However, in the

airborne case one has to deal with motion instability which complicates the processing if high precision products are required. Thanks to the aforementioned algorithms, capable of dealing with the inaccuracies of the navigation system and with topography, first D-InSAR results with an airborne platform have been achieved by the E-SAR system.

An example of an airborne D-InSAR product is given in Figure 3-8 which shows the surface velocity field (SVF) of the Aletsch glacier, located in the Swiss Alps. The data were acquired at L-band within the SWISAR campaign in 2006 on two consecutive days. Despite the short time span, the glacier has moved almost one meter in some areas. The MEGATOR campaign, carried out in 2007 over the Argentière and Mer de Glace glaciers in the French Alps, was also successful, hence proving the flexibility of the E-SAR system to monitor temperate glaciers.

**Traffic Monitoring**

The E-SAR and F-SAR systems use small antennas in order to avoid a gimble-based antenna steering configuration. This leads to an azimuth signal with a very high bandwidth requiring a correspondingly high PRF value.

During processing, usually only a small portion of the azimuth bandwidth (ca.150 Hz) is needed to obtain comparable resolutions in azimuth and range directions. The availability of a very high azimuth bandwidth (approx. 900 Hz at X-band for E-SAR and up to 2500 Hz for F-SAR) is beneficial for monitoring moving targets using the along-track interferometric mode, as the signal energy might be shifted outside the narrow azimuth bandwidth of conventional processing. Therefore, full azimuth bandwidth processing is required to allow MTI with sufficient accuracy. E-SAR data were used in support of the TerraSAR-X GMTI processor development.

Future work in the next two years will be focused on the further development of specific algorithms for the new airborne system F-SAR. Challenging scientific topics currently being investigated are related to airborne differential SAR interferometry and airborne SAR tomography. In addition, signal processing techniques for circular flight geometries and interferometric radar sounding applications will be developed. Finally, further processing algorithms are planned for the next years to enhance moving target indication in near real-time onboard using the new airborne F-SAR system.

## Major Campaigns

In the period from 1998 to 2008 approximately 80 E-SAR airborne SAR campaigns were performed, leading to an average of approx. 10 campaigns per year. About one third of the campaigns were dedicated to research topics (e.g. new operation modes and/or applications), another third to system tests and hardware developments. The remaining third were performed in standard operation modes.

The main objectives of the airborne flight campaigns are:

- Development of innovative SAR modes or operation configurations
- Development and demonstration of novel techniques and new applications
- Preparatory experiments for future SAR satellite systems, supporting the data product development as well as system specification.

Although E-SAR was originally intended to be an experimental system, today it has a high degree of operationalisation and is a reliable source of high-quality radar data for a large user community world wide.

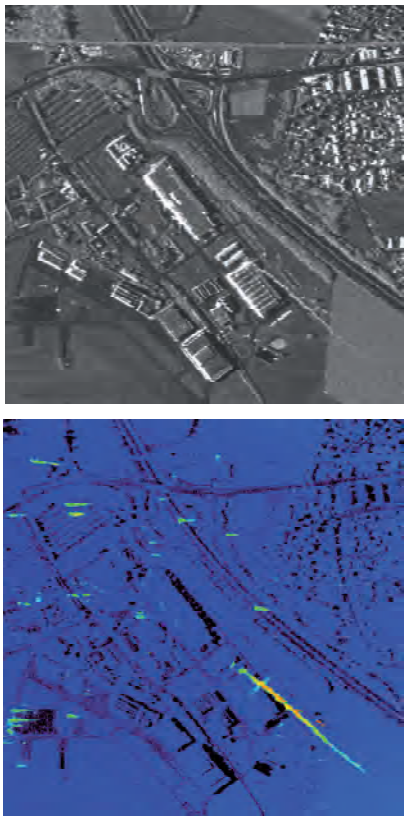

**Figure 3-9: Full azimuth bandwidth E-SAR image in X-band (above) and corresponding along-track interferometric phase. Blue colour corresponds to zero phase and represents the stationary targets. The presence of moving targets is shown in green, yellow and orange colours.**

Figure 3-10: E-SAR campaigns in Europe including the Baltic Sea near Spitsbergen, Tunisia, India and Indonesia. Red: Sea ice and land ice applications, Green: Forest applications, Yellow: Agricultural applications, Blue: Sea bottom topography and oceanography.


Figure 3-11: E-SAR test site locations across Europe. Black stars: E-SAR campaigns for TerraSAR-X and TerraSAR-L simulation. Orange circles: other campaigns.

The E-SAR campaigns are performed for different interested parties, for SME companies, universities, research institutes, as well as for European and international agencies. Approximately 70% of the campaigns performed during a year are financed through external contracts and 30% through internal DLR research funds.

With the large number of flight campaigns, a wide range of applications is covered, from areas being cartographically imaged with standard high-resolution X-band modes (with the radiometry being corrected for the terrain topography using digital surface model information), to higher quality environmental application products, for example forest height being derived from L-band polarimetric SAR interferometry.

The main application areas until now have been cartography, geology, forestry, agriculture, snow studies, glaciology (land and sea ice), urban areas, bathymetry, monitoring, and surveillance. The geographical distribution of the executed campaigns ranges from Germany to European countries as well as to South and South-East Asia and Africa. Examples of campaigns performed outside of central Europe in the last 8 years include campaigns in India, Indonesia, Svalbard, and Tunisia. In these cases the flight range of the aircraft has been a limiting factor, such that for India and Indonesia the E-SAR system had to be transported separately and installed in the aircraft just prior to the flight campaign.

All calibration and system test flights are performed close to the DLR location at Oberpfaffenhofen.

Since 2001 the Institute is following a strategy in which the data acquisitions each year are dedicated to a specific thematic research topic associated with one extensive flight campaign in order to be able to answer urgent scientific

questions. A few major campaigns of the E-SAR system, their objectives and particularities as well as first results are presented in the following.

**E-SAR Mission Highlights**

**1998**. The first demonstration of SAR tomography has been carried out at L-band. E-SAR recorded data on 14 parallel tracks over the Oberpfaffenhofen test area. As a result of the tomographic processing a height resolution of 3 m was achieved. Different backscattering mechanisms can be separated using the Pauli decomposition. The strong contributions from volume scatterers from the tree crown are clearly visible as well as the dihedral scattering and surface contribution.

**1999 – 2002**. The European space industry as well as the European Space Agency required SAR data to simulate future TerraSAR-X and TerraSAR-L data products. For the projects PROSMART, ISOCROP, TerraDEW, and Dual-band SAR Simulation DLR's E-SAR was the source of multi-frequency, multi-polarisation data for a number of different product developments. Operating in various European countries, E-SAR collected data for application to agriculture, forestry and urban planning, areas which were identified as promising. Using E-SAR data, high resolution TerraSAR simulated data products have been produced and delivered to the customers for further analysis. In this context the Institute holds a leading position amongst all airborne SAR system operators in Europe.

**2003**. The first demonstration of airborne bistatic SAR imaging has been carried out in Europe. As part of a cooperation agreement between the Institute and ONERA, a bistatic SAR experiment employing the E-SAR and RAMSES airborne SAR systems was conducted. Technical issues such as time and frequency synchronisation of both systems were resolved and the experiments were successfully executed.

**Figure 3-12: OMEGA: Digital Elevation Model of Engabreen – the glacier tongue of Svartisen, Norway acquired at X-band using single-pass SAR interferometry. The height varies by approx. 1500 meters in this sub-image of ca. 2 km x 2 km.**

In May of the same year, X-band single-pass interferometric data were acquired in support of an EU project for development of an operational monitoring system for glaciers (OMEGA). The objective was to generate a 10 km x 10 km digital elevation model of the Engabreen glacier in Norway, which was compared with laser and GPS data. Although the radar backscatter and thus the SNR was relatively low due

**Figure 3-13: INDREX II: A 15 km-long wooden bridge installed for collecting ground measurements in the Mawas peat forest test site (Kalimantan, Indonesia, 2004).**

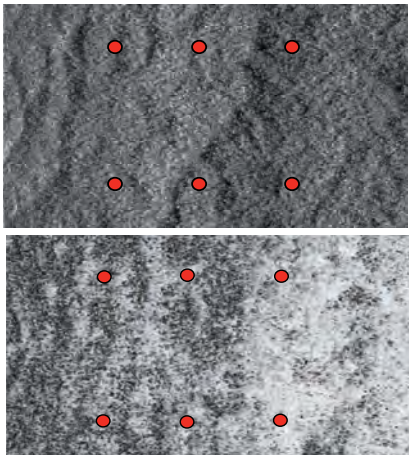

Figure 3-14: Radar backscatter (top) and interferometric coherence at L-band in HH polarisation over the hilly dense Dipterocarp forest of the Sungai Wain test site, Kalimantan, Indonesia. The red dots indicate sample locations investigated in unit circle plots (below).

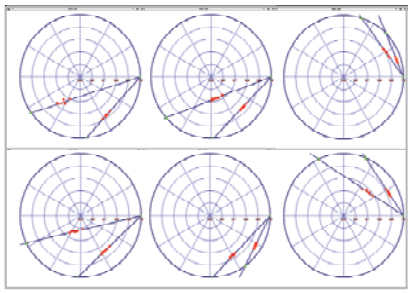

Figure 3-15: Complex coherence in L-band at different polarisations plotted on the unit circle for six sample plots (see red dots above) over the Sungai Wain test site, Kalimantan, Indonesia. The distribution of the red points along a line is due to the polarisation diversity of the ground contribution and to the random nature of the forest canopy at L-band.

Figure 3-16: INDREX II: Colour composite of three polarimetric SAR images in different carrier frequencies: RGB = P/X/L-band intensity images given as P-(HH+HV+VV)/3 / X-VV / L-(HH+HV+VV)/3. The image is geocoded (north at the top) in spatial resolution of 2 m x 2 m and depicts the Mawas test site with disturbed burned forest area (left: red) and a natural tropical forest (right: green).

to temperatures much above the melting point, successful computation of the DEM was possible, including the mosaic of several swaths.

Subsequent comparison with the laser data (obtained 4 weeks later due to continuous cloud cover) revealed an accuracy of approx. 2 m (rms value, peak-to-peak value of 4.2 m with an offset of +0.1 m) of the complete area of interest.

**2004**. From July to December 2004 the first two E-SAR campaigns in Asia, namely in India and Indonesia, were carried out. The first campaign was conducted by the Institute and the Indian Space Research Organisation (ISRO) during the post-monsoon season. E-SAR was successfully flown over arid regions, flooded, agricultural and open coal mining areas as well as sub-tropical forest regions across the Indian sub-continent. The data were processed and archived by ISRO/SAC, the Space Application Centre in Ahmedabad and are still under the authority of the Indian government. Extensive ground measurements were performed during the two months of data acquisition at P, L, C, and X-band.

Following India, the next campaign was performed in Indonesia, on Kalimantan. The objective of the INDREX-II campaign was to build up a SAR database over different tropical forest types with focus on L- and P-band polarimetric and interferometric data. The initiative for this campaign originated from the Pol-InSAR Workshop held at ESA/ESRIN in 2003. During this workshop the participating scientists identified gaps in the knowledge of SAR imaging behaviour in tropical forests. The main scientific question was to determine if L-band radar signals penetrate the dense tropical forest down to the ground and if the Random-Volume-over-Ground model is applicable in this case for the retrieval of tropical forest height measures.

Eight different forest types (example in were chosen for data acquisition on the ground and from the aircraft. More than 200 GB of raw data in 43 flight hours were acquired in polarimetric and interferometric mode and at different frequencies (X, C, L, and P-band). The length of the flight strips varied from 23 to 80 km. The E-SAR radar system was shipped separately from Germany to India and after the campaign in India to Kalimantan. Despite the high logistical effort - the transportation and integration of the radar into the aircraft, the system tests and system calibration on-site in India and Indonesia - no major technical problems occurred during the entire campaign. The overall time schedule could be followed without major delays, thus achieving all campaign objectives. All requested data could be collected with high radiometric quality and high precision in-flight navigation.

The INDREX-II data were processed and delivered to ESA, which is responsible for the distribution to the European scientific community, in 2005. The scientific questions posed at the beginning could also be answered by the detailed data analysis. Plotting the complex coherence of a selected data set at different polarisations on a unit circle shows that the loci of the coherence values (red points) are distributed along a line. This is an indication that L-band is penetrating the dense volume down to the ground. The different coherence loci would cluster at one point or would not be matched to a line, if this was not the case.

In a second step, tropical forest heights were successfully derived from Pol-InSAR data at L- and P-band. For both frequencies a similar forest height distribution has been obtained. In a first-order analysis the Pol-InSAR derived heights correspond very well to the forest heights estimated on ground. This campaign and the obtained results certainly deliver an important contribution for the future development of SAR satellites in Europe devoted to the monitoring of forested areas and their above-ground biomass.

A first demonstration of the Pol-InSAR technique using spaceborne systems was successfully performed with the PALSAR L-band instrument on-board the Japanese ALOS satellite within the Kyoto and Carbon initiative.

**2005**. Major campaigns were carried out in the Arctic and North Africa. Svalbard was selected as the ideal location for a joint DLR and AWI (Alfred Wegener Research Institute) campaign over sea and land ice (SVALEX). Two instruments were flown, the E-SAR on DLR's Do228 D-CFFU and the meteopod, laser altimeter, line scan camera and surface temperature instrument on AWI's Do228 D-CAWI.


**Figure 3-17: SVALEX 2005 – The two Do228 research aircrafts D-CFFU of DLR (left) and D-CAWI of AWI (right) at Longyearbyen airport in Svalbard. Instruments flown: E-SAR on D-CFFU and the Meteo-Pod, laser altimeter, line scan camera and surface temperature instrument on D-CAWI.**

The mission objective was to gain knowledge of the land ice volume and the sea ice structure using mainly Pol-InSAR techniques at X-, L- and P-band. In addition, a first ice sounder experiment at P-band with the E-SAR system was performed with different baselines by means of close nadir-looking antenna geometry.

Despite the arctic climate conditions in early April with temperatures below -20°C the campaign could be performed successfully; all planned data were collected and are in the process of being analysed. This campaign was funded by

**Figure 3-18: Colour composites of polarimetric radar backscatter (RGB = HH-HV-VV): Sea ice (left) and land ice (centre: L-band, right: P-band). The centre and right image correspond to the same area. Note the different features in the P-band image showing the very good penetration of the P-band signal in land ice.**

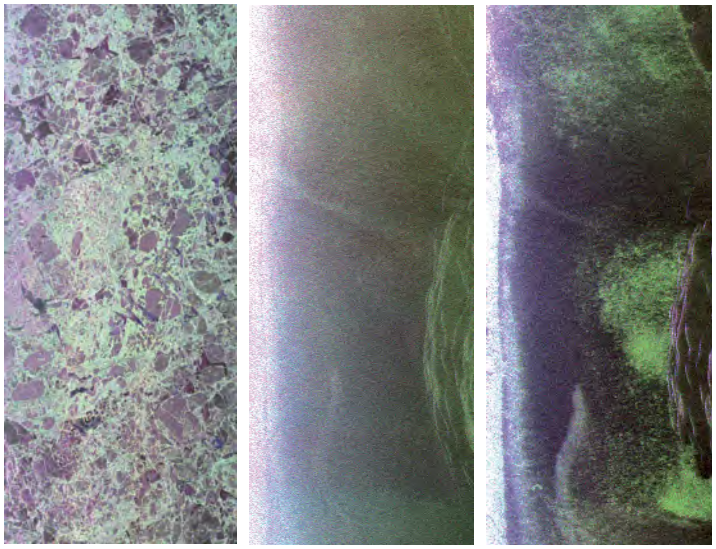

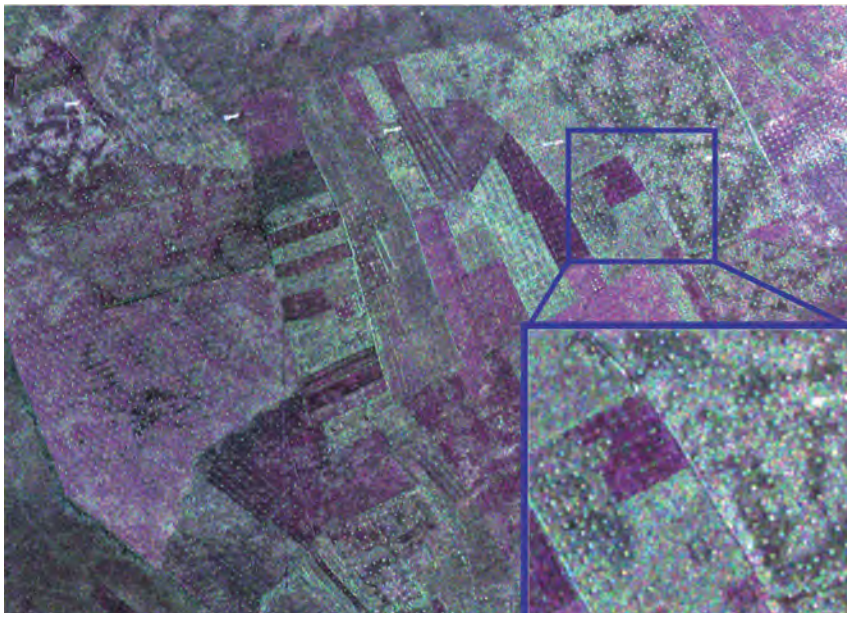

Figure 3-19: AQUIFEREX – Acquired image in C-band (RGB = HH-HV-VV polarisation) over the Ben Gardan test site in South-East Tunisia. Different irrigated fields are visible. The dots on some of the fields are regularly planted olive trees (zoom).

Figure 3-20: AGRISAR – Collection of instruments used for the validation of derived Radar and Optical data on the Demmin test site of the AGRISAR campaign.

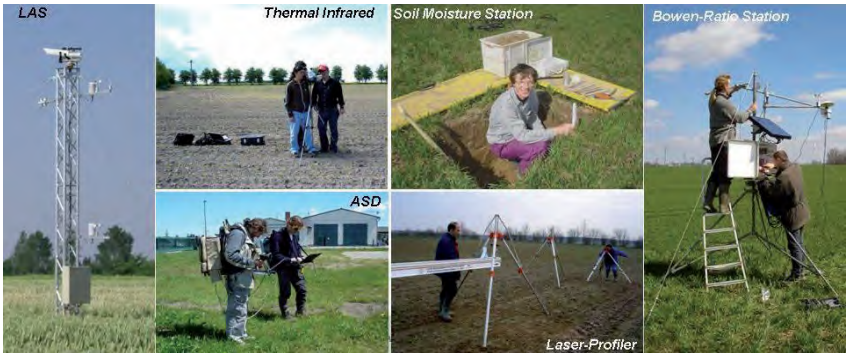


DLR in preparation for the polar year in 2007-2008 as well as for the upcoming satellite systems dedicated to Arctic and Antarctic applications (e.g. Cryosat).

AQUIFEREX was an ESA funded campaign that took place in Tunisia in November 2005. The key issues of the project were to support national authorities and international institutions with Earth Observation-based technology to better manage internationally-shared water resources and aquifers. E-SAR successfully collected X, C and L-band data. At the same time AVIS, an optical system of the Ludwig-Maximilians-Universität of Munich, recorded multispectral images. Synergetic analyses of the collected data showed a high potential for physical environmental parameter estimation, as surface soil moisture and the data have been made available for further investigations as part of ESA's AQUIFER project (an ESA TIGER demonstrator initiative).

**2006**. The year 2006 was dedicated to build up a SAR data base for agricultural vegetation and surface parameter estimation over entire vegetation period (acquisition time of four months, April to August). For this purpose a test site in Northern Germany was chosen that had near ideal conditions, with huge fields up to 25 ha and a long-term acquisition program with 12 weather stations in the surrounding area. The AGRISAR campaign was funded by ESA to support space segment activities with respect to the GMES / Sentinel Programme to address open questions concerning system constellations (single, dual, quad polarisation, revisit time, etc.).
15 Institutions with approximately 60 persons were working on-site collecting ground vegetation and surface data that could be useful for airborne data interpretation. This campaign supports the scientific community in developing model and inversion algorithms for parameter estimation.

**2007**. In 2007 the main focus was dedicated to ice applications. The importance of understanding slow and fast changes of glaciers and sea ice processes is essential for understanding climate change. In the frame of the ICESAR campaign that contributed to the performance analysis and definition of future satellites such as CryoSAT-2, Sentinel-1 and BIOMASS ESA supported a radar campaign to the arctic region. The main objectives of this campaign were to acquire radar and optical data over sea and land ice. Three different test areas for sea ice were chosen inferring different ice types, whereas for

the land ice two defined areas were chosen that are also part of the CroySAT-2 long-term validation program. The land ice test sites are located on the Island Nordauslandet on the Austfonna ice cap. Each test site covers an area approximately 12 km long and 3 km wide. One is located directly on the summit of the ice cap and the other on the lower part of the glacier. They are characterised by homogenous and heterogeneous areas in terms of topography. The same test areas were chosen as in 2005 in order to compare image results for a temporal baseline of two years. Not only long-term change but also short-term change was intended to be mapped. Therefore, with a temporal baseline of one month a second data acquisition campaign over land ice was performed (March and April 2007). The data were acquired at X, C, L and P-band and also with different interferometric baselines. In addition a P-band sounder experiment over the same test site was performed. For calibration and flight track reconstruction purposes during the first land ice campaign two DLR researchers installed 6 corner reflectors (1.5 m and 90 cm blade length) distributed over the test sites and operated a differential GPS. During the second campaign a team from the CryoVEX campaign monitored the corner reflectors and recorded the differential GPS signals. The complete data set is available over the ESA data portal. The campaign was executed in collaboration between DLR, AWI, and ESA.

Combined with ICESAR, a second campaign dedicated to forest parameter estimation was executed – BIOSAR 2007. The area of interest was chosen to be a well-managed forest that has a long record of intensive ground observations and is located in Southern Sweden – Remningstorp test site. The main objective of this campaign was to collect SAR data at L- and P-band over boreal like forest for above ground forest biomass and height estimation.


Figure 3-21: ICESAR 2007 – Airport of Longyerbyen with the two research aircrafts and air view of Svalbard seen from the aircraft (left) and the base station at Oxford where the differential GPS was operated (right), corner reflector installation at the summit and campaign executing team from AWI and DLR.

In particular the variation in time of the interferometric coherence was the main topic of investigation. In view of the goal data acquisition of short time differences of 15 minutes to long time variations of 56 days were performed. Data were acquired prior to and after the ICESAR, where the first flights were executed on the way to Svalbard in March, the second one on the way back to Germany at the beginning of April, and the third again coming back from Svalbard at the end of April. In addition to the temporal variation, the effect of bandwidth reduction in the spaceborne case from 100 to 6 MHz was also a main topic of investigation. To this aim satellite image simulations after data acquisition were performed. This campaign was supported by ESA in the frame of the Earth Explorer mission BIOMASS. The ground activities were performed in cooperation with FOI and SLU.

In the same year a smaller agricultural campaign – OPAQUE was executed in May over the Weisseritz Watershed with the objective to derive surface parameters as input for hydrological modelling. The campaign was performed

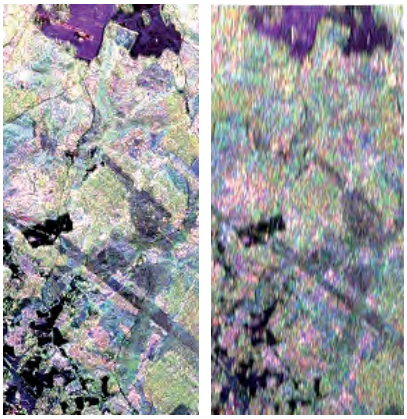

Figure 3-22: Fully polarimetric image in P-Band (RGB Pauli vector) of Remningstorp, Sweden. Left: 100 MHz, right: 6 MHz bandwidth.

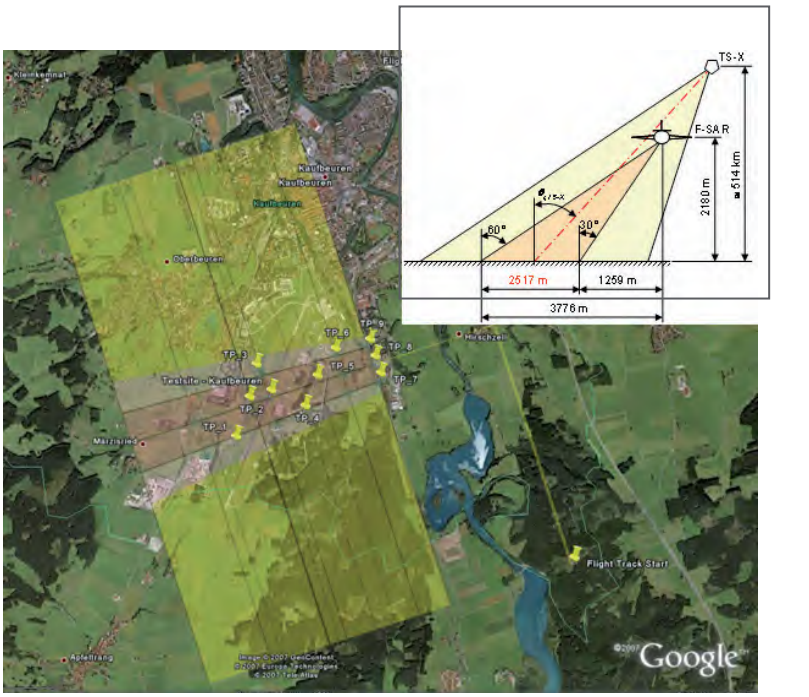


**Figure 3-23: Bistatic experiment between spaceborne and airborne SAR instrument – Mission planning with TerraSAR-X (yellow swath) and F-SAR (red swath) for a bistatic observation of TerraSAR-X signals using F-SAR as receiver. The yellow markers corresponding to deployed corner reflectors and transponders for radar signal validation.**

in cooperation with the University of Potsdam and GFZ. The main difference from the AGRISAR campaign is the test site with strong topographic variations and the use of longer wavelength (P-band) for a deeper penetration into the soil surface. Apart from measuring vegetation and soil parameters with conventional methods ground penetrating radar (GPR) was also used for parameter validation.

A first demonstration of a bistatic flight with the new airborne radar system (F-SAR) at X-band in combination with the TerraSAR-X satellite was successful performed in November. The TerraSAR-X satellite was transmitting and the F-SAR system received the raw signals. For validation purposes three corner reflectors were positioned at the Kaufbeuren airport, the main test site.

**2008**. One of the major campaigns in 2008 was the follow up of the boreal like forest SAR observations - BIOSAR 2008. The purpose of this forest campaign was to acquire data at longer wavelength over an area with mild relief using radar backscattering signal and multi-baseline polarimetric SAR interferometry. For this the test site Krycklan was chosen with a more boreal type of forest and a gentle topographic variations (location: 64 degree latitude North). The campaign was performed at the beginning of October acquiring one major flight strip with a length of approximately 12 km. Two smaller strips with a length of 4 km at 45° and 90° angles to this track were also collected to provide different viewing directions. Data analysis is still ongoing.

This year the first campaign in combination with a radiometer was also executed over agricultural fields for surface moisture estimation. In the frame of SARTEO a 200 km-long strip at the Rur watershed was acquired using L-band polarimetry in order to compare both derived soil moisture observations. The soil moisture algorithm for SAR is under development.

## Polarimetric SAR Interferometry

Today Polarimetric SAR Interferometry (Pol-InSAR) is an established remote sensing technique that allows the estimation of the 3-D structure of natural volume scatterers. Interferometric observables are highly sensitive to the spatial variability of vertical structure parameters and allow accurate 3-D localisation of the scattering centre. On the other hand, scattering polarimetry is sensitive to the shape, orientation and dielectric properties of scatterers and allows the identification and/or separation of scattering mechanisms of natural media.

In polarimetric interferometry both techniques are coherently combined to provide sensitivity to the vertical distribution of scattering mechanisms. Hence, it becomes possible to investigate the 3-D structure of volume scatterers and to extract information about the underlying scattering processes using only a single frequency polarimetric radar sensor. This promises a break-through in solving essential radar remote sensing problems. Indeed, structural parameters of volume scatterers in the biosphere and cryosphere such as vegetation height, structure, biomass and moisture, or snow and ice depth, layering and moisture, are critical inputs for ecological process modelling and enable monitoring and understanding of ecosystem change.

From the very beginning, the Institute developed the new technique of Pol-InSAR leading to expertise in sensor technology, system and instrument design and performance analysis as well as processing, modelling and inversion techniques. The Institute's E-SAR sensor was the first to demonstrate airborne polarimetric repeat-pass interferometry at L- and P-band - initiating the development of Pol-InSAR technology in Europe.

In the following, an overview of the activities, advances and achievements in Pol-InSAR techniques and applications developed over the last 8 years is provided.

**Forest Applications**

Across the different application fields, the maturity of Pol-InSAR applications is very diverse. Forest applications are by far the most developed and a success story. The analysis of the first Pol-InSAR data provided by the SIR-C/X-SAR mission indicated the potential of combining polarimetry with interferometry for forest applications. As a next step, the Institute developed the sensor technology and processing expertise to acquire and process Pol-InSAR data with the E-SAR system in a repeat-pass interferometric mode.

In addition, theory, modelling and inversion techniques have been addressed and advanced in close cooperation with international partners. Early airborne experiments in the late 90s have found their continuation in a series of successful Pol-InSAR demonstration campaigns across Europe performed in cooperation with academic and commercial institutions providing in situ forest expertise. These have culminated in INDREX-II – a large-scale airborne experiment sponsored by ESA for the demonstration of Pol-InSAR techniques in tropical forest environments. The airborne campaign BIOSAR 2007, for the investigation of temporal decorrelation from zero to 56 days, and BIOSAR 2008, for the investigation of the effect of topography on forest-biomass estimation, both over boreal-like forests, were supported by ESA in the frame of the Earth Explorer programme for the selected mission BIOMASS.

Today, several model-based forest parameter inversion approaches, which combine dual or fully polarimetric data with single or multiple baseline interferometric measurements have been proposed, discussed and validated as part of several ESA-funded R&D studies. The main forest vegetation parameters that can be potentially estimated from polarimetric and interferometric data inversion are described below.

*Forest height* is one of the most important parameters in forestry along with basal area and tree species or species composition. Being a standard parameter in forest inventories, forest height is difficult to measure on the ground and typical estimation errors are given with 10% accuracy yet increase

**Figure 3-24: BIOSAR 2008 mission planning – Flight strips over a part of the Krycklan forest area, Sweden. Multi-baseline flights in L- and P-band (dark blue) and a smaller part of the test site additionally observed in viewing angles of 45 and 90 degrees (light blue) with L- and P-band for polarimetry.**

**Figure 3-25: Boreal forest at the Krycklan test site in mid Sweden (above) and a meshed corner reflector with side length of 5 m deployed at the test site (below).**

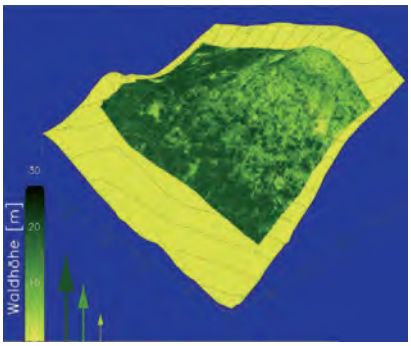


Figure 3-26: Example of the estimation of forest height using airborne Pol-InSAR data in L-band. Perspective view of forest height and topographical variation (Test site: Fichtelgebirge, Germany). Validation results are shown below.

with forest height and density. It describes dynamic forest development, modelling and inventory. Forest height estimation from polarimetric single and multi-baseline data has been demonstrated in a series of airborne experiments over a variety of natural and commercial as well as temperate and boreal test sites characterised by different stand and terrain conditions. The validation indicates an estimation accuracy on the order of 10-20% compared to the forest top height. The estimation performance is widely independent of terrain and/or forest conditions. The results from INDREX-II verify the inversion performance at L-band (and at P-band) for dense tropical forest conditions.

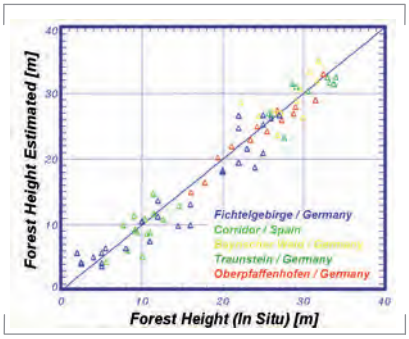


Figure 3-27: Pol-InSAR forest height validation over 5 European test sites representing a wide range of forest and topographic conditions.

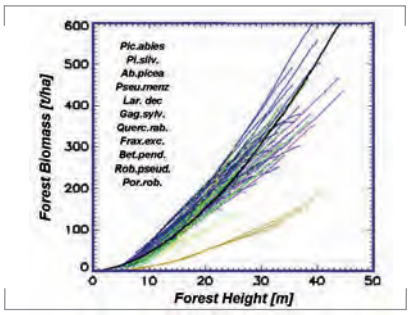


Figure 3-28: Forest height to biomass relationship for eleven most common European and North American tree species accounting for varying site and thinning conditions. It demonstrates that the allometric estimation of forest biomass from forest height is robust, does not saturate and is therefore a good candidate for above ground biomass inventory.

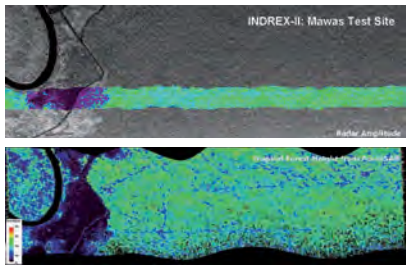


Figure 3-29: Tropical forest height maps from a peat swamp forest – obtained from Lidar measurements (top: coloured stripe) and by single baseline Pol-InSAR data inversion at L-band (bottom) in the framework of the INDREX-II experiment in Indonesia at the Mawas test site in Kalimantan.

Forest height is more than a single parameter in forestry application. It is used to characterise forest conditions. From a federal-funded large-scale experiment over the Traunstein forest from 2003-2008 changes in forest height through time could be observed and is an important indicator of stand condition.

*Forest biomass* is the most integrative forest parameter essential for ecological modelling and forest inventory and is today the largest unknown in global ecosystem change modelling. The development of forest height estimation in terms of Pol-InSAR initiated the development and evaluation of allometric biomass estimation schemes in collaboration with academic institutions with forest ecology and modelling expertise. Indeed, allometric estimation of forest biomass from forest height is robust and does not saturate and is therefore a good candidate for above ground biomass inventory. This very fundamental biological (allometric) relationship between forest height and forest biomass varies only about 10-15% with site conditions and only about 15-20% across species – exceptions are very fast growing pioneer species with very light woods such as poplar and birch. This makes the estimation of forest biomass even in inhomogeneous and natural forest conditions possible by only knowing forest height. The estimation accuracy varies between 20 and 40% up to biomass levels of 450 t/ha.

The achieved experimental results are in accordance with general allometric relations for different temperate, boreal and tropical forest ecosystems and with predictions of generalised forest structure models underlying the general character and thus the validity of the

height-biomass relationship. However, the largest uncertainties in the height-to-biomass relationship are due to density variations (natural or anthropogenic) especially in low density forest conditions, as present in boreal and savannah forest ecosystems. To reduce the biomass estimation uncertainty and increase the robustness of the methodology, the incorporation of additional information such as basal area becomes important, especially in low density, open canopy forest conditions and is still being investigated.

*Forest canopy* structure is a key forest ecosystem parameter. Regarding the estimation of forest biomass, vertical structure information is important as it allows a significant reduction of the biomass estimation error. However, the extraction of forest structure requires baseline diversity in addition to polarisation diversity in the observation vector. Dual and multi-baseline Pol-InSAR is a very promising configuration for the extraction of structure information and a new research topic in the field of polarimetric interferometry. In addition a new published method is investigated for vertical structure estimation using single baseline polarimetric coherence tomography (PCT).

Forest parameter (height and biomass) estimation from Pol-InSAR data has reached a pre-operational stage. As part of ESA's Pol-InSAR Mission and Application Study the actual state of Pol-InSAR techniques and technology has been evaluated and proven with respect to operational information product generation accounting for the technological constraints of actual and/or future satellite missions. Towards a first in-orbit demonstration of the Pol-InSAR technique the Institute is a member of the JAXA's ALOS Carbon & Kyoto Initiative and is responsible for Pol-InSAR forest parameter estimation. However, the temporal decorrelation limits the ALOS Pol-InSAR demonstration to favourable data sets only.

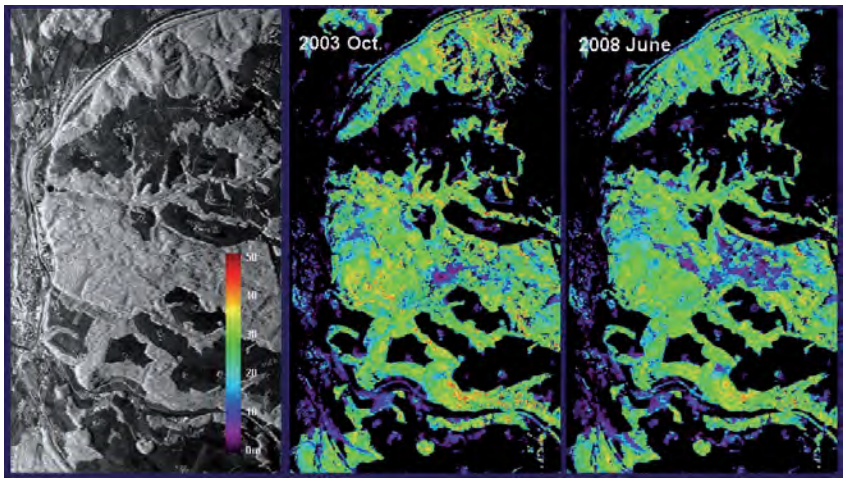


**Figure 3-30: Forest height monitoring – Radar backscatter (left), forest height in 2003 (middle) and in 2008 (right). The depicted forest heights range from 0 to 50 m (black to red). In the middle of the image a drastic change in forest height is observed caused by a strong storm in the beginning of 2007: *Kyril*.**

Aspiring to global monitoring, the wide spectrum of scientific and technological Pol-InSAR expertise developed within the Institute culminated in HABITAT, a European mission proposal for global above-ground biomass inventory and change monitoring submitted in answer to ESA's Call for Ideas for the Next Earth Explorer Core Missions in 2005. The selection was in favour of a P-band satellite mission, BIOMASS, where Pol-InSAR is used for the estimation of biomass through forest height.

**Agricultural Applications**

From the EM scattering point of view, agricultural scatterers can be divided into two categories:

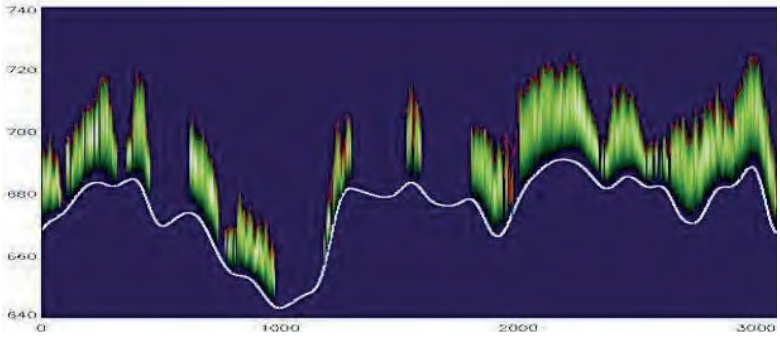


**Figure 3-31: Vertical forest structure profile derived from single-baseline data for the Traunstein forest in Southern Germany. The green variation represents the signal intensity at different heights on hilly terrain. It is the first result of a new published method for vertical structure estimation using single baseline polarimetric coherence tomography (PCT).**

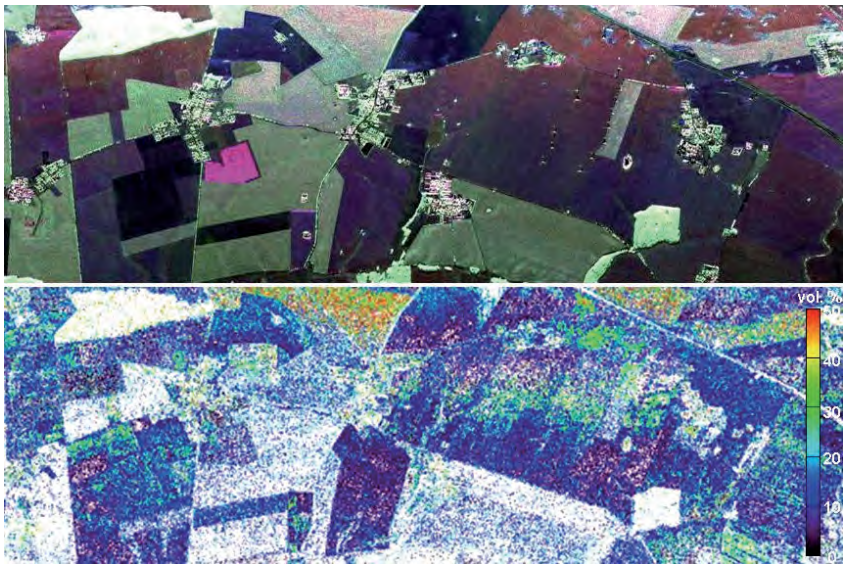


**Figure 3-32: Latest inversion result of soil moisture. L-band image (top) of a test site in Northern Germany, RGB image: HH+VV (blue), HH-VV (red), HV (green), and soil moisture map (bottom) derived from the coherent polarimetric X-Bragg model. The soil moisture ranges between 5 and 40 vol. % from blue to red. The data have been acquired as part of the AGRISAR project.**

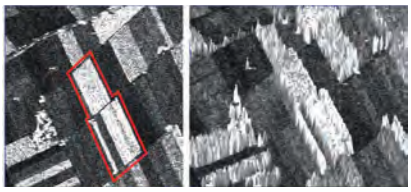

**Figure 3-33: SAR image (left) and 3-D height map (right) of a corn field retrieved from single-baseline Pol-InSAR data inversion. Test site: Küttighoffen, Switzerland.**

*Bare surfaces* are characterised by a direct surface interaction. In this case only the geometric and dielectric properties of the surface affect the scattered wave. Indeed, inversion of soil-moisture and roughness for fully polarimetric data has been further developed and validated while an alternative roughness inversion algorithm from Pol-InSAR data has been proposed.

*On vegetated surfaces* the waves first propagate through the vegetation layer and then interact with the underlying surface. Vegetation and surface scattering are superimposed. In contrast to forest vegetation applications, quantitative agricultural vegetation Pol-InSAR applications are still in an early phase of development. The significant differences in vegetation height, structure and attenuation values and in the propagation properties through the vegetation layer make the adoption of forest concepts for agricultural applications questionable and ineffective. Opposed to forest applications, where lower frequencies are an advantage, agricultural vegetation monitoring is rather a high frequency Pol-InSAR application – a fact that makes airborne repeat-pass demonstration a challenge.

Nevertheless, in the last few years dedicated airborne campaigns and indoor measurements provided the required initialisation for the development of dedicated agricultural applications:

*Vegetation layer height estimation:* The height of agricultural vegetation is an important input parameter for the estimation of crop biomass. Furthermore, monitoring of agricultural plant height at different stages of development allows direct measurements of crop health and yield. Early results demonstrated the potential of estimating height in the case of large differential extinction crop values (see Figure at 3-33).

*Extinction of the vegetation layer:* Density and water content of the vegetation layer affects the extinction of the forward propagating wave. As opposed to the forest case, the scatterers within the agriculture vegetation layer are characterised by an orientation correlation introducing anisotropic propagation effects and differential extinction. The extinction coefficient and its variation with polarisation are related to structural attributes such as the leaf area index (LAI) of the vegetation and orientation effects of vegetation structure. Furthermore, knowledge of the differential extinction is strongly related to the vegetation moisture content and this, in turn, is an essential parameter for agricultural cultivation management. First positive experimental results point towards a successful development of Pol-InSAR for agricultural applications.

*Moisture Content of the Underlying Surface:* Underlying surface moisture is significant for farming optimisation and predictive hydrological modelling. This importance combined with the absence

of an alternative remote sensing method for even rough estimation makes the inversion of the dielectric properties of the underlying surface a challenge. The potential of Pol-InSAR techniques is currently being addressed as part of an ongoing ESA-funded R&D study. A first attempt is to decompose different scattering mechanisms in order to extract the pure surface scattering mechanism and then to apply surface scattering models on this component for soil moisture inversion. A modified version of a polarimetric decomposition has been applied.

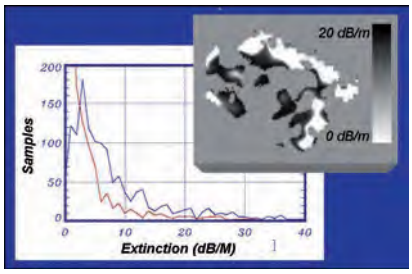


**Figure 3-34: Extinction estimates (red HH, blue VV) and spatial differential extinction distribution over a cornfield derived from Pol-InSAR data inversion (Test site: Alling, Germany). Knowledge of the differential extinction is strongly related to the vegetation moisture content and this, in turn, is an essential parameter for agricultural cultivation management. These first positive experimental results point towards a successful development of Pol-InSAR for agricultural applications.**

**Ice and Snow Applications**

The cryosphere is dominated by ice and snow scattering volumes. Admittedly, the understanding and development of Pol-InSAR applications with respect to ice and snow is currently at a very early stage.

First E-SAR airborne campaigns provided appropriate data sets initiating data analysis and leading to first results:

- A multi-baseline Pol-InSAR experiment in the Austrian Alps demonstrated that snow acts as a volume scatterer even at L-band and that there is a strong dependence of the interferometric coherence on polarisation. This is due to the strong underlying ground scattering component and is similar to the agriculture vegetation case. Local snow depths have been estimated.

- In 2005 and 2007, an extensive multi-frequency/multi-baseline Pol-InSAR experiment was flown in Svalbard, Norway, and was supported by ground measurements. The analysis and interpretation is ongoing. One of the first observations was that between these two years the ice volume structure changed.

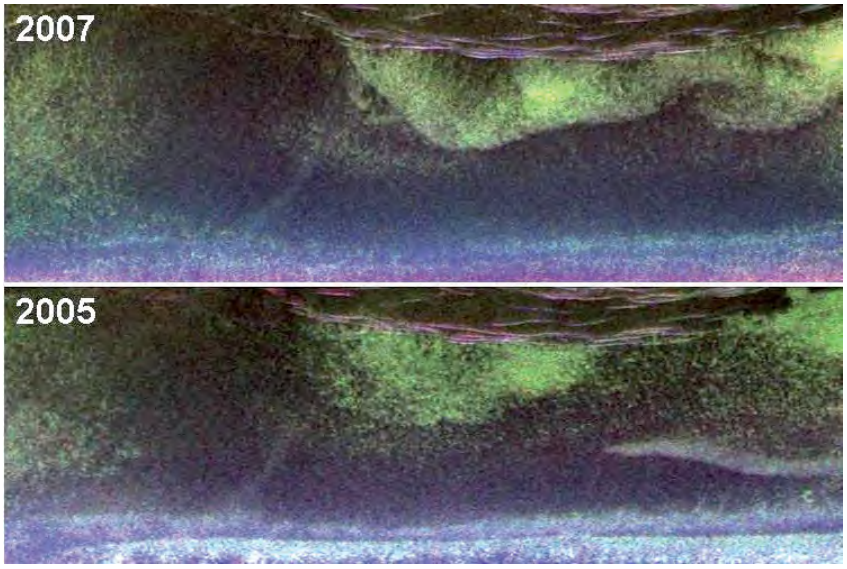


**Figure 3-35: Change detection between two years, 2005 (bottom) and 2007 (top) of data acquisition at P-band. It can be clearly seen that some ice features were changing during that time. The acquisition was made in the same month and same test area with a time interval of two years (test site Svalbard, Austfonna Ice Cap).**

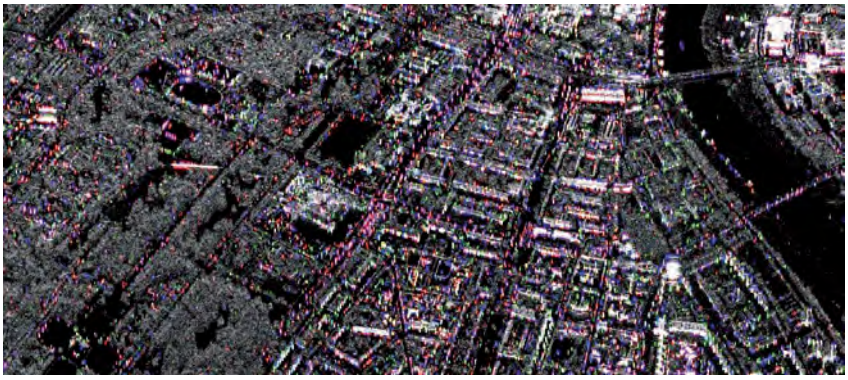

Figure 3-36: Coherent scatterers in the historical city centre of Dresden, Germany, at different polarisations: HH (red), VV (blue), HV (green), right: river Elbe.


Figure 3-37: PolSAR Pro – A polarimetric SAR data processing and educational tool – Version 3.0.


Figure 3-38: Scientific exchange: European conference on Pol-InSAR topics. Pol-InSAR Workshops 2003, 2005, 2007 and next year's 2009 organised by ESA at ESRIN comply with the rapid development in this field.

**Urban Areas**

One of the new Pol-InSAR applications recently proposed by the Institute is the identification and characterisation of point-like scatterers - so called coherent scatterers - in urban environments. Urban areas are not volume scatterers in the conventional sense but can be seen as a discrete vertical distribution of scatterers. Coherent scatterers are deterministic scatterers located at different heights within the "urban volume" and can be identified by using spectral correlation of individual or multiple images.

Accordingly, their localisation can be performed with a limited number of SAR observations, acquired with a short or even without a temporal baseline. The strong polarimetric behaviour of point-scatterers makes polarimetric observation diversity important for achieving large coherent scatterer densities. Figure 3-36 shows the first demonstration of coherent scatterers performed on L-band Pol-InSAR data sets acquired by the E-SAR system over the city of Dresden. The coherent scatterers are colour-coded according to the lexicographic polarimetric basis and are superimposed on the amplitude image.

After localisation of coherent scatterers, polarimetry furthermore allows the identification and description of scatterers in terms of canonical scattering processes (e.g. dihedral, surface, dipole type) and enables the characterisation of geometric and dielectric properties. There is a wide spectrum of potential applications for coherent scatterers ranging from polarimetric/interferometric calibration and urban DEM generation to information extraction from individual scatterers and change monitoring.

The rapid development of Pol-InSAR techniques combined with ESA's interest in coordinating the European activities and establishing a forum for scientific

exchange finally manifested in the Pol-InSAR 2003, 2005, 2007 and next year's 2009 workshops organised by ESA at ESRIN. The workshops assessed the state of the art in the field and formulated recommendations for algorithm development and new products, as well as future missions and applications. The Institute was involved in the scientific organisation of the workshops and participated with key contributions.

As a direct result of the recommendations made at the first Pol-InSAR Workshop, the *Polarimetric SAR Data Processing and Educational Tool* has been developed under ESA contract by a consortium comprising the University of Rennes 1, DLR and AEL Consultants. POLSARPRO aims to facilitate the accessibility and exploitation of multi-polarised SAR data sets. A wide-ranging tutorial and comprehensive documentation provide grounding in polarimetry and polarimetric interferometry necessary to stimulate research and development of scientific applications that exploit polarimetric data and techniques. All results of the POLSARPRO project are distributed by ESA free of charge.

Looking into the future, Pol-InSAR techniques will be faced with the potential and the challenges arising from an extended observation space provided by multi-baseline, multi-frequency, bi- and multistatic sensor configurations forcing the evolution of quantitative measurement and information product generation in SAR remote sensing.

# Tomography

As presented in the previous section, polarimetric SAR interferometry is a suitable technique for measuring vegetation height and for inferring biomass via suitable models. However, it is not possible to obtain information about the vertical backscattering structure of the volume without using appropriate models with a-priori information of the volume scatterer distribution. SAR tomography allows a three-dimensional (3-D) imaging of the volume, i.e. it allows a vertical separation of scattering centres at different heights. It is a direct measurement technique in the sense that it does not require a model.

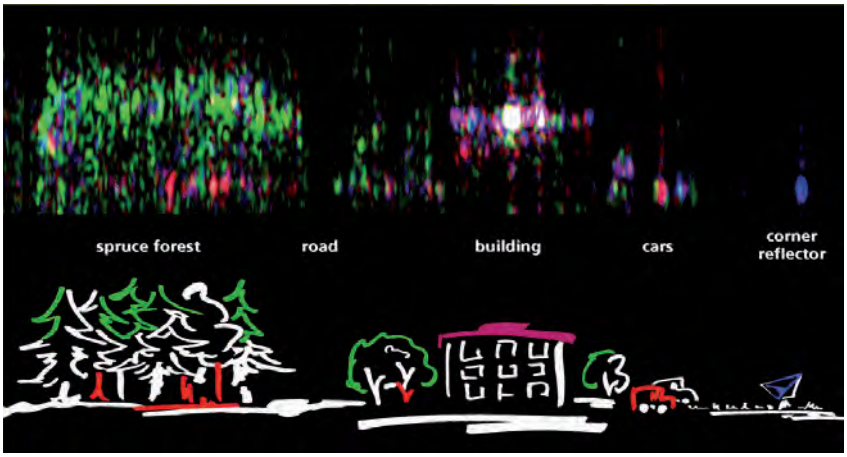


**Figure 3-39: First demonstration of airborne polarimetric SAR tomography. Colours illustrate different scattering mechanisms (red - dihedral, green - volume, blue - surface scattering). The plot represents the tomographic signal intensity as a function of height. Lower plot: An artist's view of the imaged area.**

The tomographic imaging technique can be understood as the generation of an additional synthetic aperture perpendicular to the flight track. This synthetic aperture consists of several parallel tracks or orbits with a horizontal or vertical displacement. A larger span of this aperture provides better resolution in the third dimension (height), and closer spacing between adjacent tracks influences favourably the unambiguous height range, i.e., the volume height to be imaged. Therefore, it is beneficial to obtain as many tracks as possible at an adequate minimum distance from each other. Typically, the number of images N is between 5 and 15 in order to be able to distinguish N-1 layers in the volume.

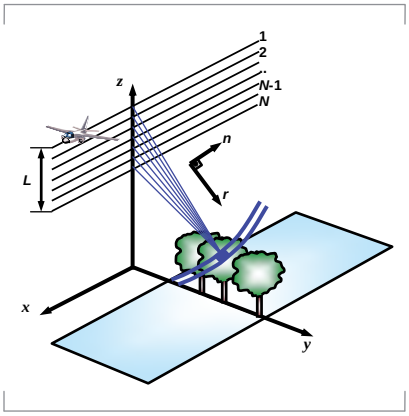


**Figure 3-40: Flight geometry for 3-D imaging via SAR tomography using repeat-pass flight acquisitions. A bistatic configuration consisting of several micro-satellites flying in formation can be used in case of a spaceborne system realisation.**

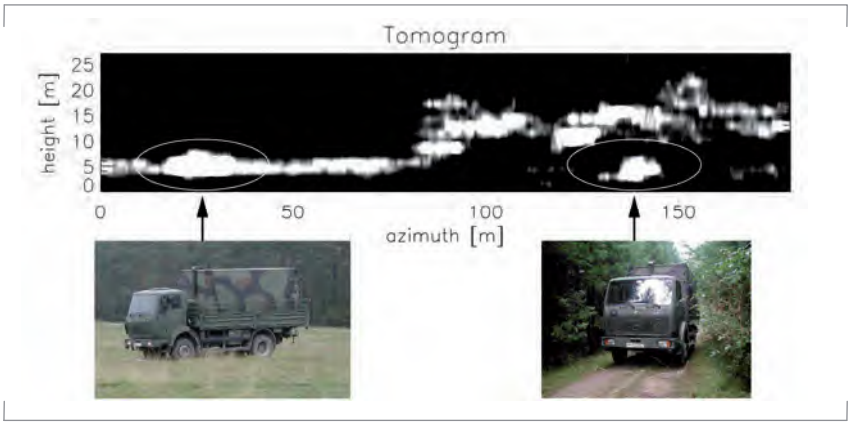


**Figure 3-41: Tomogram representing two trucks placed inside and outside the canopy. The target share the same range coordinate. The flight path is parallel to the track where the two trucks have been placed. The hidden target, as well as the vegetation over it, is clearly represented.**

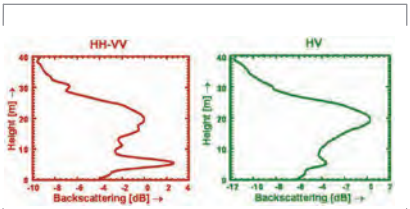


**Figure 3-42: Distribution of backscatter intensity vs. height for a spruce forest in different polarisations (HH-VV and HV). The plot on the left shows the strong reflection at approx. 5 m height caused by the double bounce scattering due to the interaction between tree trunk and ground (observed in the HH-VV channel of the Pauli representation). On the right the dominant reflection of the canopy observed in the cross-polarisation channel (HV+VH) is recognised.**

For generating a tomographic image (tomogram), the first step is a standard two-dimensional (2-D) processing that includes advanced techniques for estimating the residual motion errors. The second step consists in focusing in the third dimension. Nowadays it is possible to select the most suitable focusing approach depending on the particular need. For a qualitative interpretation of the data, the standard Fourier processing can be applied because of its coherent nature and the possibility to exploit the polarimetric information.

The first demonstration of SAR tomography has been carried out in 1998 at DLR by means of an internal campaign: 14 tracks of full-polarimetric L-band data were acquired by the E-SAR system at a nominal spacing of 20 m for a total tomographic aperture of 260 m. Investigations of a spruce forest area revealed the potential of SAR tomography, especially in combination with polarimetry to allow a good indication of forest height in approximately 20 m.

In 2006, another tomographic campaign, carried out in collaboration with the *Electromagnetic Remote Sensing Defence Technology Centre* and *eOsphere Limited* (formerly *Vexcel UK*) had the goal to determine how SAR tomography is suitable for target detection purposes. In this case, high resolution tomograms are required and, therefore, Fourier processing does not represent the best solution since several methods, derived from direction of arrival estimation (DOA) techniques can be applied and outperform the Fourier one concerning this parameter.

Due to the higher required resolution, the tomographic aperture has been enlarged to 400 m, therefore 21 tracks separated by a baseline of 20 m have been flown. Figure 3-41 summarises the main result of this campaign.
The tomogram is obtained by means of the Capon method as it is possible to observe the hidden target (not detectable in a single SAR image). It is clearly visible and its height can be roughly estimated.

It is worth to remember that the Capon method is not coherent (like most of the methods derived from DOA techniques). Therefore a polarimetric analysis cannot be carried out.

For both experiments, the irregular track spacing associated with the motion errors and the limitations of the navigation system accuracy turned out to be a challenge in the development of the tomographic processing chain. The temporal decorrelation between the images has been kept under control since both campaigns have been carried out within a few hours.

The repeat-pass scenario used in these demonstrations requires a relatively high effort to acquire a single tomographic data set. Today's research work concentrates on the reduction of the number of acquisitions by means of spectral estimation techniques. SAR tomography can also be implemented for a satellite configuration. Anyhow,

due to the large temporal baseline among the acquisitions, spaceborne SAR tomography showed mainly its advantages on urban areas than on vegetated ones.

## The new Airborne SAR – F-SAR

F-SAR identifies the successor of the well-known E-SAR system and is under development at the Institute. The development was triggered by the strong demand of E-SAR users and customers for data being simultaneously acquired at different wavelengths and polarisations, as well as by the demand for very high range resolution. E-SAR cannot cope with these requirements due to design and technological limitations. F-SAR is a totally new development, utilising most modern hardware and commercial off-the-shelf components. As for E-SAR DLR's Dornier Do228-212 aircraft is the first choice as platform for the new system.

F-SAR is a fully modular system and will operate at X, C, S, L and P-bands with

- Simultaneous data acquisition in minimum three out of five frequency bands
- fully polarimetric capability in all frequency bands
- single-pass polarimetric interferometry capability in X and S-band
- four recording channels with data rates of up to 2 Gbit/s per unit
- precise internal calibration (relative accuracy better than 1 dB)
- fully reconfigurable operation modes including capability for digital beamforming on receive.

Furthermore, repeat-pass Pol-InSAR will be a standard measurement mode. Range resolution in each frequency band has been defined by specific user

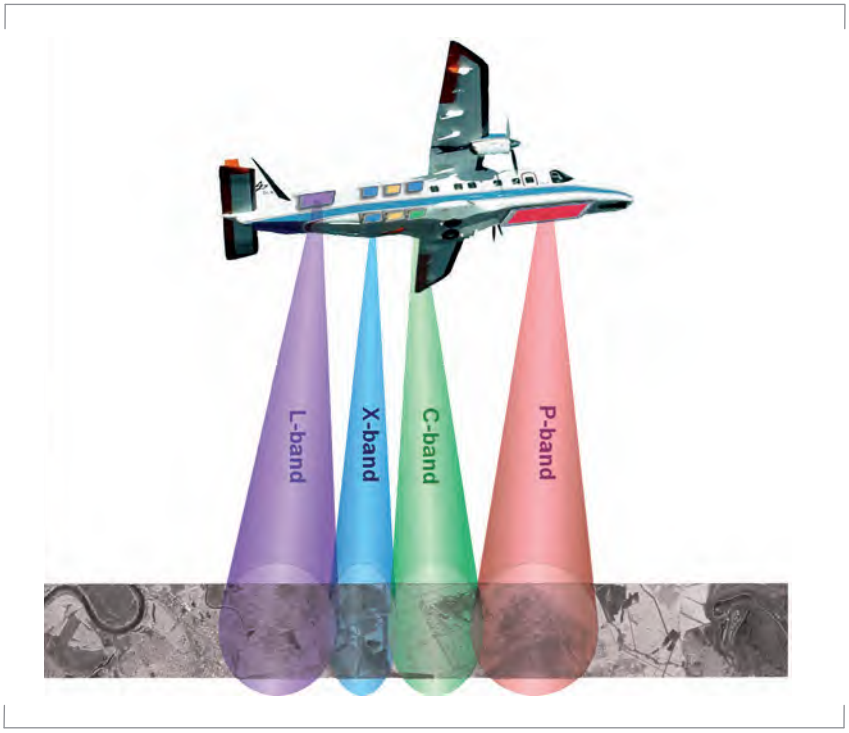


**Figure 3-43: An Artist's view of F-SAR acquiring data simultaneously in X, C, L and P-band.**

**Figure 3-44: New F-SAR antenna mount attached behind the wing to the right-hand side of the aircraft allowing 7 antennas to be integrated: 3x X-band (blue), 1x C-band (green), 2x S-band (light blue), 1x L-band (purple). As with E-SAR, the P-band antenna is separately mounted underneath the cockpit.**

**Figure 3-45: F-SAR antenna mount (red circle) under test. The aerodynamic properties are being investigated. The new antenna mount allows an easy exchange of individual antennas in the future.**

Table 3-2: F-SAR Technical Parameters

| | X | C | S | L | P |
|---|---|---|---|---|---|
| **RF** [GHz] | 9.60 | 5.30 | 3.25 | 1.325 | 0.35 |
| **Bw** [MHz] | 800 | 400 | 300 | 150 | 100 |
| **PRF** [KHz] | 5 | 5 | 5 | 10 | 12 |
| **PT** [kW] | 2.50 | 2.20 | 2.20 | 0.70 | 0.70 |
| **Rg res.** [m] | 0.3 | 0.6 | 0.75 | 1.5 | 2.25 |
| **Az res.** [m] | 0.2 | 0.3 | 0.35 | 0.4 | 1.5 |
| **Rg cov.** [km] | 12.5 (at max. bandwidth) | | | | |
| **Sampling** | 8 Bit real;<br>1 Giga sample or 500 Mega samples; max number of samples 64 K per range line; 4 recording channels | | | | |
| **Data rate** | 192 MByte/s (max. per rec. channel) | | | | |

requirements. While 100 MHz has been adopted for P-band, a Step Frequency approach is used to achieve up to 800 MHz effective signal bandwidth at X-band to satisfy the requirement for very high resolution.

The F-SAR system comprises a basic system control and data acquisition sub-system to which individual RF subsystem modules are connected. System control is based on an extended CAN bus and Ethernet concept. This gives the necessary flexibility and the degrees of freedom to configure the

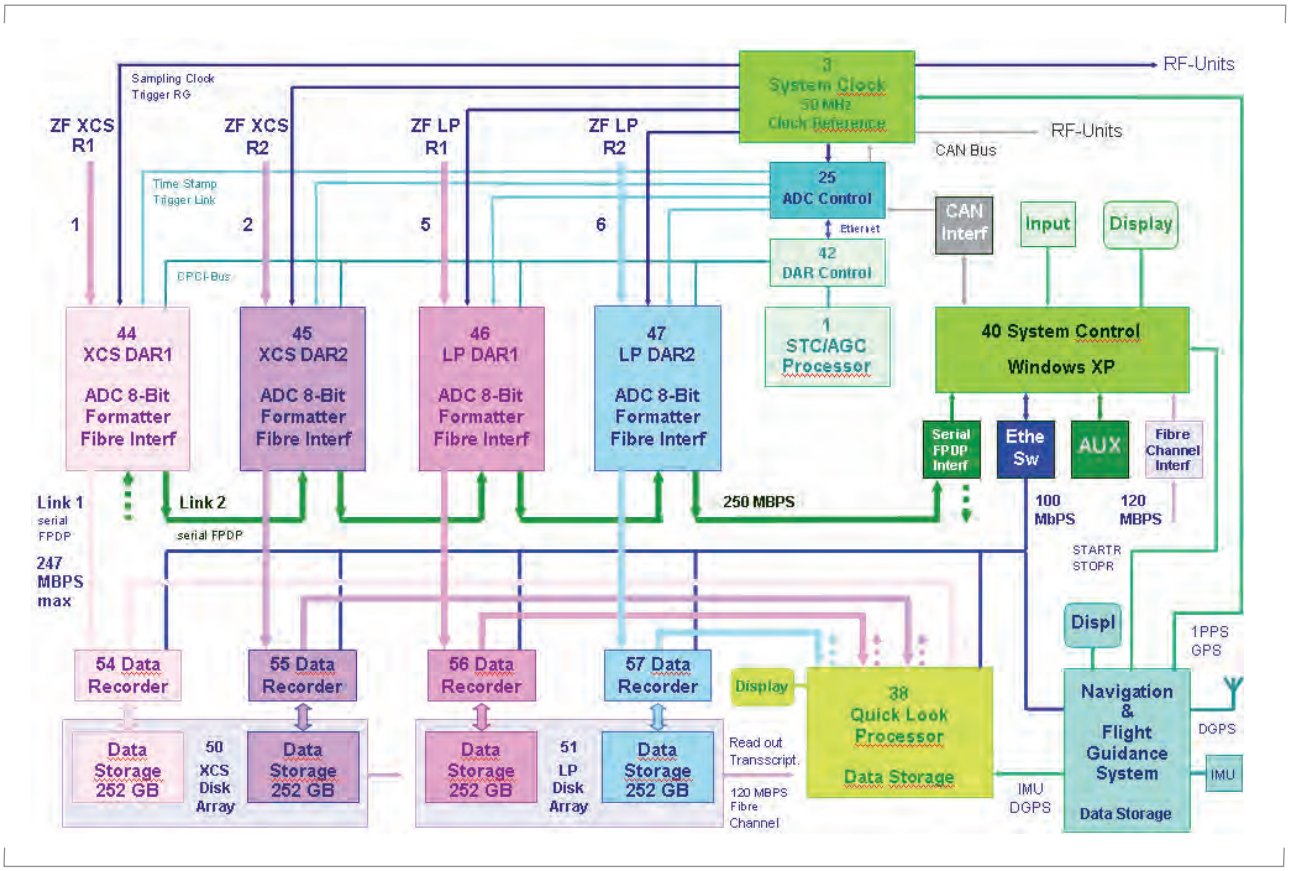


Figure 3-46: Block diagram of the F-SAR system control and data acquisition sub-system.

system optimally for carrying out the desired measurements and experiments such as bistatic SAR. Further, the concept makes an extension to any other RF band an easier task.

A new antenna mount designed to fix planar array antennas to the aircraft is under development. Fully fledged in multi-frequency configuration it holds 7 right-looking dual polarised antennas: X-band (3), C-band (1), S-band (2) and L-band (1). The P-band antenna is mounted under the nose of the aircraft as indicated in the Artist's view.

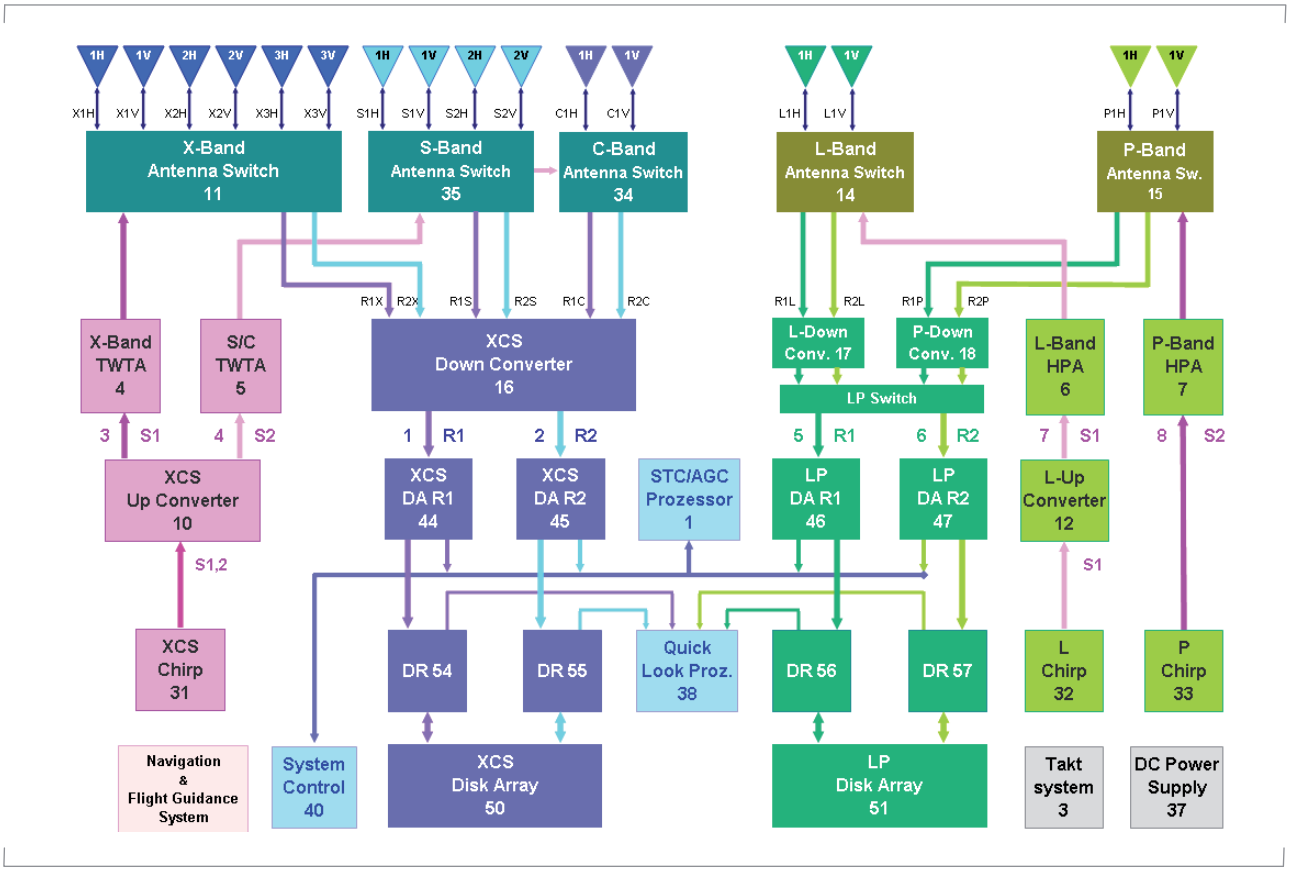


Figure 3-47: F-SAR system configuration for multi-frequency and polarimetric operation in X, C, S, L, P-band including single-pass interferometric capabilities in X and S-band.

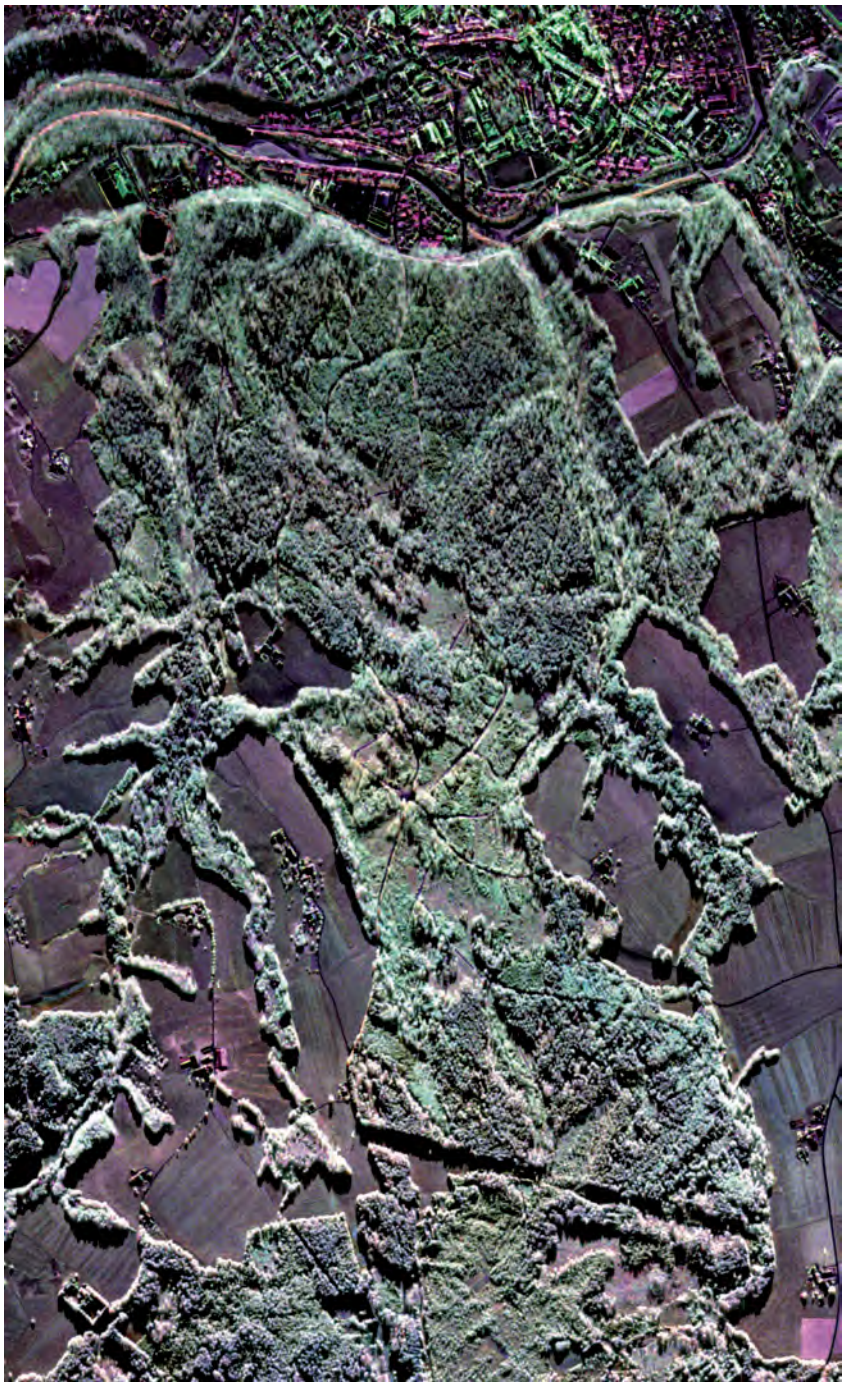

**Figure 3-48: One of the first fully polarimetric X-band images acquired with F-SAR (Traunstein, Germany).**

One important advantage of the antenna mount will be that it makes it easier to change the antenna configuration and to mount other antennas, avoiding individual airworthiness certification procedures at the same time. The antenna mount has passed all aerodynamic flight tests successfully.

The radar is designed to cover an off-nadir angle range of 25 to 55 degrees at altitudes of up to 6000 m above sea level, which is the maximum operating altitude of the Do228.

A central computer unit controls the radar via CAN bus and Ethernet. There are four modes of operation:

- System configuration,
- System test,
- Internal calibration,
- Radar operation.

The required synchronous timing and clock signals are generated in the main timing unit with less than 6 ps jitter and rise times of less than 80 ps. A 50 MHz ultra-stable quartz oscillator is the reference. The IGI D-GPS/INS based precision navigation system delivers a GPS 1 PPS signal which regularly triggers an absolute time stamp in the raw data header.

In its basic configuration the radar operates with four 1-GS ADC. The timing unit allows for two additional ADC. Each ADC unit has integrated raw data formatting thus the number of recording channels can be easily increased if needed. High-speed data recording units are connected via optical fibre. A second optical fibre links the ADCs to the central computer unit (monitoring bus) for internal calibration and system monitoring. Quick-look processing will be implemented via dedicated hardware and an optical fibre link to the data recording units. Online and/or offline operation is possible.

F-SAR is in the building phase and laboratory tests are following each completed development step.

The maiden flight of the new radar was in November 2006. Since then several SAR experiments (GMTI, bistatic imaging etc.) were conducted in X-band beside standard system functional tests.

In November 2007, we obtained a first fully polarimetric X-band image with 300 MHz bandwidth during a test flight. The radar demonstrated a very good system performance measured on trihedral reflectors. We measured an ISLR of about 16-20 dB in range and azimuth. A geometric resolution of 0.5 m in slant range and 1 m in azimuth at four looks was obtained.

Meanwhile X-band is considered to be pre-operational. Recently, in November 2008, F-SAR successfully completed its first dual frequency flights in X/C and X/S-band. The X/S-band combination is the first ever flown fully polarimetric dual-frequency configuration with F-SAR.

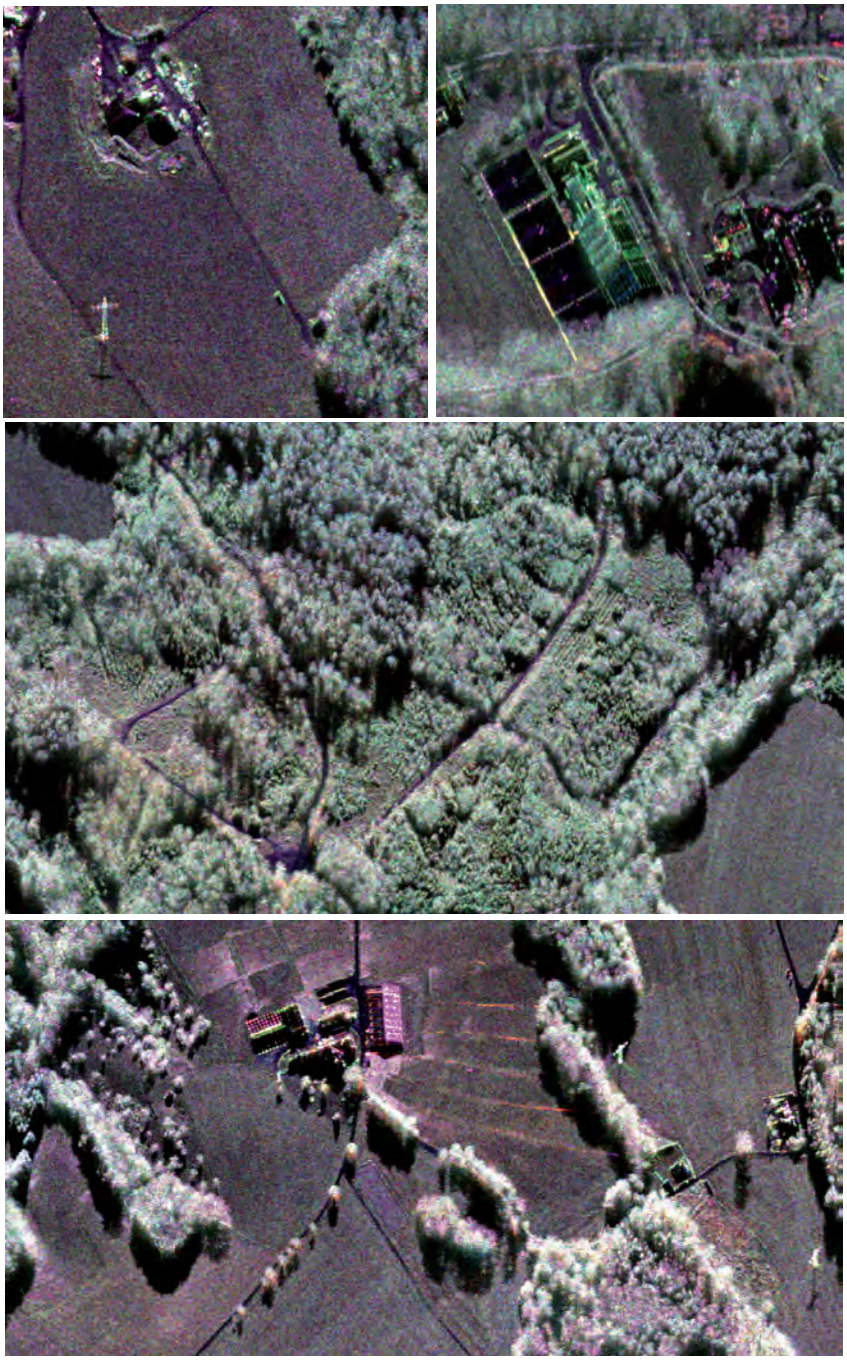

**Figure 3-49: X-band image details: Electrical tower with shadow (above, left), a large pitch-roofed building with tennis courts partly covered under trees mapped towards the radar (above, right), forest crossways (middle), farm houses and individual trees with shadows along the road (below).**

# The Institute Today

## Spaceborne SAR

## Airborne SAR

## Microwave Systems: Research and Technology

- Bistatic and Multistatic SAR
- Digital Beamforming
- Inverse SAR Imaging
- Traffic Monitoring
- End-to-End SAR Simulation
- SAR Performance Analysis
- Radar Calibration
- Antenna Technology
- Signatures
- Radiometry: Imaging Techniques
- Weather Radar
- Propagation

## Institute's Personnel

# Microwave Systems: Research and Technology

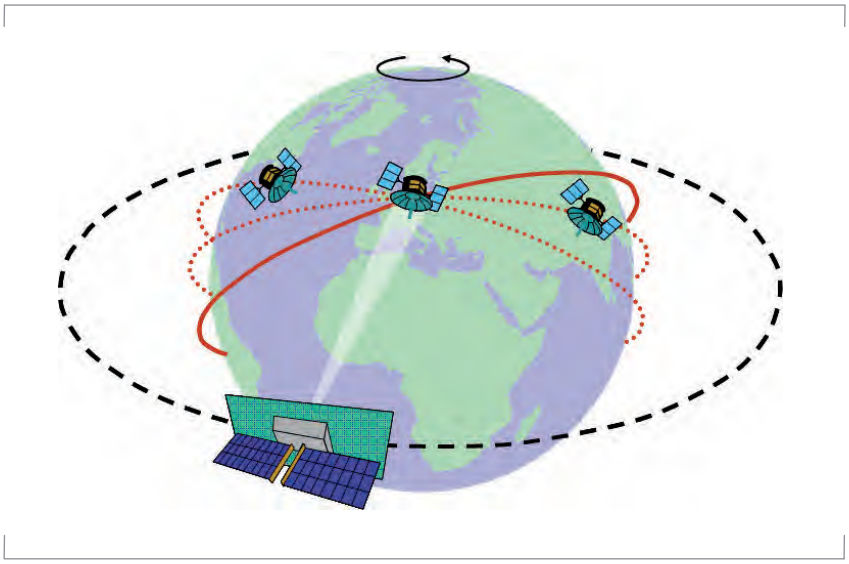

Figure 4-1: Bistatic SAR system consisting of a geostationary illuminator with multiple receivers mounted on small satellites in low Earth orbit.

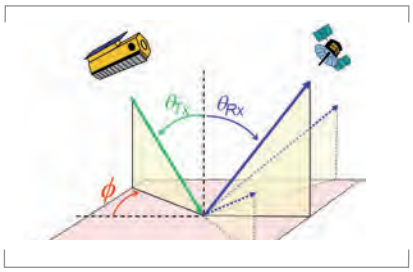


Figure 4-2: Scattering geometry of bistatic and multistatic (dotted) SAR systems with different incidence θTx and departure θRx angles for the transmit and receive signals. The planes are also offset by ϕ.

## Bistatic and Multistatic SAR

Bistatic and multistatic synthetic aperture radar operates with transmit and receive antennas mounted on separate platforms (see Figure 4-2). Such a spatial separation has operational advantages, increasing the capability, reliability and flexibility of future SAR missions and generating new, innovative data products.

Interest in such systems has significantly increased in the last few years and bistatic SAR (one transmitter, one receiver) is now a major topic at many international remote sensing conferences. This upsurge goes hand in hand with progress in satellite navigation, communications and miniaturisation, allowing the realisation of concepts previously regarded as unfeasible. TanDEM-X will be the first bistatic SAR in space and a big step forward is expected from the bistatic experiments planned during this mission.

Eventually, the capabilities of such systems may cause a paradigm shift in radar remote sensing, replacing conventional large and complex monostatic radar satellites by clusters of small and low-cost microsatellites operating in consort. By distributing the functions, modular and scalable designs are conceivable, reducing the mission risk and enabling a wealth of new imaging modes, which can even be dynamically reconfigured to serve changing tasks. Some capabilities are:

- Single-pass cross-track interferometry for the derivation of global, high precision DEMs
- Along-track interferometry for global measurements of ocean currents and sea ice drift
- Polarimetric SAR interferometry for forest mapping and global biomass estimates
- Ambiguity suppression for wide swath SAR imaging with high resolution
- Frequent monitoring for the detection of fast scene changes and timely information
- Multi-baseline SAR tomography for 3-D imaging of semi-transparent volume scatterers
- Multi-aperture ground moving target indication for large area traffic monitoring
- Double differential SAR interferometry for the measurement of vertical scene displacements
- Multi-angle SAR imaging for improved segmentation, classification and object recognition

**Mission Definition and Constellation Design**

An important parameter in defining a spaceborne SAR mission is the selection of a suitable orbit. This becomes even more important for bistatic and multistatic radar missions, where two or more satellites must cooperate to acquire the necessary data. One example is a system for frequent monitoring, whereby a dedicated radar transmitter located in geostationary orbit illuminates the scene and multiple

receivers in low Earth orbit collect the scattered radar echoes (see Figure 4-1). This distribution of tasks allows the use of small, low-cost microsatellites as receivers, thereby reducing the revisit time without excessive cost.

Different requirements arise for multistatic SAR interferometry, which calls for close satellite formations. Several concepts suitable for across-track and along-track interferometry have been studied and patented. One example is the Helix formation for TanDEM-X which provides suitable baselines for cross-track interferometry and ensures at the same time a safe satellite separation without any collision risk. Another example is the Trinodal Pendulum which uses three satellites with different ascending nodes to acquire multibaseline interferograms in a single pass.

*Performance Estimation*

The geometry of a bistatic SAR differs significantly from that of a monostatic SAR. An example is the geostationary illuminator concept of (Figure 4-1). The long transmit path remains almost constant, while the relatively short and fast varying receiver path provides the Doppler modulation for high resolution SAR imaging.

Such systems require new algorithms for performance analysis necessitating the development of a bistatic performance estimator. Figure 4-3 shows the predicted sensitivity for the geostationary illuminator system and demonstrates the feasibility of such a system with a moderate transmit power aperture product of $10^5$ $Wm^2$.

A detailed model was also developed for the analysis of the interferometric performance of multistatic satellite constellations. This model was used, for instance, to predict the height accuracies for the TanDEM-X mission. For an ESA study on polarimetric and interferometric missions it was used to predict the performance of spaceborne Pol-InSAR systems.

## Bistatic and Multistatic SAR Processing

Bistatic SAR systems require new processing algorithms for high resolution SAR imaging. Bistatic SAR data from stable configurations, where the relative position of the two platforms remains fixed, can often be processed by suitable adaptations of monostatic processing algorithms. However, more sophisticated algorithms are required to focus the bistatic returns from configurations where the transmitter-receiver separation changes during the data take. Figure 4-4 shows the successfully processed image from a hybrid bistatic SAR experiment using TerraSAR-X as illuminator and F-SAR as receiver.

Multistatic SAR data require different processing approaches. The combination of the signals from multiple receivers can be linear, as in the case of digital

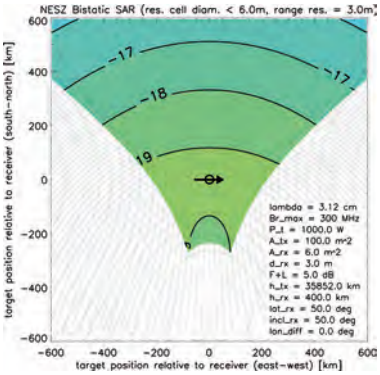


**Figure 4-3: Noise equivalent sigma zero (NESZ) in $dBm^2/m^2$ for a bistatic SAR combining a geostationary illuminator with a LEO receiver. The grey lines show the contours of constant range and Doppler in an Earth tangent plane spanning an area of 1200 km x 1200 km. The receiver motion is indicated by the arrow. It shows the predicted sensitivity for the geostationary illuminator system in the previous figure and demonstrates the feasibility of such a system with a moderate transmit power aperture product of $10^5$ $Wm^2$.**

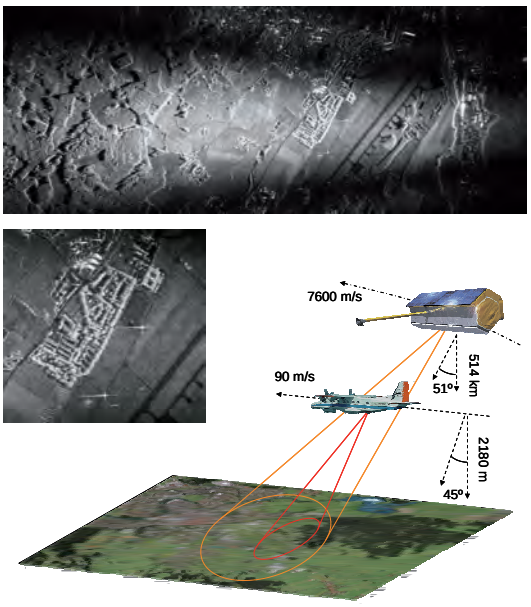


**Figure 4-4: Bistatic SAR image from a hybrid airborne-spaceborne SAR experiment conducted in November 2007.**

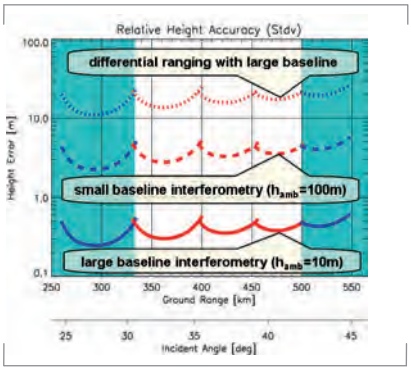


**Figure 4-5: Predicted DEM performance for multi-baseline single-pass data acquisition. The interferometric height accuracy is shown for two baselines corresponding to a height of ambiguity of 100 m (dashed) and 10 m (solid). The dotted line is the predicted height accuracy for differential ranging. The height accuracy from differential ranging remains below the height of ambiguity of the small baseline interferometry, thus enabling efficient ambiguity suppression without the need for phase unwrapping.**

beamforming, or non-linear, as required for the various interferometric modes. By using these techniques in combination, it is possible to significantly improve the performance. An example is the synergistic use of multi-baseline cross-track interferometry with differential ranging (see Figure 4-5). This enables the generation of ultra high-resolution DEMs with sub-meter height accuracy without the need for phase unwrapping, which can be a challenge for conventional interferometry. Large interferometric baselines can be used, the phase ambiguities of individual pixels being resolved by means of differential time delay measurements.

Further potential arises from multiple aperture sensing for the suppression of range and azimuth ambiguities.

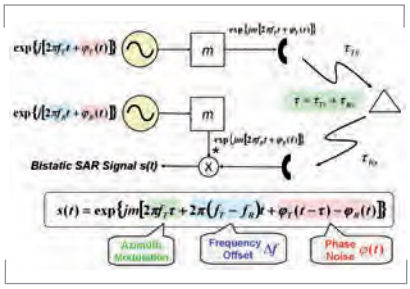


**Figure 4-6: Derivation of base-band bistatic phase errors after down conversion; fT and fR denote the transmit and receive oscillator frequencies, φT and φR are the corresponding phase errors, and τ is the travel time of the radar pulse.**

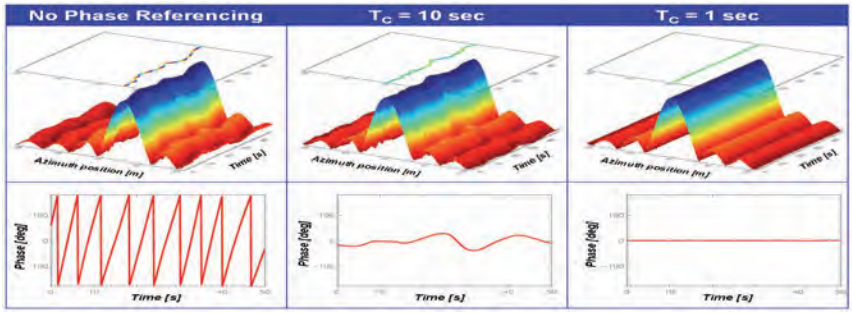


**Figure 4-7: Simulated bistatic SAR impulse response in L-band. The upper plots show the simulated profile of the azimuth response without synchronisation (left), phase referencing every ten seconds (middle), and phase referencing every second (right). The lower plots show the corresponding impulse response phase errors in the range from -180° to + 180°.**

For example, a coherent combination of the signals from multiple receivers separated in an along-track formation, a so-called sparse aperture SAR, achieves suppression of azimuth ambiguities by taking advantage of a new multi-aperture signal reconstruction algorithm. It is then possible to:

- improve the azimuth resolution
- increase the imaged swath width, and
- reduce the required antenna area.

Sparse aperture configurations are also well suited to GMTI and traffic monitoring applications, enabling efficient clutter suppression and high accuracy velocity measurements.

### Synchronisation of Bistatic SAR Systems

Further investigations address the impact of local oscillator stability during bistatic and multistatic SAR data acquisitions. Oscillator errors deserve special attention in distributed coherent radars, since there is no cancellation of low frequency phase errors as in a monostatic SAR, where the same oscillator signal is used in the transmitter and receiver (see Figure 4-6). To investigate the errors, a system model was developed, which describes the resulting phase fluctuations. Analytic expressions were then derived for typical errors like the time variant shift, spurious sidelobes, and the broadening of the impulse response, as well as the low frequency phase modulation of the focused SAR signal. To combat the degradation, several synchronisation strategies were developed.

Figure 4-7 shows the reduction of the azimuth impulse response deterioration by using a periodic phase referencing concept. This synchronisation technique will be implemented for the TanDEM-X mission, where radar pulses are periodically exchanged between the instruments via dedicated horn antennas.

### New Multistatic Imaging Techniques

A wealth of new bistatic and multistatic SAR imaging techniques has been suggested in the last years. Examples are range resolution enhancement beyond the ITU bandwidth limitations, 3-D tomographic mapping, or the measurement of small height changes by double differential SAR interferometry. Further potential arises from a combination of bistatic radar with digital beamforming on receive.

Another opportunity is the parasitic use of communication and navigation satellites, which provide a free illumination source. In order to explore the capabilities and limitations of such parasitic systems, an experimental setup has been built as shown in Figure 4-8. First results are very promising and yield well-focused impulse responses using the television signals from the Astra digital TV satellites for scene illumination. In a future step, the receiving antennas will be moved on tracks to demonstrate synthetic aperture imaging.

### Bistatic Airborne SAR Experiment

In order to explore the potentials and challenges associated with bistatic radar, DLR and ONERA conducted a joint bistatic airborne SAR experiment with their radar systems E-SAR and RAMSES in February 2003 in southern France. Two bistatic configurations (see Figure 4-9) were flown.

In the first configuration, a quasi monostatic mode, the two planes flew very close to each other to acquire interferometric data in a single-pass across-track configuration with a vertical separation of about 20 m. This successfully demonstrated two-platform bistatic SAR interferometry for the first time.

The second geometrical configuration was designed to acquire images with different bistatic angles. An impressive result is shown in Figure 4-10 which is

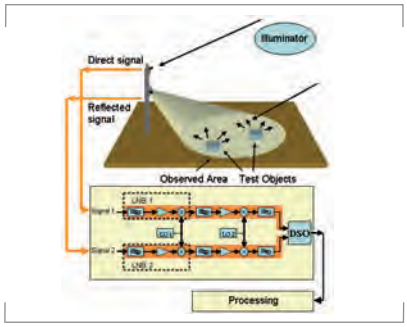


**Figure 4-8: Experimental setup for the demonstration of radar imaging based on illumination from a digital TV satellite. One antenna directed at the satellite receives a reference signal while a second antenna directed at the scene receives the reflected signals from the targets. Range focusing is achieved by correlating the two signals.**

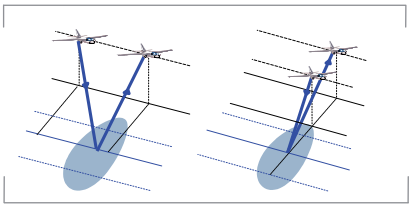

**Figure 4-9: Bistatic airborne SAR experiment. Left: the two aircrafts on the ground and in the air (inset) – Above: The two bistatic configurations. Left: Quasi monostatic geometry with the aircraft following closely on the same track, right: bistatic geometry.**

**Figure 4-10: Colour composite of three SAR images with different bistatic angles, showing the clear differentiation of surface features.**

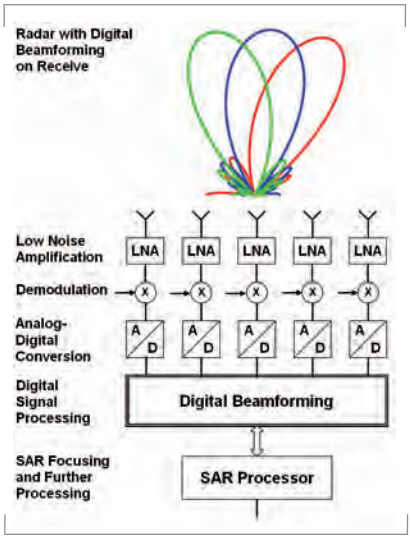


**Figure 4-11: Schematic of digital beamforming on receive. The signal from each sub-aperture element is independently amplified, down-converted, and digitised. The digital processing enables flexible and adaptive beamforming after signal reception.**

**Figure 4-12: Top: Antenna system attached to the skids of the helicopter. Bottom: SIREV antenna with 56 receiving subarrays.**

an overlay of three SAR images with different bistatic angles. The strong colour variation between the different areas in the image demonstrates the high information content in multistatic SAR products.

The results from the bistatic SAR experiments clearly demonstrate the feasibility of bistatic SAR imaging and its great potential for the extraction of highly informative scene parameters.

Bistatic and multistatic radar is a rapidly emerging technique with great potential for a broad range of innovative remote sensing applications. The combination of practical experience and theoretical expertise makes the Institute a key player in this strategically important field.

## Digital Beamforming

Digital beamforming (DBF) is a technique where the receiving antenna of a radar system is split into multiple sub-apertures. In contrast to analogue beamforming (e.g. as employed in TerraSAR-X) the signal from each sub-aperture element is separately amplified, down-converted, and digitised (see Figure 4-11). The signals are combined with a digital bus, avoiding the combiners of conventional antenna arrays and, hence, potentially simplifying antenna integration. The coherent combination of the sub-aperture signals allows the formation of multiple beams with adaptable shapes.

Digital beamforming is a powerful technique to gather additional information about the direction of scattered radar echoes during the acquisition of radar images.

**Sector Imaging Radar**

A first demonstration of the potential of digital beamforming on receive was the development of an innovative forward looking imaging radar for enhanced vision. The technique generates high-quality radar images in any desired direction, and is, hence, also suitable for forward looking airborne radars (FLAR).

The system is based on a DLR patent and denoted Sector Imaging Radar for Enhanced Vision, SIREV. In contrast to SAR systems, no relative motion is required between the sensor and the targets. The high frame repetition frequency enables the detection and measurement of very rapid changes in dynamic scenes. Further modes are interferometric mapping, as well as a true 3-D tomographic imaging of semi-transparent scatterers.

To verify and demonstrate SIREV an X-band experimental system was assembled and flown on a helicopter. An antenna was built in cooperation with IHE, University of Karlsruhe, with sequential switching of the receiving antenna elements and was connected to existing radar hardware of the company Aerosensing. The available bandwidth of 100 MHz and the wavelength limited the image resolution, but were sufficient to prove the concept. Figure 4-12 illustrates the antenna system and its attachment to the helicopter. The work was funded by Atlas Elektronik GmbH.

A fast processing algorithm was developed for SIREV, which allows accurate, phase preserving image formation. Raw data were obtained from a demonstration flight close to Oberpfaffenhofen. Motion errors of the platform were extracted from an analysis of the recorded data, avoiding the necessity of an inertial navigation system (Figure 4-13).

The results show good agreement with theory. After image formation, coherent and incoherent averaging were applied

to improve the image quality. The required motion compensation for coherent averaging was derived directly from the recorded data by evaluating the interferometric phase difference between subsequent SIREV images (Figure 4-14). The final result was an image sequence composed of several thousand images (an animation is available at http://www.dlr.de/hr/sirev). The right hand side of this figure shows one image of this sequence.

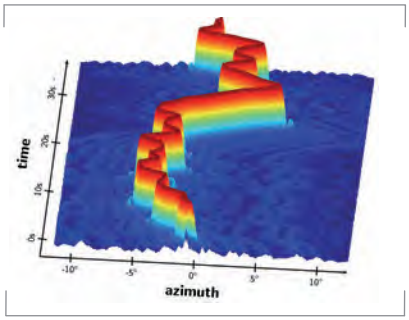


Figure 4-13: Temporal sequence of a corner reflector response obtained as the helicopter moved forward. The result shows good azimuth focusing in spite of the helicopter motion

### High-Resolution Wide-Swath SAR Imaging

The unambiguous swath width and the achievable azimuth resolution pose contradicting requirements on SAR system design. To overcome this inherent limitation, several innovative techniques have been suggested based on splitting the receiving antenna into multiple sub-apertures with individual receiver channels.

An example for such a system is the High Resolution Wide Swath (HRWS) SAR which combines the displaced phase centre (DPC) technique in azimuth with time variant beam steering in elevation (Figure 4-15). The DPC technique is used to gather for each transmitted pulse additional samples along the synthetic aperture to suppress azimuth ambiguities. The time variant beam steering in elevation is used to improve the SNR without reducing the swath width. This is achieved by steering the narrow receive beam in real time such that it follows the radar pulse as it travels over the ground.

The HRWS concept has also been extended to more advanced modes, enabling a wider unambiguous swath without the necessity to increase the antenna length.

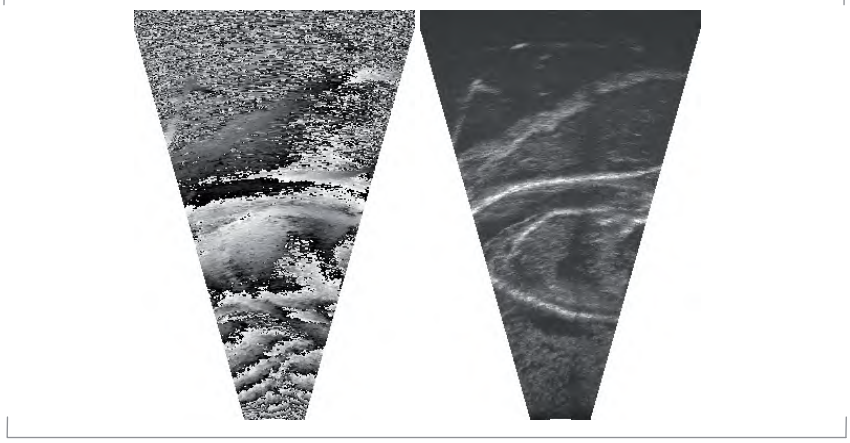

Figure 4-14: Left: Interferogram between successive SIREV images. Right: SIREV image of the Lech river.

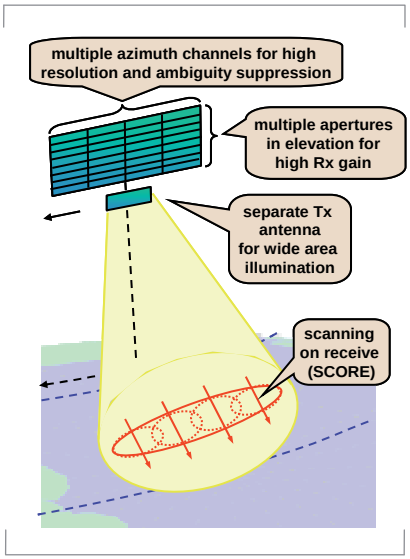


Figure 4-15: High-Resolution Wide-Swath (HRWS) SAR system. The combination of the displaced phase center technique with time variant beam steering in elevation enables large area imaging with high resolution.

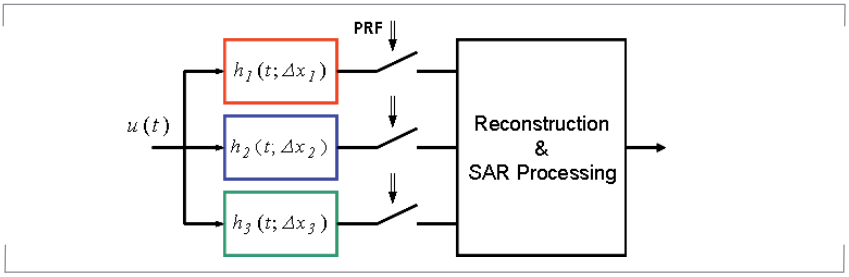


Figure 4-16: Multi-channel linear systems model for multiple aperture SAR. The SAR data acquisition is described by the linear filters on the left. The sampling with a pulse repetition frequency PRF, which is lower than the Nyquist rate, introduces ambiguities for each channel. The unambiguous SAR signal can then be recovered by a joint coherent processing of the recorded signals from all receiver channels.

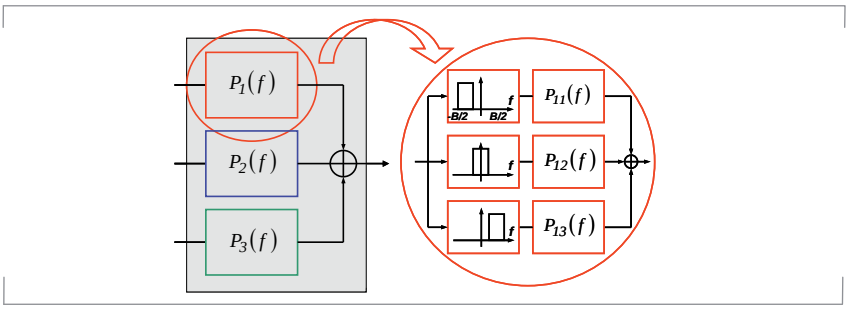


Figure 4-17: Unambiguous signal reconstruction in a multiple aperture SAR with three channels. Each reconstruction filter $P_i(f)$ consists of n=3 band-pass filters $P_{ij}(f)$. The transfer functions $P_{ij}(f)$ are derived from a generalised multiple channel system matrix describing the data acquisition in the Figure above.

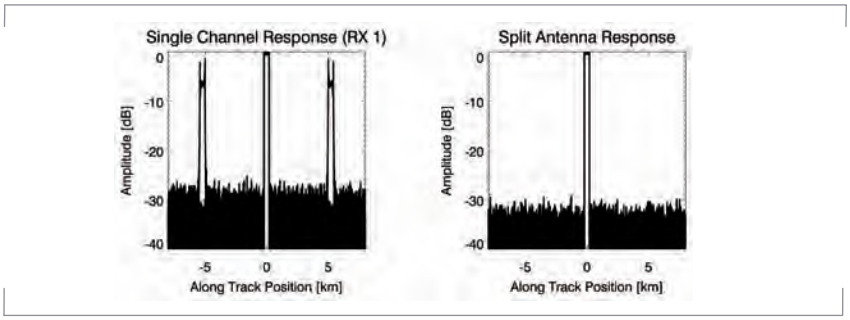


Figure 4-18: Azimuth response for one sub-aperture (left) and after non-uniform DPC antenna reconstruction (right) showing the suppression of the ambiguous responses.

### Azimuth Processing Techniques

The application of the displaced phase centre technique in a HRWS SAR system puts a stringent requirement on the PRF, which has to be chosen such that the SAR platform moves half the antenna length between successive radar pulses. This PRF ensures a uniformly sampled synthetic aperture, but it may be in conflict with the timing diagram of the SAR for some incidence angles. It also precludes the use of a higher PRF for improved azimuth ambiguity suppression.

To avoid such a restriction, a new reconstruction algorithm was developed, which can recover the unambiguous Doppler spectrum even in the case of a non-uniform DPC sampling. For this, the raw data acquisition of the multiple aperture SAR is described using a linear multi-channel systems model, as shown in Figure 4-16, where each channel on the left-hand side describes the bistatic data acquisition by one sub-aperture element. The signals are sampled with a PRF which is lower than the (Doppler) bandwidth, making the output of each channel highly aliased. The unambiguous SAR signal spectrum is then recovered by coherent multi-channel SAR processing which eliminates the ambiguous parts of the individual Doppler spectra (see Figure 4-17). This reconstruction algorithm can be regarded as a time-variant digital beamforming, which combines the individual receive signals in a general space-time processing framework.

The validity of the algorithm has been tested by simulation. Figure 4-18 shows the predicted response of the TerraSAR-X dual receive antenna mode to an extended scatterer before (left) and after (right) applying the reconstruction algorithm. It is evident that the ambiguous responses are suppressed.

The algorithm has also been applied to real SAR data acquired by the DLR E-SAR system. Figure 4-19 compares the reconstructed image (right) to the ambiguous image for one channel with a highly non-uniform sampling (left).

The azimuth processing for multi-aperture SAR systems is further being refined in ongoing contracts from ESA, DLR, and EADS Astrium. The goal of these studies is to develop a

technology demonstrator for future spaceborne HRWS missions. It has been seen that azimuth processing plays a key role in designing such systems. A first spaceborne demonstration of the new multiple aperture processing techniques is planned with the split antenna mode in TerraSAR-X.

### Beamforming in Bistatic and Multistatic SAR

Digital beamforming on receive is also of great interest in combination with bistatic SAR systems. An illustrative example is the combination of a geostationary illuminator with passive LEO receivers. Such a system has the peculiarity that the antenna footprint of the transmitter exceeds by far the size of receiver footprint. Hence, the receiver will only see a part of the illuminated footprint. Such a waste of energy can be avoided by splitting the receive antenna into multiple sub-apertures with individual receiver channels (Figure 4-20). Each element then sees a larger area on the ground, and by combining the receiver data it is possible to:

- increase the azimuth resolution,
- reduce range and azimuth ambiguities,
- detect moving objects, and
- improve the radiometric resolution.

The concept of digital beamforming on receive can further be extended to multistatic satellite configurations, where each satellite antenna forms one element of a huge, but sparsely populated aperture. The new ambiguity suppression techniques introduced in the previous section can be adjusted to such satellite formations. This enables the use of microsatellites for large satellite clusters with reconfigurable baselines. Flexible baseline selection allows new, powerful imaging modes to be realised. These can be dynamically adapted to changing demands, thus serving a broad range of remote sensing applications. First demonstrations of these highly innovative techniques will become possible with TanDEM-X which provides four independent channels with distributed phase centre positions.

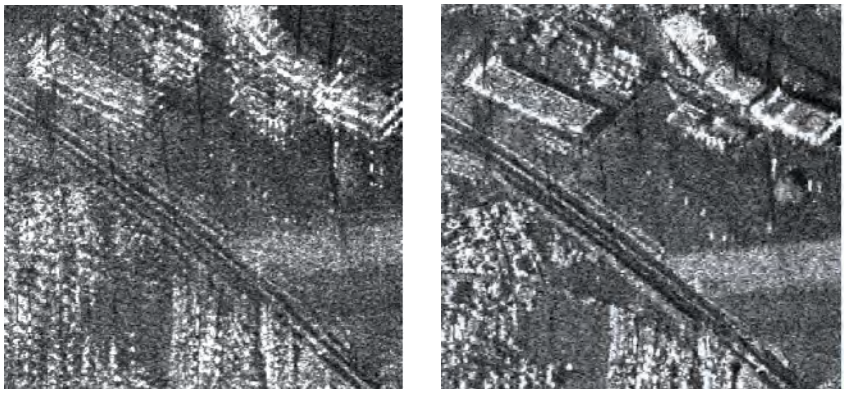

Figure 4-19: Ambiguous image for one channel with non-uniform DPC sampling (left) and after reconstruction with the ambiguities suppressed (right).

### Multiple-Input Multiple-Output (MIMO) SAR

Much research is still required to fully exploit the potentials of digital beamforming for spaceborne radar remote sensing. One example is digital beamforming on transmit with non-separable space-time waveforms. The systematic combination of such a spatiotemporal radar waveform encoding on transmit with digital beamforming on receive is an innovative concept which enables new and very powerful SAR imaging modes. Examples are superior ambiguity suppression (see Figure 4-21), improved geometric resolution and radiometric sensitivity as well as the availability of additional phase centres for along-track interferometry and moving object detection.

Digital beamforming on transmit allows furthermore a flexible distribution of the RF signal energy on the ground. This enables not only a switching between different SAR modes like spotlight, ScanSAR and HRWS stripmap, but it allows also for the simultaneous combination of multiple imaging modes in one and the same data acquisition.

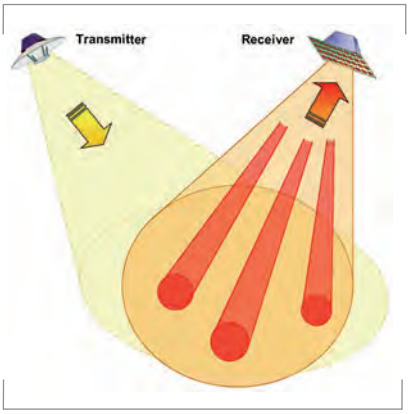


Figure 4-20: Bistatic SAR with digital beamforming on receive. The transmitter illuminates a wide area on the ground. Digital beamforming on receive allows for the formation of multiple narrow beams with high antenna gain. This improves the sensitivity without reducing the coverage, as required for high-resolution wide-swath SAR imaging.

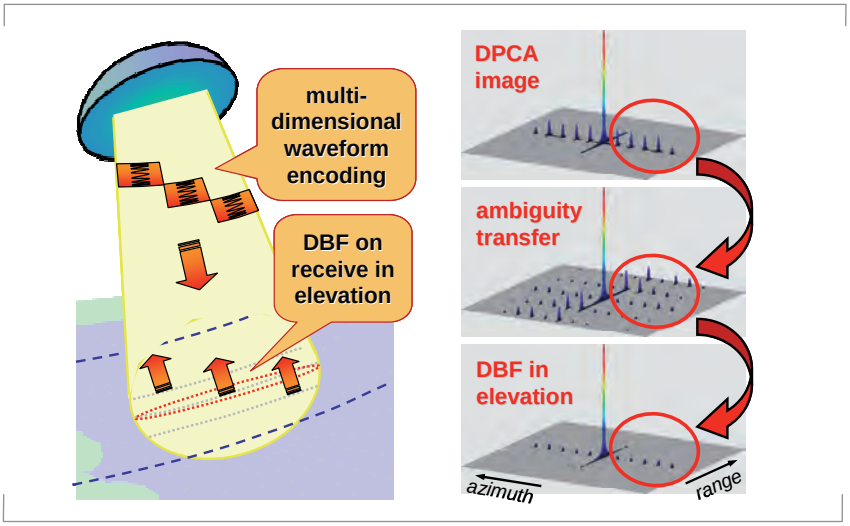


Figure 4-21: Enhanced azimuth ambiguity suppression in MIMO SAR systems by employing multi-dimensional waveform encoding on transmit.

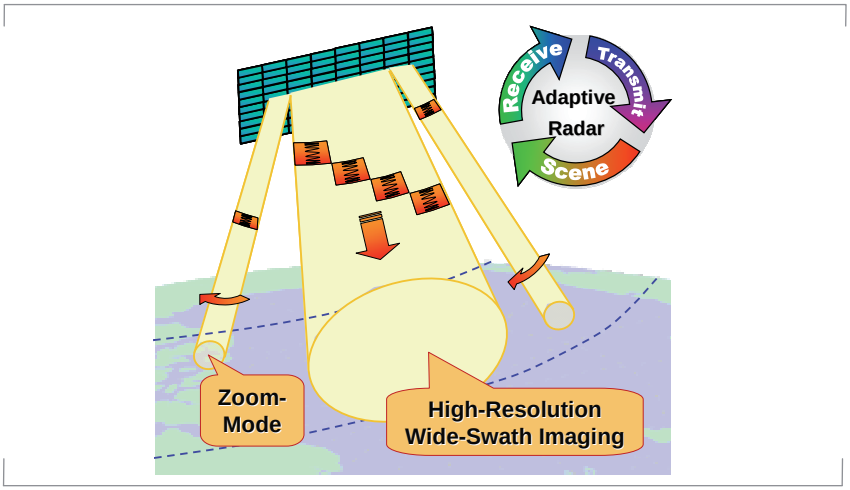


Figure 4-22: MIMO SAR with new hybrid and adaptive imaging modes.

An example for such an interleaved operation is a spotlight imaging of an area of high interest in combination with a simultaneous wide swath SAR mapping for interferometric applications. This can be achieved by enhancing the multidimensional waveform encoding with additional sub-pulses that steer highly directive transmit beams to dedicated areas on the ground (Figure 4-22). By this, one obtains a high Tx gain and a longer illumination time along the synthetic aperture, which improves both the radiometric and geometric resolution for local areas of high interest without losing wide swath coverage. Such a hybrid mode will be well suited to satisfy otherwise contradictory user requirements like the conflicts between a continuous interferometric background mission and localised high-resolution imaging requests.

The data acquisition in a MIMO SAR could even be made adaptive where more system resources are devoted to areas of high interest and/or suspicious features, thereby maximising the information gathered for a given RF power budget. This optimisation becomes possible by forming a closed loop between the radar system and its environment through the modification of the transmitted waveforms in response to the recorded radar echoes.

The innovative beamforming techniques developed in the Institute play a key role in the design of more powerful and cost-efficient SAR systems in the future. The hardware for such radars is currently being developed by EADS Astrium GmbH with funding from both DLR and ESA. Current research includes the development of new DBF modes and architectures like the combination of deployable reflector antennas with digital feed arrays, the development of efficient multi-channel data processing and compression techniques, and the use of digital beamforming techniques for new applications like tsunami warning or wide area traffic monitoring.

Reliable global reconnaissance using remote sensing techniques requires a weather and time independent detection, recognition, and identification capability. High-resolution spaceborne radar systems, such as planned for reconnaissance or implemented on TerraSAR-X, is an appropriate instrument.

When designing such a mission the availability of representative radar data from ground measurements is important, i.e. for the analysis, understanding and simulation of complex target signatures and to provide reference signatures for automatic target recognition (ATR). Inverse SAR (ISAR) imaging allows the collection of very precise high-resolution radar signatures from objects. For a spaceborne radar system the imaging geometry is similar and differs only by geometrical transformation and rotation as shown in Figure 4-23.

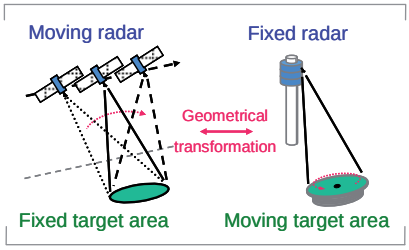


Figure 4-23: Geometry of a spotlight SAR (left) and tower-turntable ISAR (right). Azimuth resolution is achieved by the relative rotary motion between sensor and target. For far field conditions the measured signatures are identical for both scenarios.

## Inverse SAR Imaging - ISAR

Using ISAR techniques, a high spatial resolution in the decimetre range is accomplished by rotating an object on a turntable with respect to a spatially fixed broadband radar system, and by recording a sequence of corresponding radar range echoes within a specific azimuth angle area. The measurements discussed here were performed at a range distance to the turntable of about 60 m. The typical incidence angles range from 24° to 50°, since only those angles are feasible for a spaceborne radar due to transmit power limitations. The turntable usually is covered with soil and grass to provide a natural background. Calibration targets (e.g. corner reflectors and top hats) are arranged close to the turntable to allow an off-line data correction. In front of the turntable, a radar fence prevents disturbing reflections caused by the machinery from below the table.

The first generation experimental X-band radar system was based on a pulsed stepped-frequency waveform using a network analyzer (NWA). Another device contains the transmitter, the receiver, and the pulse modulator. The received and low-noise amplified signal is transferred to the NWA for I-Q detection. An angle encoder delivers the azimuth position of the turntable, and a PC controls the whole measurement system and stores the data.

Figure 4-24 shows some typical results of the whole data processing chain. The left column represents the coarse target orientation on the turntable, the middle column the distribution of the scattering centres, and in the third the distribution of the robust scatterers is illustrated. The signatures were generated using a polar format processing. These images illustrate the different character of radar images compared to their corresponding optical images, being mainly caused by the coherent signal processing, the steep incidence angle, and the monostatic illumination.

Once the corrected processing of the radar raw data has been performed in order to obtain radar cross section (RCS) images of the target, an automatic target recognition (ATR) approach is required to extract a maximum of information from the scene of interest. Since many of the typical targets of interest very often produce up to thirty characteristic scattering centres, a sufficient suppression of noise, artifacts, and sidelobes is mandatory.

The right column in Figure 4-24 shows the images of the extracted robust scatterers after applying adequate filtering. In order to investigate the ATR capabilities and performance of such 2-D-signatures, a template-matching method had been selected. This recognition and/or identification approach is designed to be tolerant with

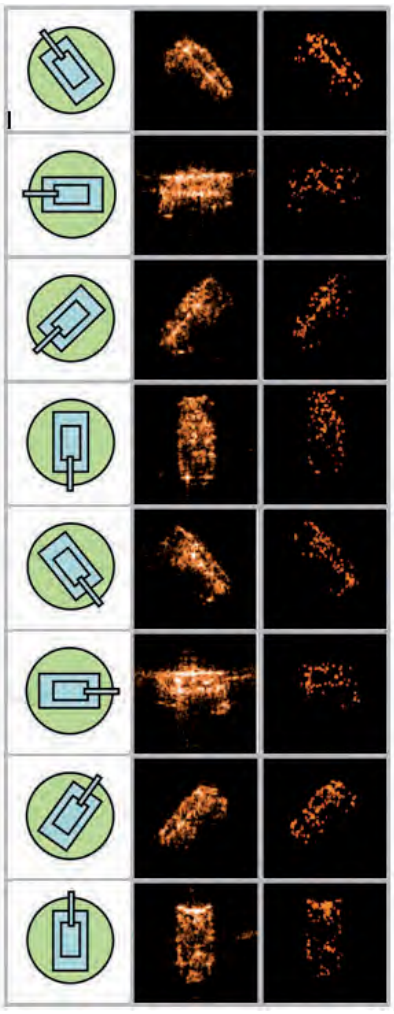

Figure 4-24: First column: Sketch of the actual target orientation; Second column: Reconstructed RCS image; Third column: Image showing the position of persistent scatterers.

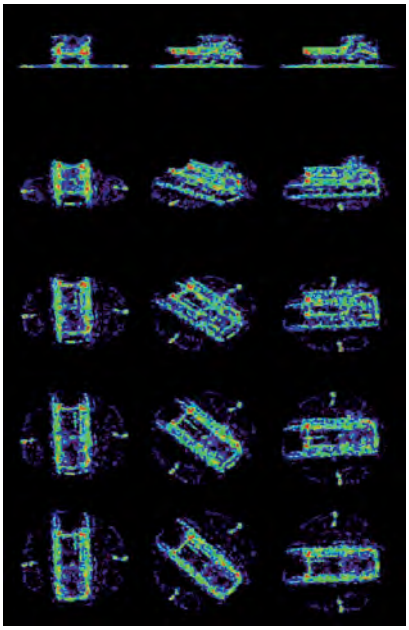

Figure 4-25: Different perspectives of the 3-D radar image of a small truck. First column: 0° azimuth, Second: 45°, Third: 90°, First row: 90° elevation, Second: 67.5°, Third: 45°, Fourth: 22.5°, Fifth: 0°.

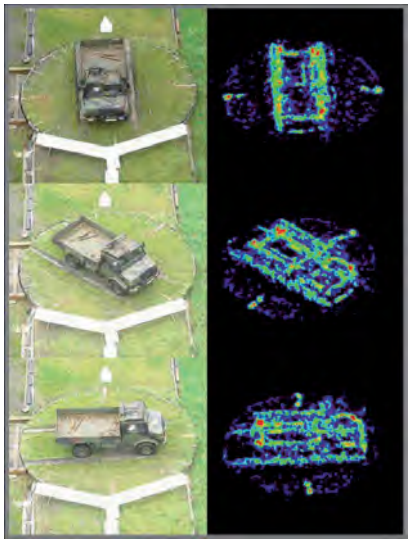

Figure 4-26: Photographs and corresponding perspectives of the 3D ISAR image (45° elevation).

respect to moderate differences between test and training data. Here a principal advantage is given by the robustness against artificially removed or generated new scattering centres. For the application of this approach an experimental data base of about two dozen civil and military vehicles was necessary and built up.

**Three-dimensional ISAR Techniques**

The correlation methods using adequately preprocessing can perform reasonable ATR performance. Nevertheless, the effort for building up a training data base by measurements as well as by simulations is tremendous. An approach for limiting the overall effort is enabled by the identification of robust scattering centre locations on a typical target of interest, thus determining those target parts being worthwhile for further efforts in the simulation. Therefore specific tower-turntable ISAR measurements are undertaken for generating three-dimensional (3-D) data sets by spanning a synthetic aperture not only in azimuth, but also in elevation.

Here the image generation is accomplished by the coherent integration of the calibrated raw data in the spatial frequency domain. The polar-format method enables the usage of a 3-D Fourier transform with the correct localisation of the raw data samples in the spectral domain. Therefore a kind of interpolation is applied to calculate the spectral data on an orthogonal equidistant grid.

First experiments on the tower-turntable were undertaken with a lorry of the type "Unimog" as the test object. In order to enhance the visual perception, the final result is composed by an incoherent superposition of all the single images of a complete turntable rotation. Once the 3-D image was built, it enables to change arbitrarily the perspective on the scatterer cloud. Such a variation of the viewpoint can simplify the determination of the object structure.

Figure 4-25 shows several projections of the 3-D radar image for three azimuth and five elevation directions including the front view in the upper left, the side view in the upper right, and the top view in the lower row. Also, four additional small reference trihedrals on the turntable besides the target are visible in the radar images. Due to the limited availability of the tower-turntable facility, the aperture sampling in elevation is sparse and irregular. Hence the corresponding ambiguities in the spatial domain had to be suppressed using a-priori knowledge of the volume pixels to be considered. In the projections of the 3-D image, especially the wheel rims, the front mudguards, and the rear corners of the loading platform are well distinguishable.

A helpful feature of the 3-D radar image representation is its direct comparability to an optical image as shown in Figure 4-26 which is in contrast to the 2-D case. Consequently the applied 3-D ISAR imaging enables an analysis for the determination of those target parts, which are most relevant for the radar backscattering.

**Signature Analysis of Urban Structures**

A further challenge for data interpretation is the composition of SAR images of urban structures. In fact the basic mechanism of the reflection and scattering behaviour has to be understood in very much detail. Theoretical models exist and can be used, but experimental data from a controlled environment are rather sparsely available. Urban structures are quite complicated with respect to backscattering and multi-bouncing mechanisms contributing to the received echo signals. In addition to a high number of possible material classes and surface roughness, a multitude of geometrical realisations of single objects or complete object areas

exist. Hence, the interpretation of the observed RCS and the understanding of how it is generated require the investigation of rather basic structures, which can be the basic components of more complicated objects. Such basic objects can be simple dielectric walls being erected in the vicinity of a dielectric foreground. This arrangement is highly present in an urban structure by buildings along roads or those located on a rather natural ground. Such typical wall structures have been constructed and measured fully-polarimetrically in the X-band by ISAR techniques.

Therefore a square-shaped house-like structure in the centre of the turntable as shown in Figure 4-27 was built. The size of the four walls was about 2 m in width and 1 m in height. Four different materials for the walls have been used – plywood, brickwork, plasterboard and gas concrete, whereas the roof was made of microwave absorber in order to avoid multiple reflections inside the house. The foregrounds have been changed between short dense grass, concrete, and smooth metal in order to arrange easily several realistic combinations.

Initially the ISAR raw data, i.e. about 3600 complex frequency profiles for 360° azimuth angle, are coherently processed into 144 single RCS images for 2.5° azimuth step size. In a next step those all are incoherently superimposed to one final image by selecting for each pixel of this image the strongest RCS value of all 144 images at this pixel location. This method allows a rather global comparison of the radar backscatter behavior for each illumination direction of the wall structure.

As an example, three images are shown for all polarisation combinations in Figure 4-28. The polarisation is indicated in the upper left corner, while a colour bar on the right illustrates the calibrated RCS values. Additionally the wall materials are specified for each wall side. For clarity only for an inner disc area of 5 m diameter the RCS values are shown. Outside, only some groups of small trihedral reflectors of different quantity are visible, which have been used as additional indicators for the wall type. The RCS of the trihedral reflectors was reduced by 30 dB in order to be in the range of the grass clutter.

Initially it stands out that the RCS of the HH polarisation has the highest values followed by the VV and the HV combinations. For HH all wall materials show a considerable backscatter. For VV only brick and plasterboard, and for HV only brick and gas concrete are significantly above the grass clutter level. Note that the groups of trihedral reflectors are not visible in the HV image as expected.

Figure 4-29 shows the maximum RCS values for each measured wall-foreground and each polarisation combination. Along the abscissa the foreground materials are indicated, and on the graph's top the wall materials are specified and marked in terms of colour. The values of identical polarisation combination are connected by lines. In general a high variability in radar return depending on the material combination and the polarisation can be observed.

### New Experimental Radar Development

In the last few years the new experimental high-performance multi-functional radar system UniRad (Universal-Radar) has been developed and constructed. The system shall serve for ISAR measurements within a tower-turntable arrangement, and as well for ground-based SAR measurements performed from a vehicle platform. Consequently fully-polarimetric high-resolution radar signatures of interesting objects can be measured, and realistic error sources for various SAR modes can be experimentally simulated.

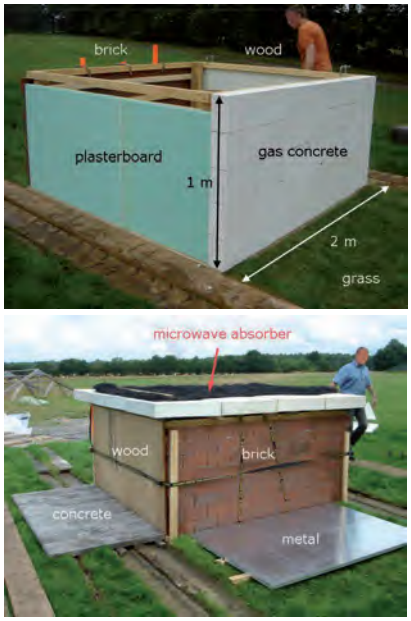


**Figure 4-27: Photographs of the wall structure during construction (top) and after completion (bottom). Visible are the different wall material types and those for simulating the foreground.**

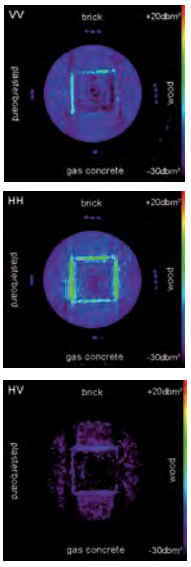


**Figure 4-28: Incoherently superimposed RCS images of the wall structure and grass as foreground for different polarisation combinations (transmit-receive).**

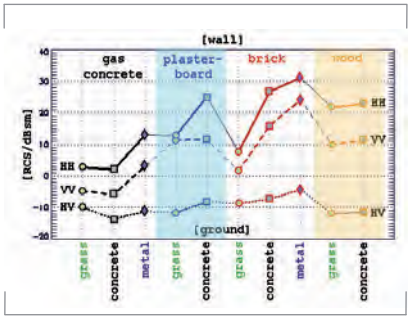


Figure 4-29: Extracted maximum RCS values from each measured wall-foreground and each polarization combination.

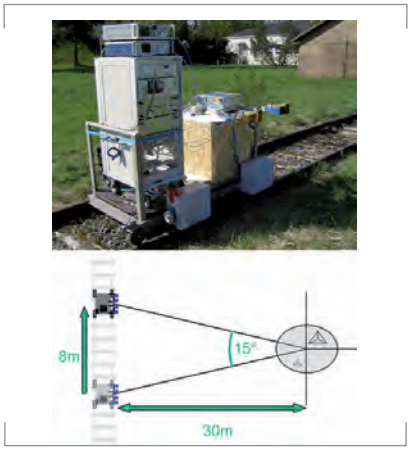


Figure 4-30: UniRad system (top) mounted on a railtrack vehicle. Four horn antennas for fully-polarimetric X-band measurements are connected. The synthetic aperture is generated by moving the side-looking radar along the railway as indicated in the top-view sketch below for a typical example.

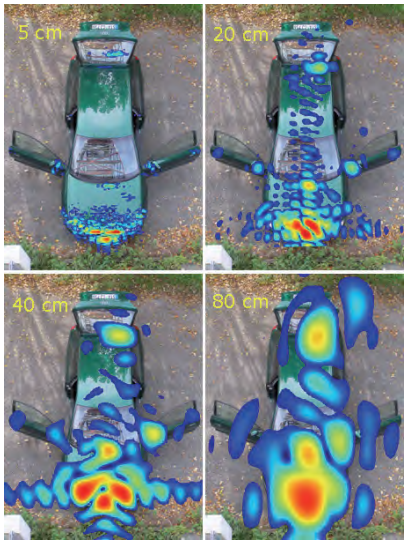


Figure 4-32: Photographs and superimposed X-band radar-cross-section signatures of a car with open doors for various spatial resolutions as indicated in the upper left edges.

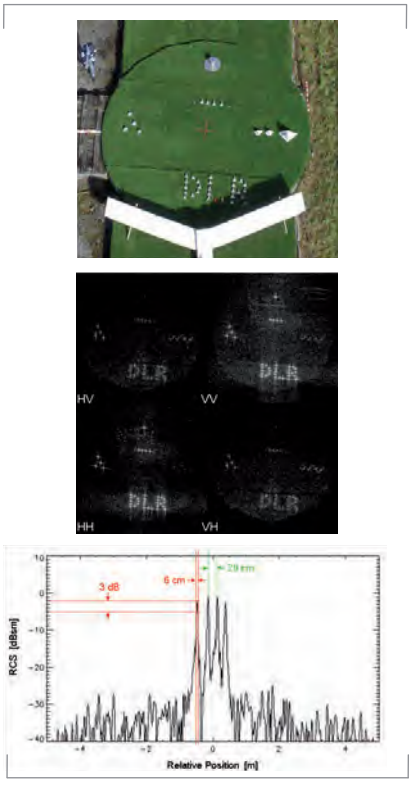


Figure 4-31: Photograph (above), RCS images of all polarisations (HV, VV, HH, VH) of a test scenario including canonical objects of different size in different patterns (middle) and RCS profile of the four trihedrals aligned in a line as visible above the DLR pattern.

The fully-polarimetric radar again is configured as a stepped-frequency system enabling now the use of up to 4 GHz bandwidth and a maximum flexibility in forming the signal shape. The modular concept allows the choice of almost any frequency band within a range of 1-18 GHz considering only a few technical restrictions. The radar consists of three main modules in order to decrease maintenance and transportation efforts: the transmitter and tunable local oscillator (LO) generator; the receiver and internal control unit; the intermediate frequency (IF) converter unit. This breakdown structure furthermore enhances crosstalk attenuation and thermal stability. Additional modules for the power supply, an external control unit using a personal computer, and a high-power amplifier (HPA) are also included in the main rack, which has a standard industrial 19" size, as shown in Figure 4-30 installed on a railtrack vehicle for SAR measurements.

In a first experiment using the new radar system the investigation of spatial resolution impacts on artificial man-made targets was of interest. X-band RCS images of four different spatial resolutions are shown in Figure 4-32 as a geometrical correct superposition to an optical photograph. The target was illuminated from the bottom by the radar beam. It is immediately obvious how the higher resolution increases the information content of the RCS images. While for 80 cm only rather the existence of an elongated object can be extracted, the 5 cm resolution allows the detection of very small object features like the front part, the rear mirrors and pulls on the doors, and the rear window wiper. Hence for proper target recognition a suitable resolution is mandatory, and such experiments allow a realistic estimation of the specific requirements.

Results from first fully-polarimetric high-resolution experiments at the tower-turntable facility are illustrated in Figure 4-31. The test scene included

trihedrals of different sizes and tophats. The letters writing 'DLR' using small trihedrals had an height of about 1 m. The image resolution was 6 cm as expected by the applied bandwidth and elevation, as can be read from the RCS profile in Figure 4-31 representing a slice through the group of four 0 dBsm trihedrals in one line in the upper central image part. The dynamic range of the RCS images is about 50 dB. Even in the cross-polar images, the trihedrals are visible due to scattering at the finite thickness of the construction plates. Even though the first imaging results of Unirad show pretty much the expected performance, some residual errors have been detected and the corresponding fine-tuning is still to be performed.

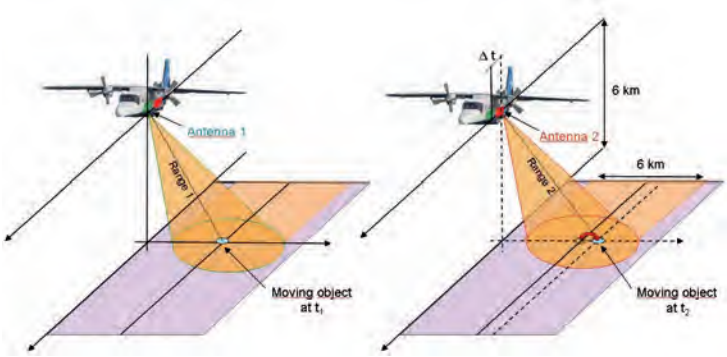


**Figure 4-33: Example of two-channel side-looking radar-target geometry used for the SAR/MTI simulations. The antennas (marked in red and green colour) are arranged in along-track direction for clutter suppression and velocity estimation.**

## Traffic Monitoring

The DLR is pursuing two coordinated traffic monitoring projects which focus on the improvement of transport management in the event of large-scale events or catastrophes. The project DELPHI at the Institute of Transportation Systems will be a basic platform for the situation assessment and integrative management. It evaluates data from airborne optical and radar sensors resulting from the project ARGOS. Under the leadership of the Remote Sensing Technology Institute in ARGOS a system for extensive and real-time capable traffic situation monitoring from an aircraft is under development that simultaneously serves as an infrastructure monitoring system by generating airborne optical or SAR images. The goal is the collection of traffic-relevant data of large areas, such as the number of vehicles, vehicle speeds, or the condition of the related infrastructure. In addition to optical sensors radar serves as an all-weather monitoring system. In ARGOS the Microwaves and Radar Institute has the leadership for the sub-project radar system. It is aimed to expand the F-SAR radar system so that data can be processed on-board in quasi-real time and that a data downlink capability can be achieved.

Already in 2005, the Institute started the predecessor project TRAMRAD (Traffic Monitoring with Radar). This project was established to investigate the possibilities of using airborne or spaceborne radar for the monitoring and control of road traffic. The goal was the definition of realisable system concepts for radar systems, which are able to frequently extract wide-area traffic data for traffic monitoring or, in extended time intervals, for traffic planning. SAR/MTI (moving target indication) methods had been studied and evaluated intensively with respect to their suitability.

In 2007 TRAMRAD was integrated in ARGOS, in which an operational airborne platform will be developed and demonstrated. Till the end of 2009 the optical sensor shall be operational and radar shall demonstrate its potential with respect to real-time capability. The experiences gained in TRAMRAD by processing the work packages MTI and multiple channel SAR systems as well as by the preparation of the F-SAR system paved the way for starting the

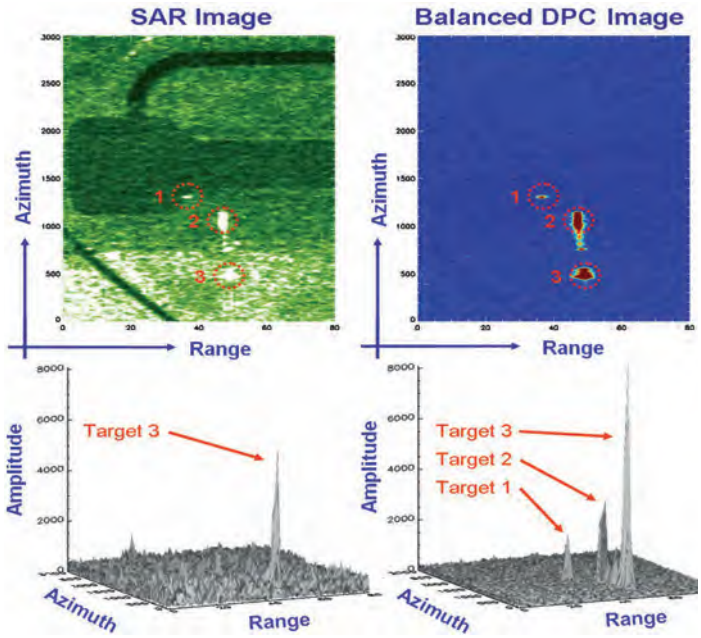


**Figure 4-34: Clutter suppression using DPC technique and channel balancing. All moving cars no. 1-3 could be detected from the DPC image on the right. The results were derived from experimental E-SAR data. Left: normal processed SAR image.**

implementation of an operational radar system for road traffic monitoring in the future.

### SAR/MTI

In general, with standard SAR processing it is not possible to detect and focus moving targets on the ground, because SAR assumes stationary scenes. One major challenge of MTI is the detection of slowly moving targets in the presence of clutter. To perform effective clutter suppression, at least two antennas arranged in the along-track direction are necessary (Figure 4-33). The achievable improvement of clutter suppression was demonstrated in TRAMRAD by processing dual-channel experimental E-SAR data (Figure 4-34) and by simulation.

A further challenge is the correct estimation of target velocities. By processing E-SAR data, experiences could be gained in the estimation of across-track velocities and Doppler slopes of moving targets which can be achieved with high accuracy by applying a matched filter bank and fractional Fourier transform in combination with along-track interferometry (ATI) and time-frequency analysis. The correct estimation of along-track velocity without using a priori knowledge, like a digital road map, is still unsolved for mult-channel systems, because the effect of along-track velocity and across-track acceleration on moving target's Doppler cannot be separated. Further investigations are necessary to overcome the problem of reliable along-track velocity estimation.

Depending on the system and antenna configuration, MTI performance can be further increased with multi-channel systems. Already, with the aid of a third receiving antenna clutter suppression can be improved, blind velocities eliminated and ambiguities in the measurement of across-track velocity resolved.

### Multiple Channel Systems

Multiple channel techniques combine array techniques with SAR processing. While classical SAR systems process the received signals either in the time domain or frequency domain, multi-channel systems, additionally, can spatially separate signals by beamforming on receive. This is necessary especially for the detection of slowly moving targets, because the received signals are ambiguous in the frequency domain but resolvable in the spatial domain. Thus, the moving target indication capability of multi-channel SAR systems is beneficially studied in the angle-Doppler domain. The sensitivity plane of a non-equidistant four-channel along-track configuration is shown in Figure 4-36. The main diagonal passing through zero Doppler at 90° (broadside direction) exhibits a sharp notch, which suppresses the clutter.

Even slow moving targets will be outside this clutter notch and, hence, remain unattenuated. As can also be seen, additional clutter notches result from spatial or temporal subsampling. Their positions are defined by the PRF and the antenna separations. The width of the clutter notch mainly depends on the overall length of the antenna.

Furthermore, in TRAMRAD Space-Time Adaptive Processing (STAP) techniques were studied and the differences between airborne and spaceborne systems investigated. Fundamental differences mainly result from the different height, velocity and stability of the platform.

**Experimental MTI-Processor**

Presently, in ARGOS a modular multichannel SAR/GMTI processor is under development (Figure 4-35) which bases on derived TRAMRAD results.

Two basic approaches are going to be implemented: the general case, that no a priori knowledge about the road map is available and a second case, that the courses of major interesting roads are known. Latter case will be realised for the demonstration of the near real-time capability of the on-board SAR/MTI processing till the end of ARGOS.

Several flight campaigns were flown with the modified F-SAR system. Figure 4-37 shows an actual result of an evaluated traffic scene corresponding to a part of the motorway A8 at Lake Chiemsee. The SAR image shows the detected vehicles on the motorway whereby the according velocities are indicated by false colours.

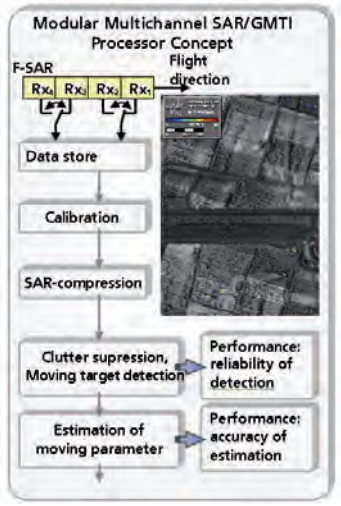


Figure 4-35: Concept of the modular structured experimental SAR/MTI processor.

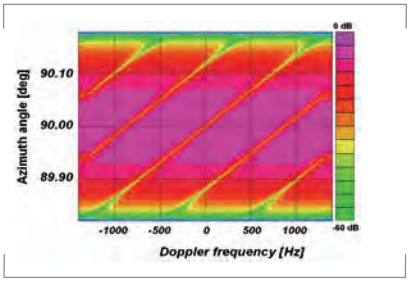


Figure 4-36: Transfer function of a four-channel non-equidistant along-track configuration plotted as a function of azimuth angle and Doppler frequency. Yellow shows the areas where signals are suppressed. Violet is maximum gain.

Figure 4-37: Detected road vehicles in beam center geometry SAR image. The scene shows a part of the Autobahn A8 at Lake Chiemsee.

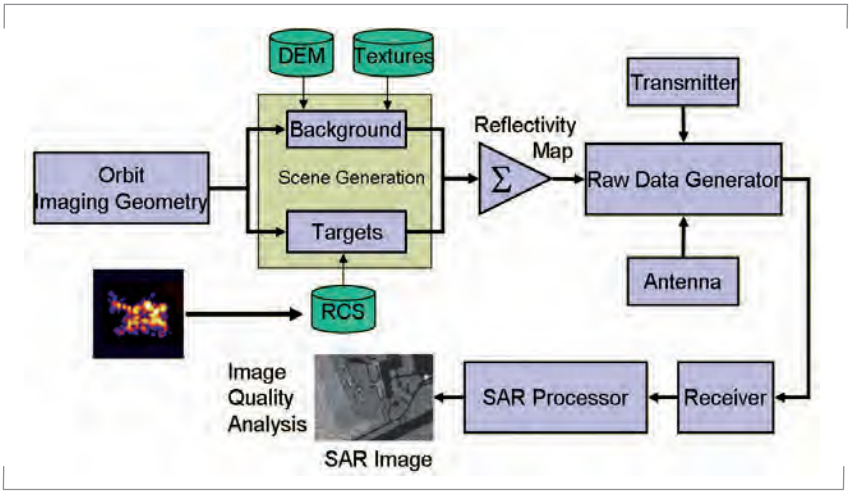


**Figure 4-38: Principal structure of SETES with the main modules for orbit and imaging geometry calculations, the generation of backscattering values, the generation of raw data, and image processing.**

# End-to-End SAR Simulation

Accurate simulation tools for the design of spaceborne synthetic aperture radar systems (SAR) are compulsory for the analysis of the system's capabilities, because ground based experimental tests are in most cases impossible and very costly. Through a simulation process it is possible to analyse the image quality parameters for a given system configuration or evaluating the effects in SAR images when this configuration is changed.

To simulate effects for different configurations of the system parameters, a SAR End-To-End Simulator (SETES) was developed. SETES is based on realistic mathematical modelling of an overall SAR system chain and generates information on the quality of the image data and its suitability to interpret target and background signatures. The simulator fulfils several objectives:

- Estimation of SAR system's capabilities and determination of trade-offs during the design phase
- Analysis and demonstration of the system's reaction to changes of operational requirements under space conditions
- Analysis and elimination of system defects and determination of their effects on the image quality
- Support for training SAR operators and image interpreters

The flexible and modular structure of the simulator allows for adjustment and extension to fulfil different tasks. The principal components of SETES are:

- The generation of the scene, including the fully polarimetric scattering behaviour of the 3-D surface and objects, and including typical SAR effects like overlay, speckle noise, shadowing, etc.
- An accurate SAR sensor simulation (antenna, transmit and receive path)
- Generation of the raw data
- Image processing and evaluation

The simulation of the whole system chain is possible but can be very time consuming. That is why a new fast SAR image simulator (SARBIS) is currently under development on the basis of SETES. This image simulator produces SAR images by using the point spread function (PSF) of a focused point target response in contrast to SETES's very expensive raw data generation module. In SARBIS the SAR image is produced through a convolution of the PSF with the reflectivity map of the scene.

**Simulation Concept of SETES**

The SAR End-To-End Simulator SETES is capable of simulating the whole SAR system's chain - from realistic raw data to a focused image of three dimensional scenes. A detailed view of the simulator's structure is given in Figure 4-38.

The toolset consists of independent modules for the different stages in a SAR system's chain. The orbit imaging geometry module calculates the state vectors of the sensor at all time steps and delivers transformation parameters

to switch between the coordinate systems of the Earth, platform, antenna and scene. The scene module is used for calculating the reflectivity values for all resolution cells in the resulting image, taking into account the geometry, material and roughness properties, speckle noise and embedded targets. This information is saved in the so-called reflectivity map. This map inputs into the raw data generation module, which delivers the raw data for the desired SAR receiving mode. The SAR processor module implements different types of algorithms, like the chirp-scaling or omega-k method and produces a focused SAR image as the end product of the system chain. Below, the main modules reflecting the basic physical models are described in more detail.

*Reflectivity Map*

The tasks of this module are to generate the backscattered reflectivity, to superimpose the RCS signatures of targets and to perform the transformation of the reflectivity data onto the slant range plane of the SAR sensor. To simulate realistic SAR raw data of extended background scenarios, the use of altitude profiles is necessary, since the influence of the relief plays a great role in the formation of the final image. It is essential to make allowance for specific SAR effects like layover, foreshortening and shadowing. Moreover, the change of the backscatter mechanism caused by different incidence angles and polarisations of the waves can be taken into account.

The starting point for generating a reflectivity map is the geometric model of the scene to be considered. This is usually given through an elevation grid with polygons as basic geometries as can be seen on the left in Figure 4-39. Moreover materials and roughness properties have to be assigned to the faces of this model. On the right in Figure 4-39, the materials are assigned to the faces of the surface model on the left by colour indexing.

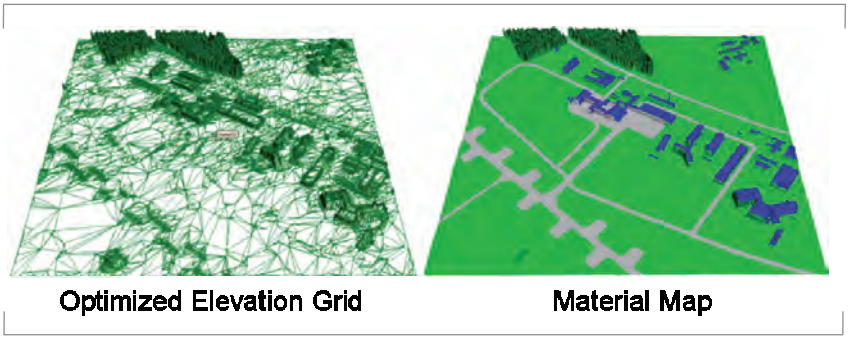


**Figure 4-39: Surface model (left) and surface model with materials attached as texture on the faces (right).**

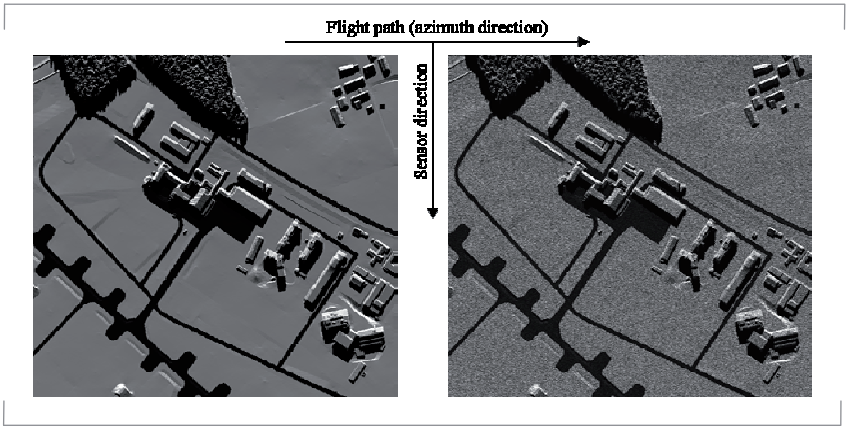


**Figure 4-40: Reflectivity map of the surface model above (left) and reflectivity map with Speckle noise inserted (right).**

In the next step the scattering matrix is calculated by different approximation methods. Currently, the software tool implements the small perturbation model (SPM) and the Kirchhoff model (KM). SPM is valid for low frequencies, where the considered geometry is much smaller than the incident wavelength. For high frequencies the approximation method KM is used. In addition to theses theoretical implementations an empirical model is inserted, where materials over a wide range of frequencies, incidence angles and roughness along with measured profiles are included. Moreover, in order to get double bounce effects into the reflectivity map the methods were extended with this feature. Additionally,

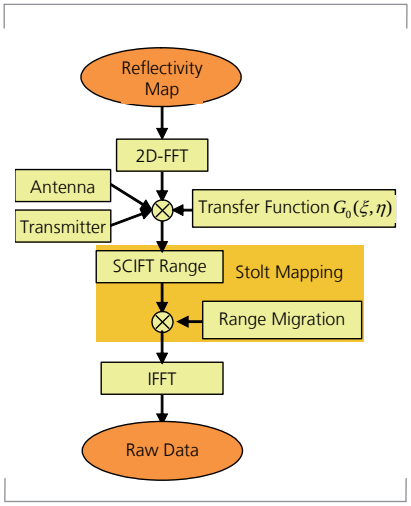


**Figure 4-41: Flow chart for the raw data generation of the stripmap mode with the space-independent part of the system transfer function and the space-variant part referred to as Stolt mapping.**

it is possible to superimpose the scattered fields of complex targets into the reflectivity map by using a database of measured targets on tower turntables.

In Figure 4-40, the reflectivity map for the surface model is shown. Only buildings, streets and woods where considered in the CAD-model, leaving out details like cars or airplanes. It is possible to insert such objects, but for showing the principle effects in SAR images this model suffices. Dark regions contribute weak parts and bright regions strong parts to the backscattered fields. Layover effects of strong double reflective fractions at buildings in sensor direction can be observed along with the shadowing effects on the opposite side. The implementation of speckle noise is directly done on the reflectivity map as can be seen on the right of Figure 4-40.

The resulting reflectivity map of the scenario is respectively input to the raw data generation module of SETES or directly convolved with the point spread function in SARBIS.

*Raw Data Generation*

The flow chart of the raw data generation module is illustrated in Figure 4-41. It shows the basic structure of the algorithm for the stripmap mode.

The raw data collected by a SAR sensor are not separable in azimuth and range directions, because of the range migration and curvature effects. In an analytical expression of the impulse response function, this dependence is given by coupling terms in the azimuth and range directions. A precisely modelled impulse response function must be considered in two dimensions. In the time domain the range dependence can be taken into account easily, but the computing time is unacceptable for the required scenario sizes. A more efficient solution is obtained by calculating the raw data in the two-dimensional frequency domain. The algorithm used is based on an analytical evaluation of the system transfer function via the stationary phase method. A detailed evaluation of the system transfer function in the Fourier domain shows that it can be formulated as the product of two factors, a space-invariant factor and a space-dependent one. The latter requires non-linear mapping of the range frequencies, usually referred to as Stolt mapping. This algorithm avoids time-consuming interpolations. It uses a Scaled Inverse Fourier Transform (SCIFT), followed by a phase shift in the azimuth-frequency range domain.

**Figure 4-42: Principal structure of SARBIS with the usage of the point spread function instead of a raw data generation module.**

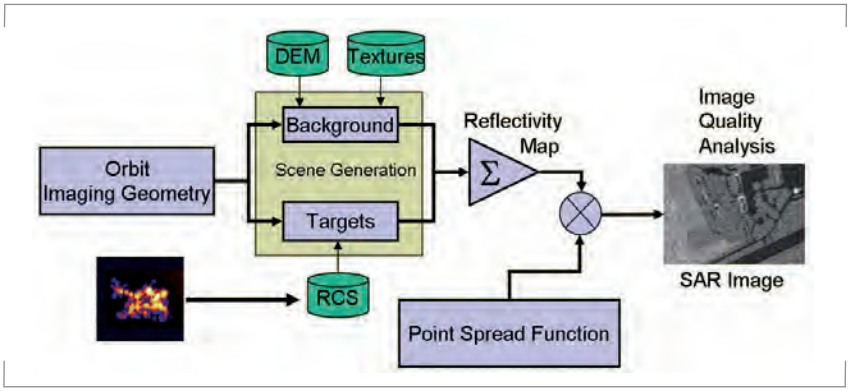


### Simulation Concept of SARBIS

The general approach of SETES gives the possibility to change every possible parameter of the SAR system chain or even the generated raw data itself. Nevertheless there exists a significant drawback, which is runtime and memory efficiency. To simulate a large down-to-Earth scene the described tool reaches its limits even with powerful computer systems.

If the primary goal of a simulation is to generate realistic image data and associated quality parameters, like the peak-to-sidelobe ratio (PSLR), it is possible to do without the costly raw data generation. This can be realised by processing the raw data of a point target response and do a convolution with the reflectivity map to produce the wanted

SAR image. A new efficient SAR image simulator (SARBIS) is currently under development using this approach. In Figure 4-42 on the bottom left the structure of this alternative procedure is shown as a modification of SETES's processing structure.

As illustrated in Figure 4-42, the concept of generating the raw data is abandoned and the convolution with the complex point spread function (PSF) of a focused point target response takes its place. The big advantage of this mechanism is the independence of the PSF from the objective scene, because only the raw data of a point target is used for its calculation. The information of the scene is solely inserted through the convolution with the reflectivity map. Through this decoupling the same PSF can be reused for several different scenes. On the other hand one can generate different PSF to study the resulting effects in the same scene or analysing the image quality parameters.

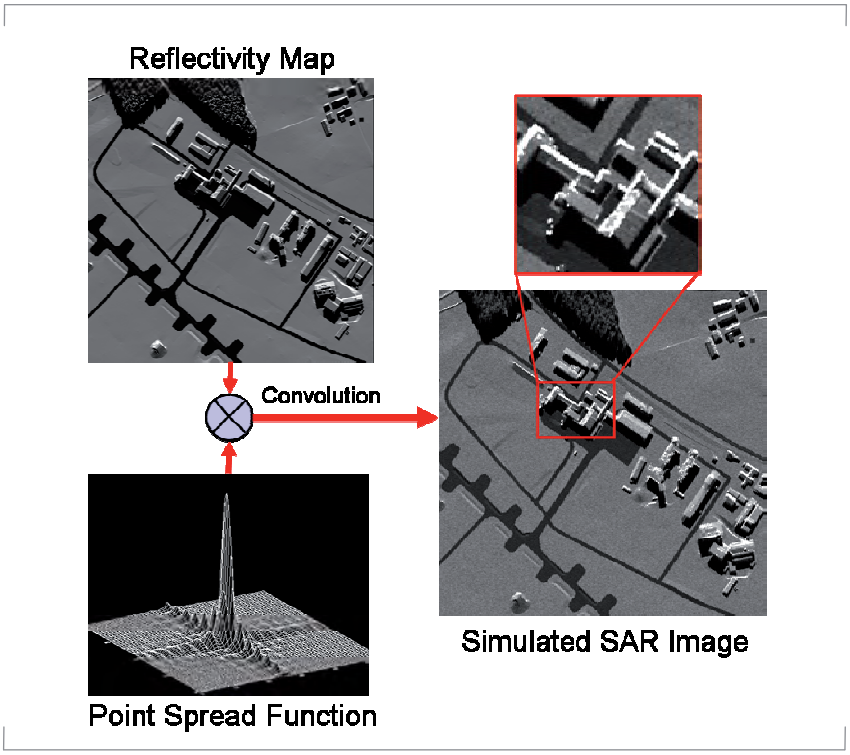


Figure 4-43: Simulation cycle of SARBIS.

*Determination of the Point Spread Function*

The SAR image is computed by processing a focussed point target response into the point spread function (PSF) and its convolution with the reflectivity map of the scene. The PSF describes how a point scatterer is imaged by the SAR and how energy due to the point target becomes spread into surrounding pixels. The PSF depends on the SAR system's parameters and on the platform behaviour. In SARBIS, the PSF is computed by generation of the raw data of the unitary point target and their focussing using a range-Doppler SAR processor.

The impulse response is spread out in range and azimuth directions. Hence, this signal has to be compressed to obtain the focussed point target response or point spread function. Figure 4-44 right shows an example for an impulse response on the left and its compressed point spread function on the right.

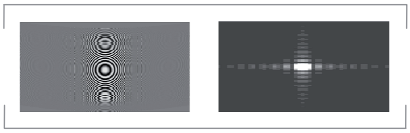

Figure 4-44: Raw data for a unitary point target (left) and pocessed point spread function (right).

After compression, the PSF results in a two-dimensional sinc-function. Since the nominal peak-to-sidelobe ratio for a sinc-function is of only about 13 dB, a weighting function is normally applied in frequency domain to reduce the sidelobes both in azimuth and range dimensions at the expense of geometrical resolution. Typical weighting functions are Hamming, Hanning, Gaussian and Blackman.

*Image generation*

Is the PSF of the SAR system known, one can produce the system output by convoluting this impulse response function with the input to the system,

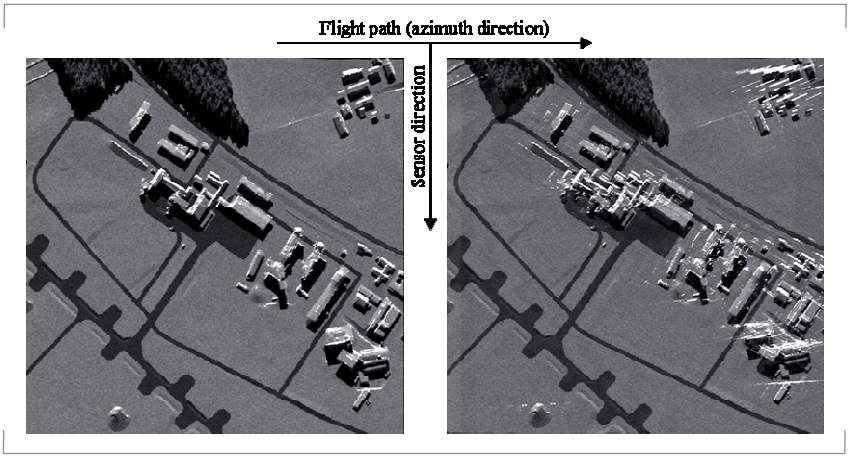


**Figure 4-45: SAR image without errors (left); SAR image with high frequency motion errors, causing ambiguities at dominant scatterers in azimuth direction (right).**

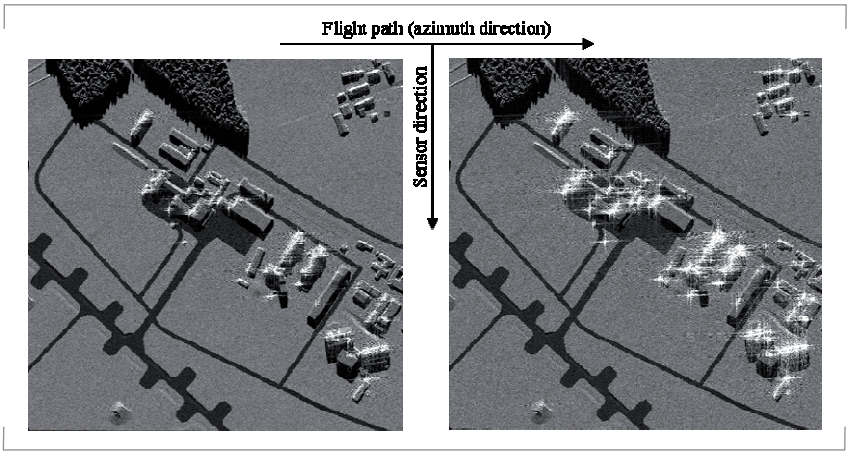


**Figure 4-46: SAR image with a PSLR = 21dB (left); SAR image with a PSLR = 13dB showing effects of poor suppression of the sidelobes (right).**

which is represented by the reflectivity map. Figure 4-43 illustrates the whole simulation cycle of SARBIS to produce SAR images. For the generation of the reflectivity map the modules of SETES are used.

**Simulation Examples**

This section introduces simulated SAR images for different effects on the point spread function. The selected scene is the one from the example before. The following SAR parameters were chosen for all scenes:

- Centre frequency: 9.6 GHz
- Bandwidth: 600 MHz
- Pulse repetition frequency: 7000 Hz
- Bandwidth of chirp: 300 MHz
- Duration of chirp: 2.5 μs
- Altitude: 2 km
- Elevation angle: 29°

In the following sections SAR image effects like motion errors and point spread functions with varying peak-to-sidelobe ratios are shown.

*Motion errors*

The following example (Figure 4-45) shows an example for a high frequency error over the synthetic aperture. For a better comparison a SAR image of the same scene without error is also shown on the left. The motion error creates ambiguities as can be clearly observed at buildings, where dominant scatterers are cloned in azimuth direction on both sides. The additional responses, often referred to as paired echoes, are due to high sidelobes in the point spread function in azimuth direction (see Figure 4-47). This phenomena is directly associated with the sinusoidal phase error. The presence of these sidelobes multiplies with the complex signal from each scatterer.

*Different peak-to-sidelobe ratios*

The application of different weighting functions on the PSF has a direct effect on image quality parameters like the PSLR. By applying a weighting the geometrical resolution goes down, but the suppression of the sidelobes gets better. The following images show these effects. The left example in Figure 4-46 illustrates a SAR image with a resulting PSLR of about 21dB, whereas the example on the right side shows a PSLR of 13dB. As can be seen in these figures the low suppression of the sidelobes causes blurring effects at dominant scatterers. The difference in geometrical

resolution can hardly be seen in the images, because they have a too small dimension in this illustration, but otherwise this effect is dominant for considerations in the design process of a SAR system. Nevertheless the change of resolution can be seen very clearly in Figure 4-48, for the corresponding point spread functions. The left diagram has a broader main-lobe than the right one, but on the other hand the damping of the sidelobes is significantly better.

*Thermal Noise*

The effects of thermal noise are implemented during image generation. The noise level is given as Noise Equivalent Sigma Zero (NESZ). The simulated SAR images in Figure 4-49 (a) - (d) illustrate the influence of the system noise for different noise levels.

The development of SETES and SARBIS will continue by extending the geometrical resolution to meet the needs of upcoming reconnaissance systems. Especially the core modules, i.e. the reflectivity map and raw data generation need to be updated.

# SAR Performance Analysis

Airborne and spaceborne SAR systems are characterised by a huge number of parameters which are interconnected in a very complex way. The development and optimisation of SAR systems therefore requires efficient software tools. The tools developed by the Institute use a modular approach to allow easy adjustment for different mission requirements or operating modes, e.g. stripmap, ScanSAR, spotlight, TOPS-SAR, bi-static modes as well as along track and across track interferometry as required for the TanDEM-X Mission. In particular, one performance tool is also used for the analysis of digital beamforming SAR systems utilising multiple channels in

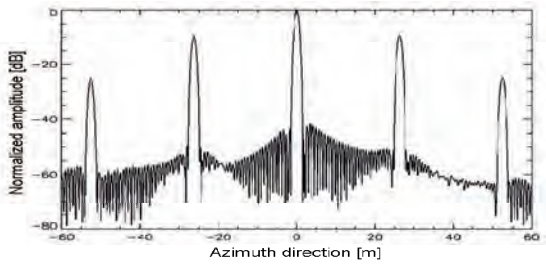


**Figure 4-47: Point spread function for a point target with an applied sinusoidal phase error with 35 cycles over the synthetic aperture and amplitude of 0.65.**

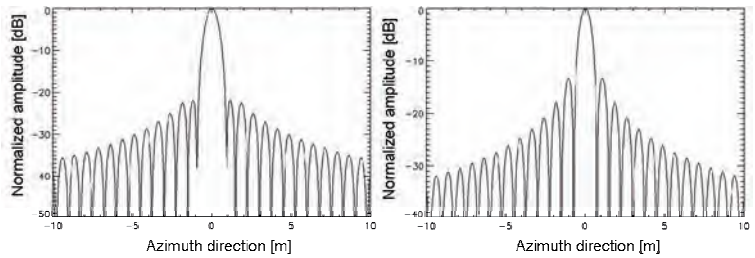


**Figure 4-48: Point spread function with a PSLR = 21dB (left) and 13dB (right).**

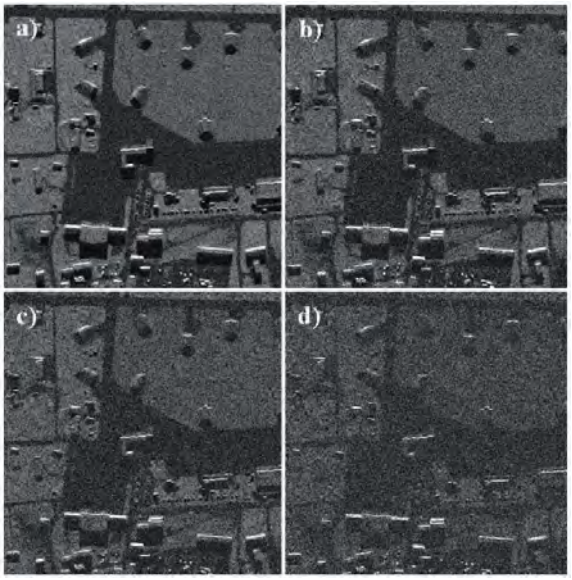


**Figure 4-49: Thermal noise effects: a) NESZ= -26 dB, b) NESZ= -20 dB, c) NESZ= -18 dB, d) NESZ= -13 dB.**

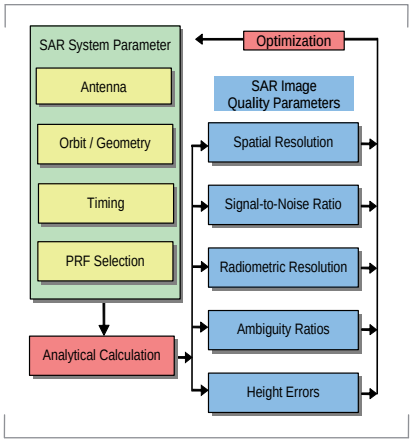


**Figure 4-50: General approach for SAR performance analysis with building blocks to describe the system parameters and optimization loops based on a trade-off with image quality parameters.**

**Figure 4-51: Screen shot of the Performance Estimator featuring some of the graphical analysis tools. From top left to bottom right: ambiguous areas, antenna patterns, PRF restrictions and the impulse response.**

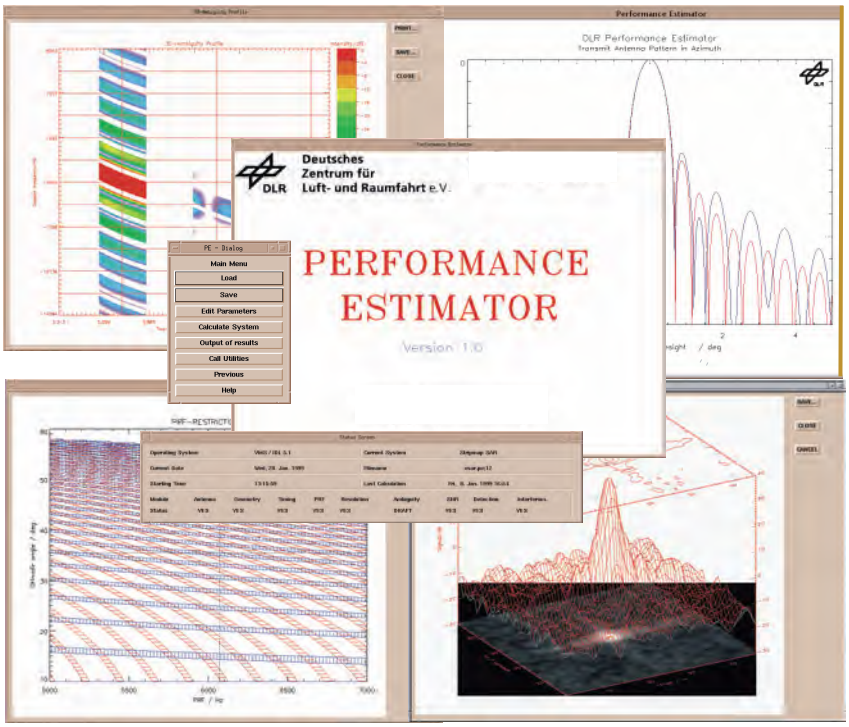


elevation and azimuth. It incorporates the highly advanced operation modes and dedicated reconstruction algorithms of these systems.

The general approach for the SAR performance analysis is depicted in Figure 4-50. The SAR system parameters are depicted by logical blocks, the most important ones being the antenna parameter computation, the imaging geometry description including the orbit, and the timing. A key parameter in the design process is the selection of the pulse repetition frequency (PRF), which is a highly constrained parameter. Once these parameters are determined in a first iteration, the quality parameters can be evaluated analytically. Prominent examples for SAR image quality parameters are spatial resolution, radiometric resolution and ambiguity ratios, or in case of an interferometric SAR, the estimated height errors of the digital elevation model. By assessment of these quality parameters the SAR system parameters can iteratively be optimised in the SAR performance analysis.

The software to perform this task is embedded in a graphical user interface and offers a variety of visualisation tools to support the interactive optimisation process (Figure 4-51). For operational purposes the calculation modules can be controlled independently from the graphical user interface to allow performance calculations as a function of arbitrary input parameter variations. With spaceborne SAR systems, for example, this allows the calculation of quality parameters as a function of the orbit position, accounting for the variation in height over ground.

### Application Examples

The orbit and imaging geometry module supports an elliptical orbit model to determine the platform velocity and position vectors by Kepler's theory in a geodetic coordinate system.
For operational purposes (e.g. TerraSAR-X), an XML-file interface to dedicated attitude- and orbit products is available to read in the state vector of the satellite.

For the attitude steering of TerraSAR-X (TS-X) the Total Zero Doppler Steering was developed. It theoretically provides zero Hz Doppler centroid, independent of incidence angle and terrain height variation. The key is to use pitch and yaw steering to align the satellite attitude to its velocity vector. Yaw and pitch angle profile as followed by the TS-X Attitude and Orbit Control System (AOCS) around one orbit.

Figure 4-52 shows the yaw and pitch angle profile as calculated by the TerraSAR-X orbit performance module. The TerraSAR-X AOCS system is following that profile around the orbits. By considering the residual SAR system errors in the performance estimation as for example the accuracy of the control loop, the residual Doppler centroid has

been estimated pre-launch to be in-between ±120 Hz for both, left and right looking geometry.

In the commissioning phase, a series of stripmap data takes from near to far range beams were acquired covering also different latitudes. The initial measurement is shown in Figure 4-53 where no dependency on latitude but a not expected dependency on incidence angle was found. The conclusion was that there must be a bias in yaw and pitch angle steering which was corrected in the star sensor transformation matrix. After correction of 0.109° in yaw and 0.066° in pitch, the Total-Zero-Doppler Steering (TZDS) worked as expected as can be seen in Figure 4-53.

The selection of the PRF is one of the most critical steps in the optimisation process. In SAR systems the time when echo data can be received is limited to the time interval between transmit pulses. Also, interference with the strong nadir echo should be avoided. The two interference conditions with transmit pulses and nadir echoes define bands of unacceptable combinations of PRF and off-nadir angle. Figure 4-54 illustrates these PRF bands and swath positions. The figure is based on the 512 PRF values flown on-board TerraSAR-X. As can be seen by the extension of the constant PRF sample values on the y-axis in the figure there is higher sampling at PRFs convenient for single polarisation data acquisition from 3000 Hz to 4600 Hz as well as for dual polarisation from 5800 Hz to 6500 Hz.

Once the PRF has been selected, the image quality parameters can be derived. Figure 4-55 illustrates an example of the azimuth impulse response analysis determining the spatial resolution and peak-to-sidelobe ratio (PSLR). The software tools support the simulation of impulse response distortions in azimuth and range due to systematic and random phase and amplitude errors. For military SAR systems a new module was developed

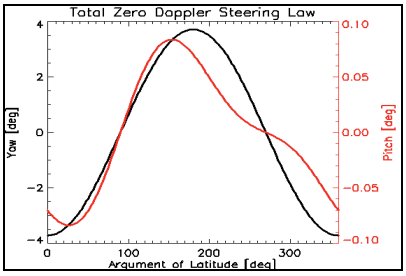


Figure 4-52: Yaw and pitch angle profile as followed by the TS-X AOCS around one orbit.

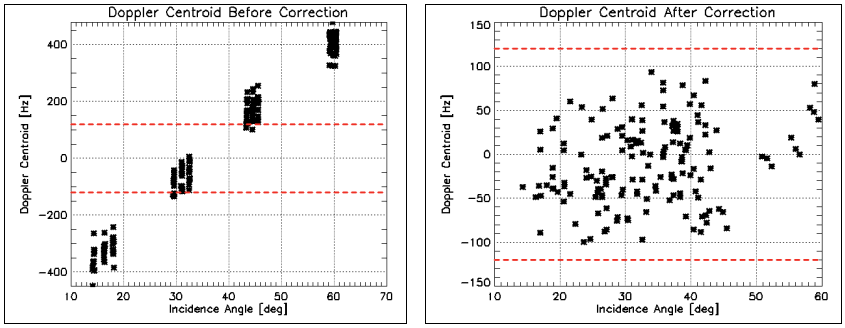


Figure 4-53: Total-Zero-Doppler Steering. Doppler centroid before (left) and after correction.

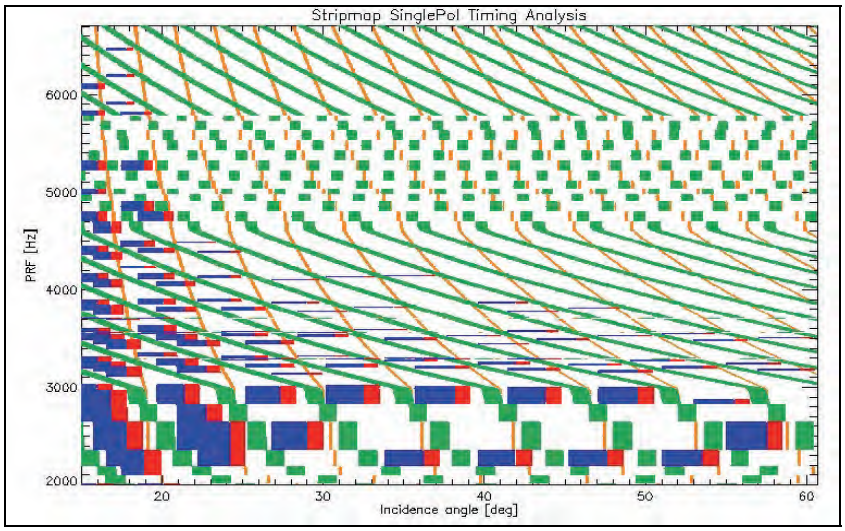


Figure 4-54: TerraSAR-X single polarisation PRF selection diagram at one dedicated orbit position with flight configuration beam swath width in blue, pulse length extensions in red, transmit interferences in green and nadir interferences in orange.

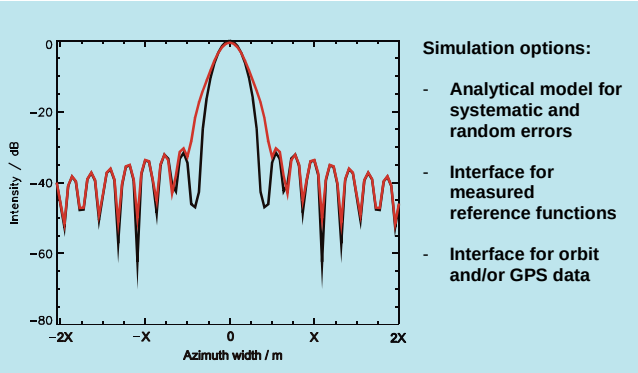


Figure 4-55: Impulse response analysis (black curve: ideal impulse response with Hamming weighting, red curve: distorted impulse response due to GPS position and velocity errors).

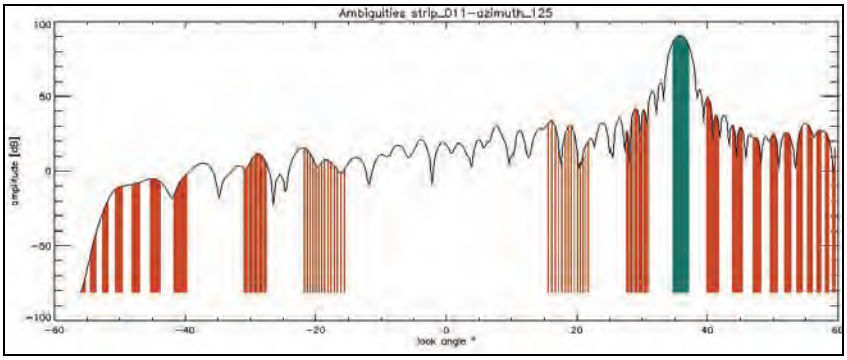


Figure 4-56: Range ambiguity analysis of TerraSAR-X stripmap beam 11 (green: desired swath area, red: ambiguous echo areas).

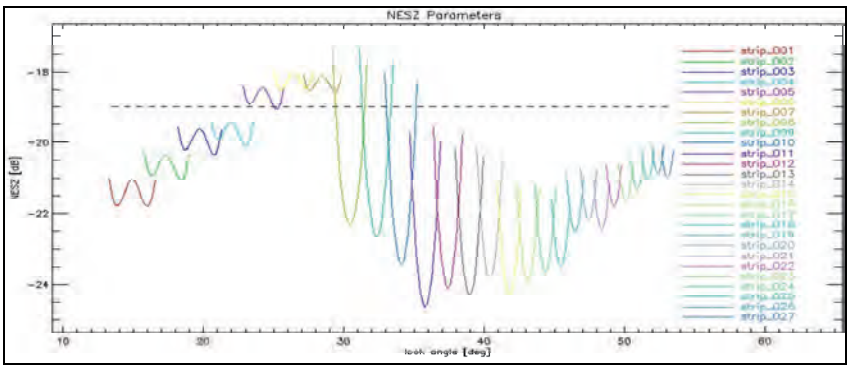


Figure 4-57: Radiometric analysis for TerraSAR-X. Different colours indicate the NESZ performance for the sub-swaths.

to process real or simulated orbit data to analyse, for example, the effects of a GPS based motion compensation and to study the possibilities of improving the spatial resolution of future SAR systems.

Figure 4-56 illustrates an example for a range ambiguity analysis. The ambiguity ratios describe the intensities of all ambiguous areas illuminated by the antenna sidelobes compared to the desired echo signal intensity. The red areas indicate the ambiguous areas and the green area the desired swath area. The range ambiguity mainly depends on the antenna pattern, the slant range and the radar reflectivity at a certain off-nadir angle.

Another important quality parameter in the radiometric analysis of a SAR system is the noise equivalent sigma zero (NESZ). This value specifies the radar reflectivity level equivalent to the noise level and is often used to describe the limiting sensitivity of SAR systems. The statistics of various scattering classes at different frequencies and polarisations are included in the software tools. Figure 4-57 illustrates a radiometric analysis of the TerraSAR-X system for several sub-swaths.

The available software tools mentioned here were tested and evaluated with data of existing spaceborne systems like ERS- 1/2, SIR-C/X-SAR, SRTM, Radarsat-1/2 and TerraSAR-X as well as airborne systems like the Institute's E-SAR. Also verification tools have been developed to comprehensively analyse measured SAR data to verify the analytically calculated image quality parameters. Figure 4-58 gives an example of one of the SAR image analysis tools. It supports the analysis of point targets, as well as the analysis of distributed targets to determine the NESZ values or the radiometric resolution. Such software tools also offer a 3-D visualisation of the backscatter characteristic of selected areas.

The software tools for performance estimation and image analysis are being continuously adjusted to the requirements of new and evolving SAR systems. The future trends for space-borne SAR systems are monostatic and multistatic SAR systems provided by constellations of small satellites with a view to improving the system response time or to realise special modes like InSAR, Pol-InSAR, MTI or bistatic measurements. The use of airborne SAR systems will be extended to high altitude platforms such as UAVs or air ships.

# Radar Calibration

Radar calibration is a traditional R&D field in the Institute with almost 20 years of experience. The primary tasks of SAR calibration are to estimate and correct systematic error contributions throughout the complete SAR system and to convert the image parameters (magnitude and phase) into geophysical units. This could be maps of RCS or backscattering coefficients in the case of standard SAR images, or Digital Elevation Models (DEMs) acquired by interferometric systems like SRTM or TanDEM-X (see Figure 4-59).

The quality of this calibration process depends on the inherent stability of the radar system and the ability to determine and monitor the radiometric and geometric characteristics.

Propagation can have an important influence on imaging performance as well as calibration accuracy. Several propagation effects occur inside the atmosphere, which need to be monitored and, where possible, corrected. Tropospheric and ionospheric effects have been analysed and are used as a basis for the calibration of SAR satellite products.

The following sections concentrate on radiometric and geometric calibration.

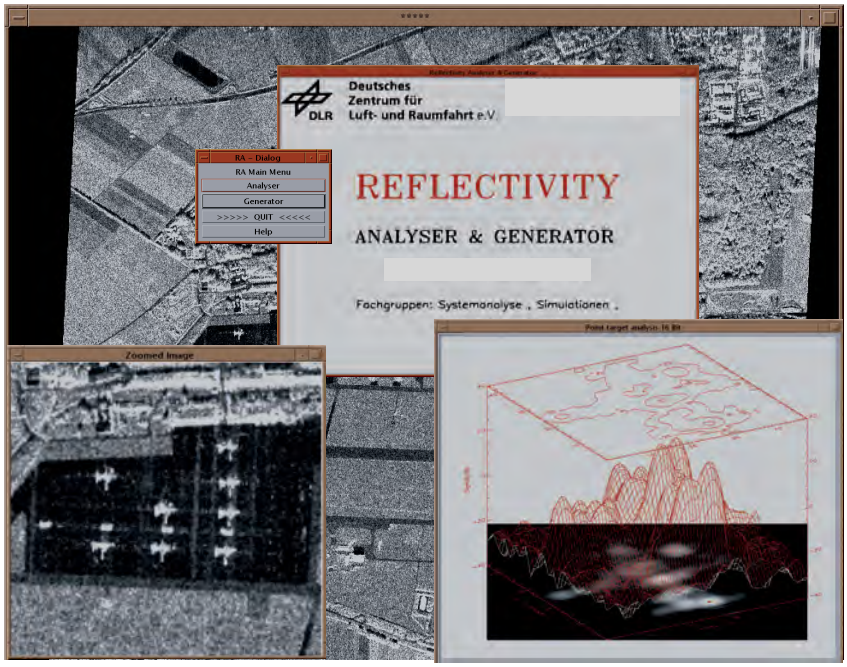


**Figure 4-58: Screen shot of the SAR image analysis tool. Background, the complete SAR image; left, close up of an area of interest; right, 3-D visualization of a target (aircraft).**

### New Calibration Concepts

In recent years, SAR antenna technology has developed from passive slotted waveguide arrays (e.g. ERS-1/2 or X-SAR) to active phased arrays (e.g. ASAR or TerraSAR-X), offering electronic beam steering capabilities required for acquisitions in different swath geometries and for operation in ScanSAR and Spotlight modes. Furthermore, with a growing number of operational applications and services, the requirements on radiometric and geometric calibration become increasingly demanding.

TerraSAR-X is an ideal example of a multiple mode high-resolution SAR and features the following operational

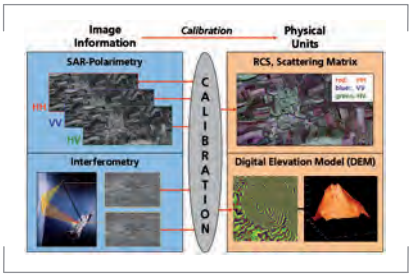


**Figure 4-59: The calibration process transforms the image information into geophysical units like RCS maps or digital elevation models.**

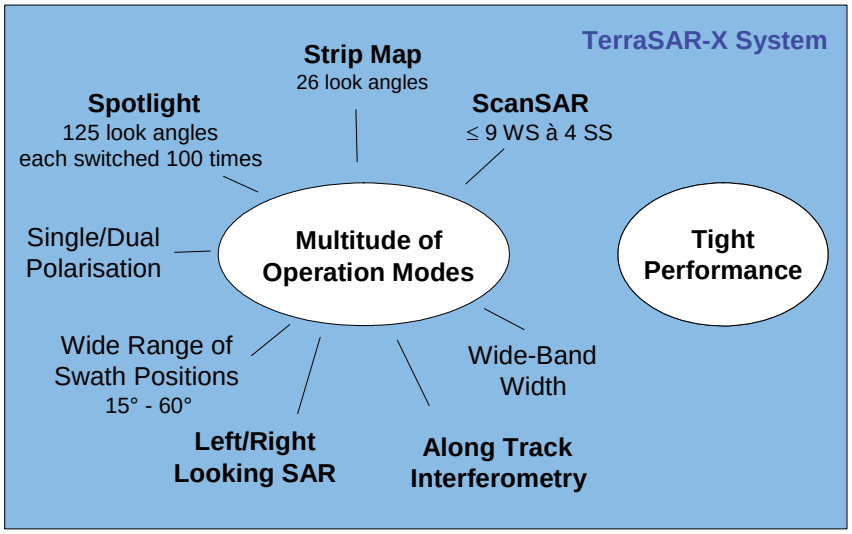


**Figure 4-60: Calibration challenges of multiple mode high-resolution SAR systems such as TerraSAR-X.**

**Figure 4-61: Rain forest scene used for radiometric calibration.**

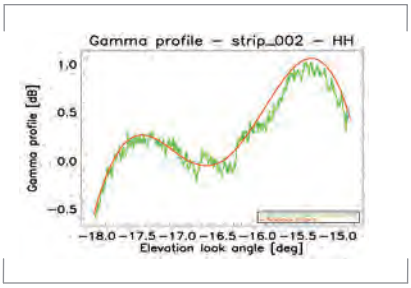


**Figure 4-62: TerraSAR-X reference elevation pattern (red line) in comparison to the measured gamma profile (green points) of the above rain forest scene.**

modes (see Figure 4-60):

- Stripmap Mode at up to 26 different look angles (swath positions)
- ScanSAR Mode in 9 different wide swath configurations each consisting of 4 sub-swaths
- Spotlight Mode at up to 125 different look angles implemented by switching between more than 100 different azimuth beams

Additionally, innovative and experimental modes have been successfully demonstrated after launch like wide-bandwidth operation or applying the novel TOPS-SAR mode for ScanSAR imaging.

Due to this high degree of flexibility of TerraSAR-X and a tight performance requirement of an absolute radiometric accuracy better than 1 dB it becomes clear that a conventional calibration approach is not feasible. For early SAR systems like ERS or X-SAR, calibration involves internal calibration of a single transmit/receive chain (via special calibration loops), the determination of a single antenna beam pattern and the absolute calibration in one or two operational modes. The real measurement of all antenna beams in all operation modes, as performed for the ASAR instrument of ENVISAT across the rainforest is too time-consuming. For current multiple beam systems (approx.10000 beams in the case of TerraSAR-X) based on active phased array antennas with hundreds of transmit/receive modules, a novel and affordable calibration concept has been developed. Important calibration tasks are already covered before launch to account for the restricted time of in-orbit calibration campaigns during the short commissioning phase. The key element of this efficient calibration concept is a novel antenna model approach.

In the frame of TerraSAR-X system development and in-orbit calibration this innovative calibration strategy has been successfully applied and is presented below.

*Antenna Model Approach*

Active phased array antennas do not only have the advantage of fast and flexible control of the patterns but also the ability to be mathematically modelled. Such an antenna model provides a tool to accurately determine the antenna beam patterns based on detailed characterisation of the antenna hardware and knowledge of the antenna control parameters.

To achieve the required radiometric quality, this concept requires highly accurate pre-launch characterisation data. After pre-launch validation against near field range pattern measurements and in-flight verification, the antenna model will be used throughout the satellite lifetime to generate the antenna patterns, as required for the radiometric corrections in the SAR processing, and for beam optimisation in case of degraded antenna characteristics.

To verify the antenna model performance for the whole antenna

in space, in-orbit measurements have been performed during the commissioning phase of TerraSAR-X. On this an accuracy of ± 0.2dB has to be achieved for both, the shape of the antenna pattern within the main beam and the gain offset between different beams. The reason for that number is not only driven by the radiometric accuracy budget but also by the visibility of the gain offset in ScanSAR images. This verification was performed with a few selected beams measured in-flight and can be divided into three main tasks:

- Measurements across the Amazon rainforest to verify the elevation pattern shape (Figure 4-62),
- ScanSAR measurements across the Amazon rainforest to verify the calculated peak-to-peak gain offset between different beams (Figure 4-63) and
- Measurements using ground receivers to verify the azimuth pattern shape (Figure 4-64).

The verification of the antenna model in elevation shows a very good accordance between the simulated antenna pattern and the measured gamma profiles. The deviation and hence the accuracy of the model for the antenna in space is within the required ± 0.2 dB (peak-to-peak), which is excellent, as can be seen for the exemplary gamma profile in Figure 4-62.

The prediction of the peak-to-peak gain offset between different beams (i.e. the gain variation in the maximum relative from beam to beam), was verified evaluating the unnormalised gamma profile of ScanSAR rain forest images. Thus, the antenna model is verified to be within the required accuracy of ± 0.2 dB, now with respect to the gain offset between different beams, as shown for the exemplary result in Figure 4-63.

Comparably to elevation, the antenna model verification shows remarkable results for azimuth patterns. Measurement of transmit patterns in azimuth direction was performed using ground receivers. The result is shown in Figure 4-64 where the measured patterns (coloured) are compared to the reference pattern (red). The measured deviation within the 3 dB beamwidth is less than ± 0.1 dB (peak-to-peak).

The in-flight verification shows that the maximum deviation between the antenna model and the measurements for both the shape within the main-beam and the gain-offset between different beams is less than ± 0.2 dB (peak-to-peak). Thus, the thousands of reference patterns and the gain offset between these patterns can be precisely derived by the antenna model. Hence, the time and the effort for calibrating TerraSAR-X is extremely reduced as only a few selected beams need to be measured in-flight.

*In-Orbit Calibration Strategy*

The main goal after launch of the satellite is to provide calibrated and verified SAR data products as soon as possible. Thus, a strategy for an efficient but robust calibration method has been developed. Applying the novel antenna model approach the in-orbit calibration method can be sub-divided into six major tasks performed during commissioning of the satellite. The successive baseline calibration procedures are:

- Geometric calibration, to assign the SAR data to the geographic location on the Earth.
- Antenna pointing determination, to obtain a correct beam pointing of the antenna.
- Antenna model verification, to ensure the provision of all antenna patterns and the gain offset between different beams.
- Relative radiometric calibration, for the radiometric correction of SAR data within an illuminated scene.
- Absolute radiometric calibration,

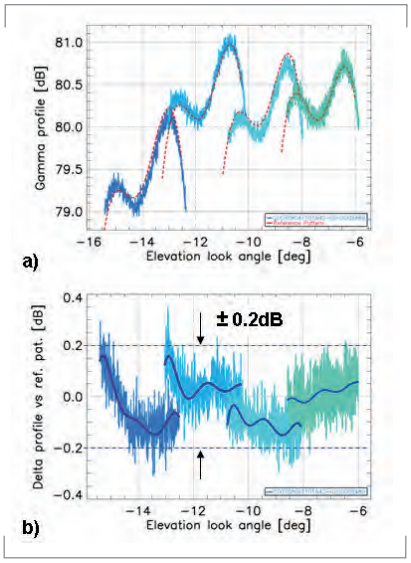


**Figure 4-63: a) Beam-to-beam gain offset verification comparing ScanSAR Beams measured (colored) and derived by the model (red), b) difference between reference and measured pattern, whereby the blue lines are fits of the difference.**

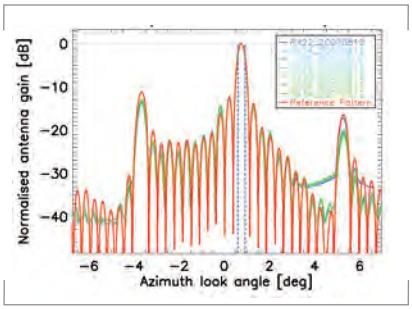


**Figure 4-64: Transmit patterns measured by ground receivers (coloured) and compared to a reference pattern (red).**

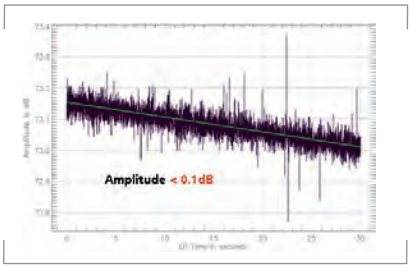


**Figure 4-65: Residual drift error of the instrument by applying the internal calibration facility, black lines: radar pulses wihtin a data take, green line: fit derived from calibration pulses.**

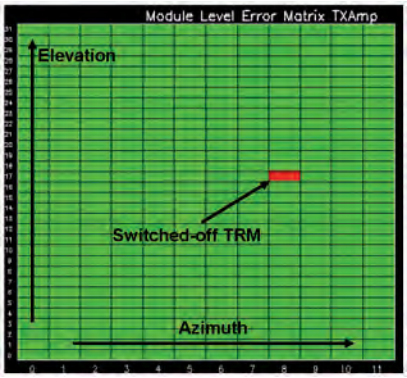


**Figure 4-66: Actual TRM Characteristics of TerraSAR-X active phased array antenna determined by PN-Gating with one TRM switched-off before launch.**

for measuring the SAR system against standard targets with well known radar cross section (RCS).

However, the success of performing all these activities within a restricted period of time for commissioning TerraSAR-X essentially depends on the radiometric stability of the instrument. Thus, an accurate facility for the internal calibration (the 6th major task) has been established and implemented for monitoring and compensating drift effects of the instrument.

*Internal Calibration and Individual TRM Characterisation*

Temperature drifts and internal hardware characteristics influence the radar signal path causing gain and phase fluctuation during data acquisition.

For monitoring and compensating these effects the radar instrument of TerraSAR-X hosts an internal calibration facility comprising both conventional internal calibration pulses and the so called PN-gating method, a further novel calibration method for characterising individual transmit/receive modules (TRM).

The TerraSAR-X instrument drift within a data take is shown in Figure 4-65 at the top left, whereby the black lines are the radar pulses and the green line is a fit derived from calibration pulses activated before and after the imaging data take. Thus, by monitoring the instrument not only by telemetry data (e.g. the temperature measured inside the instrument during operation) but also by internal calibration pulses even small drift effects can be compensated for down to an accuracy better than 0.1 dB for the amplitude and better than 1° for the phase.

Furthermore, the novel PN-gating method, developed and established at the institute for characterising individual TRMs in operation of an active phased array antenna, has now been successfully verified for the first time in orbit by TerraSAR-X. In comparison to the non-representative module stepping mode as implemented for ENVISAT/ASAR, greater accuracy can be achieved using PN coding techniques, because the TRMs are characterised under most realistic conditions while the whole antenna is operated.

Evaluation of over 40 separate measurements during commissioning phase proves that each transmit/receive module can be measured down to an accuracy of 0.2 dB and better than 2° for the phase setting. The measured characteristics of drifted or failed TRMs are written into an error matrix as plotted in Figure 4-66. This feature is directly fed into the antenna model capable of dynamic re-calibration of all antenna beams in case of detected performance degradation.

*Geometric Calibration and Pointing Determination*

The purpose of geometric calibration is the geometric assignment of the SAR system to the Earth's surface. Two major effects influence the correct localisation of the product:

- Internal electronic delay of the instrument,
- Range offset delay by propagation effects.

Measuring the TerraSAR-X system against passive targets with no internal delay and consequently no additional source of error, these effects can be determined and compensated for.

The residual error of determining the slant range derived by measuring the range delay towards deployed passive targets is shown in Figure 4-67 as function of look angle. For low and mid look angles (up to 40 deg), the slant range with a distance of about 600 km can be derived down to an accuracy of 6 cm, i.e. the range delay is determined with an accuracy better than half a

nanosecond. At higher look angles, the dispersion of the residual error increases slightly, caused by the longer way through the troposphere and the uncertainty involved. Nevertheless, considering the complete range of look angles for TerraSAR-X, a pixel localisation accuracy of 30 cm is achieved, i.e. the geometric assignment of the SAR data to the Earth surface can be calibrated down to an accuracy of almost one magnitude better than the product specification of 2 m.

By this accurate assignment, the impact of propagation effects on the range delay has been confirmed as shown in Figure 4-68. The measurements performed with TerraSAR-X verify the impact of propagation effects on the range delay for the first time by a SAR system.

An important task for correct SAR image annotation is the determination of beam pointing errors coming from mechanical and electrical antenna mis-pointing as well as attitude control offsets. These errors are measured in elevation and in azimuth using an appropriate antenna pattern over rain forest and by using ground receivers. The used patterns imply a notch in the mid of the pattern, i.e. at 0° and consequently an offset of this notch indicates a squint angle of the antenna. The offset of the notch and consequently the actual pointing of the TerraSAR-X antenna in elevation could be determined down to an accracy better than the required 0.015° as shown in Figure 4-69.

The beam pointing in flight direction could be determined likewise by notch patterns now operated in azimuth direction and measured by deployed ground receivers. The achieved pointing knowledge in azimuth is better than the required 0.002°.

Hence, by readjusting the attitude of the satellite the detected mis-pointing of the antenna beam could be removed and the remaining squint angle is in the order of the required pointing knowledge in both directions.

*Radiometric Calibration*

After the successful in-orbit verification of the antenna model thousands of beam patterns required for the relative radiometric correction during SAR data processing can be derived by the antenna model for all operation modes and all incidence angles. In order to further reduce the calibration effort, the absolute radiometric calibration is likewise based on the antenna model, i.e. real measurements against point targets with well known radar cross section have been performed on a reduced set of three beams, one with low, one with mid and one with high incidence angle. The absolute calibration factors of all other beams and modes are derived via the antenna model by applying the beam-to-beam gain prediction.

The absolute calibration factor is determined from all measured ground targets of known RCS to reference a geophysical unit to the digital numbers of each SAR image. Consequently, the absolute radiometric accuracy is defined by the standard deviation of all measurements.

For TerraSAR-X an absolute radiometric accuracy of 0.31 dB has been achieved for StripMap operation during the commissioning phase. However, considering a conservative assumption for the long term stability of the instrument, an absolute radiometric accuracy of 0.6 dB for stripmap basic products is ensured during the lifetime of TerraSAR-X.

The last important issue that must be clarified for calibrating a SAR system down to a few tenth of a dB is concerned with the absolute radiometric reference defined by the radar cross section of the reference targets

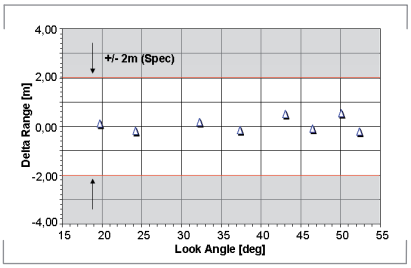


**Figure 4-67: Residual slant range offset in dependence of the look angle after correcting for instrument delay and propagation effects.**

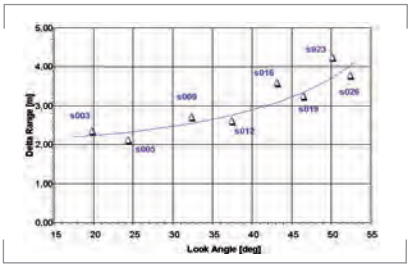


**Figure 4-68: Range offset caused by propagation effects, pink line: theoretical path extension by tropospheric refrac-tion, triangles: measurements performed by TerraSAR-X.**

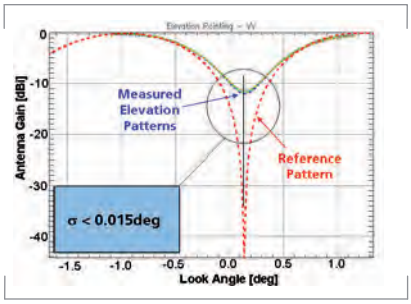


**Figure 4-69: Beam pointing in elevation determined by measured notch patterns across the rainforest.**

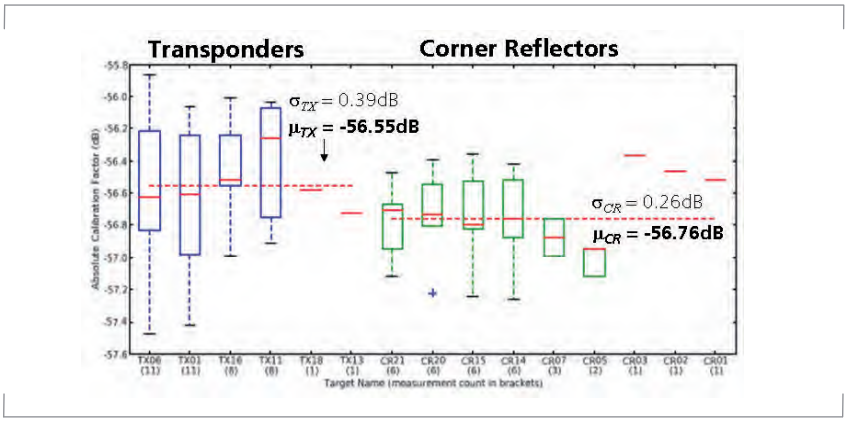


**Figure 4-70: Statistical visualisation of the absolute calibration factor derived from the two types of reference targets. Respective mean values are indicated as dashed red line.**

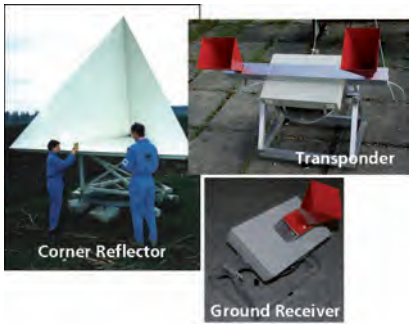


**Figure 4-71: Examples of the Institute's calibration ground equipment; left: a corner reflector with 3 m leg length, bottom: a ground receiver for measuring transmit pulses, and upper right: a transponder with adjustable RCS.**

deployed. For TerraSAR-X two different types of reference targets are deployed: corner reflectors and transponders. Thus, the absolute calibration factor can be separated depending on the type of reference target, as shown in Figure 4-70. Concentrating on the mean value (red dashed lines), both types result in nearly the same absolute calibration factor, although the determination of the radar cross section is performed in two different ways:

- In case of a transponder by electronic measurements (e.g. amplification path, antenna gain)
- In case of a corner reflector, the RCS is derived from its geometry.

Hence, two complete independent approaches are available to derive the absolute radiometric reference. Consequently, by applying both types of reference targets for TerraSAR-X, an absolute radiometric reference knowledge of ± 0.1 dB could be achieved.

Thus, at a distance of more than 500 km the complete TerraSAR-X system could be successfully adjusted and calibrated down to the accuracy of laboratory equipment.

*Calibration Facility*

The success of executing the different calibration procedures described above requires a calibration facility that is well-equipped with ground calibration hardware as well as software tools for evaluating the measurements. For this purpose the Institute has developed and established the following reliable ground equipment:

- Accurate ground targets like corner reflectors or active transponders precisely surveyed for geometric and radiometric calibration
- Ground receivers measuring the one-way azimuth pattern of a SAR antenna during an overflight
- Different analysis and evaluation tools, like CALIX, a software tool for point target analysis.

The calibration targets in Figure 4-71 are installed close to the Institute's laboratory in Oberpfaffenhofen. They have been regularly utilised for campaigns with different SAR missions (e.g. ERS-1/2, JERS-1, ASAR, ALOS, TerraSAR-X), as well as for the E-SAR calibration.

CALIX is a SAR image analysis tool featuring measurement of distributed and point targets by analysing parameters like impulse response function parameters, absolute calibration factor, target/clutter ratios, geometric analyses, as well as peak phase estimates in the case of multi-channel data. Figure 4-72 shows a screen-shot of this tool.

Worldwide, a number of new SAR missions are being implemented and novel concepts are being studied. For multi-satellite constellations like TanDEM-X or Sentinel-1 innovative calibration approaches are required to keep track with the growing complexity of SAR systems and the demand to cut down the duration of the commissioning phase. Furthermore, more cost efficient methods need to be developed. In the last years the Institute has established

a unique calibration facility supporting the calibration of missions like SRTM, ASAR, or TerraSAR-X and is consequently well prepared for the challenges of high-quality system calibration of future SAR missions.

# Antenna Technology

Technology is developed in the Institute, where suitable products are not available on the market and where the development requires close interaction with the rest of the system. The SAR antennas are an example of particular importance for the many SAR activities in the Institute. The main challenges to achieve are:

- Receive and transmit (high power) operation
- Coverage of the radar wavelengths
- Operation in various polarisations
- High gain
- Uniform illumination of the imaged swath (for high relative radiometric accuracy)
- High side-lobe suppression (for low range and azimuth ambiguities)
- Thermal stability
- Beam steering and shaping (for advanced SAR modes)

For spaceborne SAR systems, activities of the Institute are concentrated on antenna optimisation and characterisation, as required for system verification and calibration. For the airborne systems E-SAR and F-SAR, operating and licensing the SAR antennas and their mounts are additional tasks.

**Spaceborne Satellite Antennas**

Although the Institute does not construct satellite antennas, an important field is the specification, prediction and optimisation of antenna performance, particularly for active arrays as used for SAR instruments. Pattern prediction is based on the excitation coefficient settings for the array's sub-elements, on the electrical characteristics of the TRM and on the sub-element radiation patterns.

In satellite SAR missions it is of great importance to achieve high sensitivity over a large angular range (TerraSAR-X: 20° to 45° look angle), as well as good suppression of ambiguities. Hence, there is need for a software tool that optimises the antenna patterns of the satellite's electronically steered array antenna. The shaping of the pattern is obtained by varying the excitation coefficients and setting up each TRM with these coefficients. In operation, the setting is performed by up-linking appropriate commands to the SAR.

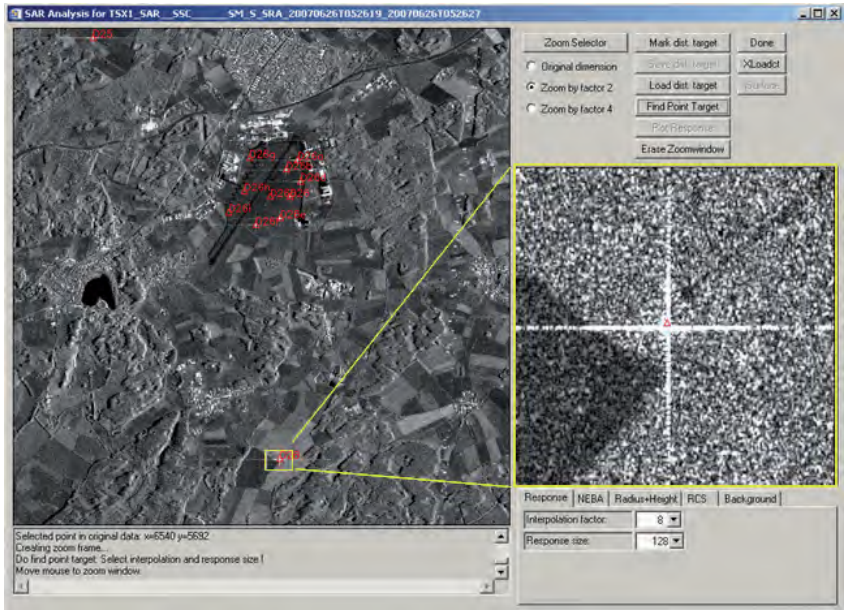


**Figure 4-72: Screen shot of the CALIX point target analysis on TerraSAR-X image over deployed calibration targets at DLR Oberpfaffenhofen calibration facility.**

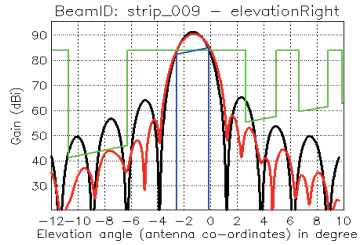


**Figure 4-73: Antenna pattern of Stripmap beam S009 for TerraSAR-X. Red curve: Optimised pattern, black curve: unoptimised pattern, green curve: Mask to be fulfilled, blue ramp: coverage region.**

**Figure 4-74: P-band antenna with the wind deflector mounted under the fuselage of DLR's Dornier Do 228.**

Figure 4-73 shows the mask, the blue line being the minimum gain mask in the coverage region and the green line, the maximum gain mask in the ambiguity regions. The black curve is the pattern without optimisation and violates the mask. The red curve is the optimised pattern which doesn't violate the ambiguity mask, while the achieved gain in the coverage region reaches the minimum required.

The Antenna Pattern Optimisation Software was first developed for the ASAR front-end under ESA/ESTEC contract. The ASAR antenna consists of 320 sub-arrays and transmit/receive modules, respectively. For TerraSAR-X, two optimisation approaches were realised and compared, an analytical method and a randomising method. The first approach uses a genetic algorithm on top of a deterministic inversion. The solution is achieved by calculating several "generations" with certain "individuals" of patterns and recombining the associated excitation coefficients through mutation.

The second method calculates thousands of different pattern realisations by randomly varying the excitation coefficients to find the optimum solution (500 realisations per second on a Pentium IV, 3.4 GHz). In case of TerraSAR-X, the second method showed better performance and results.

### Antennas for Airborne Radar Systems

The airborne SAR activities cover microwave frequencies ranging from 300 MHz to 10 GHz and require various antenna technologies, i.e. microstrip array, slotted waveguide or horn antennas. The prototype antenna development for airborne SAR has to meet airworthiness requirements, as well as the requirements given by the application.

The Institute has established a complete design and development chain for the production of prototype airborne antennas. Airworthiness certification and payload approval are carried out in cooperation with other DLR institutions. This has proven to be very successful as the example of the P-band antenna for the DLR airborne SAR shows (see Figure 4-74).

The antenna is designed for wide-band operation in P-band, i.e. in the 300 to 400 MHz frequency range. At the 80 cm wavelength the antenna has small physical dimensions of only 1.4 m by 1.4 m constrained by the width of the aircraft's fuselage. The use of materials with a high dielectric constant was required. To achieve the bandwidth of 28%, an aperture coupled, triple stacked patch element was developed (see Figure 4-75). Sixteen elements form the electrically steered array. Thus, the configuration of 4 rows was chosen with 125° phase shift per row to obtain a main beam pointing 42° off nadir, necessary for the side-looking SAR imaging geometry.

**Figure 4-75: Structure of the different layers of one radiating P-band element. Three resonating patches contribute to the radiated field.**

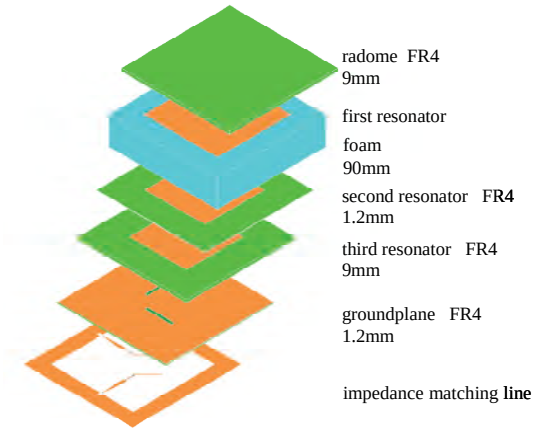

The P-band antenna is dual polarised and has a high cross-polarisation suppression of 25 dB over the useful bandwidth of 100 MHz. The design meets the specification for beam width in elevation and azimuth for both polarisation directions. In close collaboration with the DLR department of flight operations, a wind deflector was designed, built and certified together with the antenna (Figure 4-74). The whole equipment comprising antenna, power dividing network, mounting frames and deflector is 3.4 m in length and has a weight of 130 kg. Figure 4-76 shows the antenna and the results of the antenna pattern measurements.

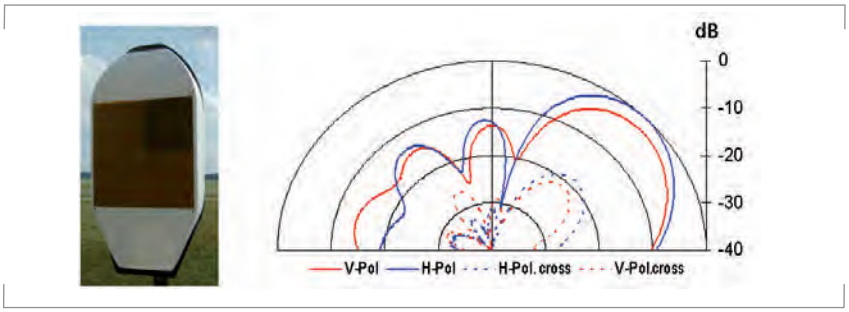


Figure 4-76: Left: Photograph of the P-band antenna mounted on the far-field measurement facility. Right: Antenna diagrams (solid blue: HH, solid red: VV, dashed: cross-pol).

A new L-band antenna to be used for the F-SAR system is an example of a phased array using patches. The antenna has a beam steering capability as well as wideband operation, high pulse power ability and low cross-polarisation level (Figure 4-77).

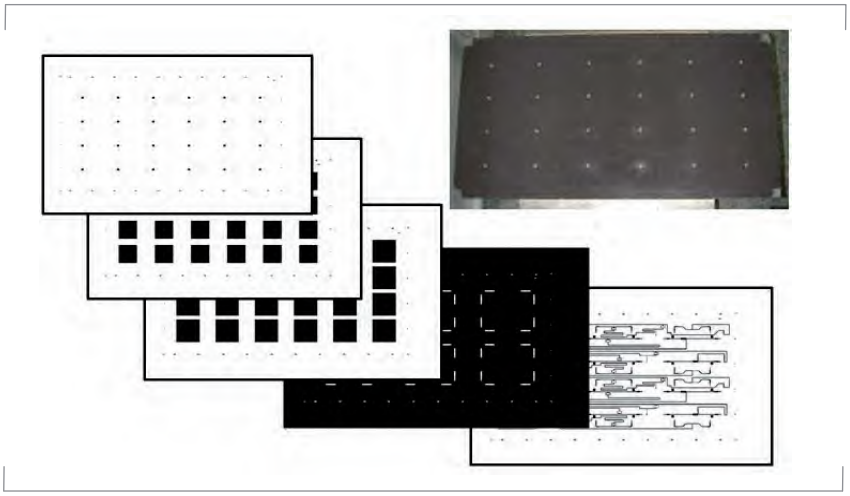

Figure 4-77: Top right: photograph of the L-band antenna for the new airborne SAR, F-SAR, together with the masks for etching the various layers.

For specific applications requiring quick solutions, slotted waveguide antennas are convenient. Figure 4-78 shows an X-band slotted waveguide antenna for SAR interferometry application. Three of these antennas are mounted on the side of the aircraft's fuselage to form an interferometer with both along-track and cross-track baselines.

**Antenna Design and Development Infrastructure**

The Institute maintains a number of antenna software design tools running on a high-performance PC. Agilent's Advanced Design System (ADS) is used for the development of planar radiating elements. The software supports the design of planar structures using a 2.5-dimensional simulator. The simulation of small groups of elements is possible, as well as the associated feed network.

For designing real 3-D structures, Ansoft's High Frequency Structure

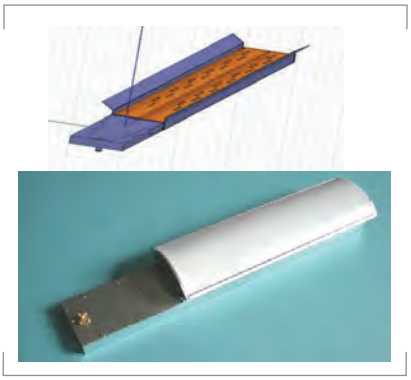

Figure 4-78: Top: Design of the X-band slotted waveguide antenna. Bottom: the prototype antenna with a Teflon.

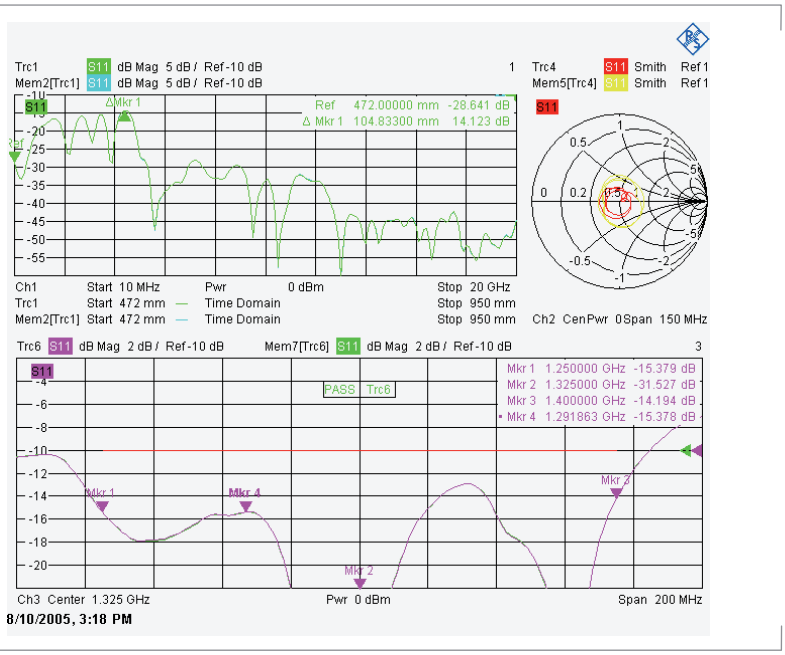


**Figure 4-79: Screen shot of the network analyser with the input impedance measurement of the L-band antenna described above. Top left: reflected power in the time domain. Top right: Smith chart of the normalised input impedance. Bottom: magnitude of the reflected power in the frequency domain.**

**Figure 4-80: DLR's airborne P-band SAR antenna mounted with its wind deflector on the antenna measurement facility AMA.**

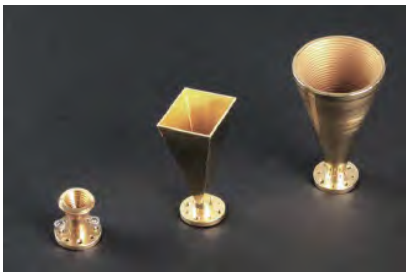

**Figure 4-81: Examples of horn antennas for millimeter wavebands. Because the machining of the inaccessible internal surfaces is impossible with conventional machines, galvanoplastic techniques have to be used.**

Simulator (HFSS) is better suited. Complex topologies are possible, limited only by the available computing power. Feko, a third software tool, produced by EM Software & Systems, is available for analysing the placement of antennas on structures.

The Institute's precision mechanics workshop handles most aspects of antenna manufacturing. The workshop is specialised in small structures and high quality products. Antennas and other microwave components are manufactured up to W-band using manual and numerically controlled machines, as well as galvanic techniques (see Figure 4-81).

The Institute maintains a laboratory equipped with latest instrumentation for antenna development. Several high-performance network analysers are used to characterise the properties of the microwave components. The new F-SAR L-band antenna is given as an example (Figure 4-79).

For antenna measurements, the far-field antenna measurement range (AMA) operated by the Institute of Communication and Navigation, is used (Figure 4-80). The major advantage is the possibility to operate the facility at very low frequencies, practically down to a few MHz, not possible in a closed chamber. However, because of the open arrangement, the measurements are weather dependent and radio frequency interference with other services cannot be excluded. Thus, the far-field antenna measurement range is unsuitable for sensitive antennas. For this reason, a new microwave laboratory complex called 'HF-TechLab', containing a compensated compact range, is in construction. The compact range will add new antenna measurement facilities and will lead to significant improvements in accuracy. Completion of the building will be at the end of November 2009. At the same time the new measurement facility will start operations.

# Signatures

The knowledge of the radar signature of a target, the scattering from the surroundings and the propagation path is essential for estimating the performance of radar systems used in both military and civil scenarios. The complexity and variability of these quantities mean that accurate models have to be relied upon.

The monostatic RCS model SIGMA based on Physical Optics (PO) has been improved in several ways. A new module to calculate edge correction contributions has been developed and implemented, and a 2-D mode as well as a stepped frequency mode have been realised. Dielectric coating can be defined by permittivity ε and permeability μ or by providing Fresnel's reflection coefficients as functions of the incidence angle. In Figure 4-82, the 2-D RCS distributions of two aircrafts are shown. Comparing the front view regions (centres of the images) the stealth behaviour of F7 is obvious.

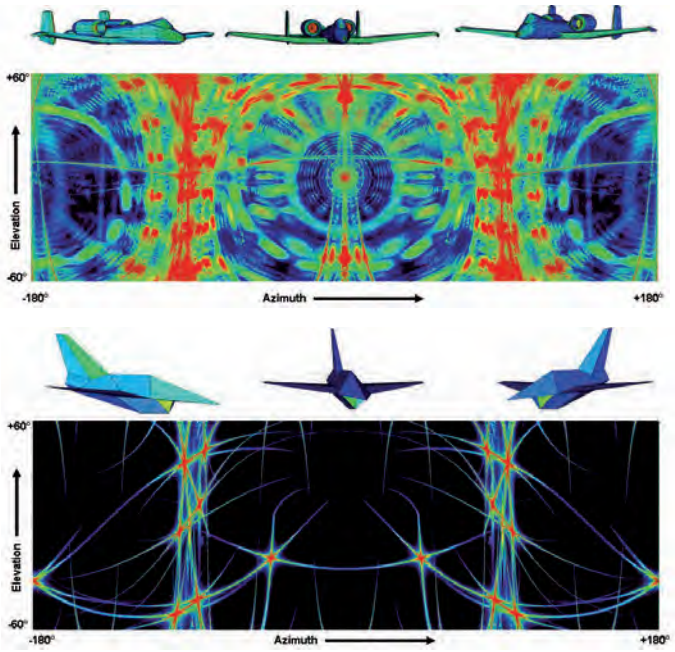


**Figure 4-82: Stealth behaviour of F7 compared to A-10 Thunderbolt: 2-D RCS of Fairchild A-10 Thunderbolt (above) and DLR stealth design F7 (below). Horizontal axis: azimuth angle (-180° .. +180°), vertical axis: elevation angle (-60° .. +60°).**

Because of the increasing importance of bistatic radar systems, the bistatic RCS simulation code BISTRO has been developed. This programme uses Physical Theory of Diffraction (PTD) to simulate the bistatic high-frequency electromagnetic scattering from man-made targets. Figure 4-83 shows a computed scattering diagram of a 10λ perfectly conducting sphere for a fixed direction of illumination and varying observation aspects. The diagram illustrates typical features of bistatic scattering, namely the dominance of forward scattering compared to backscattering and the complex structure of the scattering diagram, due to the presence of multiple sidelobes.

The developed modules of the programme have been successfully applied to various types of canonical scatterers (spheres, plates, cylinders, etc.) and complex targets (cars, aircraft). Additional modules for simulation of multiply reflected waves, edge corrections, dielectric coatings and rough surfaces are under development. Implementation of these modules will extend the applicability area of the programme and further improve the simulation accuracy. Generalisation of PTD to non-metallic structures requires an extensive research work.

In order to simulate high order reflection contributions for mono- and bistatic scattering tasks a new code SIGRAY applying the Shooting and Bouncing Rays Method has been developed. In comparison to Physical Optics this method is very time-consuming but well suited to calculate additional RCS contributions of high order reflections. Reflections of order n are treated as (n-1) specular reflections corresponding

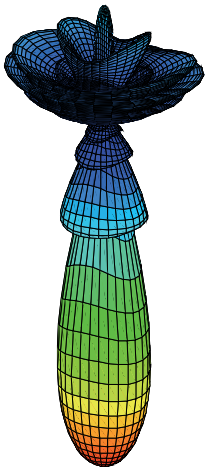

**Figure 4-83: 3-D bistatic RCS of a sphere; the radar wave is incident from the top; a pronounced maximum is seen in the forward scattering direction (lower part of the 3-D diagram).**

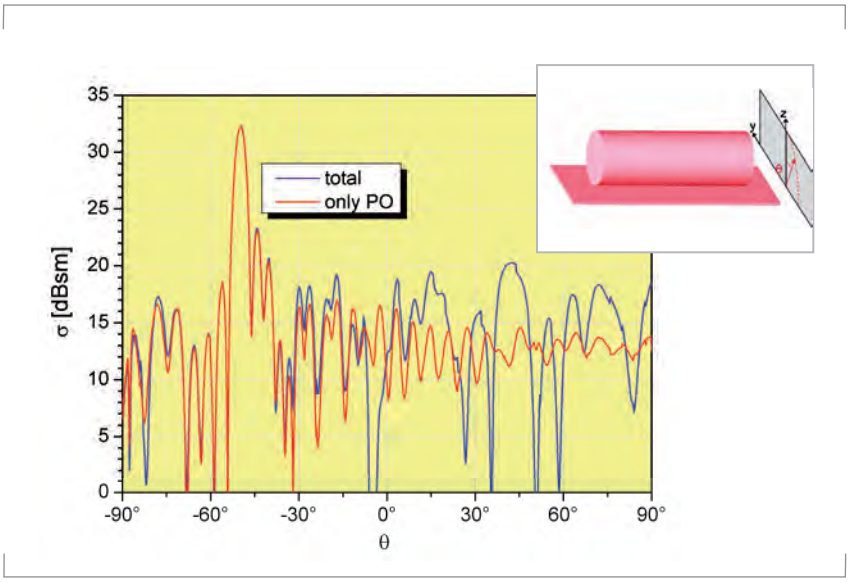


**Figure 4-84: Bistatic RCS of a cylinder near a flat panel; Transmitter: θ=+50°; Red: only PO contributions; Blue: PO plus multiple reflection contributions.**

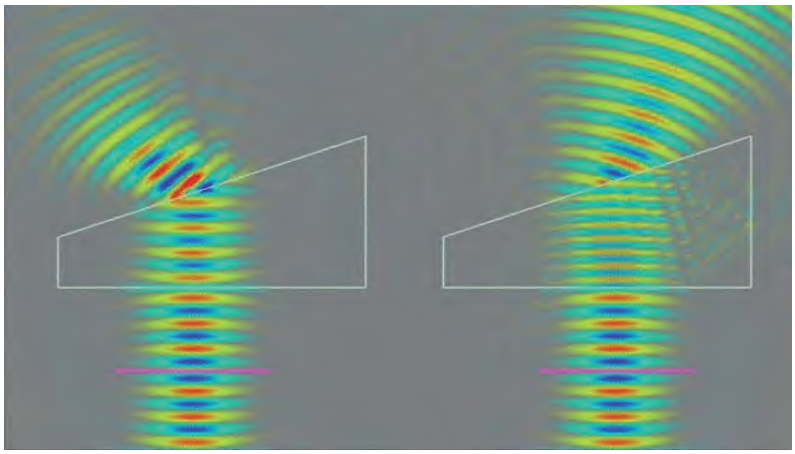

**Figure 4-85: Transmission through a metamaterial prism (left) and a prism of conventional material (right).**

to Geometrical Optics and finally one application of PO. Figure 4-84 shows the simulation results by SIGRAY on the interaction between a cylinder and a flat panel. The importance of the consideration of multiple reflection contributions in a wide angle region is obvious.

The import of 3-D geometry datasets of anthropogenic targets from popular CAD formats, its modification and repairing and finally the export to the data format used in SIGMA, BISTRO and SIGRAY are important tasks for preparing numerical simulations. All these steps have been provided and improved in the past.

In order to provid clear configuration of simulations new graphical user interfaces for SIGMA and SIGRAY have been developed (Figure 4-86). They include the visualisation of the target corresponding to the antenna positions. After starting the simulation the RCS data are shown in a graph synchronous to the actual view of the target.

Further research topics include electromagnetic properties of metamaterials and their potential applications to problems of RCS management. The concept of a metamaterial suggests a way of designing artificial materials with desired electromagnetic properties, not encountered in the nature. Current activities focus on simulations of reflection and transmission properties of metamaterial layers at microwave frequencies (Figure 4-85).

In order to assess the RCS of extended targets (i.e. terrain and water surfaces) the software tool DORTE (Detection of Objects in Realistic TErrain) is being developed. DEMs (Digital Elevation Models) are used to describe the topography and to determine shadowed areas and local incidence angles for a given radar device position. The specific radar backscattering coefficient of each terrain cell is calculated using semi-empirical and statistical clutter models.

The calculated mean values can be varied using probability density functions. The land use database CORINE (CoORdinated INformation on the Environment) of the EEA (European Environment Agency) is currently employed to assign clutter models to different areas within a DEM.

Figure 4-87 shows the graphical user interface to DORTE. This programme can be used for a quick and inexpensive estimation of the expected clutter level for virtually every place on Earth, as long as a DEM and land cover information is available. Currently the computer code is extended to handle bistatic radar configurations as well. For the future it is planned to extend the code capabilities to take different radar hardware characteristics into account.

The W-band mono- and bistatic measurement facility is operated to validate the numerical results of RCS simulation codes (Figure 4-88). Making use of the Time Domain Option of the Vector Network Analyzer a range gate is applied for suppressing disturbing signals.

Dielectric coatings may greatly influence (reduce) RCS of metallic targets. In order to determine the properties of material probes in the microwave frequency range three different measurement facilities are operated and are being developed. The Ka-band transmission measurement setup has been improved and a new computer programme to determine ε and μ written. The experiment workflow has been automated and real time data aquisitation is realised. Amongst other applications the setup was used for high temperature material measurements making use of the DLR solar furnace in Köln-Porz (Figure 4-89). These experiments have been part of a DLR project.

The X-band reflection measurement setup (Figure 4-90) has been modified concerning rotating and shifting the

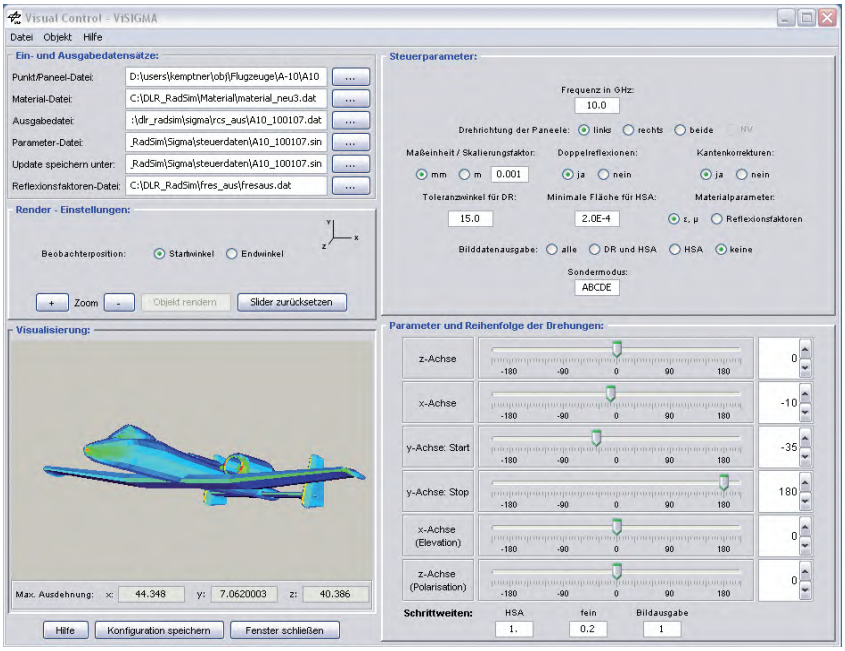


Figure 4-86: Graphical user interface for SIGMA.

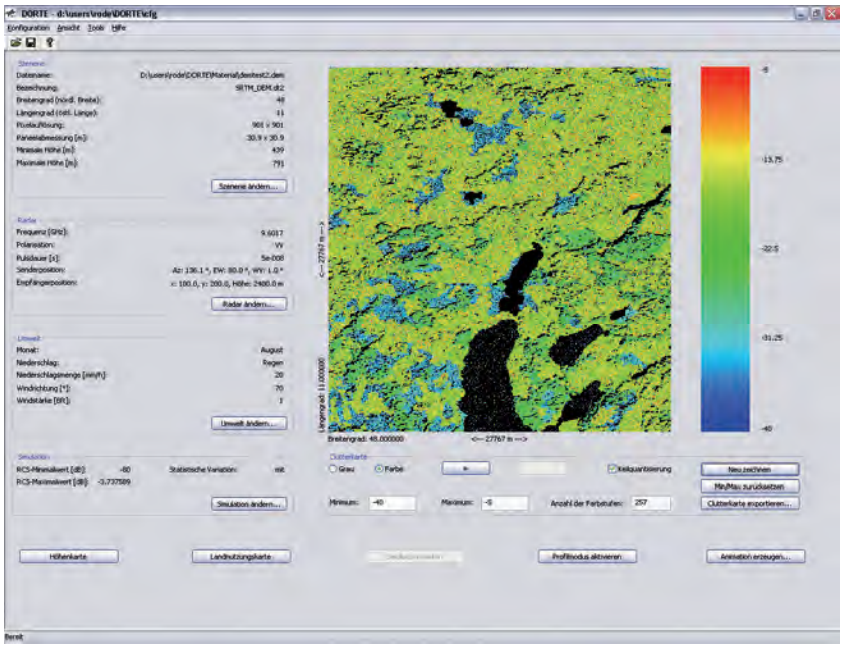

Figure 4-87: Graphical user interface of DORTE showing the X-band VV clutter distribution in the northern Ammersee region. The incidence angle is 80°, azimuth angle 136°. Dynamic range is - 40 … - 5 dB.

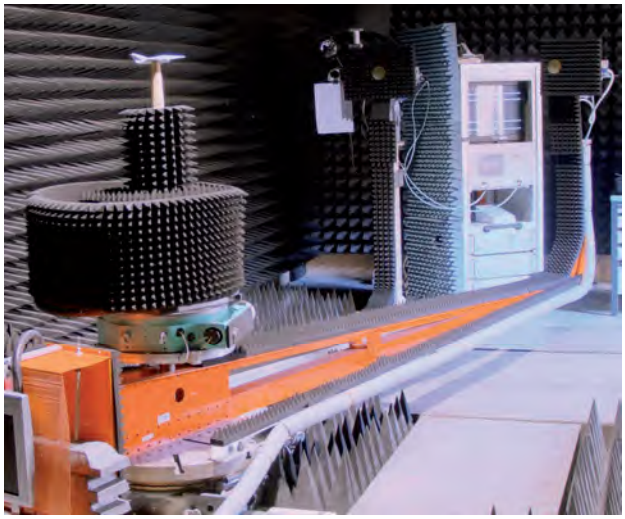

Figure 4-88: Mono- and bistatic RCS measurement facility.

Figure 4-89: Ka-band transmission measurement setup at DLR solar furnace including a material probe illuminated by focused sunlight.

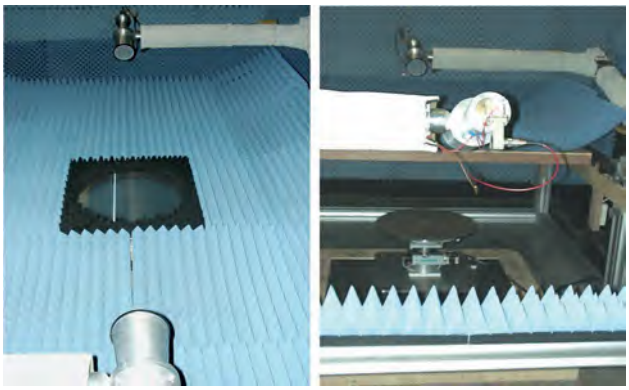

Figure 4-90: Free space reflection measurement facility.

material sample during the experiment. The full polarimetric data are measured over an extensive interval of bistatic angles by moving one antenna or both antennas synchronously. A number of different flat and rough metallic or dielectric surfaces have been measured and analysed with the aim to separate the effects of surface roughness from dielectric effects using the whole spectrum of observables and parameters. It has recently been shown that the bistatic phase is strongly related to the dielectric properties of the surface (soil moisture).

The waveguide measurement setup for transmission and reflection measurements has been extended to several frequency bands and is now available for R, S, X, Ka, Q and W-band. A new calibration procedure was established and again a new computer code was programmed to determine $\varepsilon$ and $\mu$. Some of the experiments have been performed in the framework of DLR projects on missiles and UCAV structures.

# Radiometry: Imaging Techniques

Microwave radiometry addresses the purely passive measurement of the natural thermally caused electromagnetic radiation of matter at a temperature above 0K. Microwave radiometry has a long tradition in the Institute going back more than forty years. The research on passive measurement and imaging technologies is a main working area within the radiometric activities. New requirements in spatial resolution, sensitivity, spectral diversity, penetration depth, environmental conditions, and real-time capabilities, and also new applications demand the investigation and introduction of new principles, and the refinement of existing techniques.

In general, the benefits of passive microwave techniques are
a) almost independence of poor weather, daytime, and other obstacles (e.g. dust, smoke),
b) covert operation (no transmitter),
c) no artificial irradiation of observed objects (e.g. persons) and hence also no additional electromagnetic pollution,
d) the capability of Nadir imaging in highly mountainous or urban areas, and
e) rather simple image interpretation due to quasi-optical appearance. Earth observation is mostly performed in the atmospheric windows around 35, 94, 140 and 220GHz or at lower microwaves below 20GHz.

**Present Applications of Interest**

International terrorism has reached a level where adequate countermeasures to protect the population have to be provided by the authorities. Similarly, the improved surveillance and protection of critical infrastructures attracts increased attention. Furthermore the detection of concealed objects like weapons or explosives at checkpoints becomes more and more important. Also efficient imaging systems for the purpose of natural disaster monitoring and prevention as for flooding are of major interest. Contamination by buried landmines is further on recognised as an inhumane burden on countries ravaged by war, many of these poor. In all security related cases conventional techniques are mostly too inefficient to satisfy the demands and requirements. Hence, research on these new challenges had been animated through various organisations, and therefore we also consider passive microwave sensors to improve the situation.

**Considered Imaging Principles**

The research on imaging technologies is presently focused on three principle areas:

- Line-scanner systems, which follow a more classical approach with the benefits of rather simple hardware, lower costs and expense, but they have the drawbacks of limited resolution and real-time capabilities
- Aperture synthesis systems, which are a new approach for passive Earth observation and terrestrial imaging with the benefits of high spatial resolution and real-time capabilities, but they have the drawbacks of higher costs and expense, and more complex development and operation
- Hybrids of both in order to combine benefits and reduce drawbacks, costs, and expense.

**Linescanner Developments**

Various linescanner systems for different airborne and ground-based applications have been developed at DLR during the last forty years. The linescanner principle is illustrated in Figure 4-91.

All linescanners are following typically a similar approach, where the mechanical motion of the antenna beam

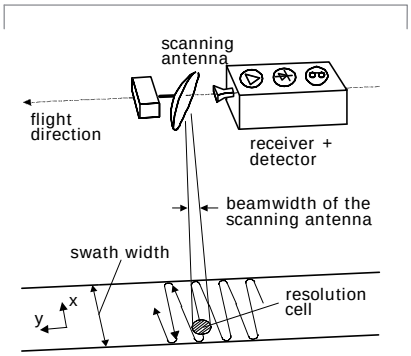


**Figure 4-91: Imaging principle of an airborne linescanner system. An oscillating parabolic mirror causes an across-track scan of the antenna beam on the ground.**

Figure 4-92: Photograph of the ABOSCA linescanner imager on top the Institute's platform roof.

Figure 4-93: Panoramic photograph of a typical scene for surveillance applications and the corresponding 90 GHz radiometric image.

is applied to two independent directions. The challenge for linescanners is to find a compromise between the image size (field of view), the spatial resolution (pixel number), the sensitivity (noise in the image), and the image acquisition time (mechanical constraints, number of receivers).

*Wide-area imaging for surveillance*

For wide-area ground-based imaging experiments the ABOSCA (German: Abbildender BOdenSCAnner) system has been developed. The main goal of this development was the capability to image a full hemisphere and to have a high flexibility concerning modifications. A rotating parabolic mirror provides an image line in elevation, and the azimuth movement of the whole unit delivers the second image dimension. A photograph of the system and a typical wide-area image are shown in Figures 4-92 and 4-93.

The single-receiver system is operated at 90, 37 and 9.6 GHz with about 0.6°, 1.5°, and 5.8° of angular far-field resolution, but it can be extended to any frequency band where ever a receiver is available and the spatial resolution is still sufficient. The measurement duration for the complete hemisphere is less than 5 minutes and the sensitivity is in the order of 0.1 K depending on the oversampling rate used.

Persons in various environments have been imaged in order to assess detection capabilities of objects carried by the persons, or of the persons themselves within the cluttered environment. Such a capability can be used to detect intruders in the surrounding of a critical infrastructure as simulated in an experiment depicted in Figure 4-94.

It is hard to detect the person neither in the optical nor in the radiometric image. However, if a radiometric difference image of the identical scene with and without the person is evaluated the person can be clearly detected. It should

be noted that the background of the two radiometer images has only slightly changed even for the large time gap between the two records, enabling a proper change detection performance.

Another example illustrates the application for intruder detection in a maritime environment. Figure 4-95 shows a person simulating a swimmer approaching the land. From an elevated perspective the detection of objects on the water surface is easily possible due to the homogeneous radiometric appearance of the water background.

The information content of radiometric imaging can be further increased by the use of polarimetry. First imaging results of a developed fully-polarimetric W-band receiver used within the ABOSCA system as shown in Figure 4-96 indicate the polarising features of dielectric surfaces. For instance, the reflection properties of the concrete ground are higher for horizontal compared to vertical polarisation. The signals of the third and fourth component of the Stokes vector are usually much smaller and hence noisier than those for the H and V channel, but they can be used to detect dielectric properties and periodic structures.

Such wide-area surveillance systems can also be used for the monitoring of the degree of manmade or natural disasters (e.g. oil pollution on the sea, extent of a flooding, extent of a forest fire) and as a sensor for the prevention of those as shown in the past (e.g. the monitoring of the seepage of dikes).

*High-resolution near-field imaging for concealed objects detection*

In order to investigate the suitable resolution and penetration requirements with respect to concealed weapons or explosives detection, the experimental system LPAS (German: Laborsystem zur Personen-Abbildung mit Scanner) as shown in Figure 4-97 was developed. Here the intention is to generate images

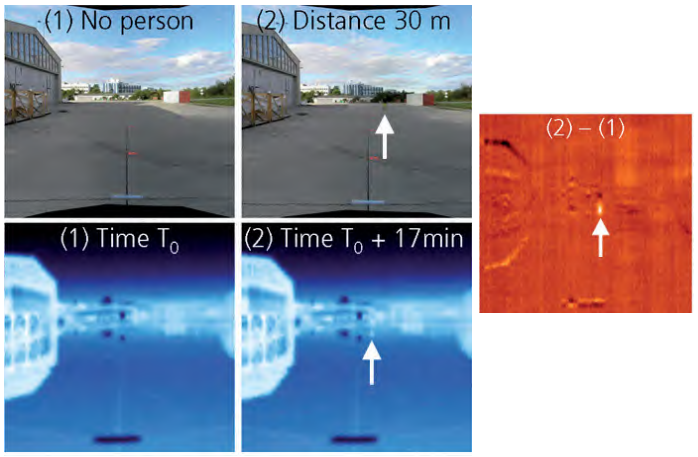


**Figure 4-94: ABOSCA imaging result of a person at a distance of 30 m in a natural urban environment: Photographs of the scene (above), radiometric images around 90 GHz (below) and a difference image (right) of the identical scene with and without the person. The white arrow indicates the position of the person.**

**Figure 4-95: ABOSCA imaging result of a person approaching the beach of a lake from the waterside. The distance was about 15 m and 8 m.**

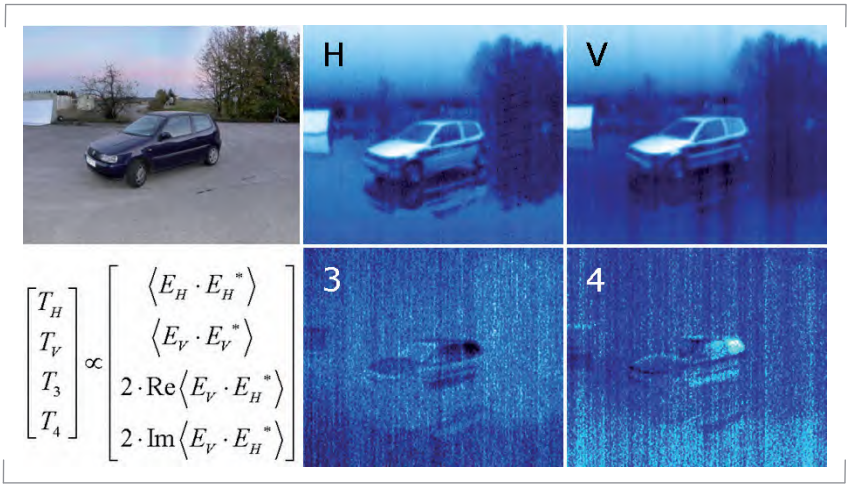


**Figure 4-96: Photograph and fully-polarimetric W-band images of a scene including a car using the ABOSCA system. The images represent horizontal (H) and vertical (V) polarisation, and the third (3) and fourth (4) component of the Stokes vector according to the indicated complex electric field representation E where Re and Im are the real and imaginary parts.**

**Figure 4-97: Photograph of the LPAS-1 radiometer imager (left), and corresponding photographs and 90 GHz imaging results of persons carrying various optically non-visible objects.**

**Figure 4-98: Photograph of the LPAS-2 radiometer imager (upper left), and corresponding photographs and 90 GHz imaging results of a person carrying various optically non-visible objects.**

of persons at a close distance of a few meters with a few centimeters of spatial resolution in short time. Hence, the system is a near-field imaging device, since the far-field condition at W-band would require a distance of at least 160 m for the used antenna size. For LPAS-1 a fixed Cassegrain antenna optimised for the near field receives the radiation from a rotating deflection plate. The vertical movement of this whole unit delivers the second image dimension. An image of a person as shown can be recorded within about 20 s, which is far from real-time, but a more light-weight and size-optimised design should allow frame rates within about 1 s using this imaging technique.

In the upper radiometric image a metallic knife wrapped in a newspaper can be recognised. In the lower image a handgun in the trouser pocket can be observed. Note that no target at all can be detected in the optical images.

For the LPAS-1 system there is only limited dwell time of the antenna footprint on the target area. Most of the rotational time of the deflection plate cannot be used for the imaging. Hence we developed a mechanism for the LPAS-2 system (patent pending) allowing the footprint to be always on the target area in order to increase the sensitivity in the image. Here again a modified Cassegrain system was used where now a tilted sub-reflector of a certain shape is rotated with a high speed as shown in Figure 4-98. The shape and tilt angle of the sub-reflector is adjusted such that the focus area of the whole MMW optics moves on an almost circular trajectory in the image plane. By moving the whole unit linearly in the vertical direction again the second image dimension is scanned. Note that the main reflector is only partially illuminated so that its size is larger than required for a certain spatial resolution. However, for many applications this fact is not a severe drawback. Here again for the first experimental version the image

acquisition time is about 15 s and can be improved to about 1 s for a single-receiver system.

The images show a person for different views carrying concealed objects under clothing or in a bag. In the upper right radiometer image (side view) a handgun in a notebook bag can be recognised. In the lower left one (front view) and right one (back view) a metal can in a cloth bag and a metal part in the trouser pocket, and a handgun under the clothing and the metal can be detected.

For the hidden object detection on people a sequence of images as in the case of a movie provides much more additional information. The reliability of the detection process and the capability of recognition are considerably improved. Hence the focus in research and development is directed towards "close to real-time" systems. It is expected that frame rates in the order of a few images per second is sufficient. In addition the optimum frequency band is not yet clear, since it has to be a compromise between penetration capability (tendency to lower frequencies) and spatial resolution (tendency to higher frequencies).

In general the detection properties of radiometer imagers are almost maintained when natural obstacles like bad weather, fog, dust, or smoke inhibit imaging at visible or infrared wavelengths. However, the spatial resolution is mostly determined and limited by the size of the moving antenna. Consequently, imagers based on electronic scanning are more attractive for high-resolution and/or real-time imaging systems. One solution for those requirements besides focal-plane array systems is the use of aperture synthesis techniques.

**Aperture Synthesis Developments**

Since the 1990s the work has focused on aperture synthesis techniques, a method capable of achieving considerably higher spatial resolution and coming from radio astronomy. Aperture synthesis uses a highly thinned aperture as shown in Figure 4-99 to perform low-redundancy imaging in the spatial frequency domain. Antennas are only mounted along the arms of the T to simulate the corresponding two-dimensional aperture. There is no mechanical movement. The image in the spatial domain has to be reconstructed via a dedicated algorithm, in the theoretically ideal case an inverse Fourier transform. Since all receiver signals are simultaneously correlated in pairs, a real-time image of the scene defined by the single-element antenna pattern can be obtained.

*Multi-spectral Imaging*

Based on former research with respect of buried landmine detection, a passive multi-spectral imaging device can be of great benefit for the detection of hidden objects behind more voluminous and denser dielectric obstacles. Since for this application the lower microwaves are more suitable and consequently the antenna size increases considerably for a sufficient spatial resolution, new imaging technologies like aperture synthesis and near-field image reconstruction processing are required. So the ANSAS (German: Abbildendes Niederfrequenz-Spektrometer mit AperturSynthese) system as shown in Figure 4-100 has been developed.

In order to explore new imaging concepts also suitable for real-time operation, a hybrid of a synthetic and a mechanical scanning was chosen as a moderate-cost approach. The antennas along the linear axis are arranged in a thinned, well-defined pattern for aperture synthesis operation along this direction. By rotating the linear axis in

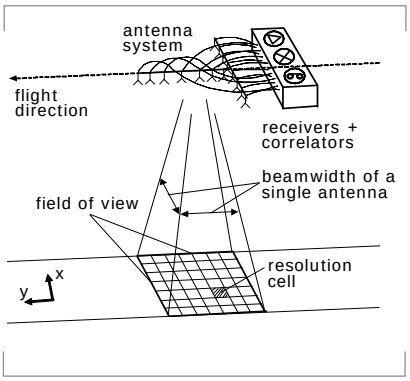


**Figure 4-99: Imaging principle of an airborne aperture synthesis imaging radiometer with a T-shaped arrangement of the receivers.**

**Figure 4-100: Photograph of the ANSAS multi-spectral hybrid radiometer system combining aperture synthesis and mechanical scanning for two-dimensional imaging. More than 15 antennas are used in order to provide similar electromagnetic properties for those antennas connected to the 15 receivers.**

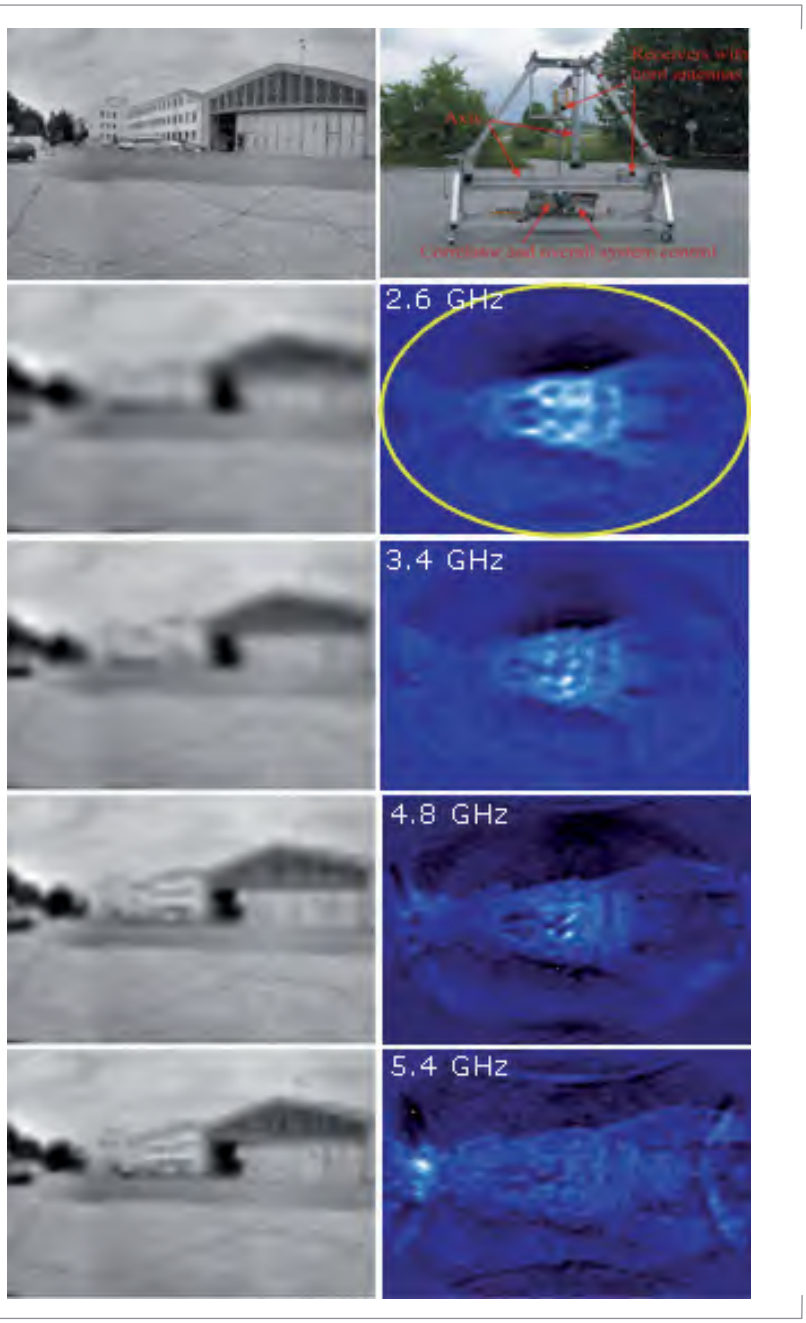


**Figure 4-101: Imaging results of the ANSAS hardware installed on a two-element interferometer with variable baseline (top right). Top left illustrates a high-resolution panoramic photograph of the scene. Below on the right the reconstructed images for various frequencies are shown, together with the optical images degraded to the corresponding spatial resolution.**

well-defined steps around its centre for 180° and performing measurements for each step, a final brightness temperature map can be reconstructed in the spatial domain for each frequency band of the multi-spectral receiver architecture. The hybrid system requires 15 receivers and 105 correlators. Each receiver operates across the band of about 1.4 to 8 GHz in a rather arbitrary number of channels of 20 MHz bandwidth in order to allow multi-spectral operation. The imaging of a scene is expected to be performed within a few minutes in the multi-spectral imaging mode. As a future goal a more operational system could use aperture synthesis in both dimensions in order to be fully real-time capable.

ANSAS is a rather complex system consisting of many challenging sub-systems like 15 Vivaldi antennas and analogue broadband heterodyne microwave receivers; a digital correlator matrix based on FPGA (Field Programmable Gate Array) technology providing 120 individual correlators; and specific image reconstruction algorithms. Hence a first proof of functional capabilities was performed operating two channels of the developed hardware in a two-element interferometer configuration. The imaging result of four arbitrary centre frequencies is shown in Figure 4-101 which had been chosen for no interference with artificial transmitters.

No calibration and no advanced image reconstruction have been applied yet. The images were generated by a Fourier inversion, which is only valid for an ideal instrument and the far-field condition. Note that the radiometric images show the reconstruction of a full hemisphere, indicated representatively as the inner part of the yellow ellipse in the 2.6 GHz image. Clearly the increase of the spatial resolution with increasing frequency can be observed, and many details corresponding to features visible in the optical images can be extracted. Note that the images as well have not been

corrected for the antenna patterns, being visible as an intensity decrease from the image centre towards the edges. Furthermore slight aliasing effects at the higher frequencies can be recognised as circular structures folding back in the images from the image edges towards the centre. It should be noted that the application of more advanced image reconstruction approaches will enable a higher image quality, allowing the detection of even much more image details.

*SMOS (Soil Moisture and Ocean Salinity) mission*

Radiometric spaceborne instruments have long been contributing to Earth observation, both for scientific research and operational services, e.g. weather prediction and climatology research. Since these applications demand an increase in reliability and precision, requiring higher spatial resolution of the radiometer, also at lower frequencies, aperture synthesis techniques have become attractive candidates for new and innovative spaceborne systems. Such an approach is currently being implemented for the SMOS mission of the European Space Agency (ESA), planned for launch in summer 2009.
The goal of SMOS is to globally map soil moisture and ocean salinity using an L-band aperture synthesis radiometer in a Y configuration.

The Institute supports the mission by participation in the SMOS science advisory group and various ESA contracts to develop image reconstruction techniques, which are mandatory for such a complex instrument. Figure 4-102 shows an artist view of the SMOS aperture synthesis radiometer. Since the array has a Y shape the corresponding sampling grid in the spatial frequency domain is hexagonal. Hence, the alias-free field of view in the spatial domain is also hexagonal. Image reconstruction has to account for all the errors introduced by

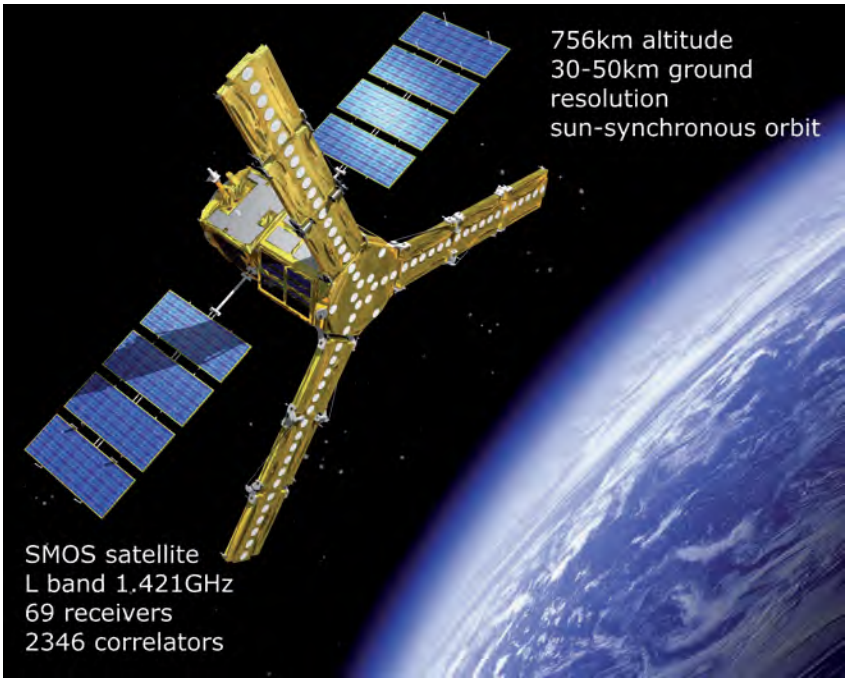


**Figure 4-102: Artist view of the SMOS aperture synthesis radiometer satellite in space.**

mismatches and imperfections in the antenna patterns, the receiver transfer functions, and the correlators, these being the ones with the largest impacts. Finally a suitable calibration is mandatory. In addition the Institute consults various German scientific groups performing ground validation/calibration experiments, and assists where possible with necessary RF measurements, for example for the detection of radio interference.

Meanwhile ESA is also considering a follow-up mission for SMOS. First ideas consider the basic SMOS concept utilising improved hardware based on the experience gathered through the SMOS development, and offering a slightly increased spatial resolution (25-50 km).

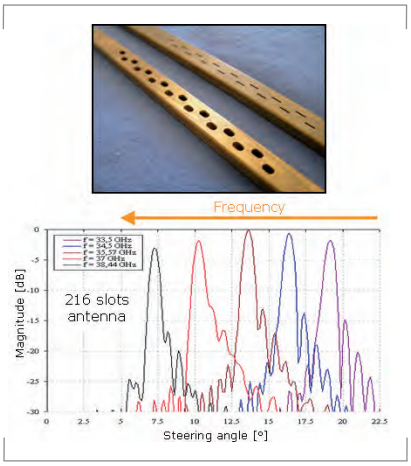


**Figure 4-103: Photograph of samples of different built slotted-waveguide antennas. The lower graph shows the angular steering capability as a function of frequency for the optimised broadband version.**

**Figure 4-104: Photograph of the manufactured Ka-band receiver board using MMIC and microstrip technology. Shown are coaxial-type connectors for the RF input (HF), the local oscillator input (LO), the upper (OSB) and lower (USB) IF sidebands, and a D-sub type for the DC power supply (DC). The blue and green boxes illustrate the size of the MMICs being otherwise hard to distinguish due to a feed size of about 1-2 mm.**

## Development of Specific Hardware Components

Various components of the required hardware are not available off-the-shelf or they are too expensive. Consequently own developments are carried out in the Institute. Recent activities for radiometric applications comprise slotted waveguide antennas, integrated receivers, and digital correlators.

*Slotted waveguide antennas*

Slotted waveguide antennas can be used to steer the antenna beam by changing frequency. Hence they are attractive as part of a fully-electronic imaging system for steering the beam in one direction. The second direction then can be accomplished by other methods like aperture synthesis, phased-array, or focal-plane-array techniques.

In order to achieve a sufficient image size in the frequency-scan direction, a challenging large bandwidth is required. Furthermore the application for radiometry demands for lowest losses across the entire scanned frequency band. Using commercial simulation tools, various Ka-band slotted-waveguide antennas as illustrated in Figure 4-103 were developed and constructed. The optimised version achieves a bandwidth of about 5 GHz (34-39 GHz) and a corresponding steering angle range of about 13° at a half-power beamwidth of about 0.6° as shown in the graph. The noise temperature of this antenna is only about 50 K from 36-38 GHz and less than 350 K at the band edges, which is quite important for radiometric applications.

*Integrated receivers*

Electronic scanning imagers require a certain number of single receiver channels in order to be able to steer the antenna beam. Since this number can be easily around several tens or hundreds, integrated receiver technology is mandatory. For current and future projects in Ka-band, an integrated receiver design was established using MMIC (Monolithic Microwave Integrated Circuit) technology. The in-house manufacturing of the whole circuit is enabled by the availability of manually to operate machine tools like a computer-assisted milling-drilling plotter or a bonding device. A first developed and manufactured part of the Ka-band receiver already including several MMICs is shown in Figure 4-104.

The module has various coaxial-to-microstrip transitions for external connections, two low-noise amplifier MMICs, an IQ mixer MMIC and a hybrid IC for separating the lower and the upper sideband, all connected via matched microstrip lines. The achieved receiver noise temperature is between 380 K and 460 K for a 34-40 GHz band including the transitions. However, although this first module already presents a suitable performance, there is room for further improvements using different bond wires, MMICs with higher performance, and modified line transitions. The actual board size is about 8 cm × 4 cm and can be kept even for the addition of further circuit parts.

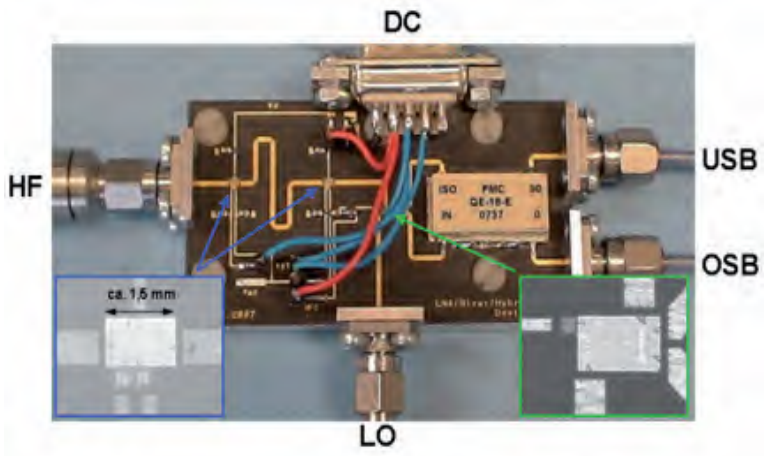

*Digital correlators*

A large number of correlators are required for applying aperture synthesis techniques. First developments in the 1990s concentrated on analogue designs using detector diodes together with appropriate phase switching of the input signals, or integrated four-quadrant multiplier circuits, both followed by adequate low-pass filters as integrators. Since analogue techniques suffer from temperature drifts and aging effects, and because future systems will require thousands of correlators, digital techniques are much more efficient.

Hence a first digital design of a one-bit correlator based on FPGA technology was established for the ANSAS instrument. The correlator board shown in Figure 4-105 consists essentially of 15 BNC connectors as inputs for all receiver channels, comparators for digitisation, the FPGA chip for the intrinsic correlation, and a USB interface for the connection to a personal computer. Within the FPGA also a FIR filter is implemented in order to provide a 90° phase shift for the complex correlation. The operating band of the correlator is 20-40 MHz, and for this range the performance for a noise signal was measured as shown in the graph. Even for large delays of up to 50 µs the measured curves for real and imaginary part follow sufficient precisely the theoretical characteristics. However, for the ANSAS instrument only a maximum delay in the order of 10 ns occur due to the maximum array dimensions of 3 m.

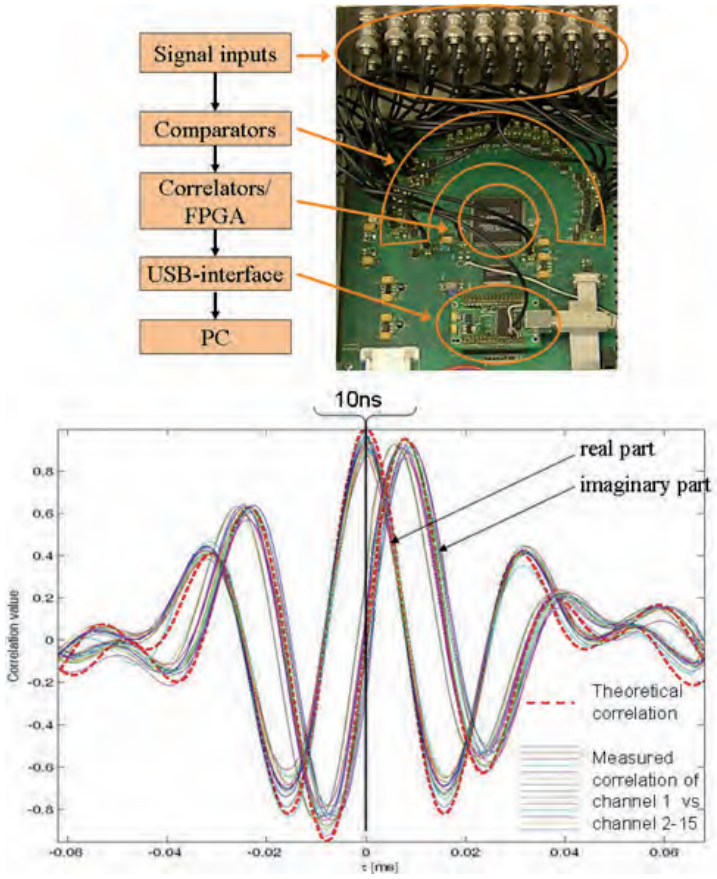


**Figure 4-105: Photograph of the digital correlator board and its functional description (top). Below the measured correlation function (real and imaginary part) over time delay for all the correlations of channel 1 versus channels 2-15 for a noisy signal is illustrated and compared with the theoretical expectation.**

# Weather Radar

The Institute is inevitably confronted by the influence of the propagation path on the imaging sensors, it is an important element in the performance computation and the system calibration. In addition, the Institute participates in European projects in the field of weather radar collaborating with other DLR institutes and external (industrial) partners. Of particular importance is the Institute of Atmospheric Physics with which the Institute shares a fully polarimetric weather radar facility (POLDIRAD). This radar is able to provide unique data for the development and verification of algorithms.

**EU AMPER Project**

The AMPER project (Application of Multi-parameter Polarimetry in Environmental Remote Sensing) was funded by the European Commission over the period from January 2003 until December 2005. The Institute was

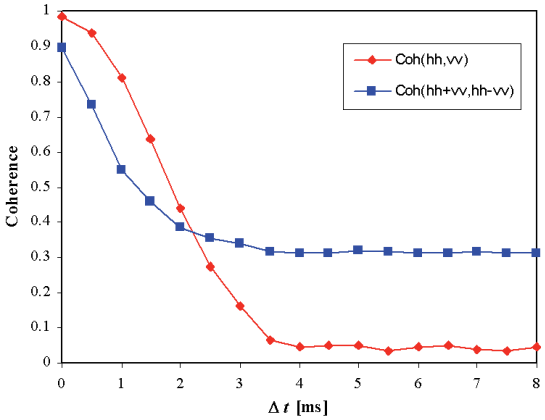


**Figure 4-106: Dependence on the measurement interval Δt of the coherence for HH and VV polarisations (red) and the Pauli base. It shows that the decorrelation is strongly dependent on the initial polarisation base, and that this is important for the correct extraction of information.**

responsible for the overall coordination of the project and research contributions in the field of modelling and understanding atmospheric effects and distortions on coherent polarimetric radar data, as well as in the field of polarimetric target decomposition theory.

The main aim of the project was the training and research of young scientists in the area of multi-parameter polarimetry at partner organisations spread all over Europe (i.e. DLR, TU Chemnitz and Definiens Imaging GmbH, Germany; University of Essex, UK; DDRE, Denmark; UPC, Spain; MOTHESIM and University of Rennes, France; JRC, Italy). The scientific activities of the network fall into three main areas dealing with sensor systems and measured data, the underlying physics and scattering models, parameter retrieval and product generation.

The focus of modelling atmospheric effects was on the scattering of hydrometeors, particularly rain drops. The main purpose is not only to have a coherent model for simulating weather radar data, but also to create a link between observations by weather radar systems and SAR systems. Polarimetric propagation effects play an important role for both systems, and, hence, the model can be used to predict or describe the influence of propagation through a medium containing rain drops for polarimetric radars, regardless of whether they are ground-based or airborne/spaceborne. Raindrops are oblate scatterers, where the oblateness increases with the size of the rain drop, and thus rainfall produces anisotropic scattering, which can be measured with polarimetric radars. One particular problem occurs, because the four elements of the scattering matrix are not all measured at the same time but with a certain time delay, which is usually around 1 ms. During this time, the observed scattering volume (containing falling rain drops) changes and, thus, decorrelation will be seen (Figure 4-106).

Using model results and experience drawn from the literature, phase delays and amplitude effects on radar data can be predicted. Special attention has been given to the impact of such effects on the processing of SAR images. Phase changes due to atmospheric distortions have a similar behaviour to motion errors of the sensor platform and thus might not be separated from such additional error sources.

With regard to polarimetric decomposition theorems, two signal processing approaches have been applied for the first time to fully polarimetric SAR and weather radar signatures. Considerable attention is paid to the eigenvectors of the covariance matrix.

**EU CARPE DIEM Project**

In the framework of the European project CARPE DIEM (Critical Assessment of available Radar Precipitation Estimation techniques and Development of Innovative approaches for Environmental Management) several work packages with regard to polarimetric techniques have been investigated. The project contributed to the Energy, Environment and Sustainable

Development Programme for Research, Technology Development and Demonstration under the fifth Framework Programme with the goal of improving flood forecasting capabilities. The Institute's tasks comprised the exploitation of advanced radar capabilities to allow the enhanced assimilation of weather radar data from operational networks in hydrological and numerical weather prediction models. As the data source, the coherent and fully polarimetric C-band weather radar POLDIRAD was used.

The first task dealt with the use of polarimetric measurements to estimate effects of variation in drop-size distributions on the uncertainty inherent in rainfall estimates collected at different spatial and temporal scales.
The parameters particularly taken into account are the differential reflectivity and phase, which occur due to the oblate nature of rain drops. The outcome was that the differential phase could potentially still provide a more accurate estimate of the average rainfall across an area (or equivalently from a series of rapid scans averaged over a period of time).

The second task was dedicated to the problem that there is a significant lack of "ground truth" for weather radar observations, i.e. the scattering particles are usually pretty much unknown or have to be guessed by using empirical methods (mostly based on fuzzy logic classification). Polarimetry has the great advantage that the scattering can be related to the physics without a priori or empirical knowledge. Hence, Entropy-Alpha decomposition and classification (originally used for land classification in SAR imaging) has been used in order to identify different types of hydrometeors. The most important premise for a precise decomposition is the correction of differential propagation errors, which can only be performed on time series (raw) data. This type of data is usually not available, but POLDIRAD is now able to deliver also the required time series. Figure 4-107 shows a typical distribution of Entropy-Alpha values in the case of a thunderstorm, which provides a broad variation of scatterers (light rain, heavy rain, hail, sleet, snow). Using this distribution and an additional weighting with reflectivity values, a classification scheme could be compiled.

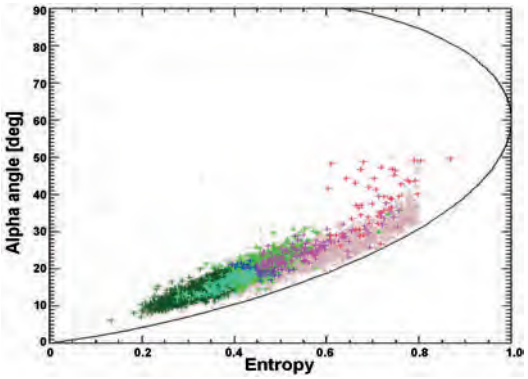


**Figure 4-107: Distribution of data points of a thunderstorm in the Entropy-Alpha plane derived from a time series measured with POLDIRAD on 2nd November 2005.**

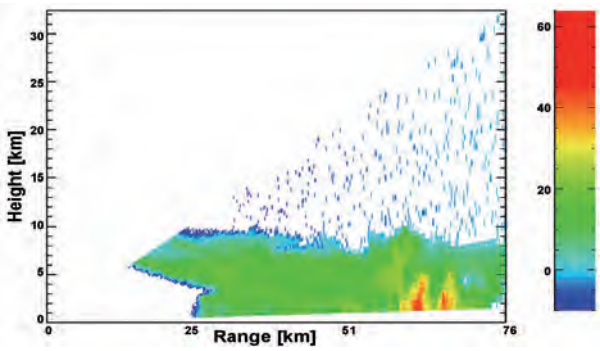


**Figure 4-108: Range-height plot of the thunderstorm in the previous image with high reflectivity values. The colours represent volume scattering in dBZ as shown in the colour scale.**

In Figure 4-108, the reflectivity can be compared with the classification result. The first impression is that this purely physically derived result is very promising, although a comparison with common techniques has still to be

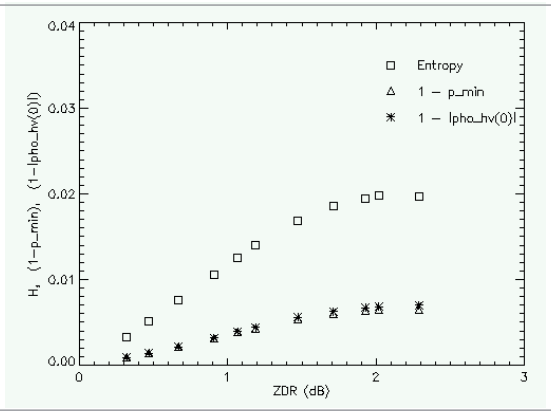


**Figure 4-109: Simulation results for a cloud of non-canted raindrops with exponential Drop Size Distribution (Marshall-Palmer). The plots reported in the graph correspond to entropy (squares), one minus the minimal degree of polarisation (triangles) and one minus the copolar correlation coefficient (asterisks).**

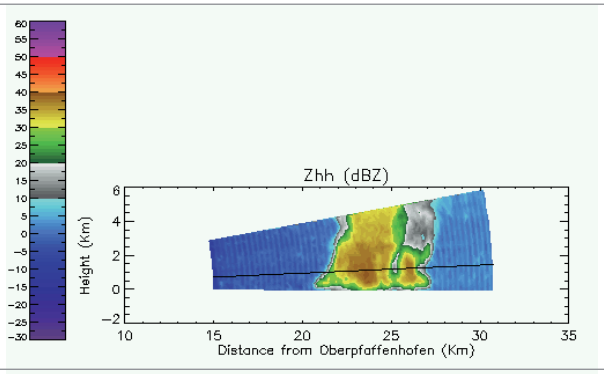


**Figure 4-110: Range-height plot of a convective event showing the reflectivity in HH polarisation. The black line indicates the cut through the cloud corresponding to the following rayplot.**

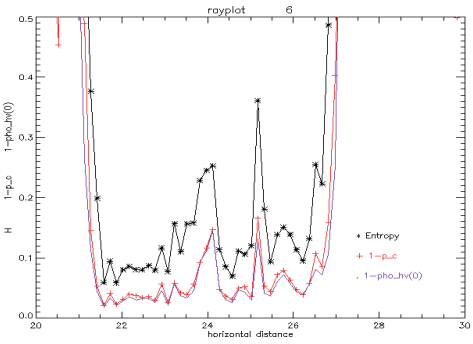


**Figure 4-111: Rayplot corresponding to the ray drawn in black in the figure above. The black line denotes the Entropy, the red and purple lines denote one minus the minimal degree of polarisation and the copolar correlation coefficient.**

performed and will be part of future activities. The method could not only improve the ability to extract weather information from terrestrial radars, but also from radars on airborne and spaceborne platforms

### Polarimetric Investigations for Hybrid Mode Weather Radars

Most weather radars today do not have the capability to measure a fully polarimetric scattering matrix (e.g POLDIRAD is one of the few offering such data). Usually only single-pol or dual-pol (hybrid polarisation) weather radars are broadly used by weather services like the Deutsche Wetterdienst (DWD). Hence, our investigations aim to place weather radar parameters in a wider context in order to exploit more general concepts like target decomposition theorems and polarisation basis transformations.

If the full scattering matrix and thus the covariance matrix is not available, polarimetric observables as the Entropy cannot be derived. However, it has been found that the degree of polarisation, which can be computed from dual-pol data, shows a similar behaviour as the Entropy to a great extent and can thus be used as a proxy for the Entropy in the analysis of weather data. A simulation of a cloud of rain drops already shows that, although the absolute values of the Entropy and the degree of polarisation are different, the trends of the two oberservables are comparable (Figure 4-109).

These theoretical results are confirmed by a case study of real weather radar data of a convective event characterised by two cores located approximately 24 and 26 km away from the radar (Figure 4-110). In correspondence of the centre of the first core (24 km) a mixture of rain and frozen, irregularly-shaped, hydrometeors is probably responsible for higher values of the reflectivity Zhh, Entropy and one minus the degree of polarisation 1-p.

### SAR Processing Techniques for Weather Radars (Rotating SAR)

In collaboration with SELEX-SI Gematronik the Institute carried out a detailed study about the possible application of SAR processing techniques to ground-based weather radar data in order to enhance the spatial (azimuthal) resolution.

At DLR a radar experiment was designed and later realised at SELEX-SI Gematronik facilities. The data were then analysed in order to obtain information about the possibility to azimuth-compress the signals scattered from hydrometeors. The results are relevant not only for ground-based weather radars but also for spaceborne weather radars, of which SAR systems can, in the limit, be considered as an example. Hydrometeors have decorrelation times in the order of milliseconds or tens of milliseconds, depending on hydrometeor type, turbulence in the resolution volume, and sounding frequency. At C-band, where European weather radars operate, the decorrelation time is approximately 10 ms. For the phase center of the antenna of a weather radar to scan the whole synthetic aperture (a sector of a circular array) an integration time approximately one order of magnitude larger is needed. The same holds also for space based synthetic aperture radars (approximately 500ms for TerraSAR-X). So, the first important result is that weather targets cannot be focussed, either with rotating ground-based weather radars or with spaceborne antennas. This should be kept in mind if weather information extraction from SAR images is to be undertaken: the weather component comes from a larger volume whereas the ground contribution (regardless whether coherent or distributed) comes from the nominal pixel resolution of the system. Also, if the weather target signal-to-noise ratio (SNR) is not enhanced by the azimuth focussing process, the same does not hold in case coherent scatterers are present in the ground scene. This renders the separation of ground clutter from weather targets even more challenging than with conventional real aperture weather radars.

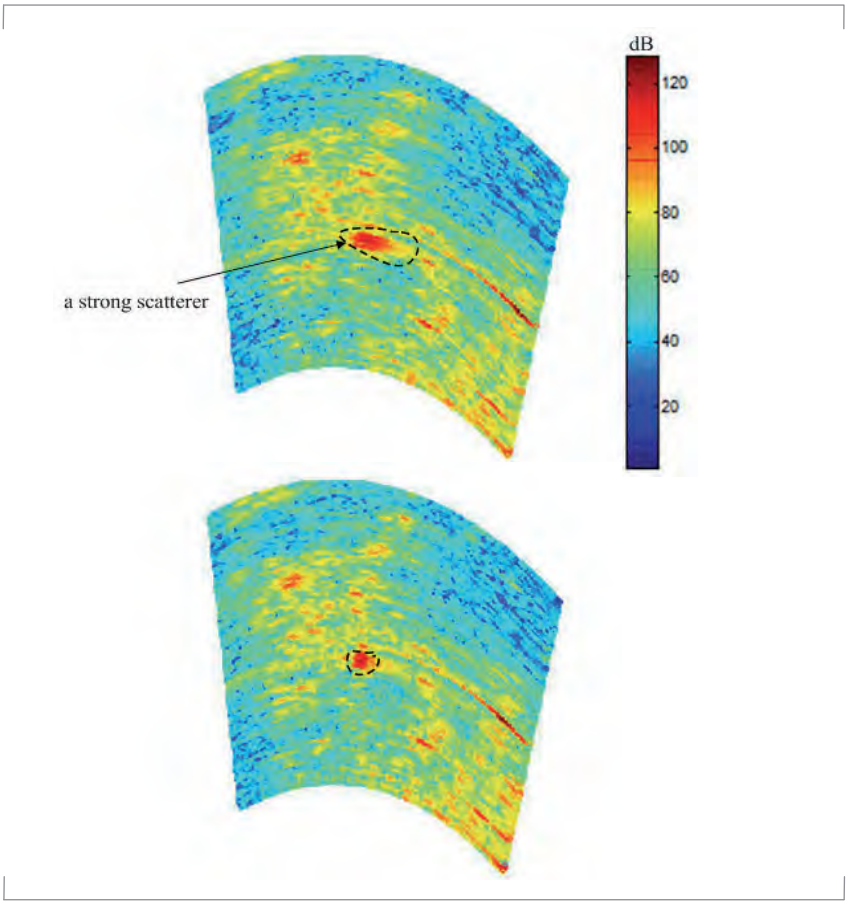


**Figure 4-112: „SAR" image corrupted by phase errors (above) and „SAR" image corrected by a RELAX-based autofocus algorithm.**

However, some applications could nevertheless be envisioned. For example, coherent targets can be focussed. Among these are ground clutter, and in this case the focussing is rather straightforward, but also flying aircrafts, and in this case autofocussing techniques can be employed to obtain

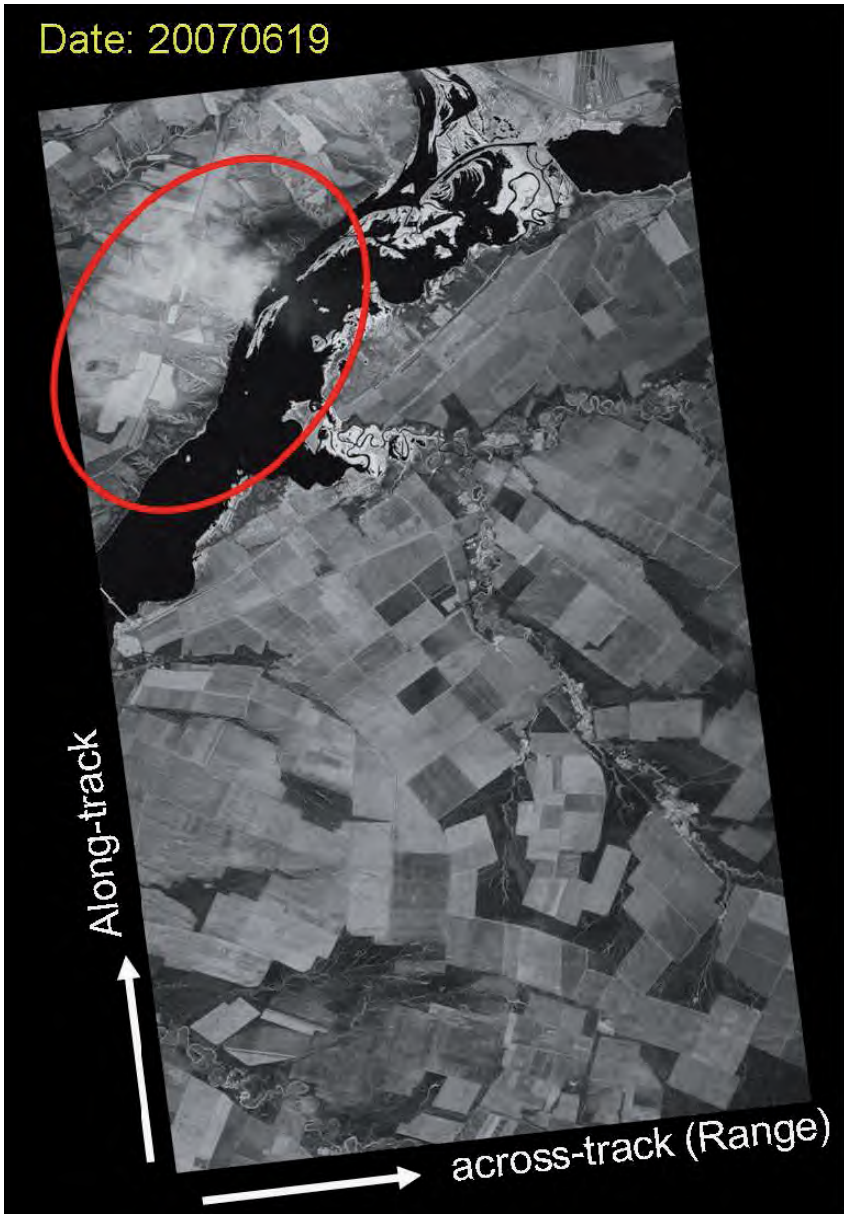


**Figure 4-113: Example of rain-cell-affected SAR signaturesre-corded with TerraSAR-X. The white shading is due to direct reflections from the rain region, whereas the darkly shaded areas are due to rain attenuated (blocked) signals from the ground. Image dimensions are 30 x 60 km.**

angular superresolution of the target (higher angular resolution with respect to the parabolic reflector). This might have applications for surveillance radars.

Also, array signal processing techniques were used in order to suppress constructively adding sidelobes resulting from closely located ground coherent targets. Figure 4-112 demonstrates the capabilities of a RELAX-based autofocus algorithm applied to the data, which gave outstandingly good results and permits to eliminate artifacts appearing due to sinc sidelobes summation.

## Propagation

Tropospheric propagation effects in radar measurements continue to play an important role at ever higher radar resolutions approaching the decimeter scale. Spaceborne Synthetic Apertur Radar (SAR) imaging is often considered to possess both day/night and all weather operational capabilities. Whereas the first argument is true since we are dealing with an active sensor; the second does not hold in cases for which the operating frequencies are above ~5 GHz.
The spectral attenuation and phase decorrelation of the polarimetric channels become apparent already at C-band and especially at X-band. During the commissioning phase of TerraSAR-X, a total of 12000 scenes were investigated for potential propagation effects and about 100 scenes revealed atmospheric effects to a visible extent. An example of the first TerraSAR-X image acquired close to Volgograd (Russia) is given in Figure 4-113. It provides an example of typical rain/precipitation induced signature modifications.

**Test Case and Comparison of SAR Data with Simultaneously Measured Ground-based Weather Radar Data**

In Figures 4-114 and 4-115, a comparison of two different types of images measured almost at the same time is provided. The Figure above shows

a TerraSAR-X image acquired in stripmap mode in ascending orbit over New York. The Figure below displays the corresponding weather radar image measured by a ground-based weather radar (WSR-88D) located close to New York City. A good agreement between visible artefacts shown in the SAR image and the reflectivity plot given in the weather radar image was observed. Such reflectivity maps display the echo intensity of the transmitted radar signals and are shown in dBZ. These maps are used to detect precipitation and evaluate storm structures. It is the best available means to compare precipitation volumes and precipitation induced signatures in SAR images. The reason is due to the high achievable spatial resolution and the possibility to measure at almost the same instant of time. The red regions in the weather radar image correspond to reflectivities up 55 dBZ, which indicate high precipitation intensities typically occurring during thunderstorms. The comparison of ground based weather radar and SAR data will be certainly useful in the process to derive rain intensity information from SAR based measurements.

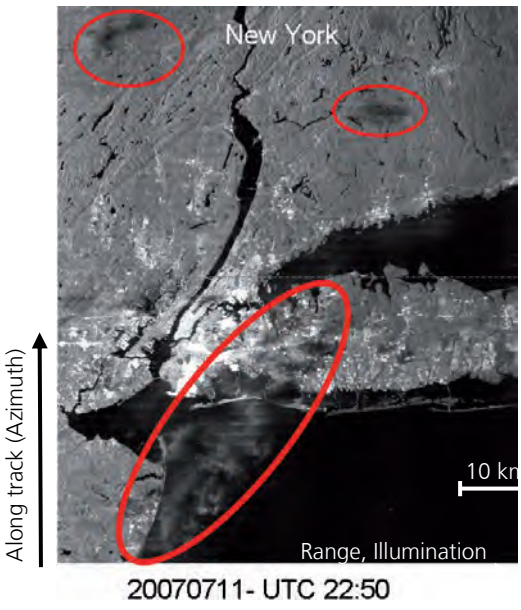


**Figure 4-114: SAR image acquired over New York in ascending orbit direction. The image dimensions are aprrox. 130 km in azimuth and 100 km in range direction.**

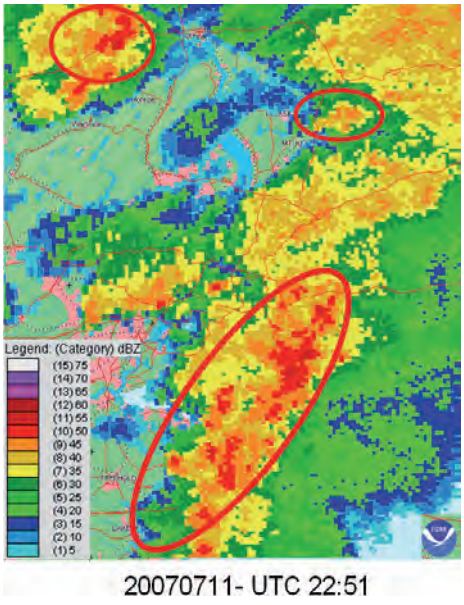


**Figure 4-115: Ground-based weather radar image acquired over New York, showing high precipitation intensities given in dBZ. A good agreement between rain induced SAR signatures (image on top) and the weather radar image (below) can be observed.**

### The Influence of Tropospheric Propagtion Effects on the Calibration of TerraSAR-X

The influence of atmospheric effects on the external calibration of SAR systems like TerraSAR-X (9.65 GHz) does, under certain circumstances, exceed the instrumental errors. Therefore, there is a demand to detect and monitor extraordinary precipitation events which might occur during the data acquisition.

Being able to detect high rain rates and subsequently to flag affected SAR data products, the rain affected SAR data products can be excluded from the external calibration procedure (XCAL).

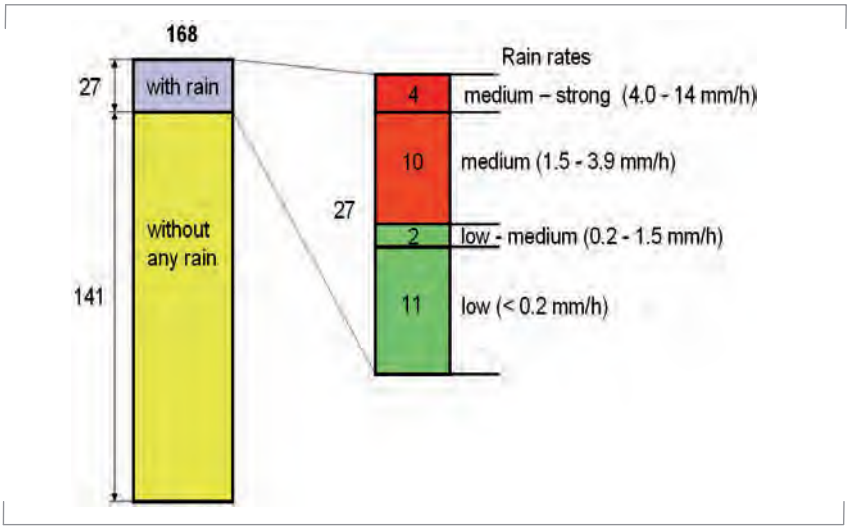


**Figure 4-116: Illustrative depiction of the weather conditions during the acquisition of the calibration data takes over the test site in Southern Bavaria.**

**Monitoring of the TerraSAR-X Test Site During the External Calibration (XCAL) Campaign**

The objective to monitor the test site during the external calibration campaign is the detection of heavy precipitation events (>14 mm/hr). Therefore, weather radar data from the weather service was utilised, which provides an update of PPIs (plan position indicator) every 15 minutes for the test site area.

For the case of TerraSAR-X the simultanously acquired weather radar measurents for each data take of TerraSAR-X have been analysed (Figure 4-116). The total number of analysed scences was 168, where 141 measurements were acquired without any precipitation. From the remaining 27 scences including rain events, 4 measurements could be identified with strong rain and they have, in turn, been excluded from the procedure to derive the averaged absolute calibration constant. Thus the overall uncertainty of the absolute calibration factor was reduced by 0.15 dB (1-sigma). Considering the finally achieved absolute radiometric accuracy of 0.31 dB (1-sigma) for TerraSAR-X, this is indeed a remarkable contribution.

# The Institute Today



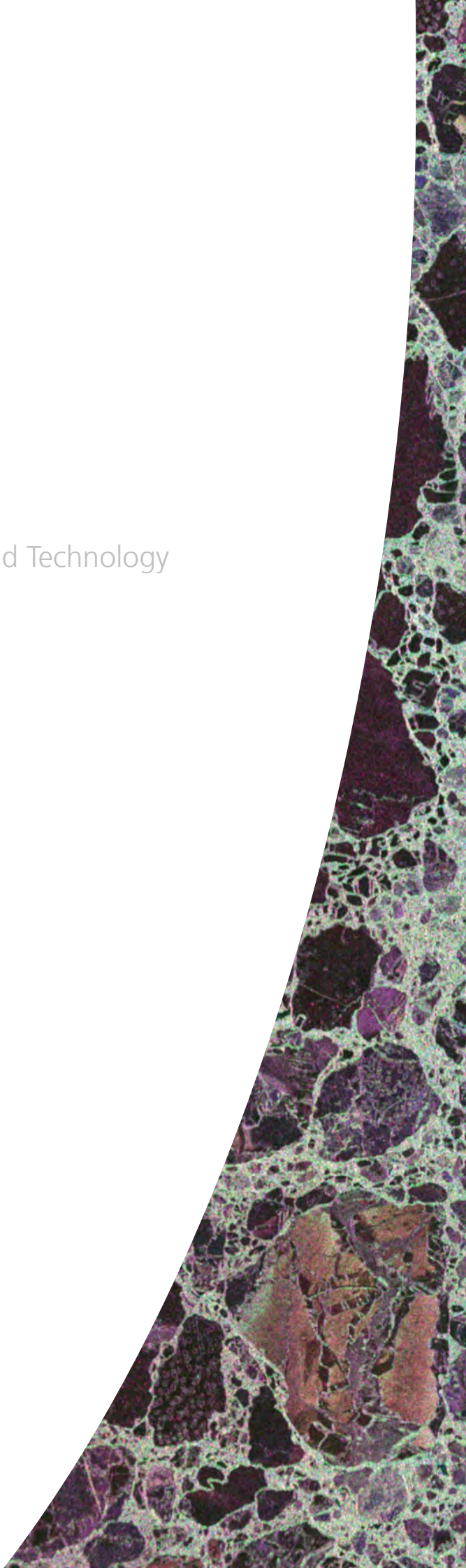

# Institute's Personnel (2008)

**Harald Anglberger**
Scientist

Dr. Federica Bordoni
Scientist

**Thomas Busche**
Scientist

**Markus Bachmann**
Scientist

**Dr. Thomas Börner**
Group Leader

**Bastian Calaminus**
Engineer

**Robert Bauer**
Engineer

**Bernd Brand**
Scientist

**Martin v. Chiari**
Scientist

**Stefan Baumgartner**
Scientist

**Benjamin Bräutigam**
Group Leader

**Ali Eren Culhaoglu**
PhD Student

**Dr. Karl-Heinz Bethke**
Quality Manager

**Dr. Stefan Buckreuß**
Group Leader

**Christoph Dahme**
IT Manager

**Johannes Böer**
Scientist

**Josè Luis Bueso Bello**
Scientist

**Dr. Andreas Danklmayer**
Scientist

**Petra Deutinger**
Secretary

**Jürgen Fiala**
Scientist

**Michele Galletti**
Scientist

**Dr. Björn Dietrich**
Group Leader

**Dr. Haucke Fiedler**
Scientist

**Rudolf Gastl**
Mechanist

**Stephan Dill**
Scientist

**Jens Fischer**
Scientist

**Nicolas Gebert**
Scientist

**Björn Döring**
Scientist

**Jean-Paul Fumelli**
Technician

**Dr. Dirk Geudtner**
Scientist

**Jan Eilers**
Scientist

**Martina Gabele**
Scientist

**Carolina Gonzalez**
Scientist

**Esra Erten**
PhD Student (DAAD)

**Bernd Gabler**
Engineer

**Christo Grigorov**
Scientist

**Peter Hackenberg**
Technician

**Daniel Höflmayr**
Technician

**Matthias Jirousek**
Scientist

**Gabriele Hager**
Personnel Administration

**Ralf Horn**
Group Leader

**Martin Keller**
Scientist

**Manfred Hager**
Scientist

**Sigurd Huber**
Scientist

**Timo Kempf**
Scientist

**Dr. Irena Hajnsek**
Group Leader

**Jaime Hueso González**
Scientist

**Dr. Erich Kemptner**
Group Leader

**Peter Heitzer**
Mechanical Lab Leader

**Koichi Iribe**
PhD Student

**Jun Su Kim**
PhD student (DAAD)

**Dr. Konrad Hiller**
Scientist

**Thomas Jagdhuber**
PhD Student

**Juliane Klämke**
Project Assistant

**Dr. Gerhard Krieger**
Head of department

**Dr. Josef Mittermayer**
Group Leader

**Lukas Orlowski**
Scientist

**Florian Kugler**
Scientist

**Prof. Dr. Alberto Moreira**
Director of the Institute

**Carlos Ortega**
Scientist

**Seungkuk Lee**
Scientist

**Gerhard Müller**
Scientist

**Dr. Andrey Osipov**
Scientist

**Markus Limbach**
Scientist

**Matteo Nannini**
Scientist

**Alicja Ossowska**
Scientist

**Alberto Di Maria**
Scientist

**Dr. Thomas Neff**
Group Leader

**Dr. István Pál**
Scientist

**Luca Marotti**
Scientist

**Anton Nottensteiner**
Group Leader

**Dr. Konstantinos Papathanassiou**
Group Leader

**Sebastian Pasch**
Technician

**Sibylle Radzuweit**
Secretary

**Dr. Rolf Scheiber**
Group Leader

**Anton Patyuchenko**
Scientist

**Dr. Andreas Reigber**
Head of Department

**Nico Schmid**
Engineer

**Dr. Markus Peichl**
Group Leader

**Frank Reinwaldt**
Technician

**Christian Schmidt**
Logistics and Controlling

**Maria Donata Polimeni**
Scientist

**Dr. Gerald Rode**
Scientist

**Rafael Schneider**
Scientist

**Dr. Pau Prats**
Scientist

**Marc Rodriguez Cassola**
Scientist

**Dr. Helmut Schön**
Scientist

**Russel Que**
Scientist

**Dr. Stefan Sauer**
Scientist

**Dirk Schrank**
Scientist

**Eric Schreiber**
PhD Student

**Dr. Rainer Speck**
Group Leader

**Stefan Thurner**
Technician

**Harald Schreiber**
Software Engineer

**Ulrich Steinbrecher**
Scientist

**Nuria Tous Ramon**
Scientist

**Clemens Schulz**
Scientist

**Prof. Dr. Helmut Süß**
Head of Department

**Renate Weist**
Institute`s Secretariat

**Daniel Schulze**
Group Leader

**Sebastian Tailhades**
Scientist

**Birgit Wilhelm**
Computer Programmer

**Dr. Marco Schwerdt**
Group Leader

**Alfred Theuerkauf**
Engineer

**Steffen Wollstadt**
Scientist

**Jayanti Sharma**
PhD Student

**Bettina Thurner**
Secretary

**Dr. Marwan Younis**
Group Leader

**Dr. Francesco De Zan**
Scientist

**Matthias Zanger**
Engineer

**Karl-Heinz Zeller**
Scientist

**Dr. Manfred Zink**
Head of Department

# Acknowledgement

A large team of Institute's members contributed to this report and their names are recognized below:

*Andres, Christian*
*Baumgartner, Stefan*
*Bethke, Karl-Heinz*
*Börner, Thomas*
*Bräutigam, Benjamin*
*Buckreuss, Stefan*
*Danklmayer, Andreas*
*Dill, Stephan*
*Dietrich, Björn Alexander*
*Döring, Björn*
*Fiedler, Hauke*
*Fischer, Jens*
*Gabele, Martina*
*Hajnsek, Irena*
*Horn, Ralf*
*Hounam, David*
*Kempf, Timo*
*Kemptner, Erich*
*Keydel, Wolfgang*
*Krieger, Gerhard*
*Limbach, Markus*
*Marquardt, Nico*
*Mittermayer, Josef*
*Neff, Thomas*
*Nottensteiner, Anton*
*Papathanassiou, Konstantinos*
*Peichl, Markus*
*Röde, Bernd*
*Scheiber, Rolf*
*Schmid, Rudolf*
*Schwerdt, Marco*
*Speck, Rainer*
*Süß, Helmut*
*Werner, Marian*
*Younis, Marwan*
*Zehetbauer, Tino*
*Zink, Manfred*

We would also like to recognize the entire Institute's staff for their exemplary engagement, hard work and outstanding research results achieved in the past years.

Alberto Moreira

# DLR at a Glance

DLR is Germany´s national research center for aeronautics and space. Its extensive research and development work in Aeronautics, Space, Energy, Transport and Security is integrated into national and international cooperative ventures.
As Germany´s space agency, DLR has been given responsibility for the forward planning and the implementation of the German space programme by the German federal government as well as for the international representation of German interests. Furthermore, Germany's largest project-management agency is also part of DLR.

Approximately 7,000 people are employed at sixteen locations in Germany: Cologne (headquarters), Augsburg, Berlin, Bonn, Braunschweig, Bremen, Goettingen, Hamburg, Juelich, Lampoldshausen, Neustrelitz, Oberpfaffenhofen, Stade, Stuttgart, Trauen, and Weilheim. DLR also operates offices in Brussels, Paris, and Washington D.C.

## Microwaves and Radar Institute

With its know-how and expertise in passive and active microwave remote sensing, the Microwaves and Radar Institute contributes to the development and advancement of ground-based, airborne and spaceborne sensors and missions. The Institute's expertise encompasses the whole end-to-end system know-how in microwave sensors. It has a number of large-scale facilities to support its research activities, including the airborne SAR (F-SAR) and a new building for microwave sensor and technology development (TechLab).

The Institute is located in Oberpfaffenhofen near Munich and has a long history dating back to the beginning of the last century. Today, the Institute focuses its research on synthetic aperture radar (SAR) techniques, sensors and applications related to remote sensing, environmental monitoring, reconnaissance and surveillance, as well as road traffic monitoring. The Institute has about 135 employees and has become the driving force of the SAR Center of Excellence at DLR. It is a leading institution in synthetic aperture radar remote sensing in Europe and worldwide.



DLR Deutsches Zentrum für Luft- und Raumfahrt e.V.
in der Helmholtz-Gemeinschaft

**Microwaves and Radar Institute**
Oberpfaffenhofen
D-82234 Weßling

www.dlr.de/HR